International Journal of Polymer Science

Advanced Polymer Particles

Guest Editors: Eri Yoshida, Takashi Kaneko, Toshifumi Satoh, Yusuf Menceloglu, and Atsuyoshi Nakayama

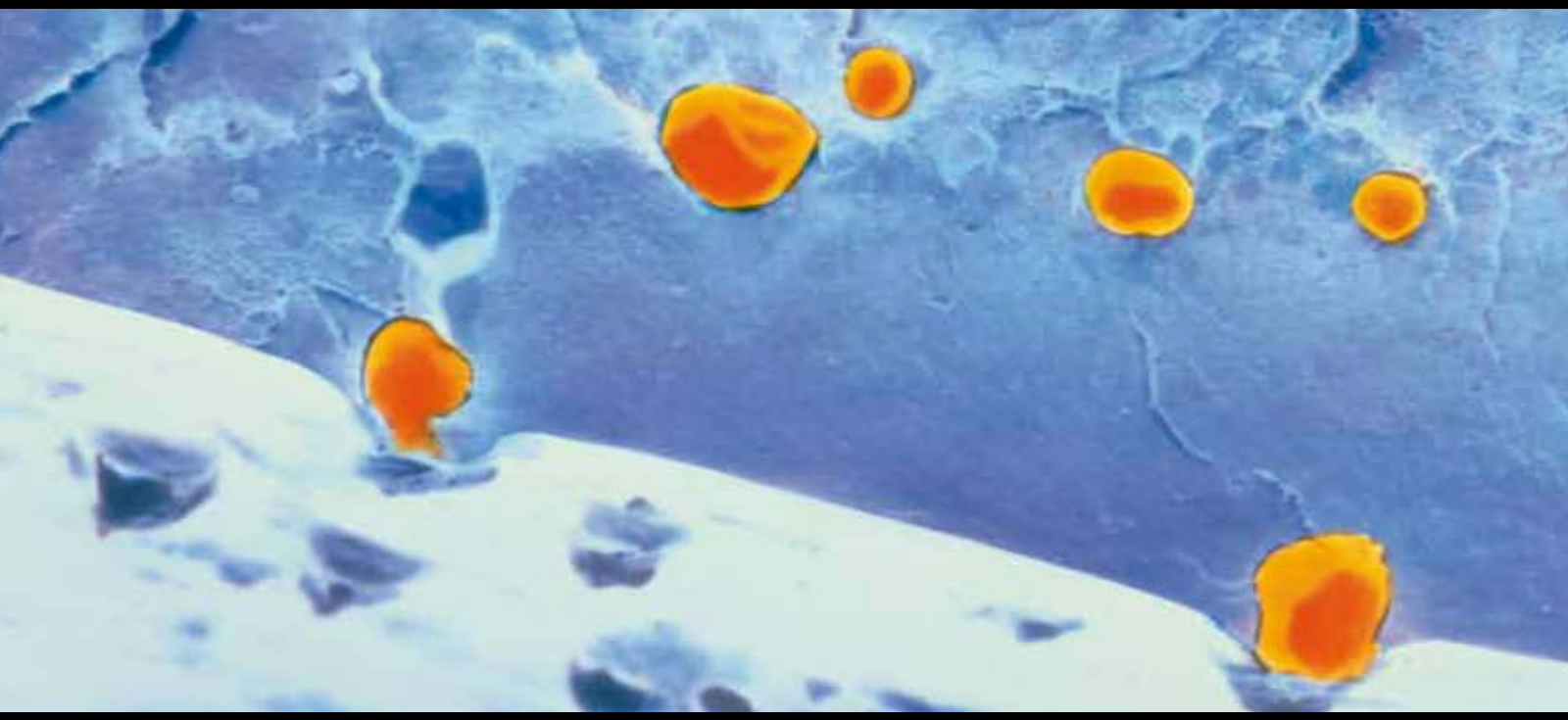

Advanced Polymer Particles

International Journal of Polymer Science

Advanced Polymer Particles

Guest Editors: Eri Yoshida, Takashi Kaneko, Toshifumi Satoh, Yusuf Menceloglu, and Atsuyoshi Nakayama

Editorial Board

Contents

Hindawi Publishing Corporation
International Journal of Polymer Science
Volume 2012, Article ID 168412, 2 pages
doi:10.1155/2012/168412

Editorial

Advanced Polymer Particles

Eri Yoshida,[1] Takashi Kaneko,[2] Toshifumi Satoh,[3] Yusuf Menceloglu,[4] and Atsuyoshi Nakayama[5]

[1] *Department of Environmental and Life Sciences, Toyohashi University of Technology, Toyohashi 441-8580, Japan*
[2] *Graduate School of Science and Technology, Niigata University, Niigata 950-2181, Japan*
[3] *Division of Biotechnology and Macromolecular Chemistry, Faculty of Engineering, Hokkaido University, Sapporo 060-8628, Japan*
[4] *Faculty of Engineering and Natural Sciences, Sabanci University, 34956 Istanbul, Turkey*
[5] *Health Research Institute, National Institute of Advanced Industrial Science and Technology, Osaka 563-8577, Japan*

Correspondence should be addressed to Eri Yoshida, eyoshida@ens.tut.ac.jp

Received 27 February 2012; Accepted 27 February 2012

Polymer particles support today industries based on cutting-edge technologies. The micro- and nanosized polymer particles have many applications in various fields, such as painting, printing, electronics, adhesives, paper manufacture, civil engineering and construction, cosmetics, and medical care. In these fields, the particles have played a significant role in improving the functions and performances of the materials. Examples include the rheology control of painting, improvement of the optical properties of luster, whiteness, and opacity in paper manufacture and cosmetics, strengthening concrete in civil engineering, and carriers of drug delivery systems and immunoassay in medical care. Thus, a wide variety of applications of polymer particles is based on the advantages over inorganic and metal particles in the fact that various methods can be utilized to prepare them that their size and forms can be strictly controlled over a wide range and that their surfaces and interior structures can be modified in great variety. The polymer particles have become a key material in creating new products and technologies. To accelerate the developments of new products and progress of technologies, we planned this special issue on advanced polymer particles. In this special issue, we have invited a few papers involving novel methods of preparing polymer particles and the polymers themselves, the methods that should promote such developments and progress.

One paper of this special issue addresses the fact that understanding the environmentally related unstable colloids, especially, floc structures and their formation mechanics to predict macroscopic transportation properties of the flocs are essential to engineering design using colloidal particles. The flocs dominate the dynamic properties of the unstable colloids, such as sediments in rivers, lakes, and brackish estuaries, and soils and cakes in waste water treatment processes. It is important to clarify the relationship between microscopic colloidal interactions and microscopic properties. In this study, a geometrical model explained the rate of sedimentation, rheological properties, and influence on flocculation of the colloids by water-soluble polymers.

Another paper of this special issue presents the preparation of the polymer particles by self-assembly of polymers containing cholesterol that forms thermotropic and lyotropic liquid crystallines, monolayers, micelles, and liposomes. These cholesterol-supported amphiphilic copolymers are self-assembled into different nanoordered structures depending on the copolymer structure in water through the strong stacking and hydrophobicity of the cholesterol. A following paper describes the fabrication of polymer particles with superhydrophobicity by self-assembly of random copolymers containing perfluoroalkyl chains in supercritical carbon dioxide. The copolymers formed micellar-structured spherical particles of hundreds of nanometers in diameter in a heterogeneous state at pressures lower than the cloud point pressure of CO_2. The surfaces coated with the spherical particles showed superhydrophobicity with the water-contact angles of over 170°.

Another paper of this special issue presents the synthesis of carbazole-supporting block, random, star, and star block copolymers that self-assemble into fluorescent micelles and three-dimensional hierarchical structures. The copolymers were prepared by the controlled/living

radical polymerizations, such as the reversible addition-fragmentation chain transfer (RAFT) polymerization and atom transfer radical polymerization (ATRP). The copolymers were also functionalized with rhenium diimine complexes to serve as a photosensitizer, while the rod-coil block copolymer was employed for a white organic electroluminescence device. A paper concerns the preparation of well-defined hyperbranched polymers expected for use as molecular capsules for carriers of drug delivery systems, nanoreactors, mixture separators, viscosity modifiers, and cross-linkers to provide functional gels. The hyperbranched polymers were prepared through polymerization using a slow monomer addition method. By this slow monomer addition technique, various highly branched polymers were obtained, such as hyperbranched poly(2-hydroxymethyloxetane), polyglycerol, and glycopolymer. Other paper is on the synthesis of rod-like structured polydendrons by the polymerization of monodendron monomers having alkoxy peripheral groups using a rhodium catalyst. The membranes prepared from the polydendrons showed high oxygen permselectivity. Finally a paper introduces the application of polymer resins to photoresists for which the molecular weights of the polymer resins are required to be strictly controlled. It is reported that the use of wet ozone was effective for removal of ionimplanted resists.

Eri Yoshida
Takashi Kaneko
Toshifumi Satoh
Yusuf Menceloglu
Atsuyoshi Nakayama

Hindawi Publishing Corporation
International Journal of Polymer Science
Volume 2012, Article ID 592759, 16 pages
doi:10.1155/2012/592759

Review Article

Nanospheres Prepared by Self-Assembly of Random Copolymers in Supercritical Carbon Dioxide

Eri Yoshida

Department of Environmental and Life Sciences, Toyohashi University of Technology, 1-1 Hibarigaoka, Tempaku-cho, Toyohashi, Aichi 441-8580, Japan

Correspondence should be addressed to Eri Yoshida, eyoshida@ens.tut.ac.jp

Received 19 August 2011; Accepted 28 November 2011

Academic Editor: Takashi Kaneko

The synthesis of spherical particles was attained by the direct self-assembly of poly[2-(perfluorooctyl)ethyl acrylate-*random*-acrylic acid], P(POA-*r*-AA), and by the indirect self-assembly poly[POA-*random*-2-(dimethylamino)ethyl acrylate], P(POA-*r*-DAA), with dicarboxylic acids in supercritical carbon dioxide ($scCO_2$). The copolymers formed spherical particles with hundreds of nanometer diameters in a heterogeneous state at pressures lower than the cloud point pressure. The formation of spherical particles was also dependent on the temperature. The formation of spherical particles could be optimized through varying the solvent quality by the manipulation of the CO_2 pressure and temperature for the different copolymer compositions. The dynamic light scattering and ^{1}H NMR studies demonstrated that the nanospheres had the micellar structures consisting of the CO_2-philic POA shells and the CO_2-phobic AA or DAA cores including the main chain cores. The nanospheres produced the superhydrophobic surfaces based on the water-proof shells of the POA units.

1. Introduction

Micro- and nanosized polymer particles have many industrial applications, such as coating [1], painting [2], cosmetics [3], adhesives [4, 5], and drug carriers [6, 7]. These spherical particles are often prepared by heterogeneous polymerizations of suspension polymerization [8, 9], dispersion polymerization [10–12], and emulsion polymerization [13–15]. While such heterogeneous polymerizations have merits in the simple procedure and particle size control, the polymerizations include problems in taking dozens of hours to produce spheres and disposing the waste solvents.

Molecular self-assembly is also important to prepare spherical particles and has advantages over the heterogeneous polymerizations in the spontaneous and environmentally benign reactions through noncovalent bond interaction. The self-assembly in supercritical carbon dioxide ($scCO_2$) has both the benefits combining its energy-saving reaction and its environmental benefits of being nontoxic, odorless, spontaneous, and volatile. The benefits also include the industrial utilities of being recyclable and having mild critical conditions (31.1°C, 73.8 bar). There have already been publications on the self-assembly in $scCO_2$; the micellization of block copolymers, such as polystyrene-*block*-poly(1,1-dihydroperfluorooctyl acrylate) [16], poly(vinyl acetate)-*block*-poly(1,1,2,2-tetrahydroperfluorooctyl acrylate) [17], poly (vinyl acetate)-*block*-poly(1,1-dihydroperfluorooctyl acrylate) [18–20], and poly(2-hydroxyethyl methacrylate)-*block*-poly(1,1-diethylsilabutane) [21], and the self-assembly of surfactants, such as ammonium carboxylate perfluoropolyether [22], bis(1H, 1H, 5H-octafluoro-*n*-pentyl) sodium sulfosuccinate, and the hybrid di-chained sulfate [23]. The self-assembly of these block copolymers and surfactants in $scCO_2$ produced spherical micelles having the perfluoroalkyl or alkylsilyl shells and the hydrocarbon or ionic cores (Scheme 1).

We found a novel and convenient method to prepare nanospheres through the direct and indirect self-assembly of random copolymers in $scCO_2$ [24–26]. This paper

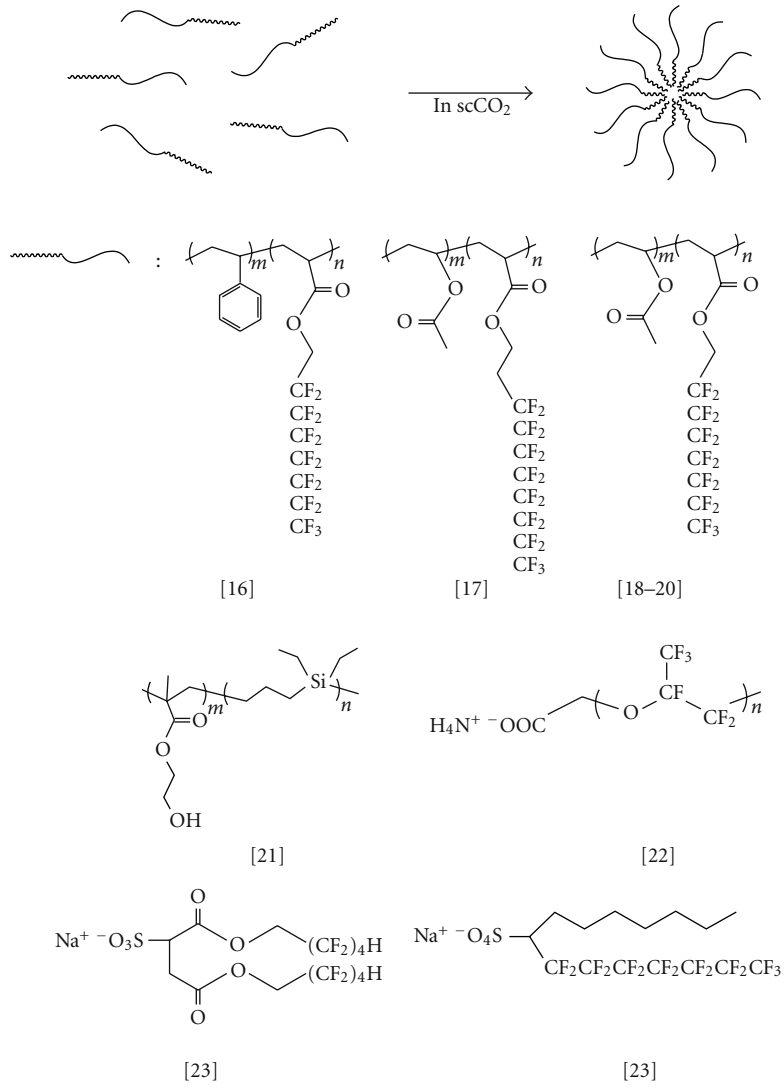

Scheme 1: The self-assembly of the block copolymers and surfactants in $scCO_2$.

Table 1: The P(POA-*r*-TBA) copolymers.

Feed ratio		Time (min)	Yield (%)	Mn^a	Mw/Mn^a	Composition[b]	
POA	TBA					POA	TBA
0.90	0.10	30	91	66,000	6.77	0.89	0.11
0.80	0.20	45	88	78,000	6.16	0.80	0.20
0.70	0.30	120	88	72,000	5.91	0.67	0.33
0.60	0.40	40	82	57,000	6.78	0.60	0.40

[a]Estimated by GPC based on poly(methyl methacrylate) standard.
[b]Estimated by ^{1}H NMR.

describes the preparation of nanospheres by the self-assembly of random copolymers containing the CO_2-philic 2-(perfluorooctyl)ethyl acrylate (POA) units.

2. Materials and Methods

2.1. Instrumentation. The ^{1}H NMR measurement was conducted using a Varian 300 FT NMR spectrometer. The gel permeation chromatography (GPC) was performed using a Tosoh GPC-8020 instrument equipped with a DP-8020 dual pump, a CO-8020 column oven, and an RI-8020 refractometer. Two polystyrene gel columns, Tosoh TSKgel GMH_{HR}-M, were used with hexafluoroisopropanol (HFIP) as the eluent at 40°C. The cloud point measurements were performed with a Nekken variable volume view cell (with a window made of tempered glass) equipped with an Eyela

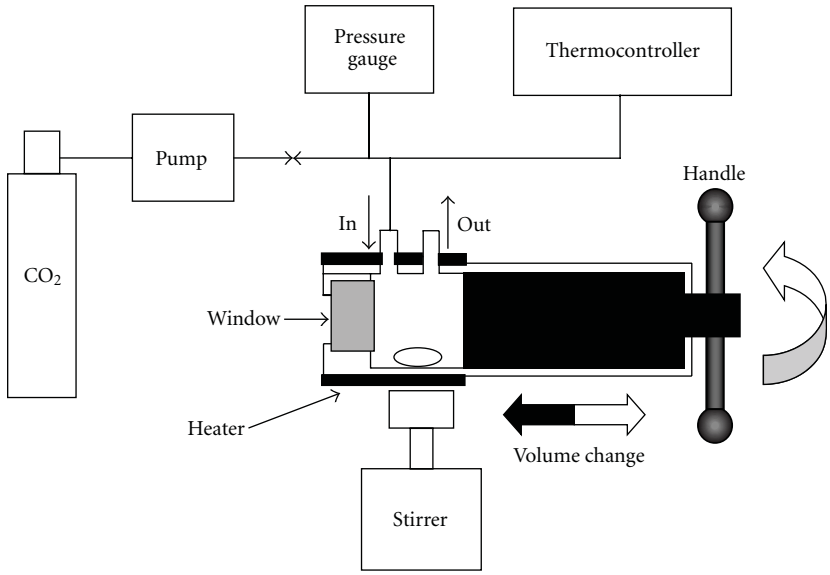

Scheme 2: A schematic of the experimental variable volume view cell.

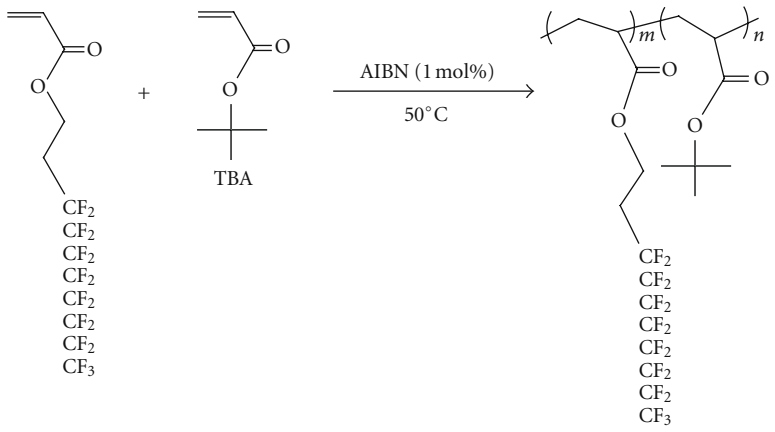

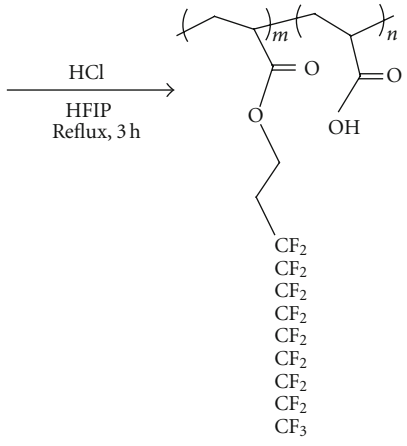

Scheme 3: Synthesis of P(POA-*r*-AA).

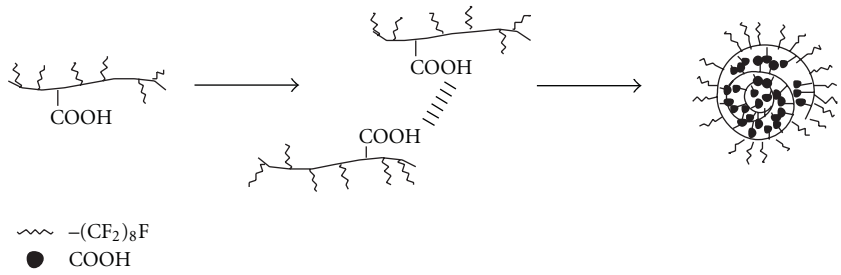

Scheme 4: A schematic of the formation of the spherical particles.

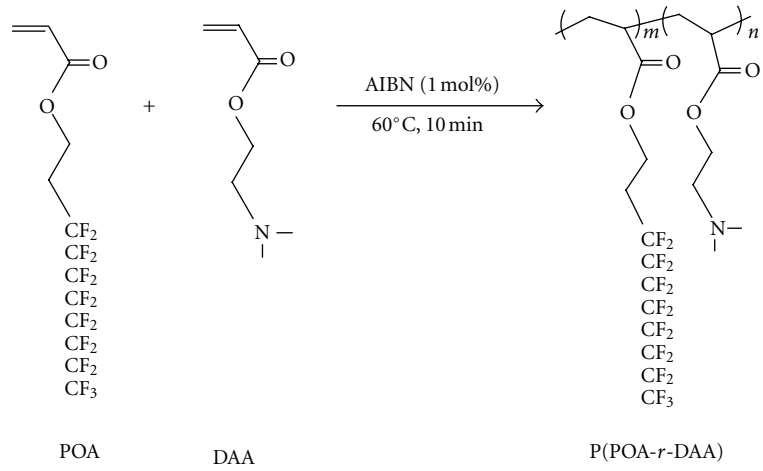

Scheme 5: Synthesis of the P(POA-*r*-DAA) random copolymers.

Table 2: The P(POA-*r*-AA) copolymers.

Composition		Yield (%)	Mn[a]	Sample name
POA	AA			
0.89	0.11	84	110,000	9/1
0.80	0.20	98	97,000	8/2
0.67	0.33	89	72,000	7/3
0.60	0.40	98	84,000	6/4

[a]Estimated by GPC based on poly(methyl methacrylate) standard.

Table 3: The P(POA-*r*-DAA) copolymers.

POA/DAA	Mn[a]	Mw/Mn[a]	Tm (°C)
9/1	58,000	10.95	60.3
8/2	55,000	8.37	55.3
7/3	50,000	7.35	47.8

[a]Estimated by GPC based on poly(methyl methacrylate) standard.

CCA-1110 cooler and a Nihon Seimitsu Kagaku NP-D-321 personal pump. The scanning electron microscopy (SEM) measurements were made using a JEOL JSM-6300 electron microscope. The Pt coating was performed using a Sanyu Denshi SC-701C-MC quick cool coater. Light scattering measurements were performed with a Photal Otsuka Electronics ELS-8000 electrophoretic light scattering spectrophotometer equipped with a system controller, an ELS controller, and an He-Ne laser operating at $\lambda = 632.8$ nm.

2.2. Materials. POA was purchased from Daikin Chemical Co. Ltd. and was deinhibited by passage through an alumina column. *tert*-Butyl acrylate (TBA) was purified by distillation under reduced pressure over calcium hydride. 2-(Dimethylamino)ethyl acrylate (DAA) was distilled under reduced pressure over calcium hydride. Hexafluorobenzene to be used as a solvent for ^{1}H NMR and light scattering measurements was also distilled over calcium hydride. Azobisisobutyronitrile (AIBN) was recrystallized from methanol. Extrapure perfluoroazelaic acid (PA), perfluorosuccinic acid (Psuc), maleic acid (Ma), succinic acid (Suc), glutaric acid (Glu), and azelaic acid (Az) were used without further purification.

2.3. Synthesis of P(POA-r-AA). POA (4.60 g, 8.88 mmol), TBA (481 mg, 3.75 mmol), and AIBN (21 mg, 0.128 mmol) were placed in an ampule. After the contents were degassed, the ampule was sealed in vacuo. The polymerization was carried out at 50°C for 2 h and was terminated by cooling with liquid nitrogen. The reaction mixture was dissolved in 40 mL of hexafluorobenzene and was poured into 1 L

Table 4: Contact angles (CAs) on the surface coated with the nanospheres.

Acid	Paz[a]	Glu[a]	PSuc[a]	Ma[b]	Suc[b]	Az[b]	None[c]	None[d]
CA (°)	165.3	171.5	170.0	165.5	164.7	171.0	161.5	96.5

[a] Acid/DAA = 0.5. [b] Acid/DAA = 1.0. [c] Treated in $scCO_2$. [d] The cast film prepared from a solution in hexafluorobenzene under atmosphere.

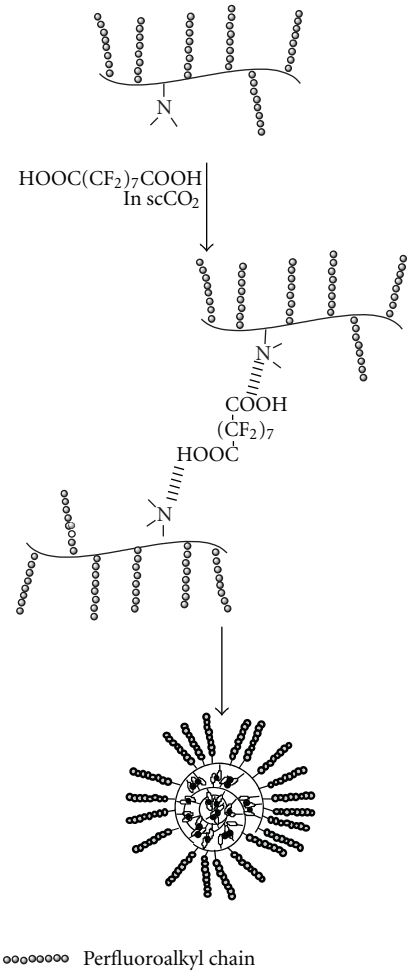

Scheme 6: A schematic of the formation of the nanospheres.

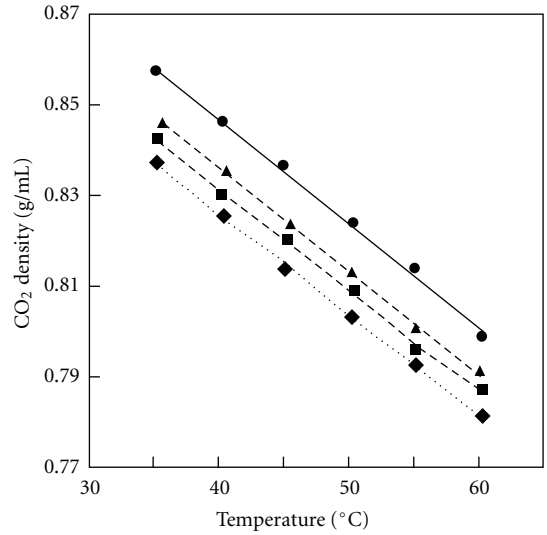

Figure 1: Plots of the experimental cloud points of the copolymers with POA/AA of 6/4 (•), 7/3 (▲), 8/2 (■), and 9/1 (♦) at each temperature versus the CO_2 density.

of methanol to precipitate a polymer. The polymer was collected and was dried in vacuo for several hours to obtain P(POA-*r*-TBA) (4.44 g). The P(POA-*r*-TBA) (2.00 g) was dissolved in HFIP (60 mL). Concentrated hydrochloric acid (2 mL) was added to the copolymer solution at room temperature, and the solution was refluxed for 3 h. After the solution was cooled to room temperature, it was concentrated to one-third of its original volume with an evaporator. The residual solution was poured into hexane (1 L) to precipitate a polymer. The polymer was purified by reprecipitation from hexafluorobenzene (5 mL) into hexane (500 mL). The resulting polymer was dried in vacuo for 5 h to obtain P(POA-*r*-AA) (1.76 g).

2.4. Synthesis of P(POA-r-DAA). POA (1.64 g, 3.16 mmol), DAA (0.198 g, 1.38 mmol), and AIBN (7.4 mg, 0.0451 mmol) were placed in ampule. After the contents were degassed, the ampule was sealed in vacuo. The polymerization was carried out at 60°C for 10 min and was terminated by cooling with liquid nitrogen. The reaction mixture was dissolved in hexafluorobenzene and poured into hexane to precipitate a polymer. The precipitate was dried in vacuo for several hours to obtain P(POA-*r*-DAA) (0.994 g).

2.5. Cloud Point Measurement. The cloud-point measurement was performed with a variable volume view cell (Scheme 2). P(POA-*r*-AA) (30 mg) was placed in the cell, then CO_2 liquefied with a cooler was added to it. The cloud point was defined as the point at which the contents of the cell turned opaque, indicating precipitation of the polymer from solution.

2.6. Preparation of Particles in $ScCO_2$. P(POA-*r*-AA) (POA/AA = 7/3, 30 mg) was placed in the variable volume view cell, then liquid CO_2 was added to it. The solution was stirred at 3620 psi and 45.0°C for 10 min. The pressure of the homogeneous solution was reduced until the cloud point (3059 psi) was reached by volume expansion. The pressure was further reduced to 2759 psi, and the heterogeneous solution was sprayed into a plastic bag made of polyethylene to collect the polymer particles (29 mg).

2.7. SEM Measurement. The polymer particles were put on a carbon adhesive tape and were subjected to SEM measurement after coated with Pt.

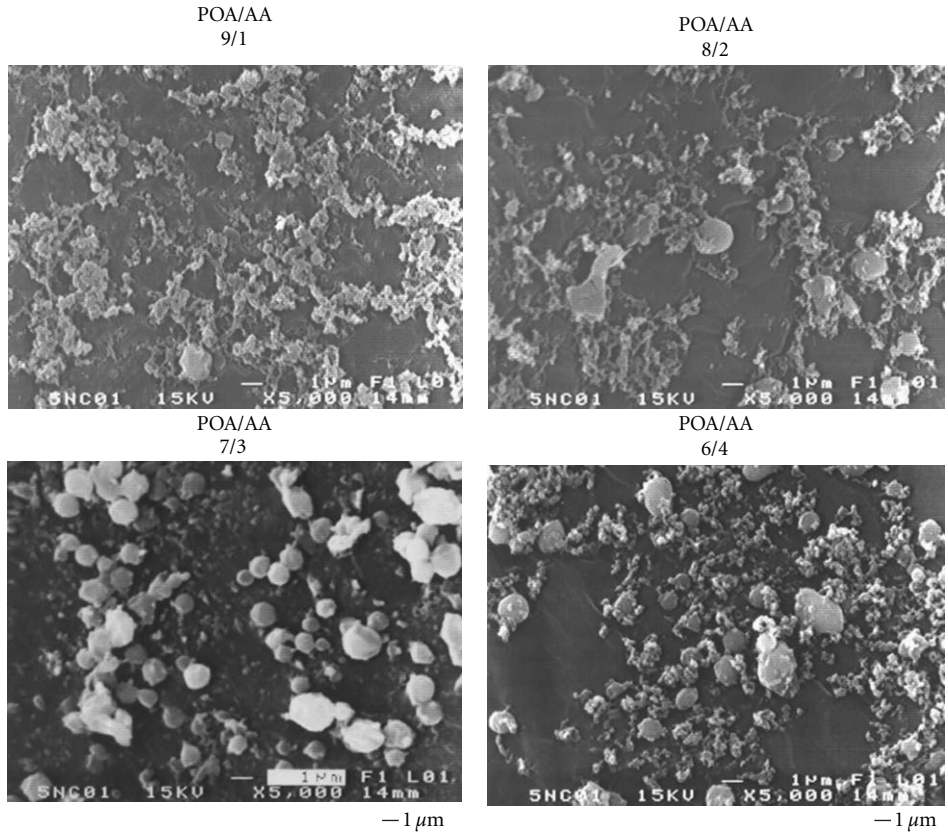

Figure 2: SEM images of the polymer particles obtained from the copolymers in $scCO_2$ at 45°C and the cloud point pressure −300 psi.

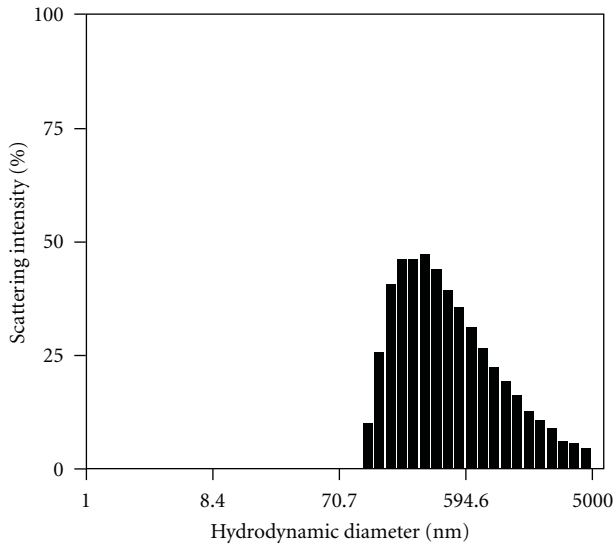

Figure 3: Scattering intensity distribution of the hydrodynamic diameter of P(POA-*r*-AA) with a 7/3 POA/AA ratio in hexafluorobenzene at 25°C and $\theta = 90°$. (copolymer) = 8.00 g/L.

2.8. Contact Angle Measurement. The surfaces completely covered with the nanospheres were prepared on a carbon adhesive tape attached to a slide glass. The contact angles were measured by dropping water (10 μL) on the nanosphere-coated surface at ambient temperature. The surface on the cast film of the copolymer was prepared directly on a slide glass from a copolymer solution in hexafluorobenzene.

2.9. Light Scattering Measurements. P(POA-*r*-AA) (24 mg) was dissolved in 3 mL of hexafluorobenzene and was subjected to light scattering at 25°C at $\theta = 90°$.

3. Direct Self-Assembly through Hydrogen Bond

The P(POA-*r*-AA) random copolymers were obtained by the hydrolysis of P(POA-*r*-TBA) prepared by the radical polymerization (Scheme 3). The hydrolysis of P(POA-*r*-TBA) was carried out in HFIP using concentrated hydrochloric acid under reflux for 3 h. The characterizations of the P(POA-*r*-TBA) and P(POA-*r*-AA) copolymers are listed in Tables 1 and 2. The molecular weight distributions of P(POA-*r*-AA) could not be estimated due to the very broad distribution.

The P(POA-*r*-AA) copolymers completely dissolved in $scCO_2$. Figure 1 shows the CO_2 density at the cloud points plotted versus temperature. The CO_2 density at the cloud points decreased as the temperature increased, indicating that the solubility of the copolymers increased with

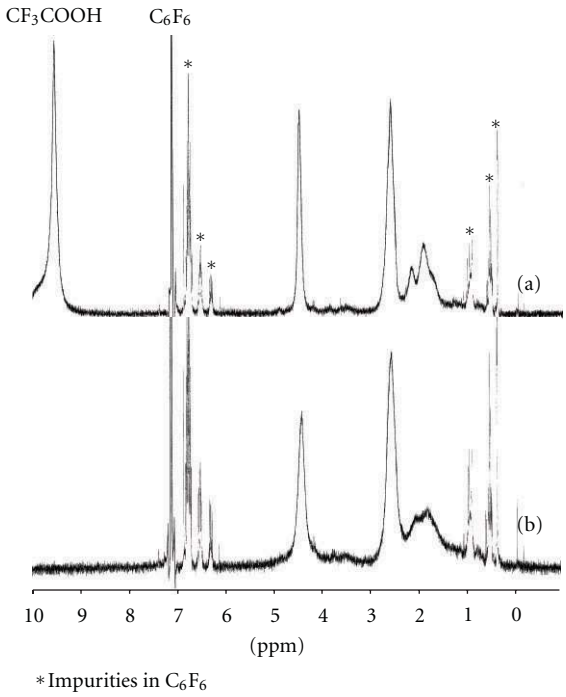

Figure 4: ^{1}H NMR spectra of P(POA-*r*-AA) with a 7/3 POA/AA ratio in the presence (a) and absence (b) of CF_3COOH. Solvent: C_6F_6 including C_6D_6.

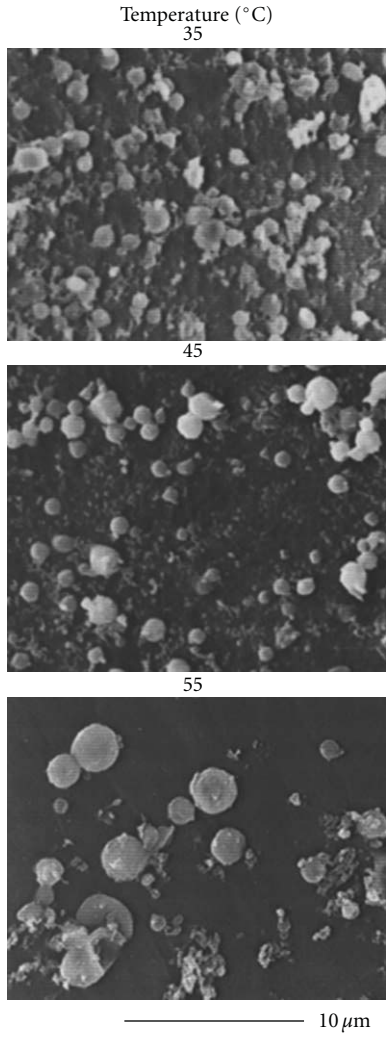

Figure 5: SEM images of the polymer particles obtained at 35, 45, and 55°C at the cloud point pressure −300 psi.

the increasing temperature. And further, the copolymer with a higher AA ratio had a lower solubility, suggesting that the hydrogen bonding based on the AA units prevented the copolymer from dissolving in $scCO_2$.

SEM observations revealed that the P(POA-*r*-AA) copolymers self-assembled into spherical particles in $scCO_2$. Figure 2 shows the SEM images of the particles obtained from the copolymer solution at 45°C in a heterogeneous state at a pressure lower than the cloud point pressure. The images included spherical particles independent of the POA/AA ratio. However, the proportion of the spherical particles was different among the various ratios. The copolymers with the 9/1 and 8/2 ratios contained some spherical particles of several micrometers in diameter and a lot of small particles with nonspecific forms. These copolymers had too low AA content to aggregate into spherical forms. The copolymer with the 6/4 ratio also contained both the spherical particles and the small particles. However, the small particles also had a spherical shape with several hundreds of nanometer diameters. It is likely that the intramolecular aggregation is preferable for the 6/4 sample due to large contribution of the hydrogen bonding based on the higher AA content. The copolymer with the 7/3 ratio produced the largest amount of spherical particles among the copolymers. Based on the SEM image of the 7/3 sample, the size of the spherical particles was estimated to be 820 nm on average, and the size distribution was 1.20 [27]. These SEM images are for the polymer particles obtained by spraying the heterogeneous solutions into the atmosphere, based on the assumption that the shapes of the particles formed in $scCO_2$ are maintained in this atmosphere at ambient temperature by rapidly releasing the CO_2 pressure.

In order to confirm the formation of the particles in solution, the light scattering measurements of the copolymer were performed in hexafluorobenzene. Hexafluorobenzene is similar to $scCO_2$ in having low polarity and the ability to dissolve fluoropolymers. Figure 3 shows the scattering intensity distribution of the hydrodynamic diameter of the particles formed by the copolymer with the 7/3 ratio in hexafluorobenzene. The intensity distribution was obtained by a Marquadt analysis of the dynamic light scattering results. The hydrodynamic diameter of the particles was estimated to be 600 nm based on the Marquadt analysis. Compared with the particle size based on the SEM image, the copolymer formed smaller particles in hexafluorobenzene. This can be accounted for by the fact that the AA units more tightly formed the particle cores in hexafluorobenzene than in $scCO_2$ because of the lower affinity of hexafluorobenzene to the AA units and also that the particles swelled when rapidly sprayed into the atmosphere.

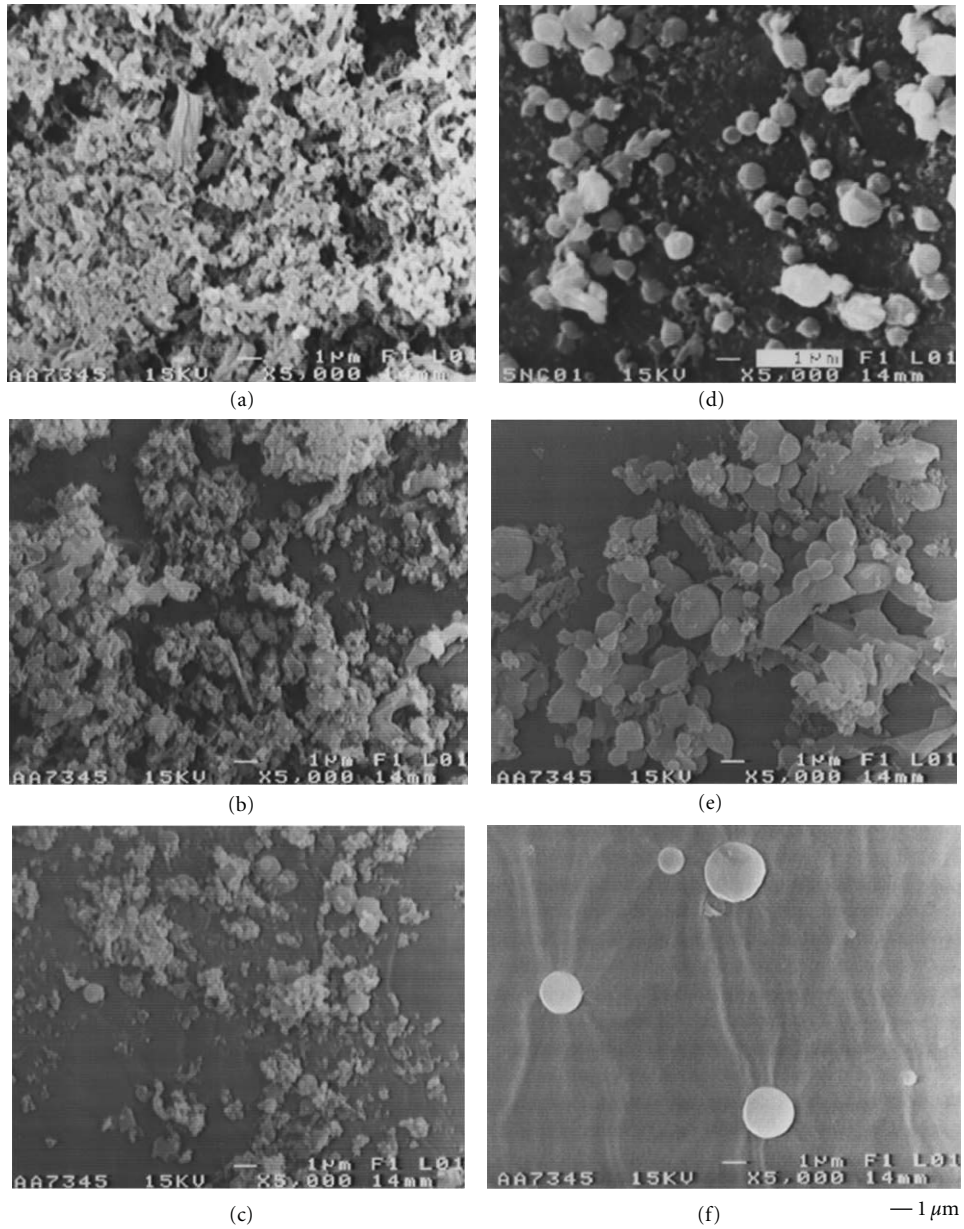

Figure 6: SEM images of the polymer particles obtained at the cloud point pressure +200 (a), ±0 (b), –100 (c), −300 (d), −900 (e), and −1500 psi (f).

The ^{1}H NMR analysis confirmed that the particles consisted of the POA unit shells and the AA unit cores. The ^{1}H NMR spectra of the copolymer in the presence and absence of trifluoroacetic acid are shown in Figures 4(a) and 4(b). The copolymer showed no aggregation in the presence of trifluoroacetic acid. The signals based on the methyne and methylene of the main chain were broadened in the absence of trifluoroacetic acid, as compared to those in its presence. This broadening of the signals indicates that the insoluble AA units and main chains were shielded from the magnetic field. Consequently, it is expected that the copolymers formed random copolymer micelles consisting of the shells of the CO_2-philic perfluorooctyl groups and the cores of the CO_2-phobic AA units and main chains when the copolymers were placed in $scCO_2$ as well as in hexafluorobenzene (Scheme 4).

The shapes of the polymer particles were dependent on temperature based on the formation by hydrogen bonding. Figure 5 shows the SEM images of the polymer particles obtained at three different temperatures in the heterogeneous state. The particles were not completely spherical at 35°C. The copolymer could not completely take a spherical shape because of the low mobility of the copolymer at this low temperature. On the other hand, the copolymer produced large

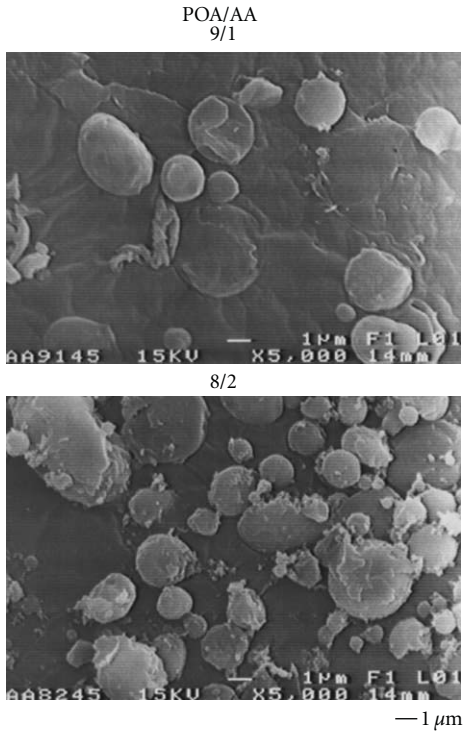

Figure 7: SEM images of the polymer particles obtained from the copolymers with 9/1 and 8/2 POA/AA ratios at 45°C and the cloud point pressure −1500 psi.

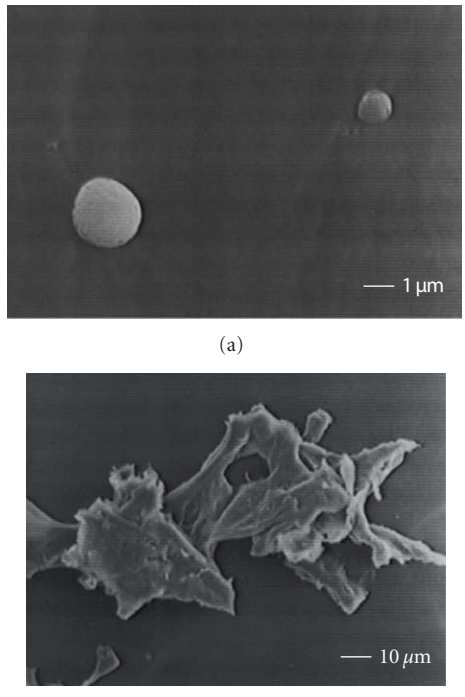

Figure 8: SEM images of the polymer particles obtained from the copolymer with a 6/4 POA/AA ratio at 45°C and the cloud point pressure −1500 psi.

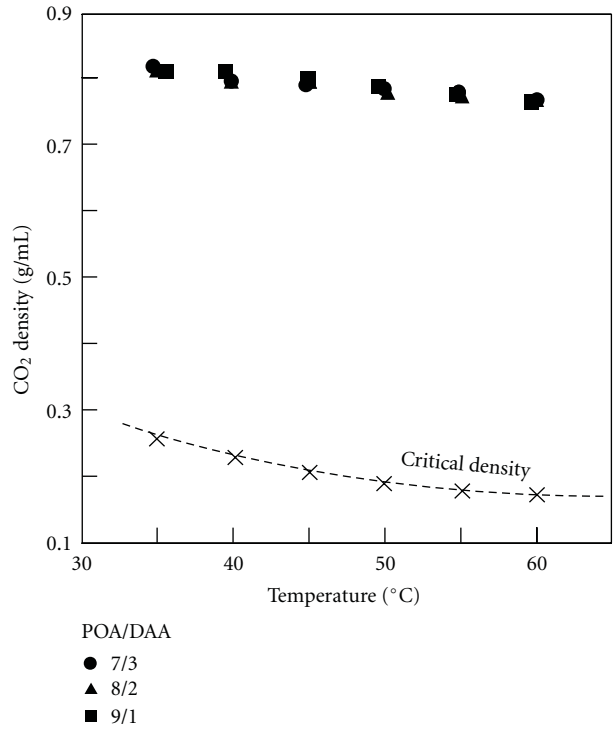

Figure 9: Plots of the experimental cloud points of the copolymers at each temperature versus the CO_2 density.

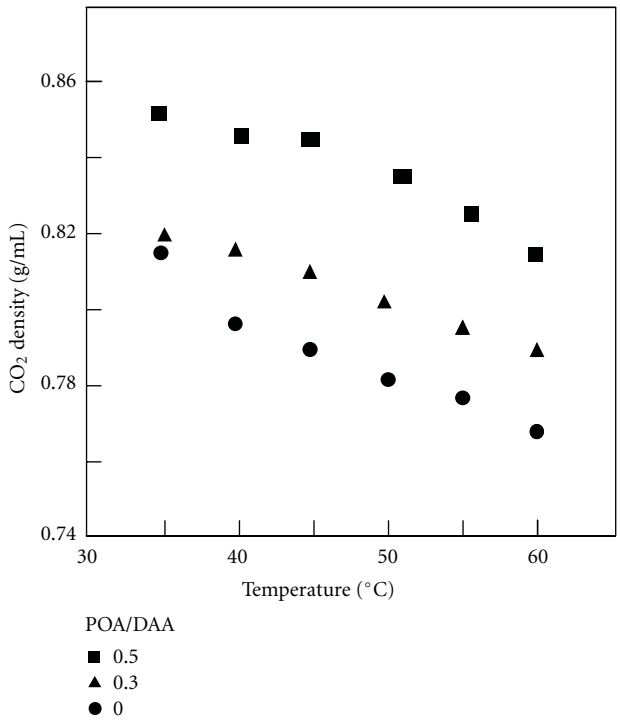

Figure 10: Plots of the cloud points of the copolymer with 7/3 of POA/DAA in the presence of PA at 0.3 and 0.5 of PA/DAA.

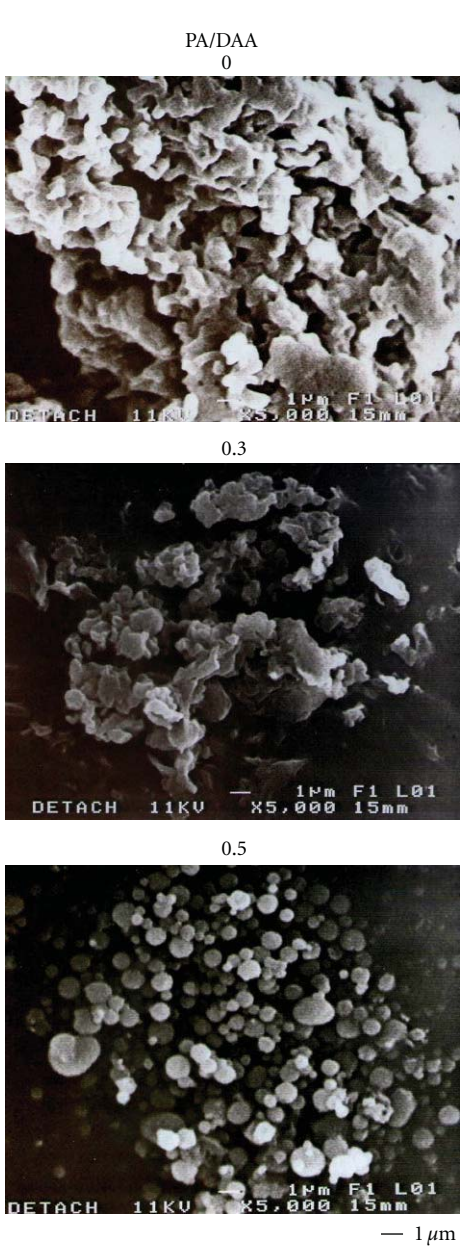

Figure 11: SEM images of the copolymer in the absence and presence of PA. POA/DAA = 7/3, heterogeneous state.

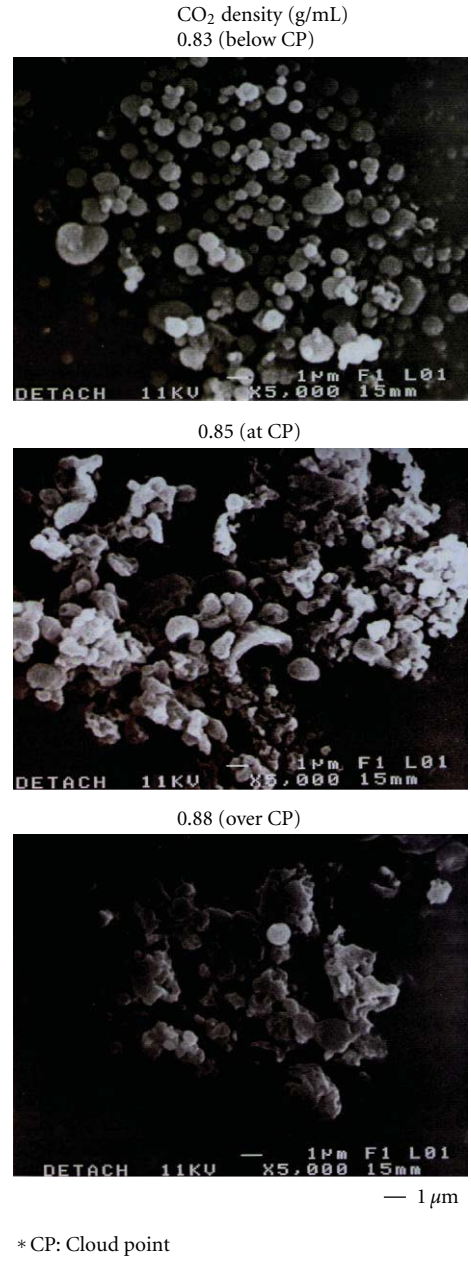

∗CP: Cloud point

Figure 12: SEM images of polymer particles obtained from the heterogeneous state below the cloud point, the state at the exact cloud point, and the homogeneous state over it. POA/DAA = 7/3, PA/DAA = 0.5.

spherical particles of several micrometers at 55°C, along with small particles with hundreds of nanometer diameters. It was considered that an increase in the mobility of the copolymer at the high temperature promoted both the intermolecular aggregation and the intramolecular association.

The self-assembly of the copolymers into spherical particles was controlled by the CO_2 pressure. Figure 6 shows the SEM images of the polymer particles produced under the different pressures. The particles produced at a pressure higher than the cloud point pressure had nonspecific forms. Spherical particles were hardly observed in the image. The particles prepared at the cloud point pressure included a small amount of spherical parts, however, most of the particles were still nonspecific. When the pressure was reduced to 100 psi lower than the cloud point pressure, the copolymer somewhat aggregated into spherical particles. At a pressure 300 psi lower than the cloud point, most of the particles had spherical shapes. However, it was observed that the spherical particles partly combined at the cloud point pressure minus 900 psi. Completely spherical and larger-sized particles were

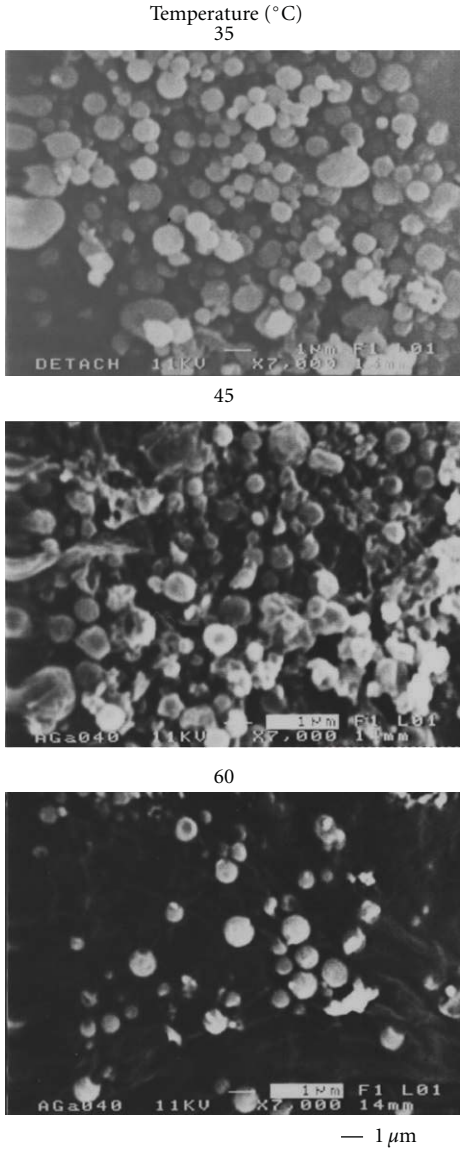

Figure 13: SEM images of the polymer particles obtained at 35, 45, and 60°C. PA/DAA = 0.5.

produced at the cloud point minus 1500 psi. It was found that more stable spherical particles were produced at the lower pressure and that the self-assembly of the copolymer was controlled through varying the solvent quality manipulated by the CO_2 pressure.

The copolymers with the 9/1 and 8/2 ratios were found to produce nearly spherical particles at the pressure 1500 psi lower than the cloud point pressure, although a few spherical particles were obtained at the cloud point pressure minus 300 psi (Figure 7). The hydrogen bonding interaction among the AA units increased with the decreasing pressure, thus the self-assembly of the copolymers into spherical particles was promoted. At the pressure 1500 psi lower than the cloud point, the copolymer with the 6/4 ratio formed not only spherical particles (Figure 8(a)), but also a small amount of nonspecific aggregates of dozens or hundreds micrometers

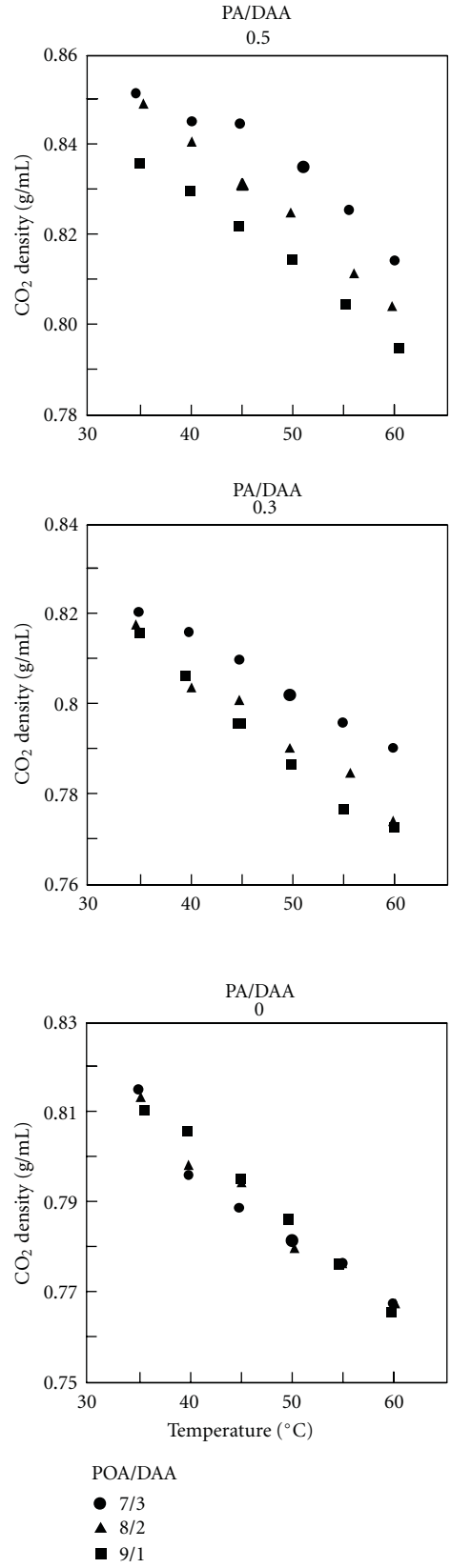

Figure 14: Plots of the cloud points of the copolymers with POA/DAA of 7/3, 8/2, and 9/1 in the absence and presence of PA at 0.3 and 0.5 of PA/DAA.

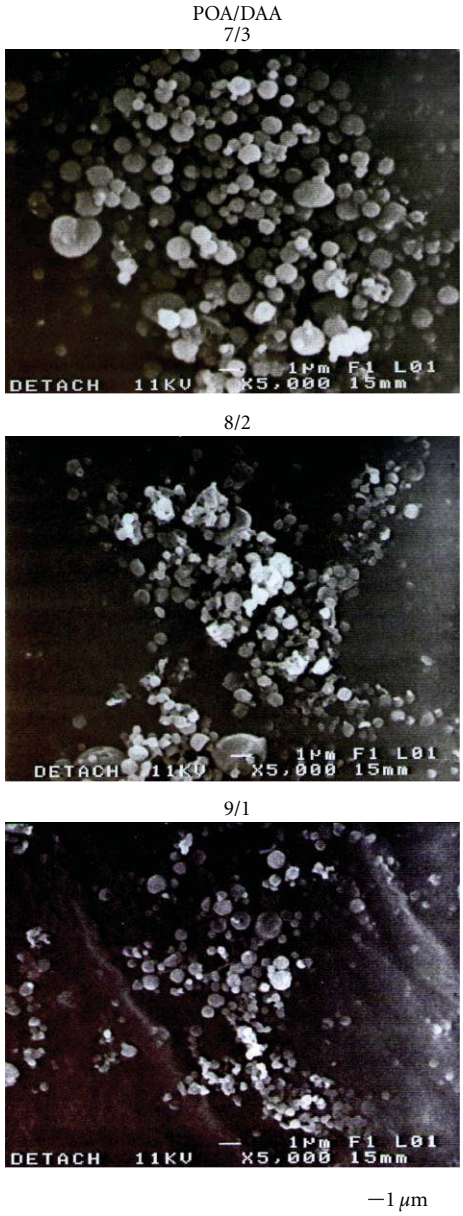

Figure 15: SEM images of the nanospheres obtained from the copolymers with POA/DAA of 7/3, 8/2, and 9/1. PA/DAA = 0.5, heterogeneous state.

(Figure 8(b)). Too strong hydrogen bonding at a very low pressure should have caused a partial second aggregation of the spherical particles into large nonspecific particles. It was deduced that the formation of spherical particles could be optimized by the manipulation of the CO_2 pressure for the different compositions of the copolymers.

4. Indirect Self-Assembly through Hydrogen Bond

It is possible to induce self-assembly for a copolymer that shows no self-assembly by itself through hydrogen bond

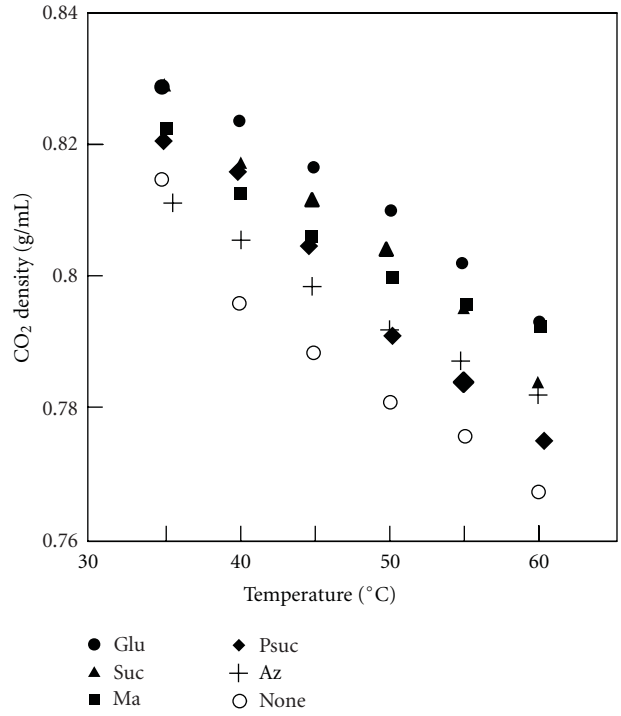

Figure 16: Plots of the experimental cloud points of the P(POA-*r*-DAA) copolymer in the presence of the dicarboxylic acids at each temperature. The acid/DAA = 0.5.

interaction with additives. P(POA-*r*-DAA) random copolymers dissolve in $scCO_2$, however, these copolymers show no self-assembly in it. The characterizations of the P(POA-*r*-DAA) copolymers prepared by radical copolymerization are listed in Table 3 (Scheme 5). Figure 9 shows the plots of the cloud points versus the CO_2 density. There was a slight difference in the cloud point among the POA/DAA ratios of the copolymers. It was found that the solubility of the copolymers in $scCO_2$ decreased in the presence of perfluoroazelaic acid (PA). Figure 10 shows the cloud points of the copolymer with 7/3 of POA/DAA in the absence and presence of PA at 0.3 and 0.5 as a molar ratio of PA to the DAA unit. As a result of increasing the amount of PA, the cloud points were shifted to a higher side of the CO_2 density. The copolymer became less soluble in the presence of PA. The decrease in the solubility should be caused by hydrogen bond cross-linking between the amino groups in the copolymer via the carboxylic groups of PA.

SEM observation demonstrated that the copolymer formed different shapes in the absence and presence of PA in $scCO_2$. Figure 11 shows the SEM images of the copolymer with and without PA. The images were obtained for the polymer particles produced in the heterogeneous state below the cloud points. The copolymer took unspecific forms in the absence of PA. There was a slight difference in the shape at 0.3 as the PA/DAA ratio. On the other hand, the copolymer had spherical forms at the 0.5 ratio. The size of the particles was ca. 700 nm. At 0.5 of PA/DAA, all the amino groups interact with the carboxylic group of PA, so that no free amino

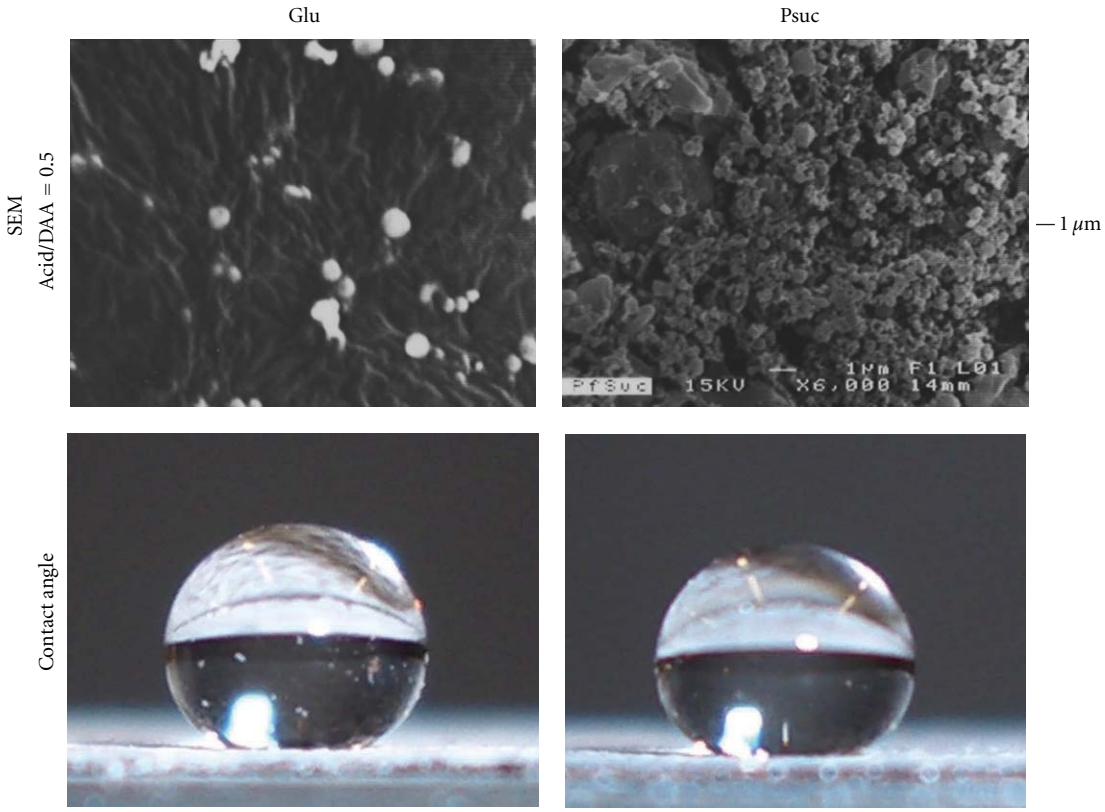

Figure 17: SEM images of the particles produced by the copolymer in the presence of Glu and Psuc, and photographs of water droplets placed on the surface coated with the particles.

groups are expected to exist in the copolymer. Therefore, the nanospheres should be formed by cross-linking between the amino groups in the copolymer through the electrostatic interaction with PA (Scheme 6).

We explored the stability of the nanospheres versus pressure. Figure 12 shows the SEM images of polymer particles obtained from three different states: the heterogeneous state below the cloud point, the state at the exact cloud point, and the homogeneous state over it. The pressure at the heterogeneous state was 300 psi lower than the cloud point pressure, while that at the homogeneous state was 500 psi higher. The particles included PA at the 0.5 ratio. The spherical particles formed in the heterogeneous state partly changed to unspecific forms as a result of increasing the pressure to the cloud point pressure. The nanospheres completely changed to unspecific forms over the cloud point. These changes were based on the cross-linking by the weak electrostatic interaction and on an increase in the solubility of the nanospheres into $scCO_2$ as a result of increasing the density of CO_2. Consequently, the shape of the polymer particles was dependent not only on the acid concentration but also on the pressure of CO_2.

The spherical shapes of the polymer particles were independent of the temperature. Figures 13 shows the SEM images of the polymer particles obtained at 35, 45, and 60°C at 0.5 of PA/DAA. The particles were prepared in the heterogeneous states at which the pressures were 300 psi lower than the cloud point pressure at each temperature. The polymer particles maintained their spherical shapes at 45 and 60°C. In addition, the copolymer with PA took more completely spherical shape with an increase in the temperature. It may be accounted for by the fact that the perfluoroalkyl chains extend much more at higher temperature, resulting in that the copolymer more easily form spherical particles at the higher temperature.

The POA/DAA ratio in the copolymer affected the cloud point and size of the nanospheres. Figure 14 shows the cloud points of three different copolymers with POA/DAA of 7/3, 8/2, and 9/1 in the presence of PA at 0.3 and 0.5 of PA/DAA. Whereas there was a negligible difference in the cloud point among the copolymers in the absence of PA, the copolymers made a marked difference in the presence of it. This difference was much greater as the amount of PA increased. The copolymer having a lower DAA content showed lower cloud point in the presence of PA. The SEM observation revealed that the copolymer with a lower DAA content formed smaller nanospheres. Figure 15 shows the SEM images of the nanospheres obtained from the copolymers with PA at the 0.5 ratio. The size of the nanospheres decreased as the DAA content decreased. The copolymer with the 8/2 ratio formed the nanospheres with ca. 600 nm as the particle size, while the 9/1 copolymer produced those with 400 nm. The decrease in the size of the nanospheres with the decrease in the DAA content may be account for by the fact that the copolymer with lower DAA content forms a lower degree of cross-linking

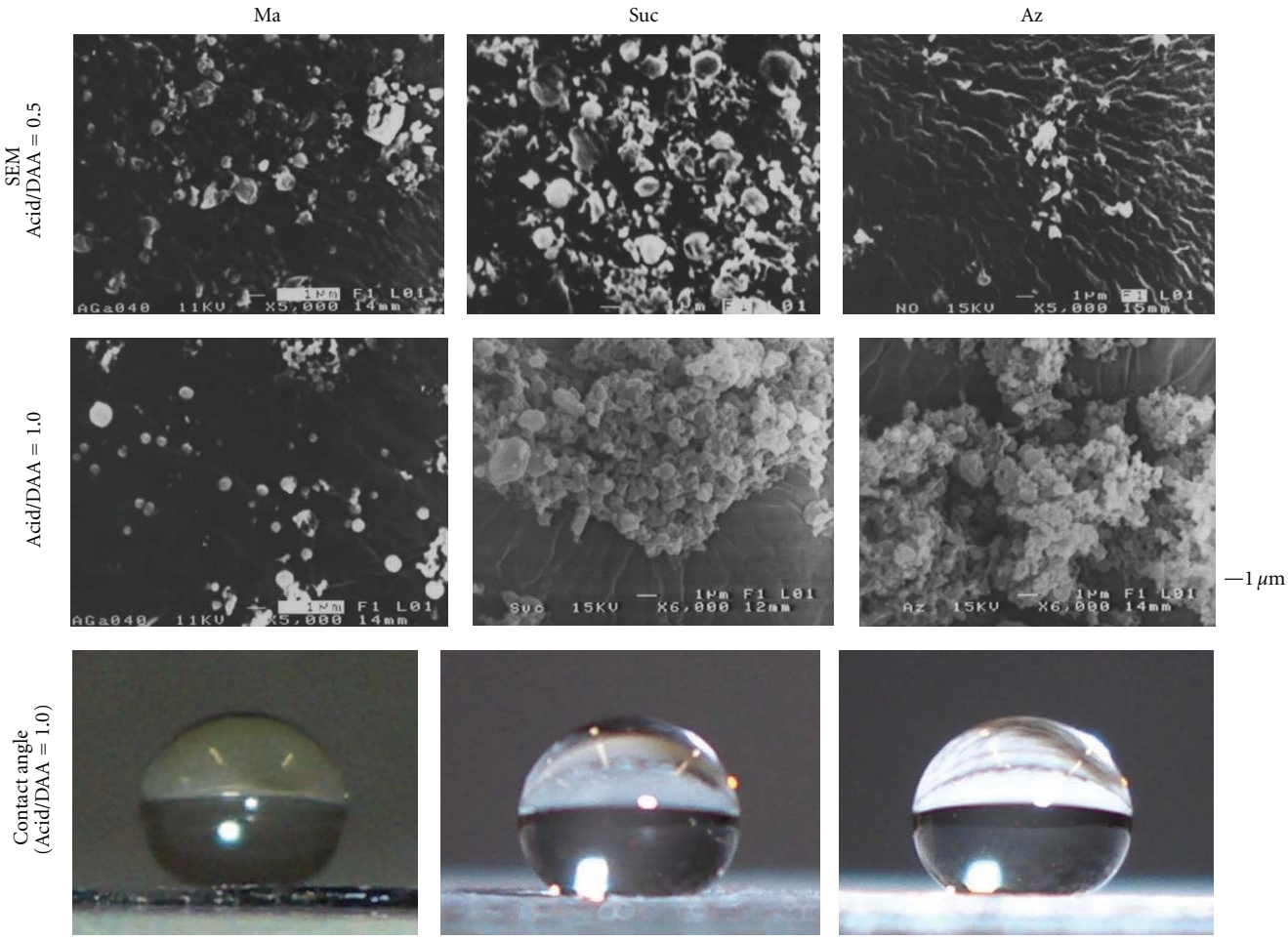

Figure 18: SEM images of the particles produced by the copolymer in the presence of Ma, Suc, and Az, and photographs of water droplets placed on the surface coated with the particles.

with the dicarboxylic acid, providing smaller aggregation numbers of the nanospheres. The nanospheres obtained from the copolymers with 8/2 and 9/1 of POA/DAA showed the same results about the amount of PA and the pressure of CO_2 as those from the copolymers with 7/3. It was deduced that the size of nanospheres was manipulated by the POA/DAA ratio in the copolymer.

The self-assembly of P(POA-*r*-DAA) by other carboxylic acids was also investigated. Figure 16 shows the plots of the experimental cloud points of the copolymer at each temperature for Psuc, Suc, Glu, Az, and Ma. The CO_2 density at the cloud points were shifted to a lower density in the order of Glu > Suc > Ma > Psuc, Az, indicating that the solubility of the particles formed by the copolymer and the acids increased in this order.

SEM observations revealed that the solubility of the particles to $scCO_2$ was dependent on the size and forms of the particles. Figures 17 and 18 show the SEM images of the particles produced by the copolymer in the presence of the respective acids. Glu and Psuc provided spherical particles at 0.5 of the acid/DAA (Figure 17). Psuc produced smaller nanospheres than Glu. On the other hand, Ma, Suc, and Az provided random forms of the copolymer rather than spherical particles at this ratio (Figure 18). Ma produced nanospheres at 1.0. Suc and Az also produced spherical particles at 1.0, however, there were very smaller particles with a several hundred nanometer size along with the nanospheres. These three acids had a lower ability to make the copolymer aggregate into nanospheres because of the weak acidity and too short or too long chain length. Consequently, there was a tendency that the solubility of the particles decreased as the form of the copolymer became spherical from the random forms. The formation of the smaller particles seems to increase the solubility of the copolymer.

The nanospheres have the shells composed of the perfluoroalkyl chains from the POA units and cores of the DAA units cross-linked through the hydrogen bonding via the acids. Therefore, the surface on the nanospheres is expected to have a high water repellence based on the perfluorinated shell. It was found that the surface coated with the nanospheres had water contact angles greater than 164° (Table 4). The largest contact angle was obtained for Glu at 171.5°. The nonspecific forms of the particles had a contact angle at 161.5° (Figure 19). The roughness of the surface

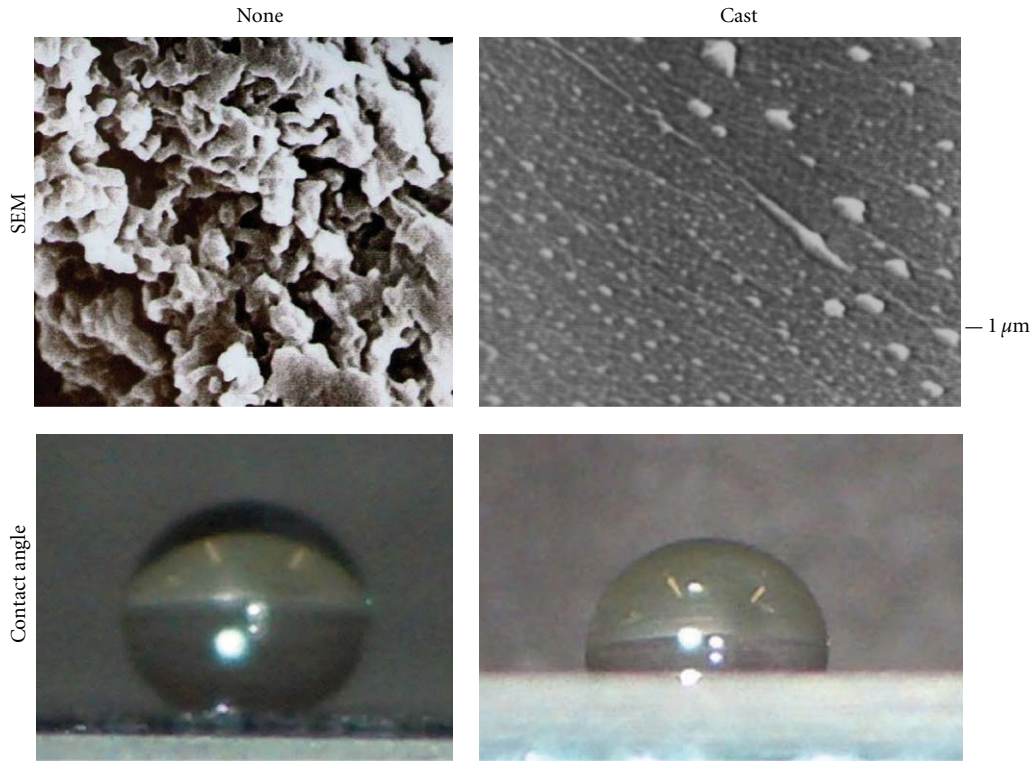

Figure 19: SEM images of the random forms produced by the copolymer and of the surface on the cast films. Also shown are photographs of water droplets placed on the surface of the random forms produced by the copolymer and of the surface on the cast films.

due to the nonspecific forms made some contribution to enhancing the hydrophobicity of the surface. On the other hand, the smooth surface of the cast films showed the small contact angle.

5. Conclusions

The synthesis of spherical particles was attained by the direct self-assembly of P(POA-*r*-AA) and by the indirect self-assembly of P(POA-*r*-DAA) with the dicarboxylic acids in $scCO_2$. The copolymers formed spherical particles with hundreds of nanometer-diameters in a heterogeneous state at pressures lower than the cloud point pressure. The formation of spherical particles was also dependent on the temperature. The formation of spherical particles could be optimized through varying the solvent quality by the manipulation of the CO_2 pressure and temperature for the different copolymer compositions. The dynamic light scattering and ^1H NMR studies demonstrated that the nanospheres had the micellar structures consisting of the CO_2-philic POA shells and the CO_2-phobic AA or DAA cores including the main chain cores. The nanospheres had the superhydrophobicity based on the water-proof shells of the POA units. This study demonstrated that the nanospheres prepared by the self-assembly in $scCO_2$ produced the superhydrophobic surfaces.

References

[1] Y. K. Ha, H. S. Song, H. J. Lee, and J. H. Kim, "Preparation of core particles for toner application by membrane emulsification," *Colloids and Surfaces A*, vol. 162, no. 1–3, pp. 289–293, 2000.

[2] L. A. Simpson, J. Robb, J. Banford, P. F. Dietz, and J. Temperley, "Composite pigmentary material," Eur Pat Appl EP 573150 A2 8 Dec: 14, 1993.

[3] D. S. Schlossman, "Method of coupling cosmetic materials and cosmetics containing coupled materials," US 5314683 A1 24 May: 12, 1994.

[4] B. Bohnel and D. L. Schlosser, "Aqueous, repositionable, high peel strength pressure sensitive adhesives," Eur Pat Appl EP 439941 A1 7 Aug: 11, 1991.

[5] S. Di and V. Frank, "Aqueous high performance contact adhesive containing microspheres," Eur Pat Appl EP 534393 A1 31 Mar: 9, 1993.

[6] K. A. Yoon and D. J. Burgess, "Effect of cationic surfactant on transport of model drugs in emulsion systems," *Journal of Pharmacy and Pharmacology*, vol. 49, no. 5, pp. 478–484, 1997.

[7] M. J. Lawrence, S. M. Lawrence, and D. J. Barlow, "Aggregation and surface properties of synthetic double-chain non-ionic surfactants in aqueous solution," *Journal of Pharmacy and Pharmacology*, vol. 49, no. 6, pp. 594–600, 1997.

[8] M. Zerfa and B. W. Brooks, "Experimental investigation of vinyl chloride drop behavior during suspension polymerization," *Journal of Applied Polymer Science*, vol. 65, no. 1, pp. 127–134, 1997.

[9] G. Wang, M. Li, and X. Chen, "Inverse suspension polymerization of sodium acrylate," *Journal of Applied Polymer Science*, vol. 65, no. 4, pp. 789–794, 1997.

[10] Y. Chen and H. W. Yang, "Hydroxypropyl cellulose (HPC)-stabilized dispersion polymerization of styrene in polar solvents: effect of reaction parameters," *Journal of Polymer Science A*, vol. 30, no. 13, pp. 2765–2772, 1992.

[11] D. Horak, F. Svec, and J. M. J. Frechet, "Preparation of colored poly(styrene-co-butyl methacrylate) micrometer size beads with narrow size distribution by dispersion polymerization in presence of dyes," *Journal of Polymer Science A*, vol. 33, pp. 2961–2968, 1995.

[12] H. Bamnolker and S. Marcel, "Dispersion polymerization of styrene in polar solvents: effect of reaction parameters on microsphere surface composition and surface properties, size and size distribution, and molecular weight," *Journal of Polymer Science A*, vol. 34, no. 10, pp. 1857–1871, 1996.

[13] M. B. Taylor, R. D. Gilbert, and V. T. Stannett, "Radiation-initiated inverse emulsion polymerization of vinylpyrrolidone," *Journal of Applied Polymer Science*, vol. 53, no. 10, pp. 1385–1390, 1994.

[14] F. Sun and E. Ruckenstein, "Preparation of high molecular weight monodisperse polystyrene latexes by concentrated emulsion polymerization," *Journal of Applied Polymer Science*, vol. 48, no. 7, pp. 1279–1288, 1993.

[15] C. S. Chern and Y. C. Chen, "Semibatch emulsion polymerization of butyl acrylate stabilized by a polymerizable surfactant," *Polymer Journal*, vol. 28, no. 7, pp. 627–632, 1996.

[16] J. B. McClain, D. E. Betts, D. A. Canelas et al., "Design of nonionic surfactants for supercritical carbon dioxide," *Science*, vol. 274, no. 5295, pp. 2049–2052, 1996.

[17] E. Buhler, A. V. Dobrynin, J. M. DeSimone, and M. Rubinstein, "Light-scattering study of diblock copolymers in supercritical carbon dioxide: CO_2 density-induced micellization transition," *Macromolecules*, vol. 31, no. 21, pp. 7347–7355, 1998.

[18] S. Zhou and B. Chu, "Self-assembly behavior of a diblock copolymer of poly(1-dihydroperfluorooctyl acrylate) and poly(vinyl acetate) in supercritical carbon dioxide," *Macromolecules*, vol. 31, no. 22, pp. 7746–7755, 1998.

[19] C. Baysal, B. Erman, and B. Chu, "Conformational features of poly(1-dihydroperfluorooctyl acrylate) and poly(vinyl acetate) diblock oligomers in supercritical carbon dioxide," *Journal of Chemical Physics*, vol. 114, no. 12, pp. 5444–5449, 2001.

[20] F. Triolo, A. Triolo, R. Triolo et al., "Critical micelle density for the self-assembly of block copolymer surfactants in supercritical carbon dioxide," *Langmuir*, vol. 16, no. 2, pp. 416–421, 2000.

[21] M. Nakano, M. Deguchi, K. Matsumoto, H. Matsuoka, and H. Yamaöka, "Self-assembly of poly(l,l-diethylsilabutane)-*block*-poly(2-hydroxyethyl methacrylate) block copolymer. 1. Micelle formation and micelle-unimer-reversed micelle transition by solvent composition," *Macromolecules*, vol. 32, no. 22, pp. 7437–7443, 1999.

[22] E. D. Niemeyer and F. V. Bright, "The pH within PFPE reverse micelles formed in supercritical CO_2," *Journal of Physical Chemistry B*, vol. 102, no. 8, pp. 1474–1478, 1998.

[23] D. C. Steytler and J. D. Holmes, "Aggregation and solubilisation in near critical CO_2 studied by scattering methods," *Current Opinion in Colloid and Interface Science*, vol. 3, no. 3, pp. 299–304, 1998.

[24] E. Yoshida and A. Mineyama, "Synthesis of spherical particles by self-assembly of poly[2-(perfluorooctyl)ethyl acrylate-co-acrylic acid] in supercritical carbon dioxide," *Colloid and Polymer Science*, vol. 286, no. 8-9, pp. 975–981, 2008.

[25] E. Yoshida and A. Nagakubo, "Convenient synthesis of microspheres by self-assembly of random copolymers in supercritical carbon dioxide," *Colloid and Polymer Science*, vol. 285, no. 4, pp. 441–447, 2007.

[26] E. Yoshida and A. Nagakubo, "Superhydrophobic surfaces of microspheres obtained by self-assembly of poly[2-(perfluorooctyl)ethyl acrylate-*ran*-2-(dimethylamino)ethyl acrylate] in supercritical carbon dioxide," *Colloid and Polymer Science*, vol. 285, no. 11, pp. 1293–1297, 2007.

[27] S. Kobayahshi, H. Uyama, I. Yamamoto, and Y. Matsumoto, "Preparation of monodispered poly(methyl methacrylate) particle in the size of mícron range," *Polymer Journal*, vol. 22, no. 8, pp. 759–761, 1990.

Hindawi Publishing Corporation
International Journal of Polymer Science
Volume 2012, Article ID 170912, 18 pages
doi:10.1155/2012/170912

Review Article

Novel Complex Polymers with Carbazole Functionality by Controlled Radical Polymerization

Kazuhiro Nakabayashi and Hideharu Mori

Department of Polymer Science and Engineering, Department of Organic Device Engineering, Graduate School of Science and Engineering, Yamagata University, 4-3-16, Jonan, Yonezawa 992-8510, Japan

Correspondence should be addressed to Hideharu Mori, h.mori@yz.yamagata-u.ac.jp

Received 27 September 2011; Accepted 8 December 2011

Academic Editor: Toshifumi Satoh

This review summarizes recent advances in the design and synthesis of novel complex polymers with carbazole moieties using controlled radical polymerization techniques. We focus on the polymeric architectures of block copolymers, star polymers, including star block copolymers and miktoarm star copolymers, comb-shaped copolymers, and hybrids. Controlled radical polymerization of *N*-vinylcarbazole (NVC) and styrene and (meth)acrylate derivatives having carbazole moieties is well advanced, leading to the well-controlled synthesis of complex macromolecules. Characteristic optoelectronic properties, assembled structures, and three-dimensional architectures are briefly introduced.

1. Introduction

Polymers with carbazole groups are of considerable scientific and industrial interest because of their attractive features, such as their hole-transporting, high charge-carrier, and electroluminescent properties [1]. The hole-transporting ability of carbazole-containing polymers makes them especially useful for applications in organic electronics. Numerous studies have been devoted to carbazole-containing polymers as a result of the success of poly(*N*-vinylcarbazole), poly(NVC), in electrophotographic applications [1]. Recent developments in this field are mostly connected to applications in polymeric light-emitting diodes, organic photorefractive materials, and photovoltaic devices. For example, conjugated poly(3,6-carbazole) and poly(2,7-carbazole) derivatives having carbazole moieties in the main chain have been employed for applications in solar cells and white-light-emitting diodes [2–4]. Carbazole-containing polymers can be divided into two general groups: polymers containing carbazole moieties in the main chain, or those containing carbazole moieties in the side chains. Poly(NVC) belongs to the group of polymers having carbazolyl groups in the side chains. A variety of polymers with pendant carbazolyl groups has been reported, including polyacrylate [5, 6], polymethacrylate [7–10], and polystyrene [11, 12] derivatives. Many factors play crucial roles in the manipulation of their properties and practical applications, such as their chemical structures, polymer architectures, conformation, location, and stacking of carbazole units. However, it was difficult to control their molecular weights and architectures, because most of these polymers with pendant carbazolyl groups have been traditionally synthesized by conventional radical polymerization. To manipulate their unique electronic and photonic functions, it is desirable to establish precise synthetic methods of controlling molecular weight, polydispersity, topology, composition, and functions. This can be achieved by using controlled polymerization systems.

In the past few decades, considerable attention has been given to the self-assembly of block copolymers, because of the feasibility of using them to generate nanostructured materials and their numerous potential applications in separation technology, controlled drug delivery and release, and smart catalyst separation technology [13–17]. Traditional amphiphilic block copolymers containing chemically connected hydrophilic and hydrophobic segments provide a great variety of morphologies in selective solvents, for example, water, in which micellar aggregates occur as a result of the association of the insoluble blocks. Block copolymers

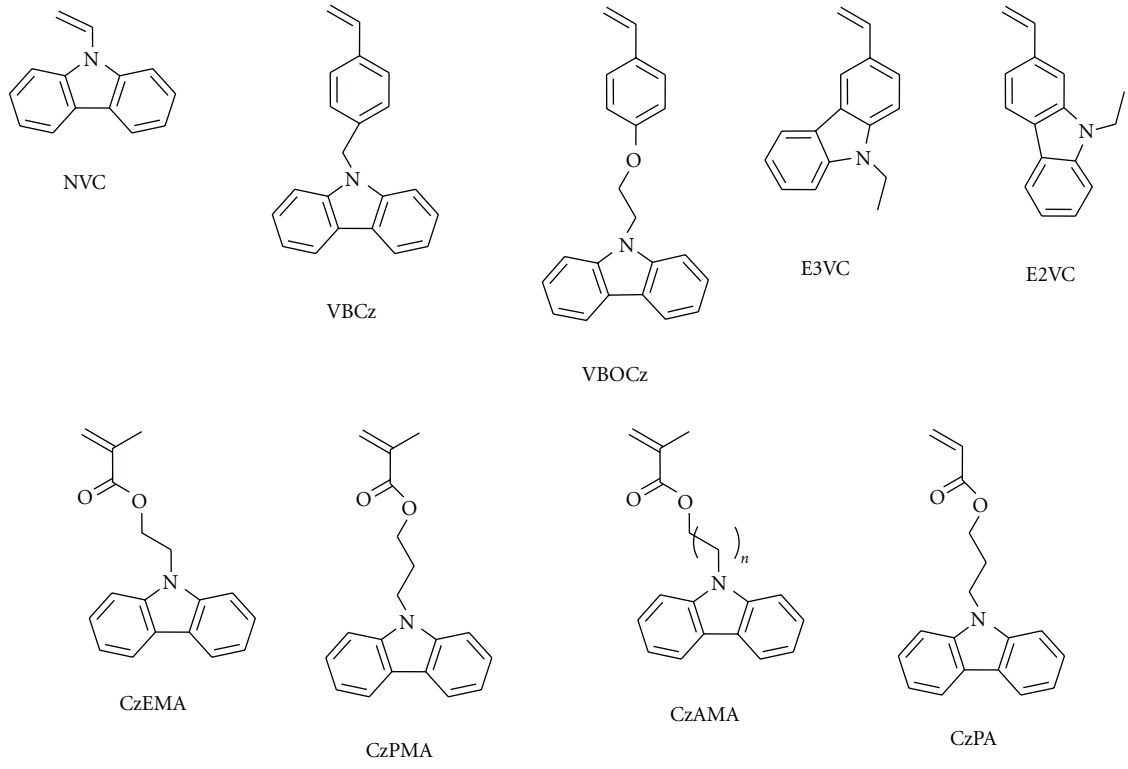

Scheme 1: Representative examples of carbazole-containing vinyl monomers used for controlled radical polymerizations.

incorporating semiconducting segments and characteristic optoelectronic functions have attracted significant research interest [18–23]. Block copolymers are emerging as a promising class of materials for optoelectronic applications, such as organic light-emitting devices, photovoltaics, and organic field-effect transistors, because of their ability to form a variety of ordered structures via self-assembly processes. Depending on the chemical nature of the functional segments and their composition, block copolymers provide a great opportunity to tune their chemical, physical, and optoelectronic properties and assembled structures.

Controlled radical polymerization (aka controlled/"living" radical polymerization or reversible deactivation radical polymerization) combines the benefits of the robust nature of conventional radical polymerization with the capability to prepare well-defined macromolecular architectures common to living polymerization techniques. This method has facilitated the synthesis of various functional polymers with predetermined molecular weights, narrow molecular weight distribution, and controlled architectures, such as star and branched polymers, block and graft copolymers, using a facile approach. The synthesis of functional polymers with controlled molecular weights, low polydispersity, and complex architectures has been possible because of recent significant progress in controlled radical polymerization techniques, such as nitroxide-mediated polymerization (NMP) [24, 25], atom transfer radical polymerization (ATRP) [26, 27], reversible addition-fragmentation chain transfer (RAFT) polymerization [28–41], single electron transfer-living radical polymerization (SET-LRP) [42], organoheteroatom-mediated living radical polymerization [43], and organometallic-mediated radical polymerization [44]. All these systems are based on establishing a rapid dynamic equilibration between a minute amount of growing free radicals and a large majority of dormant species and are more tolerant of functional groups and impurities. Such controlled radical polymerization methods have become key tools for polymer synthesis, especially for synthesizing complex polymers with well-defined structures.

This review highlights recent developments in the design and synthesis of novel complex polymers with carbazole moieties using controlled radical polymerization techniques of carbazole-containing monomers, as shown in Scheme 1. We mainly focus on three classes of carbazole-containing polymers, as follows:

(i) self-assembled block copolymers including amphiphilic block copolymers, block copolymers composed of "more activated" and "less activated" monomers, rod-coil-type block copolymers, and block copolymers possessing a metal ligating functionality

(ii) branched polymers, such as star block copolymers, miktoarm star copolymers, star polymers having a metallocore, and comb-shaped copolymers;

(iii) hybrids obtained by controlled radical polymerization of carbazole-containing monomers.

2. Carbazole-Containing Block Copolymers

Block copolymers incorporating carbazole functionality have attracted significant research interest, mainly as a result of the feasibility of using them to create highly ordered structures and their potential applications in the optoelectronic fields. Depending on the ordered structures and stacking of the carbazole moiety, the three-dimensional hierarchical structures formed by self-organization of the carbazole-containing block copolymers may lead to unique electronic and photonic functions. There has been much research for the synthesis of carbazole-containing block copolymers using controlled radical polymerization of NVC. Styrene and (meth)acrylate derivatives having carbazole moieties have also been used for the controlled synthesis of carbazole-containing block copolymers.

2.1. Controlled Radical Polymerization of N-Vinylcarbazole. Poly(NVC) was the first and most widely studied polymeric photoconductor. NVC, a strong basic monomer, undergoes facile cationic polymerization with almost all cationic initiators to give poly(NVC). The living cationic polymerization of NVC with hydrogen iodine has also been reported [45]. Free radical initiators, such as azo compounds and peroxides, readily polymerize NVC, and radical polymerization was used in manufacturing the polymer [1]. Several attempts to synthesize poly(NVC) using controlled radical polymerization systems have been reported in the literature. For example, Fukuda et al. demonstrated that the control of NVC homopolymerization could not be achieved by a typical NMP, whereas the copolymerization with styrene under the same conditions proceeded in a living fashion [46]. Baethge et al. also reported the controlled NMP of styrene and NVC, while they demonstrated that the synthesis of the homopolymer, poly(NVC), with controlled molecular weights and a narrow polydispersity, was still problematic [47, 48]. Nowakowska et al. reported that the synthesis of poly(sodium styrenesulfonate-*b*-NVC) by NMP was possible only when the polymerization of NVC was conducted in the presence of acetic anhydride as an accelerator [49]. ATRP ($C_{60}Cl_n$/CuCl/2,2′-bipyridine) was also used for the synthesis of poly(NVC) having a narrow polydispersity (M_w/M_n = 1.33). However, the actual structure of the product was a star-like architecture with a C_{60} core because of multiple chlorine atoms in one initiator molecule, $C_{60}Cl_n$, and there was no information on each poly(NVC) and its detachments from the surface of C_{60} [50]. They also demonstrated that the attempt to synthesize the block copolymer, poly(NVC-*b*-styrene), using the ATRP system provided products with bimodal molecular weight distributions [51]. These previous studies failed to provide convincing proof of the controlled character of the homopolymerization of NVC, such as a kinetic investigation, evaluation of the end groups, and a chain extension experiment. The difficulties in adapting controlled radical polymerization to NVC may also be based on the fact that the NVC propagating radical is relatively unstable and thus highly reactive, mainly because of the electron-donating carbazolyl pendant ($Q = 0.26$, $e = -1.29$) [52], leading to a tendency to undergo chain transfer and chain termination reactions. In other words, systems suitable for inducing a fast interconversion between the dormant and the reactive radical species having a high electron density at the radical center derived from NVC were difficult to find.

However, recent advances in the field of controlled radical polymerization have resulted in successful controlled polymerization of NVC. Mori et al. recently synthesized poly(NVC) with predetermined molecular weights (M_n in the range of 3000–48000) and low polydispersities (M_w/M_n in the range of 1.15–1.20) by xanthate-mediated controlled radical polymerization [53]. The RAFT process is generally accomplished by performing a radical polymerization in the presence of a thiocarbonylthio compound, such as a dithioester, dithiocarbamate, trithiocarbonate, or xanthate, all of which act as reversible chain transfer agents (CTAs). When xanthates are employed, the terminology MADIX (macromolecular design via the interchange of xanthates) is frequently used to describe the process [54–56]. In general, the controlled radical polymerization of the *N*-vinyl and *O*-vinyl monomers was considered difficult, since the generated radical species are highly reactive due to their nonconjugated nature and strong electron-donating pendant groups. However, dithiocarbonates (xanthates) were recently reported to be useful for controlling the radical polymerization of highly reactive *O*-vinyl and *N*-vinyl monomers, such as vinyl acetate [57–60], *N*-vinylpyrrolidone [61–63], *N*-vinylcarbazole (NVC) [53], *N*-vinylindole derivatives [64], *N*-vinylphthalimide [65–67], *N*-vinylnaphthalimide [66], and *N*-vinylimidazolium salts [68].

Both the MADIX and RAFT processes are based on the generally accepted reversible addition-fragmentation chain transfer mechanism between an active and a dormant species. To achieve control of the radical polymerization via the RAFT/MADIX process, a delicate balance of the forward and reverse rates of addition (k_{add} and k_{-add}) and fragmentation (k_β and $k_{-\beta}$), together with the rates of reinitiation (k_i) and propagation (k_p), is required. Because the NVC propagating radical is a poor homolytic leaving group, the fragmentation of the RAFT-adduct radical (intermediate radical) is thought to be very slow when dithioesters are used, resulting in insufficient control of the polymerization. In contrast, the xanthate-type CTA is useful for achieving controlled radical polymerization of NVC, because it increases electron density at the radical center, which may lead to the destabilization of the RAFT-adduct radicals relative to the normal dithioester-type CTA and an increase in the fragmentation rate. The electron-donating *O*-alkyl substituents may lead to stabilization of the thiocarbonyl product of fragmentation through their conjugation with the C=S double bond, as shown in Scheme 2. This lowers the rate of addition of the propagating radicals to the sulfur atom, and consequently the overall rate of chain transfer [30, 57, 69–71]; whereas the introduction of electron-withdrawing groups in the Z moiety leads to an increase in the rate of addition [70].

The blocking order is crucial for the synthesis of well-defined block copolymers by the RAFT process. The first dithioester-terminated polymer, S=C(Z)S-A, in which the A block corresponds to the first polymer and Z is the stabilizing

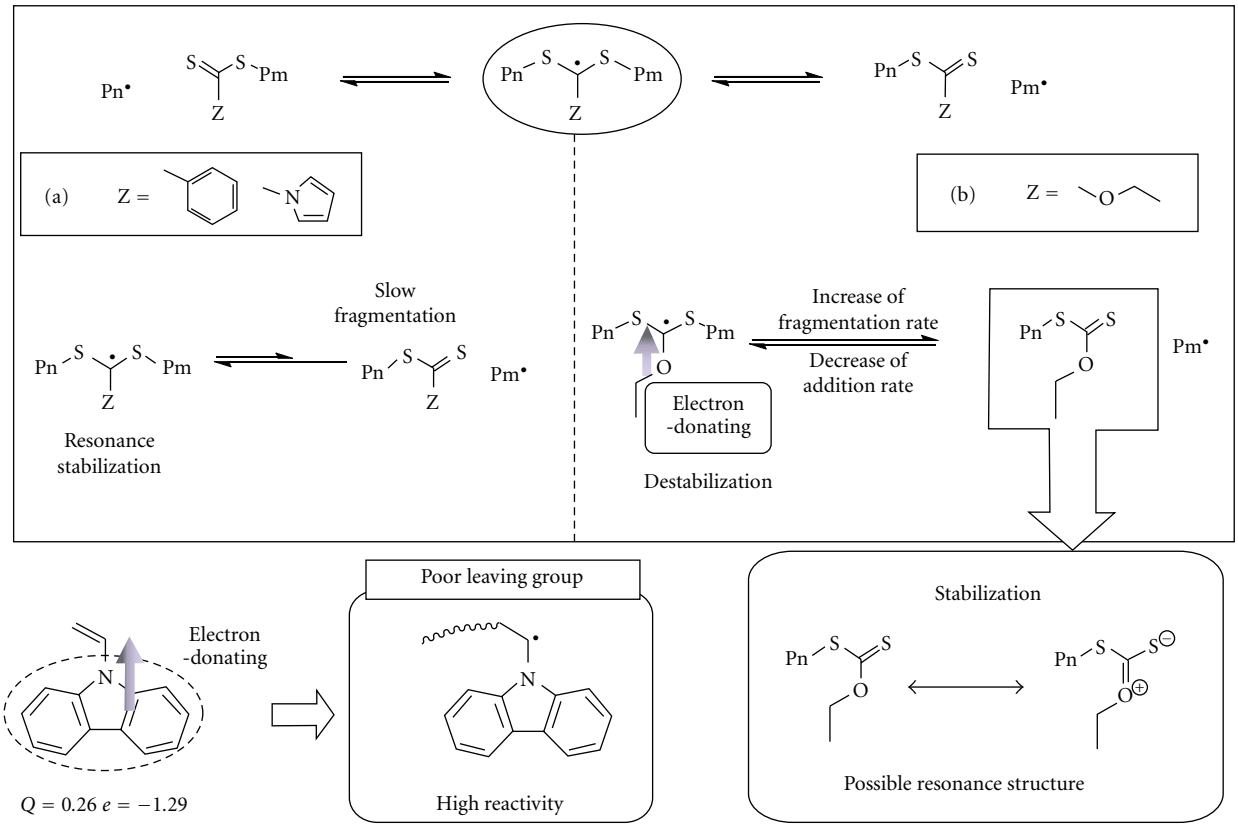

Scheme 2: Proposed mechanism of xanthate-mediated controlled radical polymerization of NVC.

group, should have a high transfer constant in the subsequent polymerization of the second monomers to give the B block [72, 73]. The rapid conversion of macro-CTA to a block copolymer is also required to achieve a block copolymer with low polydispersity, which allows all the second blocks to be initiated at approximately the same time [74, 75].

The xanthate-mediated controlled radical polymerization of NVC was also applied for the synthesis of well-defined block copolymers involving a poly(NVC) segment. For example, a well-defined block copolymer involving a poly(lithium vinyl sulfonate) segment was synthesized by RAFT polymerization of a vinyl sulfonate ester, neopentyl ethenesulfonate, using xanthate-terminated poly(NVC) macro-CTA, followed by deprotection (Scheme 3) [76]. The resulting product can be regarded as an amphiphilic block copolymer, comprising poly(lithium vinyl sulfonate) as a strong anionic polyelectrolyte and poly(NVC) as a hydrophobic segment. Amphiphilic block copolymers, poly(NVC)-*b*-poly(*N*-vinylpyrrolidone), were prepared by xanthate-mediated RAFT polymerization (Scheme 4) [77]. The amphiphilic block copolymers dissolved in several organic solvents; however, depending on their composition, formed either micelles or large aggregates in methanol. The presence of globular aggregates was confirmed by tapping mode atomic force microscopy. The xanthate-mediated RAFT polymerization of NVC was applied for the synthesis of three types of block copolymers, poly(ethylene glycol)-*b*-poly(NVC), poly(NVC)-*b*-poly(vinyl acetate), and poly(NVC)-*b*-poly(vinyl alcohol), as shown in Scheme 5 [78].

Well-defined pH- and thermomultiresponsive fluorescent micelles based on the self-assembly of diblock copolymers, poly(*N*-isopropylacrylamide-*co*-NVC)-*b*-poly[2-(dimethylamino)ethyl acrylate], were obtained by RAFT copolymerization of *N*-isopropylacrylamide and NVC followed by chain extension in the presence of 2-(dimethylamino)ethyl acrylate [79]. The micelles were formed in aqueous solutions in a wide range of temperatures, and their sizes increased from 40 to 65 nm when the pH was varied from basic to acidic. Cross-linking of the poly[2-(dimethylamino)ethyl acrylate)]-containing shell with 1,2-bis(2-iodoethoxy)ethane results in spherical soft nanoparticles. The presence of NVC in concentrations as low as 4% in the core of the micelles was reported to allow the nanoparticles to be tagged by fluorescence, making them well suited to therapeutic applications.

The synthesis of poly(NVC)-based block copolymers functionalized with rhenium diimine complexes or pendant terpyridine ligands was reported [80]. The copolymers were synthesized by RAFT polymerization, and they exhibited interesting morphological properties as a result of the phase separation between different blocks. It was demonstrated that the rhenium complex polymer block could function as a photosensitizer, while the terpyridine-containing polymer

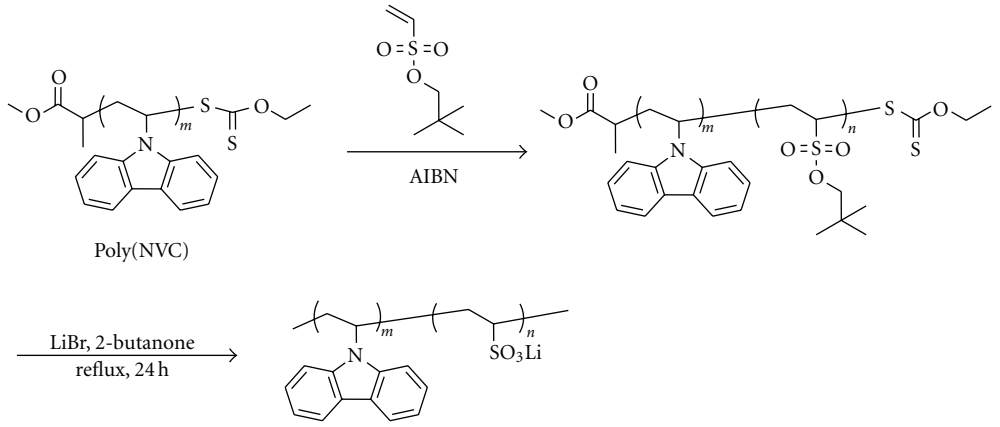

Scheme 3: Synthesis of poly(NVC)-*b*-poly(lithium vinyl sulfonate) by RAFT polymerization of neopentyl ethenesulfonate using poly(NVC) as macro-CTA and subsequent deprotection.

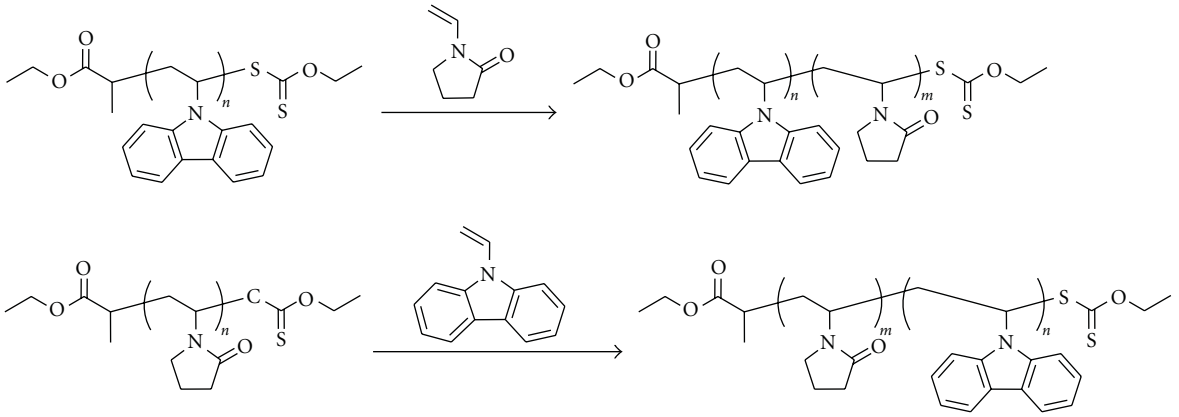

Scheme 4: Synthesis of poly(NVC)-*b*-poly(*N*-vinylpyrrolidone) by xanthate-mediated RAFT polymerization.

block can be used as a template for nanofabrication by selective deposition of zinc complexes.

Generally, the selection of the RAFT agent is dictated by the types of monomer being polymerized. The RAFT agents (dithioesters, trithiocarbonates) suitable for controlling polymerization of "more activated" monomers (e.g., styrene, acrylates, and methacrylates) tend to inhibit polymerization of "less activated" monomers (e.g., NVC, vinyl acetate, and *N*-vinylpyrrolidone). Similarly, RAFT agents suitable for polymerizations of "less activated" monomers tend to give little or poor control over polymerizations of "more activated" monomers. Hence, the synthesis of block copolymers composed of "less activated" and "more activated" monomers was difficult. Recently, switchable RAFT polymerization using *N*-(4-pyridinyl)-*N*-methyldithiocarbamates was found to provide excellent control over polymerization of "less activated" monomers and, after addition of 1 equivelant of a protic or Lewis acid, become effective in controlling polymerization of "more activated" monomers [81]. Switchable RAFT polymerization allowed the synthesis of poly(methyl acrylate)-*b*-poly(NVC) with narrow molecular weight distributions. The preparation of unimodal low dispersity block copolymers of poly(*N*, *N*-dimethylacrylamide) with NVC was also conducted by switchable RAFT polymerization [82]. The controlled radical polymerizations of "less activated" monomers, NVC, vinyl acetate, and *N*-vinylpyrrolidone, were successfully achieved in the presence of a disulfide, isopropylxanthic disulfide, using AIBN as the initiator [83]. The use of RAFT polymerization for the synthesis of optoelectronic polymers was recently reviewed by Moad et al [22]. The polymerization proceeded via MADIX process, where xanthate was formed *in situ* from the reaction of AIBN and isopropylxanthic disulfide. Organoheteroatom-mediated living radical polymerization using organotellurium, organostibine, and organobismuthine chain transfer agents were also useful methods for achieving the controlled character of polymerization of conjugated and nonconjugated monomers [43].

A rod-coil block copolymer consisting of poly(3-hexylthiophene) and poly(NVC) was synthesized by RAFT polymerization of NVC using trichiocarbonate-teminated poly(3-hexylthiophene) as a macro-CTA (Scheme 6) [84]. The rod-coil block copolymer was employed for a white organic electroluminescence device. It is possible to suppress energy transfer from poly(NVC) as wide bandgap units to poly(3-hexylthiophene) as low bandgap blocks by obtaining

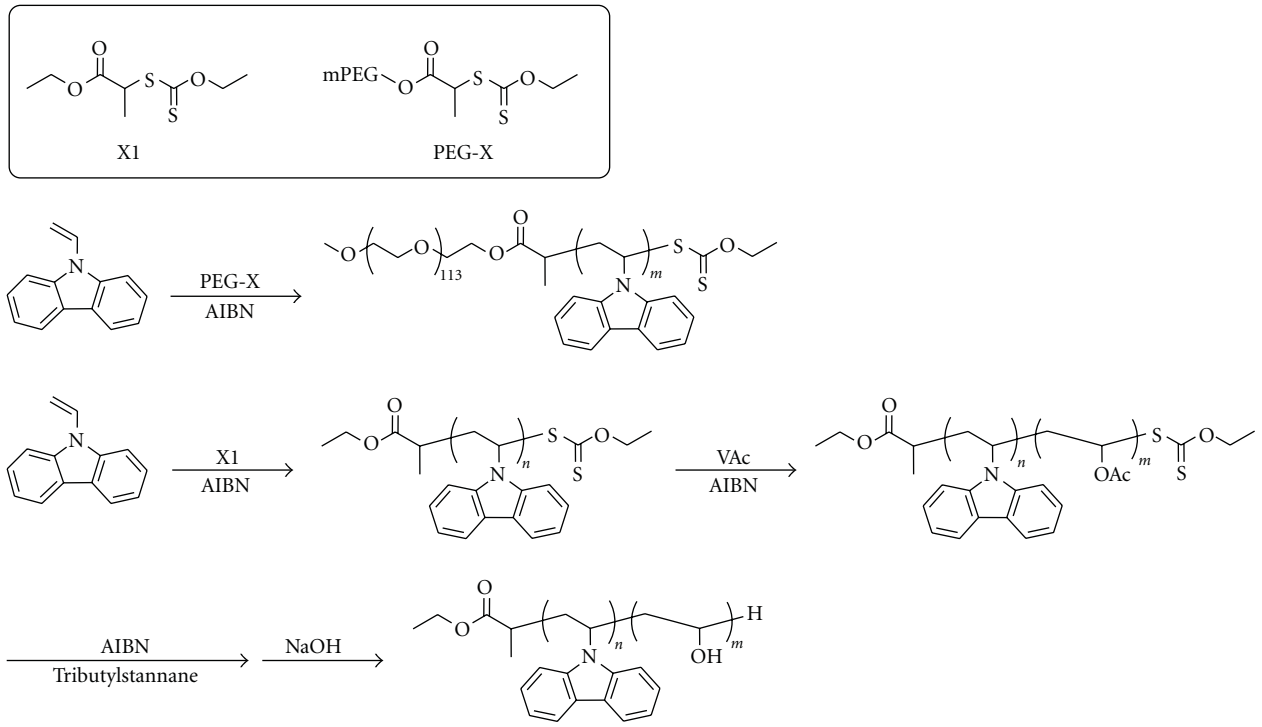

Scheme 5: Synthesis of poly(ethylene glycol)-*b*-poly(NVC), poly(NVC)-*b*-poly(vinyl acetate), and poly(NVC)-*b*-poly(vinyl alcohol) by xanthate-mediated RAFT polymerization.

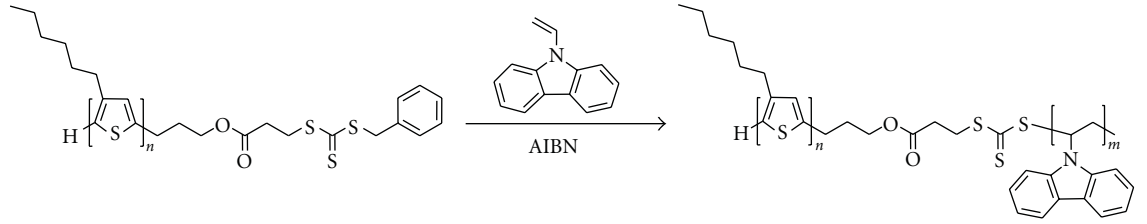

Scheme 6: Synthesis of poly(3-hexylthiophene)-*b*-poly(NVC) by RAFT polymerization.

the phase-separated domains from thin films of the resulting block copolymer, yielding dual emissions for white electroluminescence with a CIE coordination of (0.34, 0.33).

The homopolymerization of NVC was performed with ATRP with Cu(I)/Cu(II)/2,2′-bipyridine as the catalyst system at 90°C in toluene [85]. *N*-2-Bromoethyl carbazole was used as the initiator, and the optimized ratio of Cu(I) to Cu(II) was found to be 1/0.3. The resulting poly(NVC) was used as a macroinitiator for the ATRP of methyl methacrylate, and this resulted in the formation of a block copolymer. The order of blocking is considered to be also crucial for ATRP or NMP as RAFT process. The polymerization of NVC and 3-(9H-carbazole-9-yl)propyl methacrylate (CzPMA) was carried out using various controlled radical polymerization methods, such as ATRP, single electron transfer-living radical polymerization (SET-LRP), and single electron transfer initiation followed by RAFT (SET-RAFT) [86]. In the case of NVC, well-controlled polymerization with narrow molecular weight distribution was achieved by high-temperature ATRP, while SET-RAFT polymerization was relatively slow and controlled at ambient temperature. In the case of CzPMA, SET-RAFT was more suitable for ambient temperature polymerization. The synthesis of diblock copolymers was achieved from poly(NVC) and poly(CzPMA) macroinitiators using a flavanone-based methacrylate as the second monomer. The emission spectra of these block copolymers showed higher intensities compared with homopolymers.

2.2. Controlled Radical Polymerization of Styrene Derivatives Having Carbazole Moieties. The functional polymer containing carbazole units was successfully prepared via nitroxide-mediated radical polymerization of 9-(4-vinylbenzyl)-9H-carbazole (VBCz) [87]. New nonconjugated random copolymers containing pendant electron-donating poly(VBCz) and electron-accepting 2-phenyl-5-(4-vinylphenyl)-1,3,4-oxadiazole or 2-(4-vinylbiphenyl)-5-(4-phenyl)-1,3,4-oxadiazole were successfully synthesized by

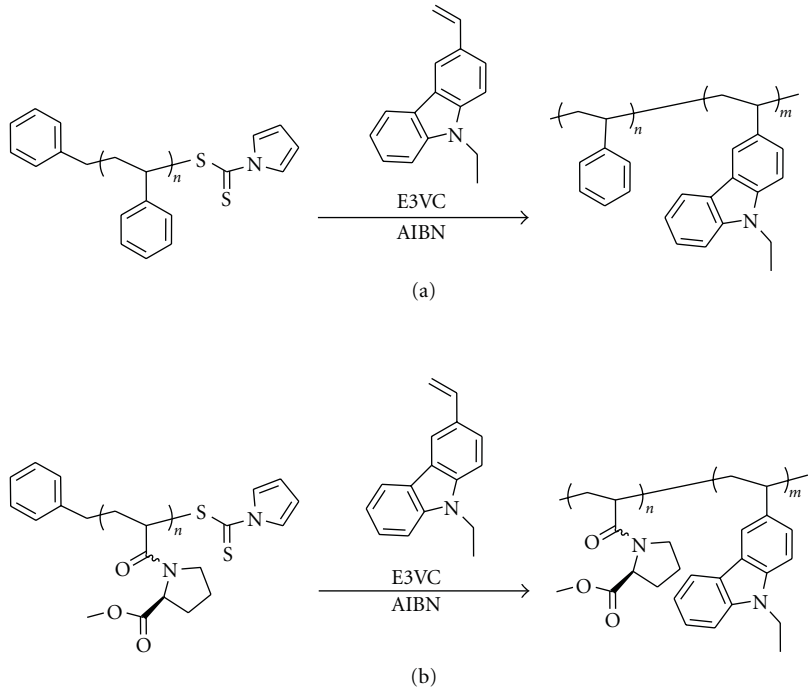

Scheme 7: Synthesis of block copolymers by RAFT polymerization of E3VC.

the NMP method [88]. The electrical switching behavior, based on the ITO/ polymer/Al device configuration, could be tuned through the donor/acceptor ratio or acceptor trapping ability. The controlled nitroxide-mediated homopolymerization of VBCz and the copolymerization of methyl methacrylate with varying amounts of VBCz were accomplished by using 10 mol % nitroxide relative to 2-({tert-butyl[1-(diethoxyphosphoryl)-2,2-dimethylpropyl]amino}oxy)-2-methylpropionic acid [89]. VBCz was found to be an effective controlling comonomer for NMP of methyl methacrylate, and such low levels of VBCz comonomer ensured transparency in the final copolymer. Well-defined cyclic polymers, cyclic poly(VBCz), with differing molecular weights were efficiently prepared by successive ATRP and a click reaction [90].

N-ethyl-3-vinylcarbazole (E3VC) was also employed as a carbazole-containing monomer, which can be regarded as a styrene derivative. The controlled RAFT polymerization of E3VC was performed using benzyl 1-pyrrolecarbodithioate as a suitable CTA to afford well-defined poly(E3VC) in which the carbazole unit is directly bound to the polymer main chain [91]. Well-defined block copolymers with poly(E3VC) segments have been synthesized using dithiocarbamate-terminated polystyrene as a macro-CTA (Scheme 7(a)). Amino-acid-containing amphiphilic block copolymers composed of poly(E3VC) as a hydrophobic segment and poly(*N*-acryloyl-L-proline methyl ester) [92, 93] as a hydrophilic segment were prepared by RAFT polymerization (Scheme 7(b)) [94]. Formation of micelles consisting of a hydrophobic core of poly(E3VC) and a hydrophilic shell of poly(*N*-acryloyl-L-proline methyl ester) was observed in methanol, which is a selective solvent for the poly(*N*-acryloyl-L-proline methyl ester) segment. The chiroptical properties were affected by the assembled structure induced by the selective solvent and were evaluated by fluorescence and circular dichroism spectra.

N-Ethyl-2-vinylcarbazole (E2VC) is a monomer structurally similar to the styrenes, which are known to polymerize well by NMP [95]. Polymerization of E2VC from a unimolecular alkoxyamine was reported to show a molecular weight that increases steadily with time, whereas termination or decomposition of the "living" radical ends was clearly evident. Nevertheless, a sufficient fraction of the chains remained living that poly(E2VC)-*b*-polystyrene could be formed by chain extension of the poly(E2VC) macroinitiator with styrene.

2.3. Controlled Radical Polymerization of (Meth)Acrylate Derivatives Having Carbazole Moieties. Photorefractive active block copolymers were successfully synthesized via ATRP of acrylate containing liquid crystalline moieties and hole transporting carbazole moieties [96]. The photorefractive characteristics of the copolymers indicated a higher diffraction efficiency and larger coupling gain for the block copolymer, compared to the corresponding statistical random copolymer. The controlled radical polymerization of 2-(*N*-carbazolyl)ethyl methacrylate (CzEMA) and 4-(5-(4-*tert*-butylphenyl-1,3,4-oxadiazol-2-yl)phenyl) methacrylate via the RAFT process has been studied for the synthesis of functional polymers with hole- or electron-transfer ability [97]. RAFT polymerization of these monomers using cumyl dithiobenzoate as a suitable CTA and AIBN as an initiator afforded well-defined polymethacrylates having hole- and electron-transporting groups. Monomers containing a

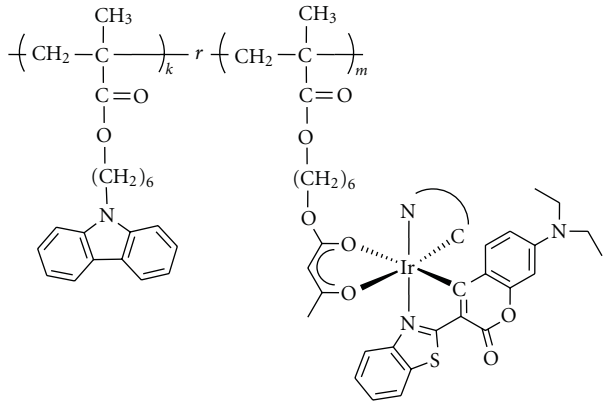

Scheme 8: Methacrylate copolymers containing phosphorescent Ir(III)-complex and carbazole moiety.

chromophore group, that is, 9-anthrylmethyl methacrylate and CzEMA, were copolymerized with methyl methacrylate using ATRP, resulting in two series of copolymers with various amounts of included chromophore units [98]. Luminescence comparison demonstrated more intense light emission by polymethacrylates with carbazolyl groups than by copolymers with anthryl groups. The wavelength of emitted light also differed in the range of blue–violet and blue–green fluorescence for carbazolyl and anthryl copolymers, respectively.

A methacrylate-functionalized phosphorescent Ir(III)-complex was copolymerized with a methacrylate-functionalized carbazole-derivative using ATRP (Scheme 8), with the aim of applying this type of host-guest-system to organic light-emitting devices [99]. In the system, the emission originated almost exclusively from the complex, suggesting efficient intrachain energy transfer.

3. Carbazole-Containing Branched Polymers

3.1. Star Polymer/Star Block Copolymer/Miktoarm Star Copolymer. There are two basic routes for synthesizing star polymers [100]: the "core first" method (polymerization from multifunctional initiators or microgels), and the "arm first" method, in which growing polymer chain ends are reacted with a multifunctional terminating agent or a divinyl compound. The use of multifunctional initiators or terminators leads to stars with a well-known (though often, low) number of arms; while the use of microgels or divinyl compounds leads to a rather broad arm number distribution, with a high average arm number. The design and synthesis of novel star copolymers having characteristic architectures, such as star block copolymers and heteroarm or miktoarm (mixed) star polymers, are attracting significant attention because of their interesting structures and properties [17, 101–106]. Amphiphilic star block copolymers and miktoarm star polymers can form a variety of superstructures as a result of self-organization, and the resulting assembled structures should be governed by the branched architecture, as well as the chemical nature of the components, their composition, and molecular weight.

The xanthate-mediated RAFT polymerization of NVC was also applied for the synthesis of star polymers [107]. RAFT polymerization was employed for the purpose, using three different xanthate-type tetrafunctional CTAs: two *Z*-designed CTAs having different *R* (leaving) groups in which the *Z* (stabilizing) groups are linked to the core, and one *R*-designed CTA. The *R*-group approach was found to be the most efficient for the controlled synthesis of four-arm poly(NVC) stars having low polydispersities and controlled molecular weights. Amphiphilic star block copolymers were synthesized by the polymerization of NVC using the poly(acrylic acid) star, which was prepared from the R-designed tetrafunctional CTA (Scheme 9) [108]. DLS measurements of the amphiphilic stars in THF solution, which is a good solvent for both components, suggested the existence of unimolecular star micelles. In contrast, the formations of the micelles and inverse micelles were observed in water, which is a good solvent only for the poly(acrylic acid) segment, and in $CHCl_3$, which is a good solvent only for poly(NVC) segment. The absorbance and fluorescence spectra indicated that specific conformations of amphiphilic stars, like micelles and inverse micelles, affected the characteristic optoelectronic properties.

Star polymers containing chemically different arms are designated heteroarm or miktoarm (mixed arm) star polymers when they comprise two or more different kinds of arms, respectively. Their unique architectures cause them to reveal interesting properties in the solid state and in solution [109]. A novel amphiphilic A_3B miktoarm star copolymer, poly(*N*-isopropylacrylamide)$_3$-poly(NVC), was successfully synthesized by a combination of single-electron transfer living radical polymerization and RAFT polymerization (Scheme 10) [110]. First, the well-defined three-armed poly(*N*-isopropylacrylamide) was prepared via SET-LRP of *N*-isopropylacrylamide using a tetrafunctional bromoxanthate iniferter (Xanthate-Br_3) as the initiator and Cu(0)/PMDETA as a catalyst system. Secondly, the target amphiphilic A_3B miktoarm star copolymer was prepared via RAFT polymerization of NVC employing three-armed poly(*N*-isopropylacrylamide) having a xanthate moiety as the macro-CTA. The amphiphilic A_3B miktoarm star

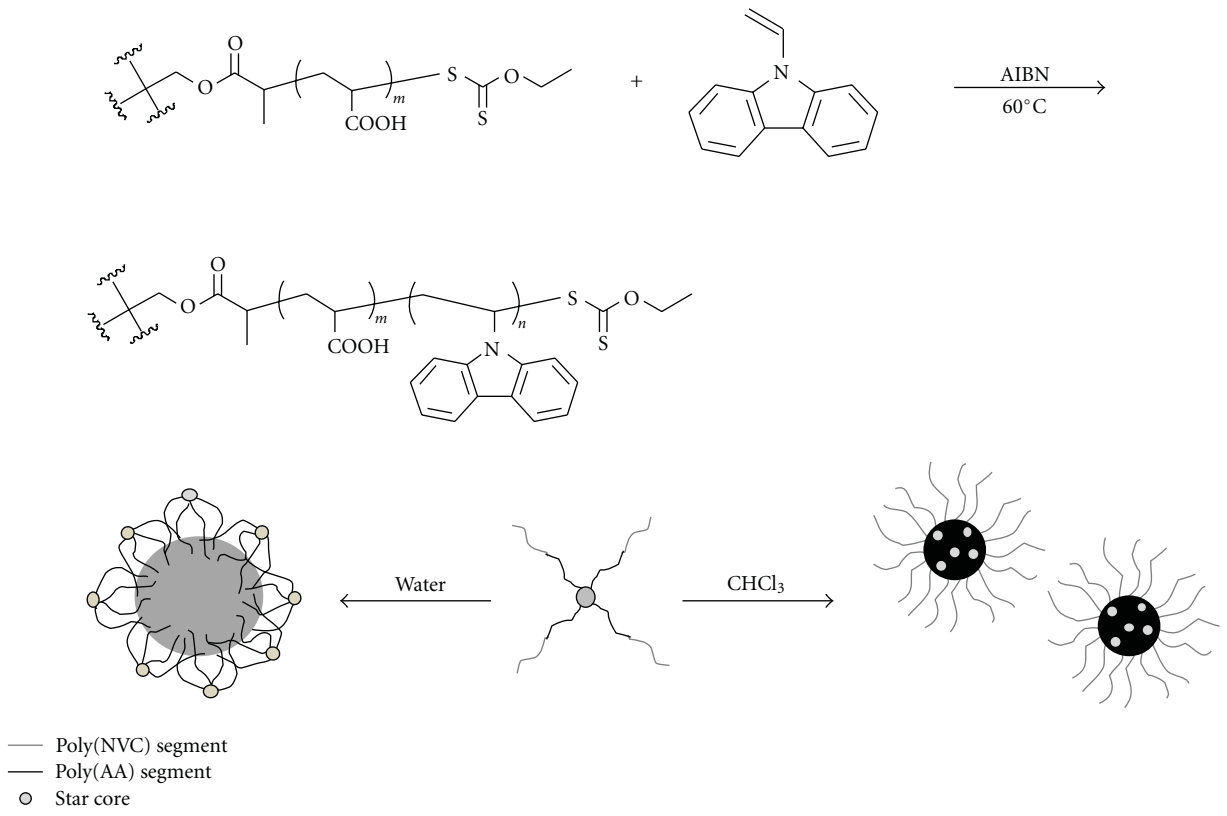

Scheme 9: Synthesis and assembled structures of amphiphilic star block copolymers.

copolymer showed an increase in the fluorescence intensity of micelle with temperature and had good temperature reversibility.

Styrene-type monomer, VBCz, and methacrylate-type monomer, 2-(9H-carbazole-9-yl)ethyl methacrylate (CzEMA), were polymerized to star polymers via ATRP using zinc 5,10,15,20-tetrakis(4-(2-methyl-2-bromopropoxy) phenyl) porphyrin as an initiator (Scheme 11) [111]. The emission spectra of the two star polymers, poly(VBCz) and poly (CzEMA) stars, displayed red light emission in the solid state, while those of the two monomers showed blue light emission, suggesting the effective energy transfer from the carbazole to the Zn porphyrin core. It was demonstrated that the flexible arms of star polymers can effectively hinder π-π interaction of the porphyrin cores and present aggregation, which would lead to fluorescent self-quenching in the solid state.

A derivative Ru(II) complex with radical initiating sites was employed in the ATRP of functional N-(ω'-alkylcarbazoly) methacrylates to provide linear metallopolymers with the metal chromophores at one terminus of the polymer chain [112]. Similar Ru(II) complexes with one and three initiating sites were also employed as metalloinitiators for ATRP of N-(ω'-alkylcarbazoly) methacrylates with $NiBr_2(PPh_3)_2$ as a catalyst (Scheme 12) [113]. Star-like three-armed polymers could be obtained from the metalloinitiators with three initiating sites.

3.2. Comb-Shaped Copolymers. There have been very few reports of the synthesis of comb-shaped copolymers with carbazole-containing segments. These comb-shaped copolymers can be regarded as cylindrical polymer brushes having the same number of side chains as the degree of polymerization of the main chain. These cylindrical polymer brushes with carbazole-containing segments are architecturally interesting for both experimental and theoretical chemists because of the possibility of forming extended chain conformations, based on the intramolecular excluded-volume interactions between side chains densely grafted to the backbone. The homopolymerization of macromonomers, "grafting onto" and "grafting from" can be used in much the same way as conventional graft copolymers and comb-shaped copolymers. The "grafting from" method was mainly employed for the synthesis of comb-shaped copolymers with carbazole-containing segments.

The comb-shaped copolymer having poly(VBCz) side chains was prepared via NMP of VBCz using a macro-TEMPO agent, which was synthesized by anion ring-opening polymerization of 4-glycidyloxy-2,2,6,6-tetramethylpiperidine1oxyl (Scheme 13) [114]. The fluorescence, ultraviolet intensities, and cyclic voltammetries of the comb-shaped copolymers with different molecular weights showed a regular order. It was reported that the highest occupied molecular orbital (HOMO) and lowest unoccupied molecular orbital (LUMO) energy levels accompanied by bandgaps

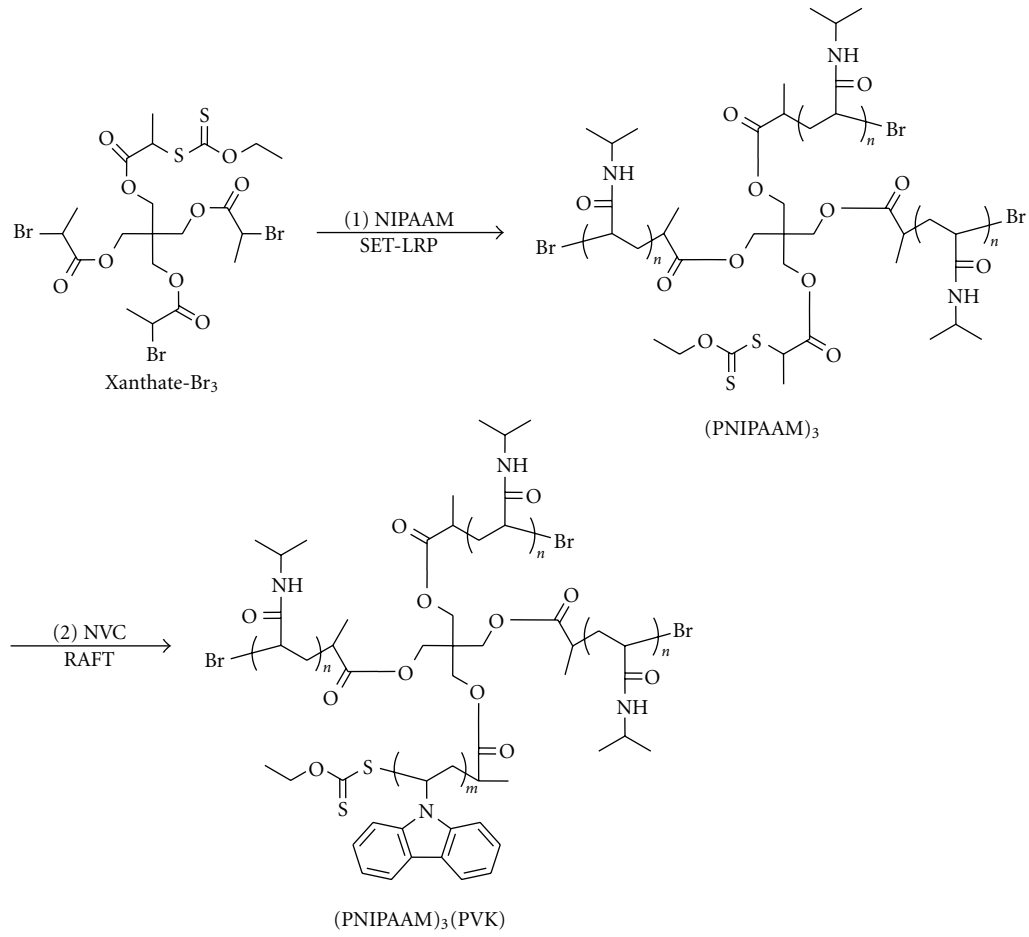

Scheme 10: Synthesis of A_3B miktoarm star copolymer, poly(*N*-isopropylacrylamide)$_3$-poly(NVC).

were adjustable via molecular weights of the polymers, which should be favorable to the application of these polymers in electronic devices.

A new light-emitting and hole transporting comb-shaped copolymer was prepared via ATRP of an acrylate monomer, 3-(*N*-carbazolyl)propyl acrylate (CzPA), initiated by a macroinitiator with ATRP initiating sites distributed along a polythiophene backbone (Scheme 14). This polymer can be regarded as a rod-coil-type comb-shaped copolymer, in which the polythiophene rod is located in the backbone and the poly(CzPA) coil is located in the side chain. The energy transfer process from the poly(CzPA) side chains to the polythiophene backbone was evidenced in both the solution and film states. Electroluminescence devices fabricated from the copolymer demonstrated that the copolymer could act as both a light emissive and hole-transporting material [115].

4. Carbazole-Containing Hybrids

Carbazole-containing polymer chains attached to planar and spherical surfaces have recently attracted much interest as candidates for various optoelectronic industrial applications. Electroactive substrates, such as carbon nanotubes, fullerene, graphene, and quantum dots, were mainly employed. The so-called "grafting onto," and "grafting from" methods can be used for the synthesis of carbazole-containing hybrids. In the "grafting from" process, the side chains of the brush are formed via controlled radical polymerizations involving ATRP and NMP initiated by the pendant initiating groups on the surface. When RAFT polymerization was employed, the CTA moiety was attached to the surface. Well-defined polymer brushes with high grafting density and rather narrow distributions can be obtained using this method. The "grafting onto" technique was frequently used for the synthesis of the hybrids, in which the carbazole-containing polymers were attached to the substrates by adsorption or chemical reaction of end-functionalized polymers or block copolymers onto the surfaces.

The poly(NVC)-grafted multiwalled carbon nanotubes hybrid materials were synthesized by RAFT polymerization of NVC in the presence of a trithiocarbonate-type CTA functionalized covalently onto multiwalled carbon nanotubes (Scheme 15) [116]. Incorporation of poly(NVC) onto the surfaces of the multiwalled carbon nanotubes can considerably improve their solubility and processability. Hybrid materials that are suitable candidates for viable optical limiting devices exhibit significant nonlinear optical

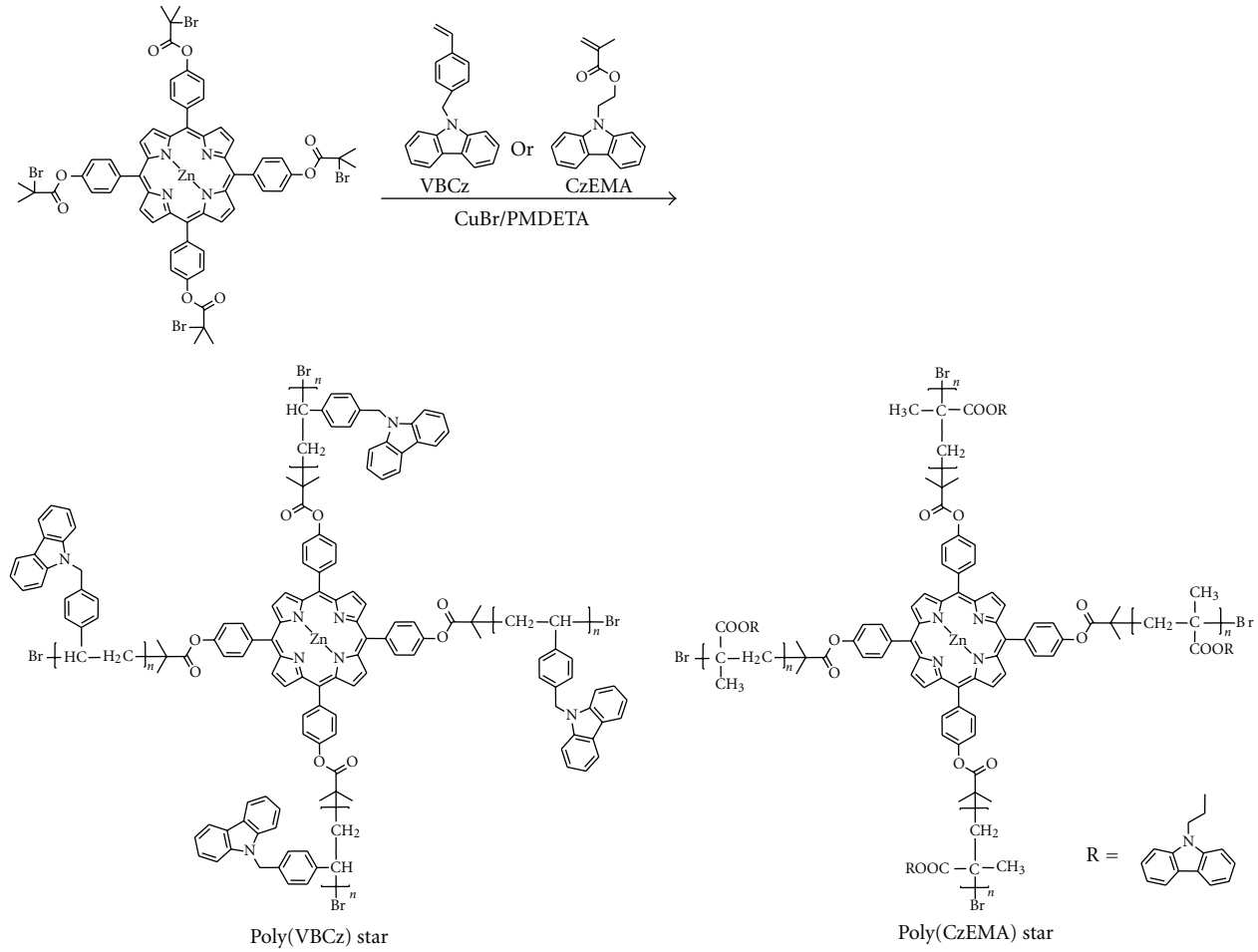

Scheme 11: Synthesis of star polymers via ATRP using zinc porphyrin as a tetrafunctional initiator.

responses. Poly(NVC) chemically modified graphene oxide was obtained by RAFT polymerization of a trithiocarbonate type-CTA functionalized on graphene oxide [117, 118]. The resulting hybrid material showed good solubility in organic solvents and a significant energy bandgap in the vicinity of 2.49 eV [118]. The poly(NVC)-C_{60} composites were synthesized by ATRP ($C_{60}Cl_n$/CuCl/2,2′-bipyridine) of NVC [50, 119, 120]. The photoconducting properties of poly(NVC)-C_{60} composites were also investigated.

The CdSe-polymer composite was prepared via ATRP of NVC on functionalized CdSe quantum dots (Scheme 16) [121, 122]. It was revealed that grafting poly(NVC) onto the surface of CdSe nanocrystals would reduce the bandgap of poly(NVC) and cause a red shift in the emission peak. The nanocrystal-polymer nanocomposite was employed as the electron acceptor in polymer bulk heterojunction solar cells. Ultrasound-assisted bulk synthesis of CdS-poly(NVC) nanocomposites was reported via RAFT polymerization [123]. Poly(methyl methacrylate)/zinc oxide (ZnO) or carbazole-containing polymers, poly(CzEMA)/ZnO nanocomposites, which are composed of high molecular weight polymers with narrow molecular weight distributions and ZnO quantum dots, were prepared by ATRP [124]. 2-Bromo-2-methylpropionyl group was introduced onto the ZnO nanoparticle surfaces, which was employed for the surface-initiated ATRP.

The styrene derivative having a carbazole moiety (VBCz) was employed for the synthesis of bifunctional nanoparticles with fluorescence and magnetism by surface-initiated iron(III)-mediated ATRP with activators generated by electron transfer (AGET ATRP) [125]. VBCz was grafted from magnetic nanoparticles (ferroferric oxide) via AGET ATRP, using $FeCl_3 * 6H_2O$ as the catalyst, tris(3,6-dioxaheptyl)amine as the ligand, and ascorbic acid as the reducing agent. Another interesting system involves the synthesis of multistimuli-response hybrid nanoparticles with magnetic cores and thermoresponsive fluorescence-labeled shells by surface-initiated RAFT polymerization using carbazole-containing CTA-functionalized magnetic silica nanoparticles [126].

Polymer brushes refer to an assembly of polymer chains, which are tethered by one end to a surface or an interface. Surface-initiated polymerization has the advantage of allowing easy modification of surface properties by varying the composition of the polymer brush, grafting density, and the degree of polymerization. Electrochemically

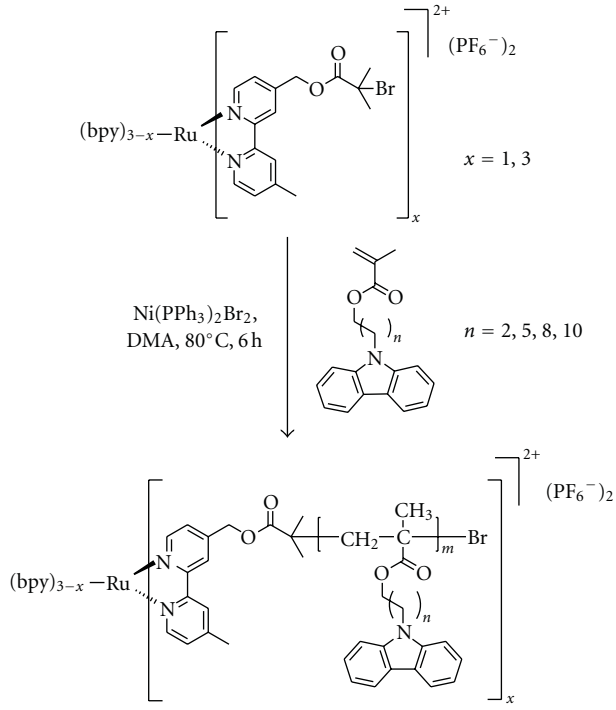

Scheme 12: Synthesis of three-armed polymer by ATRP of the carbazole-containing methacrylates with a metalloinitiator.

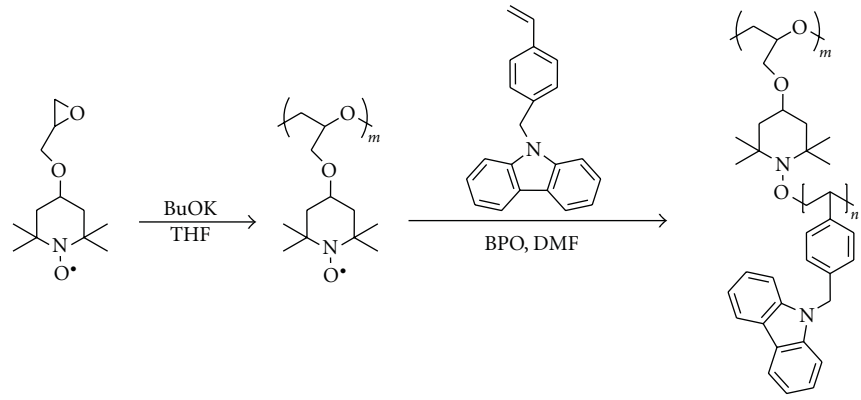

Scheme 13: Synthesis of a comb-shaped copolymer having poly(VBCz) side chains.

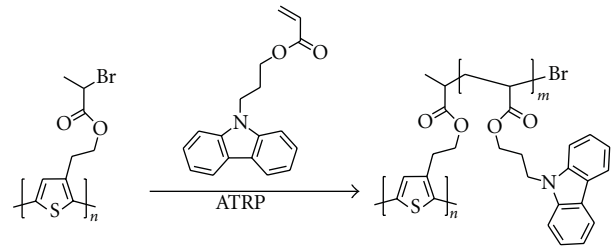

Scheme 14: Synthesis of a comb-shaped copolymer by ATRP of CzPA from a polythiophene backbone.

crosslinked surface-grafted poly(NVC) brushes have been demonstrated as hole transport layers on a photovoltaic device using surface-initiated polymerization [127, 128]. The pendant carbazole group made the poly(NVC) an electrochemically cross-linkable precursor, capable of forming conjugated polymer network films. The covalent linkage of the poly(NVC) brush allowed for direct electroluminescent device preparation on modified ITO, giving the advantage of strong adhesion to ITO with possible long-term stability against acid dopants and oxygen. Surface-initiated ATRP of

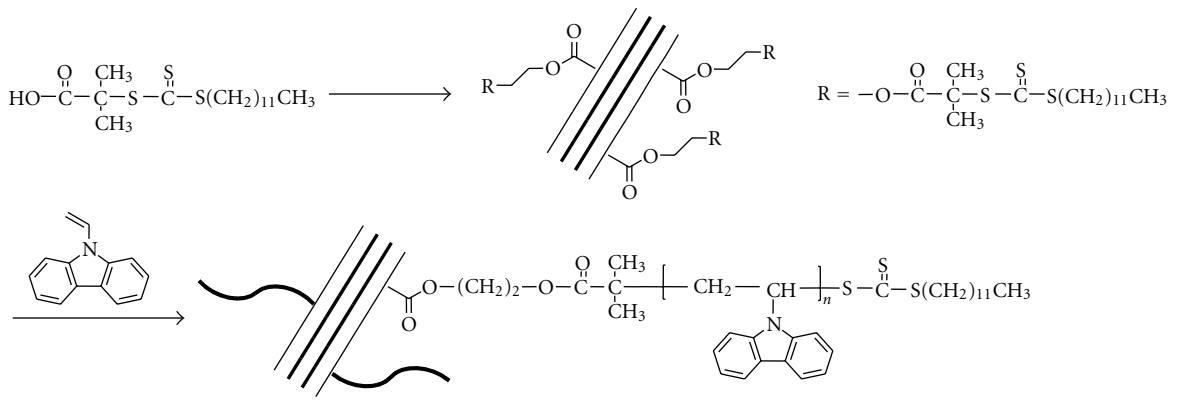

Scheme 15: Synthesis of poly(NVC)-grafted multiwalled carbon nanotubes by RAFT polymerization of NVC.

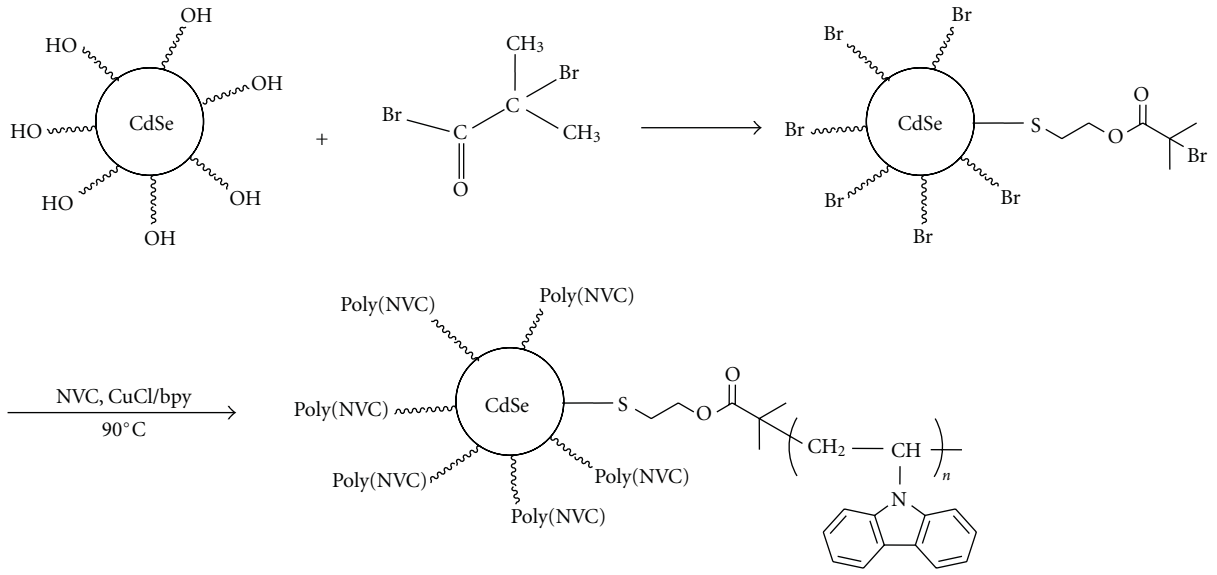

Scheme 16: Synthesis of CdSe-polymer composite by ATRP of NVC.

9-(2-(4-vinyl(benzyloxy)ethyl)-9H-carbazole (VBOCz) was also employed for the synthesis of carbazole-based polymer brushes on silicon surfaces [129]. Conductance switching at a voltage of about 2.1 V was observed in the memory device based on the brushes.

5. Conclusion

This review has summarized the approaches to synthesis of a variety of tailor-made polymers containing carbazole functionality. The combination of different polymerization mechanisms, self-organization of block copolymers, and surface-initiated polymerization have allowed great advances in the design and synthesis of various nano- and mesoscale polymeric materials with sophisticated structures, in addition to recent progress in controlled radical polymerization techniques. The synthetic methodologies for novel architectures, characteristic bulk, and solution properties related to the self-organization process, and a wide range of applications of block copolymers containing poly(NVC) segments have been extensively investigated in the last decade. Controlled radical polymerization of NVC, styrene, and (meth)acrylate derivatives having the carbazole moiety were well advanced, leading to the well-controlled synthesis of complex macromolecules, such as star polymers, star block copolymers, and polymer brushes with the carbazole functionality. The carbazole-containing complex macromolecules can be combined with a broad range of functional groups, such as fluorophores, electroactive groups, dyes, and other biorelated materials. These carbazole-containing polymers with well-defined architectures can provide viable tailored materials with unique electronic and photonic properties for a wide range of applications, including polymeric light-emitting materials, and organic photorefractive materials.

References

[1] J. V. Grazulevicius, P. Strohriegl, J. Pielichowski, and K. Pielichowski, "Carbazole-containing polymers: synthesis,

properties and applications," *Progress in Polymer Science*, vol. 28, no. 9, pp. 1297–1353, 2003.

[2] P. L. T. Boudreault, S. Beaupré, and M. Leclerc, "Polycarbazoles for plastic electronics," *Polymer Chemistry*, vol. 1, no. 2, pp. 127–136, 2010.

[3] S. Beaupré, P. L. T. Boudreault, and M. Leclrec, "Solar-energy production and energy-efficient lighting: photovoltaic devices and white-light-emitting diodes using poly(2,7-fluorene), poly(2,7-carbazole), and poly(2,7-dibenzosilole) derivatives," *Advanced Materials*, vol. 22, no. 8, pp. E6–E27, 2010.

[4] J. Li and A. C. Grimsdale, "Carbazole-based polymers for organic photovoltaic devices," *Chemical Society Reviews*, vol. 39, no. 7, pp. 2399–2410, 2010.

[5] T. Uryu, H. Ohkawa, and R. Oshima, "Synthesis and High Hole Mobility of Isotactic Poly(2-*N*-carbazolylethyl acrylate)," *Macromolecules*, vol. 20, p. 705, 1987.

[6] C. J. Hu, R. Oshima, S. Sato, and M. Seno, "Synthesis and photoinduced discharge characteristics of polyacrylates with pendant carbazole group," *Journal of Polymer Science Part C*, vol. 26, no. 10, pp. 441–446, 1988.

[7] M. Keyanpour-Rad, A. Ledwith, A. Hallam et al., "Some photophysical properties of five new carbazole-containing methacrylate polymers," *Macromolecules*, vol. 11, no. 6, pp. 1114–1118, 1978.

[8] F. S. Du, Z. C. Li, W. Hong, Q. Y. Cao, and F. M. Li, "Vinyl monomers bearing chromophore moieties and their polymers. XI. Synthesis and photochemical behavior of carbazole-containing methacrylic monomers and their polymers," *Journal of Polymer Science Part A*, vol. 38, no. 4, pp. 679–688, 2000.

[9] A. Ledwith, N. J. Rowley, and S. M. Walker, "Fluorescence emission from poly[2-(9-ethyl)carbazolyl-methylmethacrylate]," *Polymer*, vol. 22, no. 4, pp. 435–436, 1981.

[10] S. Barik and S. Valiyaveettil, "Synthesis and self-assembly of copolymers with pendant electroactive units," *Macromolecules*, vol. 41, no. 17, pp. 6376–6386, 2008.

[11] T. Kanbara, Y. Yokokawa, and K. Hasegawa, "Palladium-catalyzed modification of poly(p-bromostyrene) with carbazole and related heteroarenes containing an N-H bond and their properties," *Journal of Polymer Science Part A*, vol. 38, no. 1, pp. 28–34, 2000.

[12] Y. S. Cho, S. W. Kim, C. S. Ihn, and J. S. Lee, "Anionic polymerization of 4-(9-carbazolyl)methylstyrene," *Polymer*, vol. 42, no. 18, pp. 7611–7616, 2001.

[13] S. Förster and T. Plantenberg, "From self-organizing polymers to nanohybrid and biomaterials," *Angewandte Chemie International Edition*, vol. 41, no. 5, pp. 688–714, 2002.

[14] T. Liu, C. Burger, and B. Chu, "Nanofabrication in polymer matrices," *Progress in Polymer Science*, vol. 28, no. 1, pp. 5–26, 2003.

[15] D. E. Discher and A. Eisenberg, "Polymer vesicles," *Science*, vol. 297, no. 5583, pp. 967–973, 2002.

[16] M. Sauer and W. Meier, "Polymer nanocontainers with controlled permeability," *Australian Journal of Chemistry*, vol. 54, no. 3, pp. 149–151, 2001.

[17] G. Riess, "Micellization of block copolymers," *Progress in Polymer Science*, vol. 28, no. 7, pp. 1107–1170, 2003.

[18] F. J. M. Hoeben, P. Jonkheijm, E. W. Meijer, and A. P. H. J. Schenning, "About supramolecular assemblies of π-conjugated systems," *Chemical Reviews*, vol. 105, no. 4, pp. 1491–1546, 2005.

[19] J. Liu, E. Sheina, T. Kowalewski, and R. D. McCullough, "Tuning the electrical conductivity and self-assembly of regioregular polythiophene by block copolymerization: nanowire morphologies in new di-and triblock copolymers," *Angewandte Chemie International Edition*, vol. 41, no. 2, pp. 329–332, 2002.

[20] R. A. Segalman, B. McCulloch, S. Kirmayer, and J. J. Urban, "Block copolymers for organic optoelectronics," *Macromolecules*, vol. 42, no. 23, pp. 9205–9216, 2009.

[21] I. Botiz and S. B. Darling, "Optoelectronics using block copolymers," *Materials Today*, vol. 13, no. 5, pp. 42–51, 2010.

[22] G. Moad, M. Chen, M. Häussler, A. Postma, E. Rizzardo, and S. H. Thang, "Functional polymers for optoelectronic applications by RAFT polymerization," *Polymer Chemistry*, vol. 2, no. 3, pp. 492–519, 2011.

[23] A. de Cuendias, R. C. Hiorns, E. Cloutet, L. Vignau, and H. Cramail, "Conjugated rod-coil block copolymers and optoelectronic applications," *Polymer International*, vol. 59, no. 11, pp. 1452–1476, 2010.

[24] C. J. Hawker, A. W. Bosman, and E. Harth, "New polymer synthesis by nitroxide mediated living radical polymerizations," *Chemical Reviews*, vol. 101, no. 12, pp. 3661–3688, 2001.

[25] R. B. Grubbs, "Nitroxide-mediated radical polymerization: limitations and versatility," *Polymer Reviews*, vol. 51, no. 2, pp. 104–137, 2011.

[26] K. Matyjaszewski and J. Xia, "Atom transfer radical polymerization," *Chemical Reviews*, vol. 101, no. 9, pp. 2921–2990, 2001.

[27] M. Kamigaito, T. Ando, and M. Sawamoto, "Metal-catalyzed living radical polymerization," *Chemical Reviews*, vol. 101, no. 12, pp. 3689–3745, 2001.

[28] J. Chiefari, Y. K. Chong, F. Ercole et al., "Living free-radical polymerization by reversible addition—fragmentation chain transfer: the RAFT process," *Macromolecules*, vol. 31, no. 16, pp. 5559–5562, 1998.

[29] C. Barner-Kowollik, T. P. Davis, J. P. A. Heuts, M. H. Stenzel, P. Vana, and M. Whittaker, "RAFTing down under: tales of missing radicals, fancy architectures, and mysterious holes," *Journal of Polymer Science Part A*, vol. 41, no. 3, pp. 365–375, 2003.

[30] G. Moad, E. Rizzardo, and S. H. Thang, "Living radical polymerization by the RAFT process," *Australian Journal of Chemistry*, vol. 58, no. 6, pp. 379–410, 2005.

[31] C. L. McCormick and A. B. Lowe, "Aqueous RAFT polymerization: recent developments in synthesis of functional water-soluble (Co)polymers with controlled structures," *Accounts of Chemical Research*, vol. 37, no. 5, pp. 312–325, 2004.

[32] S. Perrier and P. Takolpuckdee, "Macromolecular design via reversible addition-fragmentation chain transfer (RAFT)/xanthates (MADIX) polymerization," *Journal of Polymer Science Part A*, vol. 43, no. 22, pp. 5347–5393, 2005.

[33] A. Favier and M. T. Charreyre, "Experimental requirements for an efficient control of free-radical polymerizations via the reversible addition-fragmentation chain transfer (RAFT) process," *Macromolecular Rapid Communications*, vol. 27, no. 9, pp. 653–692, 2006.

[34] G. Moad, E. Rizzardo, and S. H. Thang, "Living radical polymerization by the RAFT process—a first update," *Australian Journal of Chemistry*, vol. 59, no. 10, pp. 669–692, 2006.

[35] A. B. Lowe and C. L. McCormick, "Reversible addition-fragmentation chain transfer (RAFT) radical polymerization and the synthesis of water-soluble (co)polymers under homogeneous conditions in organic and aqueous media," *Progress in Polymer Science*, vol. 32, no. 3, pp. 283–351, 2007.

[36] C. Barner-Kowollik, M. Buback, B. Charleux et al., "Mechanism and kinetics of dithiobenzoate-mediated RAFT polymerization. I. The current situation," *Journal of Polymer Science Part A*, vol. 44, no. 20, pp. 5809–5831, 2006.

[37] M. L. Coote, E. H. Krenske, and E. I. Izgorodina, "Computational studies of RAFT polymerization-mechanistic insights and practical applications," *Macromolecular Rapid Communications*, vol. 27, no. 7, pp. 473–497, 2006.

[38] L. Barner, T. P. Davis, M. H. Stenzel, and C. Barner-Kowollik, "Complex macromolecular architectures by reversible addition fragmentation chain transfer chemistry: theory and practice," *Macromolecular Rapid Communications*, vol. 28, no. 5, pp. 539–559, 2007.

[39] A. Goto and T. Fukuda, "Kinetics of living radical polymerization," *Progress in Polymer Science*, vol. 29, no. 4, pp. 329–385, 2004.

[40] G. Moad, E. Rizzardo, and S. H. Thang, "Radical addition-fragmentation chemistry in polymer synthesis," *Polymer*, vol. 49, no. 5, pp. 1079–1131, 2008.

[41] C. Barner-Kowollik, *Handbook of RAFT Polymerization*, Wiley-VCH, Weinheim, Germany, 2007.

[42] B. M. Rosen and V. Percec, "Single-electron transfer and single-electron transfer degenerative chain transfer living radical polymerization," *Chemical Reviews*, vol. 109, no. 11, pp. 5069–5119, 2009.

[43] S. Yamago, "Precision polymer synthesis by degenerative transfer controlled/living radical polymerization using organotellurium, organostibine, and organobismuthine chain-transfer agents," *Chemical Reviews*, vol. 109, no. 11, pp. 5051–5068, 2009.

[44] M. Hurtgen, C. Detrembleur, C. Jerome, and A. Debuigne, "Insight into organometallic-mediated radical polymerization," *Polymer Reviews*, vol. 51, no. 2, pp. 188–213, 2011.

[45] M. Sawamoto, J. Fujimori, and T. Higashimura, "Living cationic polymerization of N-vinylcarbazole initiated by hydrogen iodide," *Macromolecules*, vol. 20, no. 5, pp. 916–920, 1987.

[46] T. Fukuda, T. Terauchi, A. Goto, Y. Tsujii, T. Miyamoto, and Y. Shimizu, "Well-defined block copolymers comprising styrene-acrylonitrile random copolymer sequences synthesized by "living" radical polymerization," *Macromolecules*, vol. 29, no. 8, pp. 3050–3052, 1996.

[47] H. Baethge, S. Butz, C. H. Han, and G. Schmidt-Naake, "Rate enhancement of the N-oxyl-controlled free radical copolymerization of styrene with N-vinylcarbazole," *Die Angewandte Makromolekulare Chemie*, vol. 267, pp. 52–56, 1999.

[48] H. Baethge, S. Butz, and G. Schmidt-Naake, "'Living' free radical copolymerization of styrene and N-vinylcarbazole," *Macromolecular Rapid Communications*, vol. 18, no. 10, pp. 911–916, 1997.

[49] M. Nowakowska, S. Zapotoczny, and A. Karewicz, "Polymeric photosensitizers. Part 4. Synthesis of poly(sodium styrenesulfonate-block-N-vinylcarbazole) by nitroxide-mediated free radical polymerization," *Polymer*, vol. 42, no. 5, pp. 1817–1823, 2001.

[50] J. Hua, D. B. Chen, Y. L. Yu et al., "Preparation of C60 bonded poly(N-vinylcarbazole) with C60Cln/CuCl/Bpy catalyst system," *Polymer Bulletin*, vol. 48, no. 2, pp. 135–141, 2002.

[51] J. Hua, D. Chen, X. Jing, L. Xu, Y. Yu, and Y. Zhang, "Preparation and photoconducting property of C60Cln-m-bonded poly(N-vinylcarbazole) with C60Cln/CuCl/Bpy catalyst system," *Journal of Applied Polymer Science*, vol. 87, no. 4, pp. 606–609, 2003.

[52] J. Brandrup and E. H. Immergut, *Polymer Handbook*, John Wiley & Sons, New York, NY, USA, 3rd edition, 1991.

[53] H. Mori, H. Ookuma, S. Nakano, and T. Endo, "Xanthate-mediated controlled radical polymerization of N-vinylcarbazole," *Macromolecular Chemistry and Physics*, vol. 207, no. 12, pp. 1005–1017, 2006.

[54] D. Charmot, P. Corpart, H. Adam, S. Z. Zard, T. Biadatti, and G. Bouhadir, "Controlled radical polymerization in dispersed media," *Macromolecular Symposia*, vol. 150, pp. 23–32, 2000.

[55] D. Taton, A. Z. Wilczewska, and M. Destarac, "Direct synthesis of double hydrophilic statistical di-and triblock copolymers comprised of acrylamide and acrylic acid units via the MADIX process," *Macromolecular Rapid Communications*, vol. 22, no. 18, pp. 1497–1503, 2001.

[56] M. Destarac, D. Taton, S. Z. Zard, T. Saleh, and Y. Six, "On the importance of xanthate substituents in the MADIX process," in *Advances in Controlled/Living Radical Polymerization*, K. Matyjaszewski, Ed., vol. 854 of *ACS Symposinum Series*, chapter 37, pp. 536–550, American Chemical Society, Washington, DC, USA, 2003.

[57] M. H. Stenzel, L. Cummins, G. E. Roberts, T. P. Davis, P. Vana, and C. Barner-Kowollik, "Xanthate mediated living polymerization of vinyl acetate: a systematic variation in MADIX/RAFT agent structure," *Macromolecular Chemistry and Physics*, vol. 204, no. 9, pp. 1160–1168, 2003.

[58] M. L. Coote and L. Radom, "Substituent effects in xanthate-mediated polymerization of vinyl acetate: Ab initio evidence for an alternative fragmentation pathway," *Macromolecules*, vol. 37, no. 2, pp. 590–596, 2004.

[59] M. H. Stenzel, T. P. Davis, and C. Barner-Kowollik, "Poly (vinyl alcohol) star polymers prepared via MADIX/RAFT polymerisation," *Chemical Communications*, vol. 10, no. 13, pp. 1546–1547, 2004.

[60] M. Destarac, D. Charmot, X. Franck, and S. Z. Zard, "Dithiocarbamates as universal reversible addition-fragmentation chain transfer agents," *Macromolecular Rapid Communications*, vol. 21, no. 15, pp. 1035–1039, 2000.

[61] T. L. U. Nguyen, K. Eagles, T. P. Davis, C. Barner-Kowollik, and M. H. Stenzel, "Investigation of the influence of the architectures of poly(vinyl pyrrolidone) polymers made via the reversible addition-fragmentation chain transfer/macromolecular design via the interchange of xanthates mechanism on the stabilization of suspension polymerizations," *Journal of Polymer Science Part A*, vol. 44, no. 15, pp. 4372–4383, 2006.

[62] D. Wan, K. Satoh, M. Kamigaito, and Y. Okamoto, "Xanthate-mediated radical polymerization of N-vinylpyrrolidone in fluoroalcohols for simultaneous control of molecular weight and tacticity," *Macromolecules*, vol. 38, no. 25, pp. 10397–10405, 2005.

[63] R. Devasia, R. L. Bindu, R. Borsali, N. Mougin, and Y. Gnanou, "Controlled radical polymerization of N-vinylpyrrolidone by reversible addition-fragmentation chain transfer process," *Macromolecular Symposia*, vol. 229, pp. 8–17, 2005.

[64] Y. Maki, H. Mori, and T. Endo, "Xanthate-mediated controlled radical polymerization of N-vinylindole derivatives," *Macromolecules*, vol. 40, no. 17, pp. 6119–6130, 2007.

[65] Y. Maki, H. Mori, and T. Endo, "Controlled RAFT polymerization of N-vinylphthalimide and its hydrazinolysis to poly(vinyl amine)," *Macromolecular Chemistry and Physics*, vol. 208, no. 24, pp. 2589–2599, 2007.

[66] Y. Maki, H. Mori, and T. Endo, "Synthesis of well-defined alternating copolymers by RAFT copolymerization of

N-vinylnaphthalimide," *Macromolecules*, vol. 41, no. 22, pp. 8397–8404, 2008.

[67] Y. Maki, H. Mori, and T. Endo, "Synthesis of amphiphilic and double-hydrophilic block copolymers containing polyvinyl amine segments by RAFT polymerization of N-vinylphthalimide," *Macromolecular Chemistry and Physics*, vol. 211, no. 1, pp. 45–56, 2010.

[68] H. Mori, M. Yanagi, and T. Endo, "RAFT polymerization of N-vinylimidazolium salts and synthesis of thermoresponsive ionic liquid block copolymers," *Macromolecules*, vol. 42, no. 21, pp. 8082–8092, 2009.

[69] G. Moad, J. Chiefari, Y. K. Chong et al., "Living free radical polymerization with reversible addition—fragmentation chain transfer (the life of RAFT)," *Polymer International*, vol. 49, no. 9, pp. 993–1001, 2000.

[70] M. Destarac, W. Bzducha, D. Taton, I. Gauthier-Gillaizeau, and S. Z. Zard, "Xanthates as chain-transfer agents in controlled radical polymerization (MADIX): structural effect of the O-alkyl group," *Macromolecular Rapid Communications*, vol. 23, no. 17, pp. 1049–1054, 2002.

[71] A. Favier, C. Barner-Kowollik, T. P. Davis, and M. H. Stenzel, "A detailed on-line FT/NIR and 1H NMR spectroscopic investigation into factors causing inhibition in xanthate-mediated vinyl acetate polymerization," *Macromolecular Chemistry and Physics*, vol. 205, no. 7, pp. 925–936, 2004.

[72] B. Y. K. Chong, T. P. T. Le, G. Moad, E. Rizzardo, and S. H. Thang, "More versatile route to block copolymers and other polymers of complex architecture by living radical polymerization: the RAFT process," *Macromolecules*, vol. 32, no. 6, pp. 2071–2074, 1999.

[73] R. T. A. Mayadunne, E. Rizzardo, J. Chiefari et al., "Living polymers by the use of trithiocarbonates as reversible addition-fragmentation chain transfer (RAFT) agents: ABA triblock copolymers by radical polymerization in two steps," *Macromolecules*, vol. 33, no. 2, pp. 243–245, 2000.

[74] Y. A. Vasilieva, D. B. Thomas, C. W. Scales, and C. L. McCormick, "Direct controlled polymerization of a cationic methacrylamido monomer in aqueous media via the RAFT process," *Macromolecules*, vol. 37, no. 8, pp. 2728–2737, 2004.

[75] P. Vana, T. P. Davis, and C. Barner-Kowollik, "Kinetic analysis of reversible addition fragmentation chain transfer (RAFT) polymerizations: conditions for inhibition, retardation, and optimum living polymerization," *Macromolecular Theory and Simulations*, vol. 11, no. 8, pp. 823–835, 2002.

[76] H. Mori, E. Kudo, Y. Saito, A. Onuma, and M. Morishima, "RAFT polymerization of vinyl sulfonate esters for the controlled synthesis of poly(lithium vinyl sulfonate) and sulfonated block copolymers," *Macromolecules*, vol. 43, no. 17, pp. 7021–7032, 2010.

[77] C. F. Huang, J. A. Yoon, and K. Matyjaszewski, "Synthesis of N-vinylcarbazole-N-vinylpyrrolidone amphiphilic block copolymers by xanthate-mediated controlled radical polymerization," *Canadian Journal of Chemistry*, vol. 88, no. 3, pp. 228–235, 2010.

[78] N. Hu, W. X. Ji, Y. Y. Tong, Z. C. Li, and E. Q. Chen, "Synthesis of diblock copolymers containing poly(N-vinylcarbazole) by reversible addition-fragmentation chain transfer polymerization," *Journal of Polymer Science Part A*, vol. 48, no. 20, pp. 4621–4626, 2010.

[79] N. Suchao-in, S. Chirachanchai, and S. Perrier, "pH-and thermo-multi-responsive fluorescent micelles from block copolymers via reversible addition fragmentation chain transfer (RAFT) polymerization," *Polymer*, vol. 50, no. 17, pp. 4151–4158, 2009.

[80] W. Y. Tam, C. S. K. Mak, A. M. C. Ng, A. B. Djurišič, and W. K. Chan, "Multifunctional poly(N-vinylcarbazole)-based block copolymers and their nanofabrication and photosensitizing properties," *Macromolecular Rapid Communications*, vol. 30, no. 8, pp. 622–626, 2009.

[81] M. Benaglia, J. Chiefari, Y. K. Chong, G. Moad, E. Rizzardo, and S. H. Thang, "Universal (Switchable) RAFT agents," *Journal of the American Chemical Society*, vol. 131, no. 20, pp. 6914–6915, 2009.

[82] D. J. Keddie, C. Guerrero-Sanchez, G. Moad, E. Rizzardo, and S. H. Thang, "Switchable reversible addition-fragmentation chain transfer (raft) polymerization in aqueous solution, n, n -dimethylacrylamide," *Macromolecules*, vol. 44, no. 17, pp. 6738–6745, 2011.

[83] Y. Yan, W. Zhang, Y. Qiu et al., "Universal xanthate-mediated controlled free radical polymerizations of the "less activated" vinyl monomers," *Journal of Polymer Science Part A*, vol. 48, no. 22, pp. 5206–5214, 2010.

[84] M. Heo, J. Kim, J. Y. Kim, and C. Yang, "A first approach to white organic electroluminescence device from a single rod-coil poly[thiophene-block-(N-vinylcarbazole)] diblock copolymer," *Macromolecular Rapid Communications*, vol. 31, no. 23, pp. 2047–2052, 2010.

[85] A. S. Brar and S. Kaur, "Atom transfer radical polymerization of N-vinyl carbazole: optimization to characterization," *Journal of Polymer Science Part A*, vol. 44, no. 5, pp. 1745–1757, 2006.

[86] N. Haridharan and R. Dhamodharan, "Controlled polymerization of carbazole-based vinyl and methacrylate monomers at ambient temperature: a comparative study through ATRP, SET, and SET-RAFT polymerizations," *Journal of Polymer Science Part A*, vol. 49, no. 4, pp. 1021–1032, 2011.

[87] W. Zhang, Y. Yan, N. Zhou et al., "Controlled synthesis and fluorescent properties of poly(9-(4-vinylbenzyl)-9H-carbazole) via nitroxide-mediated living free-radical polymerization," *European Polymer Journal*, vol. 44, no. 10, pp. 3300–3305, 2008.

[88] Y. K. Fang, C. L. Liu, and W. C. Chen, "New random copolymers with pendant carbazole donor and 1,3,4-oxadiazole acceptor for high performance memory device applications," *Journal of Materials Chemistry*, vol. 21, no. 13, pp. 4778–4786, 2011.

[89] B. Lessard, E. J. Y. Ling, M. S. T. Morin, and M. Marić, "Nitroxide-mediated radical copolymerization of methyl methacrylate controlled with a minimal amount of 9-(4-vinylbenzyl)-9H-carbazole," *Journal of Polymer Science Part A*, vol. 49, no. 4, pp. 1033–1045, 2011.

[90] X. Zhu, N. Zhou, Z. Zhang et al., "Cyclic polymers with pendent carbazole units: enhanced fluorescence and redox behavior," *Angewandte Chemie International Edition*, vol. 50, no. 29, pp. 6615–6618, 2011.

[91] H. Mori, S. Nakano, and T. Endo, "Controlled synthesis of poly(N-ethyl-3-vinylcarbazole) and block copolymers via RAFT polymerization," *Macromolecules*, vol. 38, no. 20, pp. 8192–8201, 2005.

[92] H. Mori, H. Iwaya, and T. Endo, "Structures and chiroptical properties of thermoresponsive block copolymers containing L-proline moietiesa," *Macromolecular Chemistry and Physics*, vol. 208, no. 17, pp. 1908–1918, 2007.

[93] H. Mori, H. Iwaya, and T. Endo, "Controlled synthesis of thermoresponsive polymer via RAFT polymerization of an acrylamide containing l-proline moiety," *Reactive and Functional Polymers*, vol. 67, no. 10, pp. 916–927, 2007.

[94] H. Mori and S. Okabayashi, "Synthesis, assembled structure, and chiroptical properties of amino acid-based amphiphilic block copolymers containing carbazole moiety," *Reactive and Functional Polymers*, vol. 69, no. 7, pp. 441–449, 2009.

[95] J. D. Quinn and R. A. Register, "Nitroxide-mediated radical polymerization of N-ethyl-2-vinylcarbazole," *Polymers for Advanced Technologies*, vol. 19, no. 6, pp. 556–559, 2008.

[96] K. Ogino, T. Goma, D. Kageyama, H. Sato, and N. Yonezawa, "Multifunctional block copolymers for organic photorefractive materials," *Journal of Photopolymer Science and Technology*, vol. 19, no. 3, pp. 419–424, 2006.

[97] P. Zhao, Q. D. Ling, W. Z. Wang, J. Ru, S. B. Li, and W. Huang, "Reversible addition-fragmentation chain transfer polymerization of methacrylates containing hole-or electron-transporting groups," *Journal of Polymer Science Part A*, vol. 45, no. 2, pp. 242–252, 2007.

[98] D. Neugebauer, D. Charasim, A. Swinarew et al., "Polymethacrylates with anthryl and carbazolyl groups prepared by atom transfer radical polymerization," *Polymer Journal*, vol. 43, no. 5, pp. 448–454, 2011.

[99] C. Ulbricht, C. R. Becer, A. Winter, D. Veldman, and U. S. Schubert, "Copolymers containing phosphorescent iridium(III) complexes obtained by free and controlled radical polymerization techniques," *Macromolecular Rapid Communications*, vol. 29, no. 24, pp. 1919–1925, 2008.

[100] N. Hadjichristidis, M. Pitsikalis, S. Pispas, and H. Iatrou, "Polymers with complex architecture by living anionic polymerization," *Chemical Reviews*, vol. 101, no. 12, pp. 3747–3792, 2001.

[101] A. Hirao, M. Hayashi, S. Loykulnant et al., "Precise syntheses of chain-multi-functionalized polymers, star-branched polymers, star-linear block polymers, densely branched polymers, and dendritic branched polymers based on iterative approach using functionalized 1,1-diphenylethylene derivatives," *Progress in Polymer Science*, vol. 30, no. 2, pp. 111–182, 2005.

[102] H. Mori and A. H. E. Müller, "New polymeric architectures with (meth)acrylic acid segments," *Progress in Polymer Science*, vol. 28, p. 1403, 2003.

[103] N. Hadjichristidis, H. Iatrou, M. Pitsikalis, S. Pispas, and A. Avgeropoulos, "Linear and non-linear triblock terpolymers. Synthesis, self-assembly in selective solvents and in bulk," *Progress in Polymer Science*, vol. 30, no. 7, pp. 725–782, 2005.

[104] K. V. Bernaerts and F. E. du Prez, "Dual/heterofunctional initiators for the combination of mechanistically distinct polymerization techniques," *Progress in Polymer Science*, vol. 31, no. 8, pp. 671–722, 2006.

[105] Y. Yagci and M. A. Tasdelen, "Mechanistic transformations involving living and controlled/living polymerization methods," *Progress in Polymer Science*, vol. 31, no. 12, pp. 1133–1170, 2006.

[106] D. Taton, Y. Gnanou, R. Matmour et al., "Controlled polymerizations as tools for the design of star-like and dendrimer-like polymers," *Polymer International*, vol. 55, no. 10, pp. 1138–1145, 2006.

[107] H. Mori, H. Ookuma, and T. Endo, "Synthesis of star polymers based on xanthate-mediated controlled radical polymerization of N-vinylcarbazole," *Macromolecular Symposia*, vol. 249-250, pp. 406–411, 2007.

[108] H. Mori, H. Ookuma, and T. Endo, "Poly(N-vinylcarbazole) star polymers and amphiphilic star block copolymers by xanthate-mediated controlled radical polymerization," *Macromolecules*, vol. 41, no. 19, pp. 6925–6934, 2008.

[109] N. Hadjichristidis, S. Pispas, M. Pitsikalis, H. Iatrou, and C. Vlahos, "Asymmetric star polymers: synthesis and properties," *Advances in Polymer Science*, vol. 142, pp. 71–127, 1999.

[110] W. Zhang, W. Zhaing, Z. Zhang et al., "Thermo-responsive fluorescent micelles from amphiphilic A3B miktoarm star copolymers prepared via a combination of SET-LRP and RAFT polymerization," *Journal of Polymer Science Part A*, vol. 48, no. 19, pp. 4268–4278, 2010.

[111] Y. Tao, Q. Xu, N. Li, J. Lu, L. Wang, and X. Xia, "Synthesis and photoluminescent property of star polymers with carbzole pendent and a zinc porphyrin core by ATRP," *Polymer*, vol. 52, no. 19, pp. 4261–4267, 2011.

[112] A. A. Farah and W. J. Pietro, "Atom transfer radical polymerization of N-(ω'-alkylcarbazolyl) methacrylates via the use of novel heteroleptic Ru(II) polypyridyl initiator," *Inorganica Chimica Acta*, vol. 357, no. 13, pp. 3813–3824, 2004.

[113] A. A. Farah and W. J. Pietro, "Synthesis and characterization of multifunctional polymers via atom transfer radical polymerization of N-(ω'-alkylcarbazolyl) methacrylates initiated by Ru(II) polypyridyl chromophores," *Journal of Polymer Science Part A*, vol. 43, no. 23, pp. 6057–6072, 2005.

[114] C. Chang, J. Zhu, Z. Zhang, N. Zhou, Z. Cheng, and X. Zhu, "Synthesizing and characterization of comb-shaped carbazole containing copolymer via combination of ring opening polymerization and nitroxide-mediated polymerization," *Polymer*, vol. 51, no. 9, pp. 1947–1953, 2010.

[115] J. Shen, H. Masaoka, K. Tsuchiya, and K. Ogino, "Synthesis and properties of a novel brush-type copolymers bearing thiophene backbone and 3-(N-carbazolyl)propyl acrylate side chains for light-emitting applications," *Polymer Journal*, vol. 40, no. 5, pp. 421–427, 2008.

[116] B. Zhang, J. Wang, Y. U. Chen et al., "Multiwalled carbon nanotubes covalently functionalized with poly(N-vinylcarbazole) via RAFT polymerization: synthesis and imonliner optical properties," *Journal of Polymer Science Part A*, vol. 48, no. 14, pp. 3161–3168, 2010.

[117] B. Zhang, Y. U. Chen, X. Zhuang et al., "Poly(N-vinylcarbazole) chemically modified graphene oxide," *Journal of Polymer Science Part A*, vol. 48, no. 12, pp. 2642–2649, 2010.

[118] B. Zhang, Y. Chen, L. Xu et al., "Growing poly(N-vinylcarbazole) from the surface of graphene oxide via RAFT polymerization," *Journal of Polymer Science Part A*, vol. 49, no. 9, pp. 2043–2050, 2011.

[119] J. Hua, D. Chen, X. Jing, L. Xu, Y. Yu, and Y. Zhang, "Preparation and Photoconducting Property of $C_{60}Cl_{n-m}$-Bonded Poly(*N*-vinylcarbazole) with $C_{60}Cl_n$/CuCl/Bpy Catalyst System," *Journal of Applied Polymer Science*, vol. 84, 2003.

[120] J. Hua, W. Yang, and Y. Zhu, "Optical-limiting effect of C_{60} bonded poly(*N*-vinylcarbazole) initiated with $C_{60}Cl_n$/CuCl/Bpy catalyst system," *Materials Letters*, vol. 59, p. 644, 2005.

[121] T.-L. Wang, C.-H. Yang, Y.-T. Shieh, A.-C. Yeh, L.-W. Juan, and H. C. Zeng, "Synthesis of new nanocrystal-polymer nanocomposite as the electron acceptor in polymer bulk heterojunction solar cells," *European Polymer Journal*, vol. 46, p. 634, 2009.

[122] T. L. Wang, C. H. Yang, Y. T. Shieh, and A. C. Yeh, "Synthesis of CdSe-Poly(N-vinylcarbazole) nanocomposite by atom transfer radical polymerization for potential optoelectronic applications," *Macromolecular Rapid Communications*, vol. 30, no. 19, pp. 1679–1683, 2009.

[123] M. Feng, Y. Chen, N. He et al., "Ultrasound-assisted bulk synthesis of CdS-PVK nanocomposites via RAFT

polymerization," *Journal of Polymer Science Part A*, vol. 46, no. 16, pp. 5702–5707, 2008.

[124] M. Sato, A. Kawata, S. Morito, Y. Sato, and I. Yamaguchi, "Preparation and properties of polymer/zinc oxide nanocomposites using functionalized zinc oxide quantum dots," *European Polymer Journal*, vol. 44, no. 11, pp. 3430–3438, 2008.

[125] J. Liu, W. He, L. Zhang et al., "Bifunctional Nanoparticles with Fluorescence and Magnetism via Surface-Initiated AGET ATRP Mediated by an Iron Catalyst," *Langmuir*, vol. 27, pp. 12684–12692, 2011.

[126] Q. Li, L. Zhang, L. Bai et al., "Multistimuli-responsive hybrid nanoparticles with magnetic core and thermoresponsive fluorescence-labeled shell via surface-initiated RAFT polymerization," *Soft Matter*, vol. 7, no. 15, pp. 6958–6966, 2011.

[127] T. M. Fulghum, P. Taranekar, and R. C. Advincula, "Grafting hole-transport precursor polymer brushes on ITO electrodes: surface-initiated polymerization and conjugated polymer network formation of PVK," *Macromolecules*, vol. 41, no. 15, pp. 5681–5687, 2008.

[128] M. C. Tria, K. S. Liao, N. Alley, S. Curran, and R. Advincula, "Electrochemically crosslinked surface-grafted PVK polymer brushes as a hole transport layer for organic photovoltaics," *Journal of Materials Chemistry*, vol. 21, no. 28, pp. 10261–10264, 2011.

[129] Y. Wei, D. Gao, L. Li, and S. Shang, "Memory effect in polymer brushes containing pendant carbazole groups," *Polymer*, vol. 52, no. 6, pp. 1385–1390, 2011.

Hindawi Publishing Corporation
International Journal of Polymer Science
Volume 2012, Article ID 974204, 8 pages
doi:10.1155/2012/974204

Research Article

Polymerization of Phenylacetylene-Based Monodendrons with Alkoxy Peripheral Groups and Oxygen/Nitrogen Permeation Behavior of Their Membranes

Takashi Kaneko,[1,2,3] Kazuaki Sato,[2] Yoshihiko Uchiya,[3] Masahiro Teraguchi,[1,2,3] and Toshiki Aoki[1,2,3,4]

[1] *Center for Transdisciplinary Research, Niigata University, Ikarashi 2-8050, Niigata 950-2181, Japan*
[2] *Department of Chemistry and Chemical Engineering, Faculty of Engineering, Niigata University, Ikarashi 2-8050, Niigata 950-2181, Japan*
[3] *Graduate School of Science and Technology, Niigata University, Ikarashi 2-8050, Niigata 950-2181, Japan*
[4] *Venture Business Laboratory, Niigata University, Ikarashi 2-8050, Niigata 950-2181, Japan*

Correspondence should be addressed to Takashi Kaneko, kanetaka@gs.niigata-u.ac.jp

Received 11 August 2011; Accepted 28 November 2011

Academic Editor: Eri Yoshida

Monodendron monomers with alkoxy peripheral groups were synthesized, and the focal point of monodendrons, terminal acetylene, was polymerized with rhodium catalyst to yield corresponding polydendrons with a high molecular weight. The polydendrons were soluble in common organic solvents and readily formed membranes. Oxygen permselectivity was improved in the polydendrons with a space-persistent dendritic crowd. It was found that the well-defined dendritic and rod-like structure of the polydendrons was useful for permselective membrane.

1. Introduction

The chemical structure and/or morphology of polymers play an important role for the permselectivity of nonporous membranes. Recently, dendrimers have attracted much attention in organic and polymer chemistry due to their novel properties or functions, which are based on their specific shapes and precisely defined three-dimensional structures [1–3]. Dendrimers are characterized by a regularly—and fractally—branched treelike architecture. This feature provides a nanoscale homogeneous space in the dendrimers particularly suited for rigid molecular architectures. Additionally, the center and periphery of dendrimer molecule can be modified by substituent groups, which may aid molecular recognition [4].

We have previously synthesized monodendron monomers consisting of *m*-linked phenyleneethynylene repeating unit with trimethylsilyl peripheral groups and oligo(dimethylsiloxane) chains and obtained the corresponding polydendrons by polymerization of the monomers using a rhodium (Rh) catalyst [5, 6]. The polydendrons were mechanically stable and excellent for preparing self-supporting membranes. The first-generation polydendron (polyTMS1H) membrane showed an oxygen permselectivity higher than that of the corresponding zero-generation poly(phenylacetylene) derivative (polyTMS0H). In this study, we synthesized polydendrons with alkoxy peripheral groups as shown in Scheme 1 because alkyl domain that would have better gas barrier property than that of oligo(dimethylsiloxane) domain would be suitable to study the effect of dendritic domain on the gas permselectivity. We examined the oxygen permselectivity of their membranes in relation to their chemical structures.

2. Experimental

2.1. Materials. 3,5-Dibromo-1-(3-hydroxyl-3-methylbutynyl)benzene was synthesized as previously described [7].

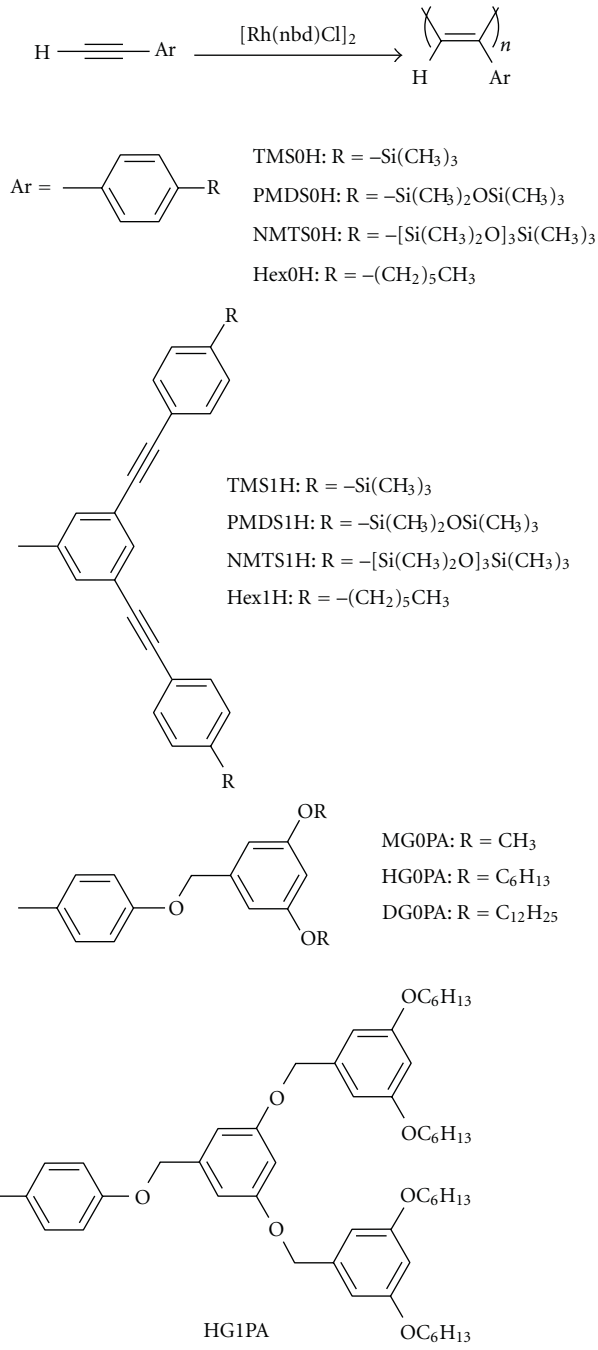

Scheme 1

3,5-Dimethoxybenzyl chloride [8], 3,5-dihexyloxybenzyl alcohol [9], 3,5-didodecyloxybenzyl alcohol [10], 3,5-bis(3,5-dihexyloxybenzyloxy)benzyl alcohol [11], and (4-hexyloxyphenyl)acetylene (**Hex0H**) [12] were synthesized according to the literature procedures. (Bicyclo [2.2.1]hepta-2,5-diene)chlororhodium(I) dimer catalyst ($[Rh(nbd)Cl]_2$) (Aldrich Co.), bis(triphenylphosphine)palladium(II) chloride (Aldrich Co.), and *n*-butyllithium (Kanto Chemical Co., Inc., 1.6 M in hexane) were used without further purification. Other conventional reagents were used as received or purified by conventional method.

2.2. Synthesis of Monomers. The general procedure of *3,5-dialkoxybenzyl chloride* is as follows. A solution of 3,5-dialkoxybenzyl alcohol (5 mmol), DMF (0.5 mL), and thionyl chloride (10 mmol) in chloroform (25 mL) was stirred at room temperature for 2–12 h. The excess thionyl chloride and solvents were evaporated under reduced pressure, and then the residue was dissolved in diethyl ether. The ether solution was washed with water, then dried over anhydrous sodium sulfate, filtered, and evaporated. Then, 3,5-dialkoxybenzyl chloride was obtained without further purification.

3,5-Dihexyloxybenzyl Chloride. Yield 94%. IR (KBr; cm^{-1}): 2872–2936 (C–H). ^{1}H NMR ($CDCl_3$, 270 MHz; ppm): δ 0.91 (t, 6H, J = 6.8 Hz, CH_3), 1.33 (m, 8H, CH_2), 1.44 (m, 4H, CH_2), 1.77 (m, 4H, CH_2), 3.93 (t, 4H, J = 6.5 Hz, CH_2O), 4.50 (s, 2H, CH_2Cl), 6.39 (t, 1H, J = 2.4 Hz, ArH), 6.51 (d, 2H, J = 2.4 Hz, ArH). ^{13}C NMR ($CDCl_3$; ppm): δ 14.10, 22.66, 25.68, 29.07, 31.55, 46.46, 68.07, 101.17, 106.78, 139.16, 160.26.

3,5-Didodecyloxybenzyl Chloride. Yield 76%. IR (KBr; cm^{-1}): 2856–2928 (C–H). ^{1}H NMR ($CDCl_3$, 500 MHz; ppm): δ 0.88 (t, 6H, J = 6.5 Hz, CH_3), 1.27 (m, 32H, CH_2), 1.44 (m, 4H, CH_2), 1.76 (m, 4H, CH_2), 3.93 (t, 4H, J = 6.5 Hz, CH_2O), 4.50 (s, 2H, CH_2Cl), 6.40 (t, 1H, J = 2.5 Hz, ArH), 6.51 (d, 2H, J = 2.5 Hz, ArH).

3,5-Bis(3,5-dihexyloxybenzyloxy)benzyl chloride. Yield 99%. IR (KBr; cm^{-1}): 2868–2944 (C–H). ^{1}H NMR ($CDCl_3$, 270 MHz; ppm): δ 0.90 (t, 12H, J = 7.0 Hz, CH_3), 1.34 (m, 16H, CH_2), 1.45 (m, 8H, CH_2), 1.76 (m, 8H, CH_2), 3.93 (t, 8H, J = 6.5 Hz, CH_2O), 4.50 (s, 2H, CH_2Cl), 4.94 (s, 4H, CH_2O), 6.40 (t, 2H, J = 2.2 Hz, ArH), 6.51 (d, 4H, J = 2.2 Hz, ArH), 6.55 (t, 1H, J = 2.2 Hz, ArH), 6.62 (d, 2H, J = 2.2 Hz, ArH). ^{13}C NMR ($CDCl_3$; ppm): δ 14.14, 22.68, 25.79, 29.27, 31.64, 46.35, 68.04, 70.15, 100.75, 101.99, 105.62, 107.53, 138.62, 139.34, 159.88, 160.33.

4-Bromo-1-(3,5-dimethoxybenzyloxy)benzene. A mixture of 4-bromophenol (13 g, 74 mmol), 3,5-dimethoxybenzyl chloride (15 g, 81 mmol), K_2CO_3 (22 g, 0.16 mol), and 18-crown-6 (3.0 g, 11 mmol) in acetone (200 mL) was refluxed for 18 h. After removal of the solvent, the residue was extracted with dichloromethane. The organic layer was washed with brine, then dried over anhydrous sodium sulfate, filtered, and evaporated. The crude product was purified by silica-gel column separation with dichloromethane/hexane (1/1 v/v) as an eluent to give 4-bromo-1-(3,5-dimethoxybenzyloxy)benzene (19 g, 58 mmol). Yield 78%; mp 75°C. TLC (dichloromethane/hexane (1/1 v/v)): R_f = 0.14. IR (KBr; cm^{-1}): 2844–2944 (C–H). ^{1}H NMR ($CDCl_3$, 270 MHz; ppm): δ 3.77 (s, 6H, CH_3), 4.96 (s, 2H, CH_2), 6.41 (t, 1H, J = 2.4 Hz, ArH), 6.55 (d, 2H, J = 2.4 Hz, ArH), 6.83 (d, 2H, J = 8.9 Hz, ArH), 7.36 (d, 2H, J = 8.9 Hz, ArH). ^{13}C NMR ($CDCl_3$; ppm): δ 55.36, 70.10, 99.80, 105.05, 113.04, 116.58, 132.13, 138.78, 157.57, 160.85.

1-(3,5-Dimethoxybenzyloxy)-4-(3-hydroxyl-3-methylbutynyl) benzene. 2-Methyl-3-butyn-2-ol (10 mL, 0.10 mol) was added to a triethylamine solution (110 mL) of 4-bromo-1-(3,5-dimethoxybenzyloxy)benzene (18 g, 55 mmol), bis (triphenylphosphine)palladium (II) chloride (0.14 g, 0.2 mmol), triphenylphosphine (0.72 g, 2.7 mmol), and copper (I) iodide (0.34 g, 1.8 mmol) under a nitrogen atmosphere. The solution was stirred for 18 h at 90°C. After cooling, the mixture was treated with aqueous 4 N HCl, extracted with dichloromethane, and washed with brine. The organic layer was dried over anhydrous sodium sulfate, and the solvent was removed under reduced pressure. The crude product was purified by silica gel column separation with dichloromethane as an eluent to give 1-(3,5-dimethoxybenzyloxy)-4-(3-hydroxyl-3-methylbutynyl)benzene (5.5 g, 17 mmol). Yield 31%. TLC (dichloromethane): R_f = 0.15. IR (KBr; cm^{-1}): 3324 (–OH), 2848–2988 (C–H), 2228 (C≡C). ^{1}H NMR ($CDCl_3$, 270 MHz; ppm): δ 1.61 (s, 6H, CH_3), 2.11 (s, 1H, –OH), 3.79 (s, 6H, CH_3), 4.99 (s, 2H, CH_2), 6.41 (t, 1H, J = 2.2 Hz, ArH), 6.56 (d, 2H, J = 2.2 Hz, ArH), 6.88 (d, 2H, J = 8.9 Hz, ArH), 7.34 (d, 2H, J = 8.9 Hz, ArH). ^{13}C NMR ($CDCl_3$; ppm): δ 31.61, 55.36, 65.61, 69.89, 81.89, 92.45, 99.82, 105.08, 114.69, 115.03, 132.94, 138.81, 158.44, 160.82.

*[4-(3,5-Dimethoxybenzyloxy)phenyl]acetylene (**MG0PA**).* Sodium hydride (2.0 g, 50 mmol) was added to a toluene solution (65 mL) of 1-(3,5-dimethoxybenzyloxy)-4-(3-hydroxyl-3-methylbutynyl)benzene (5.5 g, 17 mmol). The solution was refluxed for 2 h under a nitrogen atmosphere. After cooling, the mixture was treated with water, extracted with dichloromethane, and washed with brine. The organic layer was dried over anhydrous sodium sulfate, and the solvent was removed under reduced pressure. The crude product was purified by silica gel column separation with dichloromethane as an eluent to give **MG0PA** (1.1 g, 4.3 mmol). Yield 25%; mp 60°C. TLC (hexane): R_f = 0.75. IR (KBr; cm^{-1}): 3296 (≡C–H), 2848–2988 (C–H), 2112 (C≡C). ^{1}H NMR ($CDCl_3$, 270 MHz; ppm): δ 3.00 (s, 1H, C≡C–H), 3.78 (s, 6H, CH_3), 4.98 (s, 2H, CH_2), 6.40 (t, 1H, J = 1.9 Hz, ArH), 6.55 (d, 2H, J = 1.9 Hz, ArH), 6.89 (d, 2H, J = 8.9 Hz, ArH), 7.41 (d, 2H, J = 8.9 Hz, ArH). ^{13}C NMR ($CDCl_3$; ppm): δ 55.32, 69.87, 75.96, 83.53, 99.80, 105.04, 114.31, 114.70, 133.43, 138.71, 158.79, 160.81.

4-Bromo-1-(3,5-didodecyloxybenzyloxy)benzene. A mixture of 4-bromophenol (1.9 g, 11 mmol), 3,5-didodecyloxybenzyl chloride (6.0 g, 12 mmol), K_2CO_3 (3.3 g, 24 mmol), and 18-crown-6 (3.2 g, 12 mmol) in acetone (60 mL) was refluxed for 87 h. The mixture was worked up in the same manner as described above, and the crude product was purified by silica gel column separation with dichloromethane/hexane (1/2 v/v) as an eluent to give 4-bromo-1-(3,5-didodecyloxybenzyloxy)benzene (5.3 g, 8.3 mmol). Yield 76%. TLC (dichloromethane/hexane (1/2 v/v)): R_f = 0.90. IR (KBr; cm^{-1}): 2856–2928 (C–H). ^{1}H NMR ($CDCl_3$, 500 MHz; ppm): δ 0.88 (t, 6H, J = 6.8 Hz, CH_3), 1.26 (m, 32H, CH_2), 1.43 (m, 4H, CH_2), 1.76 (m, 4H, CH_2), 3.92 (t, 4H, J = 6.8 Hz, CH_2O), 4.95 (s, 2H, CH_2O), 6.40 (t, 1H, J = 2.3 Hz, ArH), 6.52 (d, 2H, J = 2.3 Hz, ArH), 6.84 (d, 2H, J = 8.8 Hz, ArH), 7.36 (d, 2H, J = 8.8 Hz, ArH).

1-(3,5-Didodecyloxybenzyloxy)-4-(3-hydroxyl-3-methylbutynyl)benzene. 2-Methyl-3-butyn-2-ol (1.2 mL, 12 mmol) was added to a triethylamine solution (12 mL) of 4-bromo-1-(3,5-didodecyloxybenzyloxy)benzene (4.0 g, 6.3 mmol), bis(triphenylphosphine)palladium (II) chloride (1.6 mg, 0.0022 mmol), triphenylphosphine (2.8 mg, 0.010 mmol), and copper (I) iodide (1.5 mg, 0.0077 mmol) under a nitrogen atmosphere. The solution was stirred for 24 h at 90°C. The mixture was worked up in the same manner as described above, and the crude product was purified by silica gel column separation with dichloromethane/hexane (1/2 v/v) as an eluent to give 1-(3,5-didodecyloxybenzyloxy)-4-(3-hydroxyl-3-methylbutynyl)benzene (1.6 g, 2.5 mmol). Yield 40%. IR (KBr; cm^{-1}): 3324 (–OH), 2856–2928 (C–H), 2240 (C≡C). ^{1}H NMR ($CDCl_3$, 500 MHz; ppm): δ 0.88 (t, 6H, J = 6.5 Hz, CH_3), 1.26 (m, 32H, CH_2), 1.42 (m, 4H, CH_2), 1.60 (s, 6H, CH_3), 1.76 (m, 4H, CH_2), 2.04 (s, 1H, –OH), 3.92 (t, 4H, J = 6.5 Hz, CH_2O), 4.98 (s, 2H, CH_2O), 6.40 (t, 1H, J = 2.0 Hz, ArH), 6.53 (d, 2H, J = 2.0 Hz, ArH), 6.88 (d, 2H, J = 8.5 Hz, ArH), 7.34 (d, 2H, J = 8.5 Hz, ArH). ^{13}C NMR ($CDCl_3$; ppm): δ 14.18, 22.67, 26.03, 29.23, 29.34, 29.38, 29.56, 29.58, 29.62, 29.65, 31.56, 31.91, 65.63, 68.07, 70.01, 81.96, 92.44, 100.79, 105.60, 114.80, 115.05, 133.04, 138.75, 158.70, 160.53.

*[4-(3,5-Didodecyloxybenzyloxy)phenyl]acetylene (**DG0PA**).* Catalytic amounts of sodium hydride were added to a toluene solution (12 mL) of 1-(3,5-didodecyloxybenzyloxy)-4-(3-hydroxyl-3-methylbutynyl)benzene (0.90 g, 1.4 mmol). The solution was refluxed for 3 h under a nitrogen atmosphere. The mixture was worked up in the same manner as described above, and the crude product was purified by silica gel column separation with dichloromethane/hexane (1/1 v/v) and hexane as an eluent to give **DG0PA** (0.45 g, 0.78 mmol). Yield 55%. TLC (dichloromethane/hexane (1/1 v/v)): R_f = 0.71. IR (KBr; cm^{-1}): 3328 (≡C–H), 2856–2924 (C–H), 2112 (C≡C). ^{1}H NMR ($CDCl_3$, 500 MHz; ppm): δ 0.88 (t, 6H, J = 7.0 Hz, CH_3), 1.26 (m, 32H, CH_2), 1.43 (m, 4H, CH_2), 1.76 (m, 4H, CH_2), 2.99 (s, 1H, C≡C–H), 3.92 (t, 4H, J = 6.5 Hz, CH_2O), 4.98 (s, 2H, CH_2O), 6.40 (t, 1H, J = 2.0 Hz, ArH), 6.53 (d, 2H, J = 2.0 Hz, ArH), 6.90 (d, 2H, J = 8.5 Hz, ArH), 7.41 (d, 2H, J = 8.5 Hz, ArH). ^{13}C NMR ($CDCl_3$; ppm): δ 14.11, 22.68, 26.03, 29.23, 29.34, 29.38, 29.56, 29.59, 29.63, 29.65, 31.91, 68.06, 70.02, 75.81, 83.60, 100.78, 105.56, 114.38, 114.83, 133.56, 138.66, 159.06, 160.53.

4-Iodo-1-(3,5-dihexyloxybenzyloxy)benzene. A mixture of 4-iodophenol (18 g, 80 mmol), 3,5-dihexyloxybenzyl chloride (29 g, 88 mmol), K_2CO_3 (24 g, 18 mmol), and 18-crown-6 (23 g, 88 mmol) in acetone (530 mL) was refluxed for 8 h. The mixture was worked up in the same manner as described above, and the crude product was purified by silica gel column separation with

dichloromethane/hexane (1/3 v/v) as an eluent to give 4-iodo-1-(3,5-dihexyloxybenzyloxy)benzene (37 g, 73 mmol). Yield 91%. TLC (dichloromethane/hexane (1/3 v/v)): R_f = 0.40. IR (KBr; cm^{-1}): 2872–2936 (C–H). ^{1}H NMR ($CDCl_3$, 270 MHz; ppm): δ 0.90 (t, 6H, J = 6.8 Hz, CH_3), 1.32 (m, 8H, CH_2), 1.44 (m, 4H, CH_2), 1.76 (m, 4H, CH_2), 3.92 (t, 4H, J = 6.8 Hz, CH_2O), 4.94 (s, 2H, CH_2O), 6.39 (t, 1H, J = 2.2 Hz, ArH), 6.52 (d, 2H, J = 2.2 Hz, ArH), 6.73 (d, 2H, J = 9.3 Hz, ArH), 7.53 (d, 2H, J = 9.3 Hz, ArH). ^{13}C NMR ($CDCl_3$; ppm): δ 14.13, 22.68, 25.79, 29.27, 31.64, 68.07, 70.08, 82.99, 100.72, 105.48, 117.22, 138.07, 138.57, 158.43, 160.39.

1-[4-(3,5-Dihexyloxybenzyloxy)phenyl]-2-trimethylsilylacetylene. Trimethylsilylacetylene (19 mL, 0.14 mol) was added to a triethylamine solution (140 mL) of 4-iodo-1-(3,5-dihexyloxybenzyloxy)benzene (36 g, 70 mmol), bis(triphenylphosphine)palladium (II) chloride (84 mg, 0.12 mmol), triphenylphosphine (87 mg, 0.33 mmol), and copper (I) iodide (46 mg, 0.24 mmol) under a nitrogen atmosphere. The solution was stirred for 10 h at 60°C. The mixture was worked up in the same manner as described above, and the crude product was purified by silica gel column separation with dichloromethane/hexane (1/2 v/v) as an eluent to give 1-[4-(3,5-dihexyloxybenzyloxy)phenyl]-2-trimethylsilylacetylene (25 g, 53 mmol). Yield 76%. IR (KBr; cm^{-1}): 2872–2964 (C–H), 2160 (C≡C). ^{1}H NMR ($CDCl_3$, 270 MHz; ppm): δ 0.24 (s, 9H, $Si(CH_3)_3$), 0.91 (t, 6H, J = 6.8 Hz, CH_3), 1.33 (m, 8H, CH_2), 1.45 (m, 4H, CH_2), 1.76 (m, 4H, CH_2), 3.93 (t, 4H, J = 6.5 Hz, CH_2O), 4.98 (s, 2H, CH_2O), 6.40 (t, 1H, J = 2.4 Hz, ArH), 6.53 (d, 2H, J = 2.4 Hz, ArH), 6.88 (d, 2H, J = 8.9 Hz, ArH), 7.39 (d, 2H, J = 8.9 Hz, ArH). ^{13}C NMR ($CDCl_3$; ppm): δ 0.17, 14.14, 22.68, 25.79, 29.26, 31.64, 68.05, 69.97, 92.46, 100.71, 105.07, 105.49, 114.64, 115.39, 133.33, 138.58, 158.69, 160.35.

*[4-(3,5-Dihexyloxybenzyloxy)phenyl]acetylene (**HG0PA**).* A mixture of 1-[4-(3,5-dihexyloxybenzyloxy)phenyl]-2-trimethylsilylacetylene (4.8 g, 10 mmol) and K_2CO_3 (0.14 g, 1.0 mmol) in methanol (200 mL) was stirred at room temperature for 20 h. After removal of the solvent, the residue was extracted with dichloromethane. The organic layer was washed with brine, then dried over anhydrous sodium sulfate, filtered, and evaporated. The crude product was purified by silica gel column separation with dichloromethane/hexane (1/4 v/v) as an eluent to give **HG0PA** (3.5 g, 8.4 mmol). Yield 84%. TLC (dichloromethane/hexane (1/4 v/v)): R_f = 0.76. IR (KBr; cm^{-1}): 3332 (≡C–H), 2860–2932 (C–H), 2160 (C≡C). ^{1}H NMR ($CDCl_3$, 270 MHz; ppm): δ 0.90 (t, 6H, J = 6.8 Hz, CH_3), 1.33 (m, 8H, CH_2), 1.44 (m, 4H, CH_2), 1.76 (m, 4H, CH_2), 2.99 (s, 1H, C≡C–H), 3.93 (t, 4H, J = 6.6 Hz, CH_2O), 4.96 (s, 2H, CH_2O), 6.40 (t, 1H, J = 2.2 Hz, ArH), 6.53 (d, 2H, J = 2.2 Hz, ArH), 6.89 (d, 2H, J = 8.9 Hz, ArH), 7.41 (d, 2H, J = 8.9 Hz, ArH). ^{13}C NMR ($CDCl_3$; ppm): δ 14.13, 22.68, 25.79, 29.27, 31.64, 68.08, 70.04, 75.82, 83.60, 100.75, 105.53, 114.31, 114.77, 133.47, 138.57, 158.92, 160.39.

4-Iodo-1-[3,5-bis(3,5-dihexyloxybenzyloxy)benzyloxy]benzene. A mixture of 4-iodophenol (3.7 g, 17 mmol), 3,5-bis(3,5-dihexyloxybenzyloxy)benzyl chloride (13 g, 17 mmol), K_2CO_3 (4.7 g, 34 mmol), and 18-crown-6 (0.56 g, 2.1 mmol) in acetone (130 mL) was refluxed for 115 h. The mixture was worked up in the same manner as described above, and the crude product was purified by silica gel column separation with ethyl acetate/hexane (1/8 v/v) as an eluent to give 4-iodo-1-[3,5-bis(3,5-dihexyloxybenzyloxy)benzyloxy]benzene (11 g, 12 mmol). Yield 72%. TLC (ethyl acetate/hexane (1/8 v/v)): R_f = 0.64. IR (KBr; cm^{-1}): 2864–2936 (C–H). ^{1}H NMR ($CDCl_3$, 270 MHz; ppm): δ 0.90 (t, 12H, J = 6.9 Hz, CH_3), 1.33 (m, 16H, CH_2), 1.45 (m, 8H, CH_2), 1.76 (m, 8H, CH_2), 3.93 (t, 8H, J = 6.6 Hz, CH_2O), 4.94 (s, 4H, CH_2O), 4.95 (s, 2H, CH_2O), 6.40 (t, 2H, J = 2.2 Hz, ArH), 6.54 (d, 4H, J = 2.2 Hz, ArH), 6.55 (t, 1H, J = 2.2 Hz, ArH), 6.62 (d, 2H, J = 2.2 Hz, ArH), 6.71 (d, 2H, J = 9.0 Hz, ArH), 7.53 (d, 2H, J = 9.0 Hz, ArH). ^{13}C NMR ($CDCl_3$; ppm): δ 14.15, 22.69, 25.80, 29.28, 31.64, 68.05, 69.93, 70.13, 83.07, 100.69, 101.50, 105.62, 106.11, 117.20, 138.07, 138.70, 138.75, 158.31, 159.97, 160.32.

1-{4-[3,5-Bis(3,5-dihexyloxybenzyloxy)benzyloxy]phenyl}-2-trimethylsilylacetylene. Trimethylsilylacetylene (1.4 mL, 10 mmol) was added to a triethylamine solution (10 mL) of 4-iodo-1-[3,5-bis(3,5-dihexyloxybenzyloxy)benzyloxy]benzene (4.6 g, 5.0 mmol), bis(triphenylphosphine) palladium (II) chloride (10 mg, 0.015 mmol), triphenylphosphine (4.2 mg, 0.016 mmol), and copper (I) iodide (17 mg, 0.090 mmol) under a nitrogen atmosphere. The solution was stirred for 14 h at 75°C. The mixture was worked up in the same manner as described above, and the crude product was purified by silica gel column separation with dichloromethane/hexane (1/2 v/v) as an eluent to give 1-{4-[3,5-bis(3,5-dihexyloxybenzyloxy)benzyloxy]phenyl}-2-trimethylsilylacetylene (3.5 g, 4.0 mmol). Yield 79%. IR (KBr; cm^{-1}): 2864–2936 (C–H), 2160 (C≡C). ^{1}H NMR ($CDCl_3$, 500 MHz; ppm): δ 0.24 (s, 9H, $Si(CH_3)_3$), 0.90 (t, 12H, J = 7.0 Hz, CH_3), 1.33 (m, 16H, CH_2), 1.45 (m, 8H, CH_2), 1.76 (m, 8H, CH_2), 3.93 (t, 8H, J = 6.8 Hz, CH_2O), 4.94 (s, 4H, CH_2O), 4.99 (s, 2H, CH_2O), 6.40 (t, 2H, J = 2.2 Hz, ArH), 6.54 (d, 4H, J = 2.2 Hz, ArH), 6.56 (t, 1H, J = 2.2 Hz, ArH), 6.63 (d, 2H, J = 2.2 Hz, ArH), 6.86 (d, 2H, J = 9.0 Hz, ArH), 7.38 (d, 2H, J = 9.0 Hz, ArH). ^{13}C NMR ($CDCl_3$; ppm): δ 0.04, 14.03, 22.59, 25.72, 29.21, 31.57, 68.05, 69.85, 70.15, 92.53, 100.79, 101.60, 105.11, 105.69, 106.22, 114.72, 115.55, 133.44, 138.86, 138.92, 158.76, 160.13, 160.49.

*{4-[3,5-Bis(3,5-dihexyloxybenzyloxy)benzyloxy]phenyl}acetylene (**HG1PA**).* A mixture of 1-{4-[3,5-bis(3,5-dihexyloxybenzyloxy)benzyloxy]phenyl}-2-trimethylsilylacetylene (3.5 g, 4.0 mmol) and K_2CO_3 (78 mg, 0.57 mmol) in methanol/diethyl ether (160 mL/50 mL) was stirred at room temperature for 24 h. The mixture was worked up in the same manner as described above, and the crude product was purified by silica gel column separation

with dichloromethane/hexane (1/1 v/v) as an eluent to give **HG1PA** (2.3 g, 2.8 mmol). Yield 69%. TLC (dichloromethane/hexane (1/1 v/v)): R_f = 0.43. IR (KBr; cm^{-1}): 3296 (≡C–H), 2864–2940 (C–H), 2112 (C≡C). ^{1}H NMR ($CDCl_3$, 270 MHz; ppm): δ 0.90 (t, 12H, J = 6.5 Hz, CH_3), 1.33 (m, 16H, CH_2), 1.45 (m, 8H, CH_2), 1.76 (m, 8H, CH_2), 2.99 (s, 1H, C≡C–H), 3.93 (t, 8H, J = 6.5 Hz, CH_2O), 4.94 (s, 4H, CH_2O), 4.99 (s, 2H, CH_2O), 6.40 (t, 2H, J = 2.2 Hz, ArH), 6.54 (d, 4H, J = 2.2 Hz, ArH), 6.56 (t, 1H, J = 2.2 Hz, ArH), 6.64 (d, 2H, J = 2.2 Hz, ArH), 6.88 (d, 2H, J = 8.8 Hz, ArH), 7.41 (d, 2H, J = 8.8 Hz, ArH). ^{13}C NMR ($CDCl_3$; ppm): δ 14.16, 22.70, 25.81, 29.29, 31.66, 68.06, 69.90, 70.15, 75.86, 83.58, 100.72, 101.54, 105.63, 106.16, 114.36, 114.77, 133.47, 138.72, 138.77, 158.82, 159.99, 160.35.

1-(3-Hydroxyl-3-methylbutynyl)-3,5-bis [(4-hexyloxyphenyl) ethynyl]benzene. A triethylamine (40 mL) solution of 4-[2-(3,5-dibromophenyl)ethynyl]-1-(3-hydroxyl-3-methylbutynyl) benzene (11 g, 35 mmol), **Hex0H** (14 g, 70 mmol), bis(triphenylphosphine)palladium (II) chloride (0.23 g, 0.33 mmol), triphenylphosphine (0.47 g, 1.8 mmol), and copper (I) iodide (0.24 g, 1.3 mmol) was stirred for 16 h at 95°C under a nitrogen atmosphere. The mixture was worked up in the same manner as described above, and the crude product was purified by silica gel column separation with dichloromethane as an eluent to give 1-(3-hydroxyl-3-methylbutynyl)-3,5-bis [(4-hexyloxyphenyl) ethynyl]benzene. (12 g, 21 mmol). Yield 60%. TLC (dichloromethane): R_f = 0.34. IR (KBr; cm^{-1}): 3464 (–OH), 2960 (C–H), 2212 (C≡C). ^{1}H NMR ($CDCl_3$, 500 MHz; ppm): δ 0.91 (t, 6H, J = 7.0 Hz, CH_3), 1.35 (m, 8H, CH_2), 1.46 (m, 4H, CH_2), 1.62 (s, 6H, CH_3), 1.79 (m, 4H, CH_2), 2.01 (s, 1H, OH), 3.97 (t, 4H, J = 6.7 Hz, CH_2O), 6.87 (d, 4H, J = 8.8 Hz, ArH), 7.44 (d, 4H, J = 8.8 Hz, ArH), 7.48 (d, 2H, J = 2.0 Hz, ArH), 7.57 (t, 1H, J = 2.0 Hz, ArH). ^{13}C NMR ($CDCl_3$; ppm): δ 14.03, 22.59, 25.68, 29.14, 31.41, 31.56, 65.58, 68.10, 80.87, 86.52, 90.59, 94.62, 114.58, 123.28, 124.25, 133.11, 133.35, 133.58, 133.74, 159.46.

*{3,5-Bis [(4-hexyloxyphenyl)ethynyl]phenyl} acetylene (**Hex1H**).* 1-(3-Hydroxyl-3-methylbutynyl)-3,5-bis [(4-hexyloxyphenyl)ethynyl]benzene (12 g, 22 mmol) was allowed to react with sodium hydride in the same manner as described above. The crude product was purified by silica gel column separation with dichloromethane and hexane as an eluent to give **Hex1H** (9.0 g, 18 mmol). Yield 82%. TLC (dichloromethane): R_f = 0.93. IR (NaCl; cm^{-1}): 3308 (≡C–H), 2932 (C–H), 2208 (C≡C). ^{1}H NMR ($CDCl_3$, 500 MHz; ppm): δ 0.91 (t, 6H, J = 7.0 Hz, CH_3), 1.35 (m, 8H, CH_2), 1.43 (m, 4H, CH_2), 1.78 (m, 4H, CH_2), 3.09 (s, 1H, C≡C–H), 3.97 (t, 4H, J = 6.8 Hz, CH_2O), 6.87 (d, 4H, J = 9.0 Hz, ArH), 7.44 (d, 4H, J = 9.0 Hz, ArH), 7.55 (d, 2H, J = 1.5 Hz, ArH), 7.62 (t, 1H, J = 1.5 Hz, ArH). ^{13}C NMR ($CDCl_3$; ppm): δ 14.03, 22.59, 25.69, 29.14, 31.57, 68.11, 78.03, 82.21, 86.39, 90.75, 114.52, 114.59, 122.68, 124.37, 133.14, 133.99, 134.31, 159.51.

2.3. Polymerization. An appropriate amount of monomers (typically, 0.5–1.0 g) was placed in a Schlenk tube equipped with a three-way stopcock, a rubber septum, and a Teflon-coated magnetic stirring bar. The tube was placed under vacuum, followed by a nitrogen backflush. Freshly distilled solvent was transferred to the tube, and the monomers were dissolved with stirring. The determined amount of $[Rh(nbd)Cl]_2$ and triethylamine dissolved in the solvent was added to the stirred monomers solution. The detailed polymerization conditions are tabulated in Table 1. The reaction solution was poured into methanol or methanol/benzene (3/2 v/v) to yield polymer precipitate. The precipitate was washed with the precipitant and then dried in vacuo to give a yellow polymer.

2.4. Membrane Preparation. A 5 wt% (w/v) solution of a polymer in chloroform or toluene was cast on a Teflon sheet, and the solvent was evaporated at room temperature. The resulting solid membrane was detached from the sheet and dried in vacuo for 24 hr. Thickness (L) of the membranes was 70–160 μm.

2.5. Measurement of Oxygen and Nitrogen Permeability. Oxygen and nitrogen permeability coefficients (P_{O_2} and P_{N_2}: $cm^3(STP)cm\,cm^{-2}\,s^{-1}\,cmHg^{-1}$) and the oxygen separation factor ($\alpha = P_{O_2}/P_{N_2}$) were measured by a gas chromatographic method using YANACO GTR-10 according to [13].

2.6. Other Measurements. IR spectra were measured with a Hitachi IR 270-30 spectrometer. NMR (^{1}H, ^{13}C) spectra were measured with a Varian Unity 500SW (500 MHz) or a JEOL GSX-270 (270 MHz) spectrometer. Average molecular weights (M_n and M_w) were evaluated by coupling of gel permeation chromatography and low angle laser light scattering (GPC-LALLS) at 40°C on THF eluent using Tosoh Liquid Chromatograph instruments with SD-8000, CCPD, C0-8010, LS-8000, RI-8011, and PP8010. The optical spectra were measured with a JASCO Ubest V-550DS UV-vis spectrometer. The wide-angle X-ray scattering measurements were performed using a Rigaku Geigerflex with a graphite-monochromatized Cu Kα radiation, which was supplied at 40 kV and 20 mA.

3. Results and Discussion

3.1. Polymerization of Monodendron Monomers. The monodendron monomers were polymerized by Rh catalyst, $[Rh(nbd)Cl]_2$, in the presence of triethylamine cocatalyst. The polymerization mixtures were purified by precipitating into methanol or methanol/benzene (9/1-4/3 v/v) to yield the corresponding polydendrons as yellow powders. It is well known that the Rh catalyst can selectively promote the polymerization of monosubstituted acetylenes [14–19]. Moreover, we have previously demonstrated that **TMS1H**, **PMDS1H,** and **NMTS1H** polymerize at the terminal acetylene group of the focal point [7]. The same catalyst system promotes the polymerization of **HG1PA** and **Hex1H** to yield the corresponding polymers as shown in Table 1. **HG0PA**

Table 1: Polymerization of phenylacetylene monodendrons with alkyl peripheral groups using $[Rh(nbd)CL]_2$[a].

Monomers	Yield (%)	M_w[b] ($\times 10^6$)	M_w/M_n[b]	DP[c] ($\times 10^3$)
MG0PA	60	0.92	1.4	3.4
HG0PA[d]	87	2.4	1.8	5.9
DG0PA[e]	65	2.8	2.7	4.9
HG1PA	92	6.1	1.7	7.4
Hex0H[f]	49	5.3[g]	5.2[g]	2.6
Hex1H[f]	35	8.2[g]	3.0[g]	1.6

[a] Triethylamine, $[M]_0 = 0.5$ mol/l, $[M]_0/[Cat]_0 = 2500$, 25°C, 3 hr, precipitated with MeOH/benzene (9/1 v/v).
[b] Determined from GPC-LALLS.
[c] Calculated from M_w.
[d] Ether, $[\text{triethylamine}]_0/[Cat]_0 = 20$.
[e] $[M]_0/[Cat]_0 = 5000$.
[f] Chloroform, $[M]_0/[Cat]_0 = 1000$, $[\text{triethylamine}]_0/[Cat]_0 = 20$.
[g] Determined from GPC calibrated by polystyrene standard.

and **DG0PA** gave highly soluble polymers with a high degree of polymerization ($DP > 10^3$) in spite of the larger peripheral groups in comparison with **MG0PA**. The yield and the degree of polymerization of polydendrons (i.e., poly(**HG1PA**) and poly(**Hex1H**)) are similar to those of the corresponding zero-generation polymers (i.e., poly(**HG0PA**) and poly(**Hex1H**)), since the first-generation dendrons are not too crowded to affect the polymerization ability.

3.2. Structure of Polydendrons. The polymerization of the monodendrons at the terminal acetylene group of focal point was confirmed by means of IR and ^{1}H NMR; for example, in IR and ^{1}H NMR spectra of poly(**Hex1H**), the peaks assignable to the terminal acetylene group of the monodendron **Hex1H**, that is, 3308 cm^{-1} (the stretching vibration of the ≡C–H bond) in IR spectrum and δ 3.09 (s, 1H, ≡C–H) in ^{1}H NMR, completely disappeared. The visible absorption maxima (λ_{max}) of polydendrons significantly increased due to the construction of the dendritic structure, that is, poly(**Hex0H**) (400 nm) to poly(**Hex1H**) (455 nm), and poly(**HG0PA**) (400 nm) to poly(**HG1PA**) (441 nm). A bathochromic shift has been reported for some *ortho*- and *meta*-substituted poly(phenylacetylene)s in comparison with the simple or *para*-substituted poly(phenylacetylene) [20–24]. This bathochromic shift indicates a developed π-conjugation in the main chain of polydendrons and suggests that steric hindrance and repulsion among bulky substituents at the *m*-position formed the extended main chain structure. This resulted in a highly twisted dihedral angle between the main chain and the attached phenyl rings and was counteracted by slightly or moderately twisted single bonds of the main chain. The visible absorption maxima (λ_{max}) of the first-generation polydendrons were significantly increased due to the effect of the bulky substituent at the *m*-position in comparison with the corresponding zero-generation polymers poly(**HG0PA**) and poly(**Hex1H**).

The wide-angle X-ray scattering (WAXS) of poly(**HG0PA**) and poly(**HG1PA**) was measured in film states (Table 2). The sharp peaks were observed at $2\theta = 3 - 4°$, and these sharp crystalline peaks are attributed to the (100) reflection of the pseudohexagonal lattice of rod-like molecules [7, 25]. The interplanar *d* spacing of the polymers increased with increasing generation, while the density seldom decreased. These data suggest that the increase of *d* spacing is related to the increase of the column diameter with the generation. The column diameter of the polymers estimated from *d* spacing is only slightly smaller than that of molecular modeling. (The molecular modeling was performed on the assumption of a fully extended conformation for side-chain monodendrons and distorted *cis*-transoid main chain conformation (dihedral angle = 130 deg), as described in [7].) The column diameter difference between the values estimated from *d* spacing and from molecular modeling suggests that the flexible alkyl chain as the peripheral group was bent and/or the columns slightly overlapped each other in the part of the peripheral group.

3.3. Oxygen Permselectivity of Polydendron Membranes. The polymers were soluble in common organic solvents, such as chloroform, toluene, and tetrahydrofuran. The polymers poly(**HG0PA**), poly(**Hex0H**), and poly(**Hex1H**) exhibited good film-forming abilities depending on their degree of polymerization and formed a self-supporting film colored orange due to π-conjugated main chain chromophore by the solvent-casting method.

Oxygen and nitrogen permeation were measured using air as feed gas at 298 K and 76 cmHg using poly(**HG0PA**), poly(**Hex0H**), and poly(**Hex1H**) membranes. Figure 1 shows the relationship between the oxygen permeability coefficient (P_{O_2}) and the oxygen separation factor ($\alpha = P_{O_2}/P_{N_2}$) for the polydendron membranes with the zero-generation polymer (poly(**TMS0H**), poly(**PMDS0H**), and poly(**NMTS0H**)) membranes. The oxygen permeability coefficient (P_{O_2}) of the membranes formed by first-generation polydendrons were smaller than that of the corresponding zero-generation poly(phenylacetylene) derivative. It seems that this behavior was caused by the low mobility of the stiff and crowded dendritic structure. The zero-generation poly(phenylacetylene) derivatives show a balance between

Table 2: Column structure of polydendrons.

Polymers	Generation number	Density[a] (g/cm^3)	2θ [b] (deg)	d spacing[c] (Å)	Column diameter	
					WAXS[d] (Å)	Calcd[e] (Å)
poly(**HG1PA**)[f]	1	1.068	3.1	30.5	35.2	43.0
poly(**HG0PA**)[f]	0	1.062	3.3	28.7	33.1	36.7

[a] Determined by floating method containing error of ±0.005.
[b] Crystalline peak of the wide-angle X-ray scattering (WAXS) of the polymers.
[c] Estimated from 2θ.
[d] Estimated from d (column diameter = $2d/\sqrt{3}$).
[e] Estimated from molecular modeling, which was performed as described in text. (The molecular modeling was performed on the assumption of a fully extended conformation for side-chain monodendronsn and distorted *cis*-transoid main chain conformation (dihedral angle = 130 deg), as described in [7].)

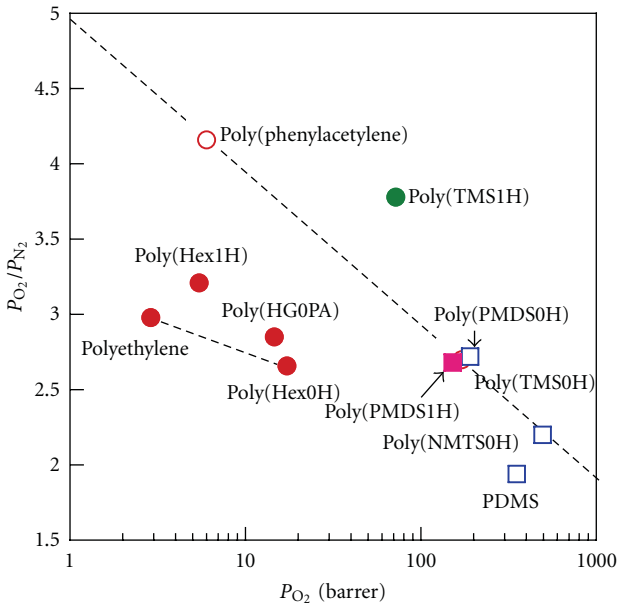

Figure 1: Permselectivity of poly(phenylacetylene) analogue membranes for O_2/N_2 separation. Poly(phenylacetylene) (PPA) and poly(**TMS0H**) from [13], poly(**PMDS0H**), poly(**NMTS0H**), poly(**TMS1H**), and poly(**PMDS1H**) from [6].

the oxygen permeability coefficient and oxygen separation factor. However, the oxygen permselectivity of the polydendrons with a trimethylsilyl group, poly(**TMS1H**), shows good performance in comparison with corresponding zero-generation poly(phenylacetylene) derivatives. In comparison, polydendrons with oligo(dimethylsiloxane) peripheral groups (i.e., poly(**PMDS1H**)) exhibited similar trend to that of the corresponding zero-generation poly(phenylacetylene) derivatives. On the other hand, polymers and polydendrons with alkoxy peripheral groups exhibited the lower oxygen permeability coefficient due to the alkyl domain that would have better gas barrier property than oligo(dimethylsiloxane) domain. But the oxygen permselectivity of poly(**Hex1H**) shows good performance in comparison with the trend between polyethylene and poly(**Hex0H**). These results suggest that the space-persistency due to the stiff and crowded dendritic structure play an important role in the high performance of the oxygen permselectivity, while the effect of the peripheral group was similar to that of the corresponding zero-generation poly(phenylacetylene) derivatives.

4. Conclusions

The phenylacetylene monomers consisting of monodendron with alkoxy peripheral groups were successfully polymerized with a Rh catalyst, $[Rh(nbd)Cl]_2$, to yield corresponding polydendrons with high molecular weight, in spite of the bulkiness of the dendritic residue and the peripheral groups. The polydendrons were fabricated to self-supporting membranes, and the membrane formed by the polydendron of first generation, poly(**Hex1H**), showed an oxygen permselectivity higher than that of the corresponding zero-generation poly(phenylacetylene) derivatives.

Acknowledgments

This work was partially supported by a Grant-in-Aid for Scientific Research (B) (no. 20310052) from JSPS and by the Mukai Science Technology Foundation.

References

[1] K. Inoue, "Functional dendrimers, hyperbranched and star polymers," *Progress in Polymer Science*, vol. 25, no. 4, pp. 453–571, 2000.
[2] D. A. Tomalia and J. M. J. Fréchet, "Discovery of dendrimers and dendritic polymers: a brief historical perspective," *Journal of Polymer Science Part A*, vol. 40, no. 16, pp. 2719–2728, 2002.
[3] J. M. J. Fréchet, "Dendrimers and other dendritic macromolecules: from building blocks to functional assemblies in nanoscience and nanotechnology," *Journal of Polymer Science Part A*, vol. 41, no. 23, pp. 3713–3725, 2003.
[4] T. Aoki and T. Kaneko, "New macromolecular architectures for permselective membranes—gas permselective membranes from dendrimers and enantioselectively permeable membranes from one-handed helical polymers," *Polymer Journal*, vol. 37, no. 10, pp. 717–735, 2005.
[5] T. Kaneko, T. Horie, M. Asano, T. Aoki, and E. Oikawa, "Polydendron: polymerization of dendritic phenylacetylene monomers," *Macromolecules*, vol. 30, no. 10, pp. 3118–3121, 1997.
[6] T. Kaneko, K. Yamamoto, M. Asano, M. Teraguchi, and T. Aoki, "Synthesis of poly(phenylacetylene)-based polydendrons consisting of a phenyleneethynylene repeating unit, and oxygen/nitrogen permeation behavior of their membranes," *Journal of Membrane Science*, vol. 278, no. 1-2, pp. 365–372, 2006.
[7] T. Kaneko, M. Asano, K. Yamamoto, and T. Aoki, "Polymerization of phenylacetylene-based monodendrons and structure of

the corresponding polydendrons," *Polymer Journal*, vol. 33, no. 11, pp. 879–890, 2001.

[8] G. Chen, W. Shan, Y. Wu, L. Ren, J. Dong, and Z. Ji, "Synthesis and anti-inflammatory activity of resveratrol analogs," *Chemical and Pharmaceutical Bulletin*, vol. 53, no. 12, pp. 1587–1590, 2005.

[9] K. Sivanandan, S. V. Aathimanikandan, C. G. Arges, C. J. Bardeen, and S. Thayumanavan, "Probing every layer in dendrons," *Journal of the American Chemical Society*, vol. 127, no. 7, pp. 2020–2021, 2005.

[10] J. F. Eckert, J. F. Nicoud, J. F. Nierengarten et al., "Fullerene-oligophenylenevinylene hybrids: synthesis, electronic properties, and incorporation in photovoltaic devices," *Journal of the American Chemical Society*, vol. 122, no. 31, pp. 7467–7479, 2000.

[11] O. Haba, K. Haga, M. Ueda, O. Morikawa, and H. Konishi, "A new photoresist based on calix[4]resorcinarene dendrimer," *Chemistry of Materials*, vol. 11, no. 2, pp. 427–432, 1999.

[12] S. Gandon, P. Mison, M. Bartholin et al., "Thermal polymerization of arylacetylenes: 1. Study of a monofunctional model compound," *Polymer*, vol. 38, no. 6, pp. 1439–1447, 1997.

[13] T. Aoki, H. Nakahara, Y. Hayakawa, M. Kokai, and E. Oikawa, "Trimethylsilyl-group containing polyphenylacetylenes for oxygen and ethanol permselective membranes," *Journal of Polymer Science Part A*, vol. 32, no. 5, pp. 849–858, 1994.

[14] M. Tabata, W. Yang, and K. Yokota, "Polymerization of m-chlorophenylacetylene initiated by [Rh(norbornadiene)CI]," *Polymer Journal*, vol. 22, no. 12, pp. 1105–1107, 1990.

[15] M. Tabata, W. Yang, and K. Yokota, "H-NMR and UV studies of Rh complexes as a stereoregular polymerization catalysts for phenylacetylenes: effects of ligands and solvents on its catalyst activity," *Journal of Polymer Science Part A*, vol. 32, no. 6, pp. 1113–1120, 1994.

[16] Y. Kishimoto, P. Eckerle, T. Miyatake et al., "Well-controlled polymerization of phenylacetylenes with organorhodium(I) complexes: mechanism and structure of the polyenes," *Journal of the American Chemical Society*, vol. 121, no. 51, pp. 12035–12044, 1999.

[17] Y. Misumi and T. Masuda, "Living polymerization of phenylacetylene by novel rhodium catalysts. Quantitative initiation and introduction of functional groups at the initiating chain end," *Macromolecules*, vol. 31, no. 21, pp. 7572–7573, 1998.

[18] Y. Misumi, K. Kanki, M. Miyake, and T. Masuda, "Living polymerization of phenylacetylene by rhodium-based ternary catalysts, (diene)Rh(I) complex/vinyllithium/phosphorus ligand. Effects of catalyst components," *Macromolecular Chemistry and Physics*, vol. 201, no. 17, pp. 2239–2244, 2000.

[19] M. Miyake, Y. Misumi, and T. Masuda, "Living polymerization of phenylacetylene by isolated rhodium complexes," *Macromolecules*, vol. 33, no. 18, pp. 6636–6639, 2000.

[20] T. Masuda and T. Higashimura, "Polyacetylenes with substituents: their synthesis and properties," *Advances in Polymer Science*, vol. 81, pp. 121–165, 1986.

[21] J. Kunzler and V. Percec, "Living polymerization of aryl substituted acetylenes by MoCl," *Journal of Polymer Science Part A*, vol. 28, no. 5, pp. 1221–1236, 1990.

[22] H. Nishide, T. Kaneko, R. Gotoh, and E. Tsuchida, "Polyacetylene derivatives with chain-sided phenoxy and galvinoxyl radicals," *Molecular Crystals and Liquid Crystals*, vol. 233, pp. 89–96, 1993.

[23] Y. Miura, M. Matsumoto, and Y. Ushitani, "Synthesis of poly(ethynylbenzene) with pendant nitroxide radicals by rhodium-catalyzed polymerization of ethynylphenyl nitroxide," *Macromolecules*, vol. 26, no. 10, pp. 2628–2630, 1993.

[24] R. R. Schrock, S. Luo, J. C. Lee, N. C. Zanetti, and W. M. Davis, "Living polymerization of (o-(trimethylsilyl)phenyl)acetylene by molybdenum imido alkylidene complexes," *Journal of the American Chemical Society*, vol. 118, no. 16, pp. 3883–3895, 1996.

[25] M. Tabata, H. Takamura, K. Yokota et al., "Pressure-induced cis to trans isomerization of poly(o-methoxyphenylacetylene) polymerized by Rh complex catalyst. A ramam, X-ray, and ESR study," *Macromolecules*, vol. 27, no. 21, pp. 6234–6236, 1994.

Hindawi Publishing Corporation
International Journal of Polymer Science
Volume 2012, Article ID 937928, 7 pages
doi:10.1155/2012/937928

Review Article

Development of an Environmentally Friendly Resist-Removal Process Using Wet Ozone

Hideo Horibe and Yousuke Goto

Department of Bioscience and Applied Chemistry, Graduate School of Science and Technology, Kanazawa Institute of Technology, 3-1 Yatsukaho, Hakusan, Ishikawa 924-0838, Japan

Correspondence should be addressed to Hideo Horibe, hhoribe@neptune.kanazawa-it.ac.jp

Received 12 August 2011; Accepted 15 November 2011

Academic Editor: Eri Yoshida

We investigated the removal of polymers with various chemical structures and the removal of ion-implanted resists using wet ozone. The removal rates of polymers that have carbon-carbon (C–C) double bonds in the main chain were high. The main chain of these polymers may be decomposed. The removal rates of polymers that have C–C double bonds in the side chain were low. The benzene ring in the side chain changes into carboxylic acid, so their ability to dissolve in water increased. The polymers without C–C double bonds were not removed. Removal of B and P ion-implanted resists became difficult with increasing acceleration energy of ions at implantation. The resist with plastic-deformation hardness that was twice as hard as that of nonimplanted resist should be removed similarly to nonimplanted resist. Using TOF-SIMS, we clarified that the molecule of cresol novolak resin was destroyed and carbonized by ion implantation.

1. Introduction

Photosensitive resin (resist) is used in the semiconductor (IC, LSI) and liquid crystal display (LCD) manufacturing process. The pattern is transferred to the resist by three processes (spin coating, exposure and development). The substrate is etched by using resist as a mask, and ions are implanted. Finally, the unneeded resist is removed. Resist removal from substrates in a semiconductor manufacturing process conventionally uses oxygen plasma [1, 2] and/or chemicals (e.g., sulfuric acid hydrogen peroxide mixture, and ammonia hydrogen peroxide mixture). Environmentally unfriendly chemicals are used in large amounts and cause environmental damage [3, 4]. Also, oxygen plasma ashing may cause oxidation of substrates and metal wiring because this process requires high temperature (above 250°C) [5, 6]. Therefore, several resist removal methods have been developed (e.g., atomic hydrogen [7–10], UV/ozone [11, 12], and YAG laser [13–15]).

We examine the wet ozone process, which is an environmentally friendly, low-temperature process. In this process, ozone gas mixed with a small amount of water is irradiated to the resist at a temperature below 100°C, and the resist changes into hydrophilic carboxylic acid by the ozone and condensed water [16–18].

Figure 1 presents a schematic diagram of the experiment apparatus for wet ozone (Mitsubishi Electric-Corp. and SPC Electronics Corp.). Ozone gas mixed with a small amount of water vapor (wet ozone) is generated by bubbling ozone gas through hot water. Also, a small amount of water vapor condenses on the resist, due to the difference in temperature ($\Delta T = T_1 - T_2$) between wet ozone (T_1) and Si wafer (T_2). The amount of water condensed on the resist was controlled by adjusting ΔT [19]. Figure 2 depicts the chemical reaction of the carbon-carbon double bond (C–C double bond) with ozone and the hydrolysis of ozonide. In resist removal using wet ozone, the C–C double bond in the benzene ring of the resist reacts with the ozone to generate ozonide [20, 21]. Ozonide is hydrolyzed by the water condensed on the resist, and carboxylic acid is generated. Finally, the carboxylic acid was washed down from the Si wafer by a pure-water rinse.

We removed base polymers that had different chemical structures and evaluated the chemical reactivity of wet ozone with the chemical structures of polymers. Also, we

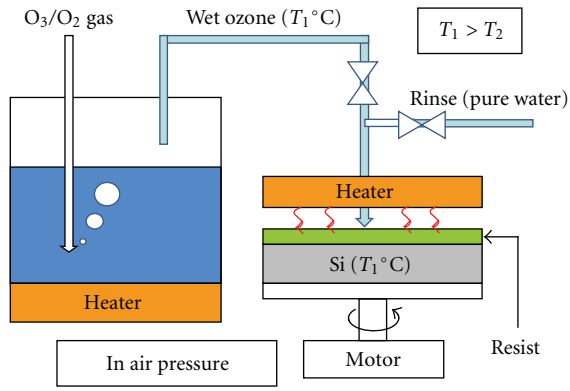

Figure 1: Experiment apparatus for resist removal using wet ozone.

Table 1: Film thickness, polymers, and solvents.

Polymer samples/solvents	Thickness (μm)
AZ6112	1.35
Novolak resin (M_w = 15000)/PGMEA	0.96
cis-1,4-polyisoprene (M_w = 38000)/xylene	0.40
PVP (M_w = 20000)/ethyl lactate	1.62
PS (M_w = 4000 ~ 20000)/toluene	0.66
PMMA (M_w = 96700)/ethyl lactate	1.30
PVC (M_w = 68750)/cyclohexanone	1.32

investigated the relationship between ion-implanted resist removability and acceleration energy of ions at implantation. We examined the structure of ion-implanted resists by SEM observation and by stripping ion-implanted resists using chemicals. We clarified the characteristics ion-implanted resists by nanoindentation [22–24] and time-of-flight secondary ion mass spectrometry (TOF-SIMS).

2. Experimental

2.1. Removal of Polymers with Various Chemical Structures Using Wet Ozone. The cycle consisted of 10 s at 2000 rpm for wet ozone irradiation, 5 s at 2000 rpm for pure-water washing, and 20 s at 1000 rpm for drying. The ozone gas concentration was 230 g/m^3 (10.2 vol%), and the flow rate was 12.5 slm. The wet ozone temperature was T_1 = 70°C, and the substrate temperature was T_2 = 60°C. Polymer removal involved estimating novolak resin and cis-1,4-polyisoprene, which have C–C double bonds in the main chain; polyvinyl phenol (PVP) polystyrene (PS), which have C–C double bonds in the side chain; and polymethyl methacrylate (PMMA) and polyvinyl chloride (PVC), which have no C–C double bond. These polymers, which were dissolved in each solvent, were spin-coated onto an Si wafer using a spin coater (ACT-300A; Active) at 2000 rpm for 20 sec and prebaked at 100°C for 1 min on a hotplate (PMC 720 series; Dataplate). Table 1 lists polymers, solvents, and film thickness for this study. We also removed a positive-tone novolak photoresist (AZ6112; AZ-Electronic Materials) as a reference.

2.2. Removal of Ion-Implanted Resists Using Wet Ozone. The wet ozone irradiation conditions were the same as those described in Section 2.1. In this study, the ion-implanted resist was a positive-tone novolak resist (AZ6112; AZ-Electronic Materials) with B and P ions implanted at a dose of 5 × 10^{14} atoms/cm^2 at each acceleration energy (10 keV, 70 keV, and 150 keV).

We observed cross-sections of ion-implanted resists using scanning electron microscopy (SEM: JSR-6360; JEOL Ltd.). SEM images were secondary electron images with an acceleration voltage of 20 kV. Also, after dissolving the ion-implanted resist into ethylene carbonate (EC), we measured the thickness of the stripped resist film. We previously clarified the presence of a damaged layer at the surface of ion-implanted resists [25–28]. Ion-implanted resists were composed of two layers (the damaged layer and the normal layer). We calculated the percentages of the damaged layer among of the ion-implanted resist. The temperature of EC was 70°C.

We examined plastic-deformation hardness by varying the maximum load from 1 to 260 mgf by nanoindentation. The loading rate was 1/2000 for loads exceeding 8 mgf and 0.004 mgf/ms (lower limit) below 8 mgf. We used a Berkovich diamond indenter with an apex angle of 115°. Also, in order to evaluate the effect of ion implantation on resists, we normalized the plastic-deformation hardness of the ion-implanted resists with that of nonimplanted resists. We refer to this value as normalized plastic-deformation hardness H_2.

In order to evaluate the composition of ion-implanted resists, we cut resists at a slant using SAICAS (NN-04; DAIPLA WINTES) and conducted composition depth profile analysis using TOF-SIMS (TOF-SIMS 5; ION-TOF). The primary ion was Bi_3^{2+}, and the acceleration voltage was 25 kV. In order to clarify the degree of hardening, we used ion-implanted resists in which B ions were implanted at a dose of 5 × 10^{15} atoms/cm^2 and some acceleration energies (10 keV, 70 keV, and 150 keV).

3. Results and Discussion

3.1. Removal of Polymers with Various Chemical Structures Using Wet Ozone. Figure 3 plots the results of removing polymers using wet ozone. Table 2 presents removal rates of each polymer using wet ozone. The removal rates of polymers that have C–C double bonds in the main chain (novolak resin and cis-1,4-polyisoprene) were highest. The removal rates of polymers that have C–C double bonds in the side chain (PVP and PS) were low compared to those of novolak resin and cis-1,4-polyisoprene. In novolak resin and cis-1,4-polyisoprene, the main chain may be decomposed by reaction of wet ozone. In PVP and PS, the benzene ring in the side chain changes into carboxylic acid by reaction with wet ozone. Thus, PVP and PS should be removed because their ability to dissolve in water increased. In contrast, the polymers that have no C–C double bond (PMMA and PVC) were not removed.

3.2. Removal of Ion-Implanted Resists Using Wet Ozone. Figure 4 plots the removal of B and P ion-implanted resists using wet ozone. Removal of B and P ion-implanted resists

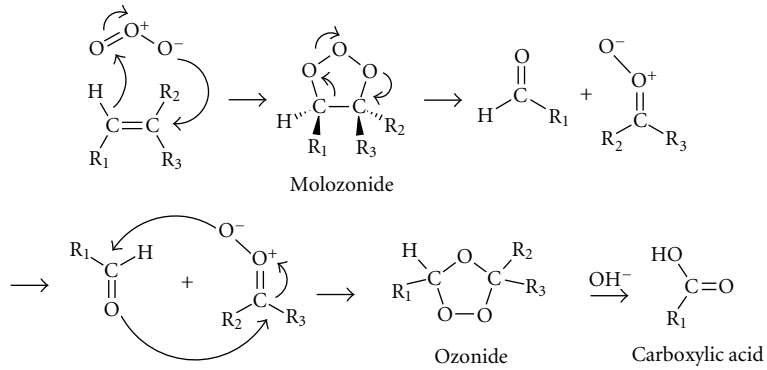

Figure 2: Chemical reaction of carbon-carbon double bond with wet ozone.

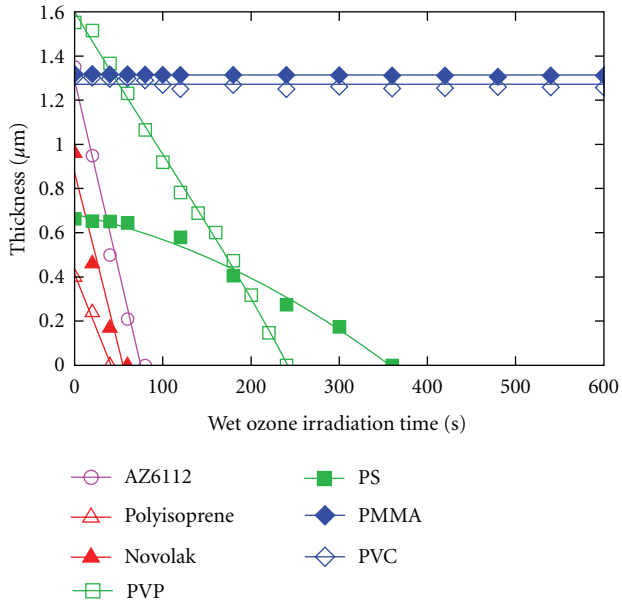

Figure 3: Dependence of polymer thickness on wet ozone irradiation time.

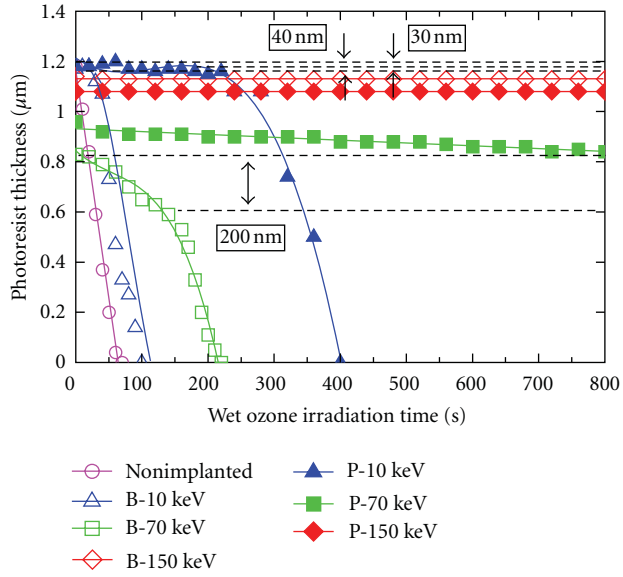

Figure 4: Removal of B and P ion-implanted resists with various acceleration energies using wet ozone.

Table 2: Removal rates of polymers using wet ozone.

Polymer samples	Removal rates (μm/min)
AZ6112	1.01
Novolak resin	0.96
cis-1,4-polyisoprene	0.61
PVP	0.35
PS	0.12
PMMA	0.01
PVC	0

became difficult with increasing acceleration energy of ions at implantation. Resist with B ions implanted at an acceleration energy of 150 keV could not be removed, nor could resist with P ions implanted at acceleration energies of 70 keV and 150 keV. Removal rate decreased with increasing acceleration energy. It was assumed that the reactivity of ozone and resists decreases with increasing acceleration energy. After the ion-implanted resist surfaces were removed, the resists were removed at the same rate as nonimplanted resists. The damaged layer formed at the surface of ion-implanted resists, and the lower layer was normal layer (nonimplanted resist). The estimated thicknesses of the damaged layer of B ion-implanted resists were 40 nm (10 keV) and 200 nm (70 keV) and that of P ion-implanted resist was 30 nm (10 keV).

3.3. SEM Images of Ion-Implanted Resist. Figure 5 presents SEM images of B and P ion-implanted resists with various acceleration energies. The ion-implanted resists are composed of two layers. The percentage of ion-implanted resist damaged layer increased with increasing acceleration energy. Table 3 lists the damaged layer thickness measured by resist removal using wet ozone, SEM images, and resist removal using chemicals. Table 4 lists the percentage of ion-implanted resist damaged layer determined by SEM and stripping of

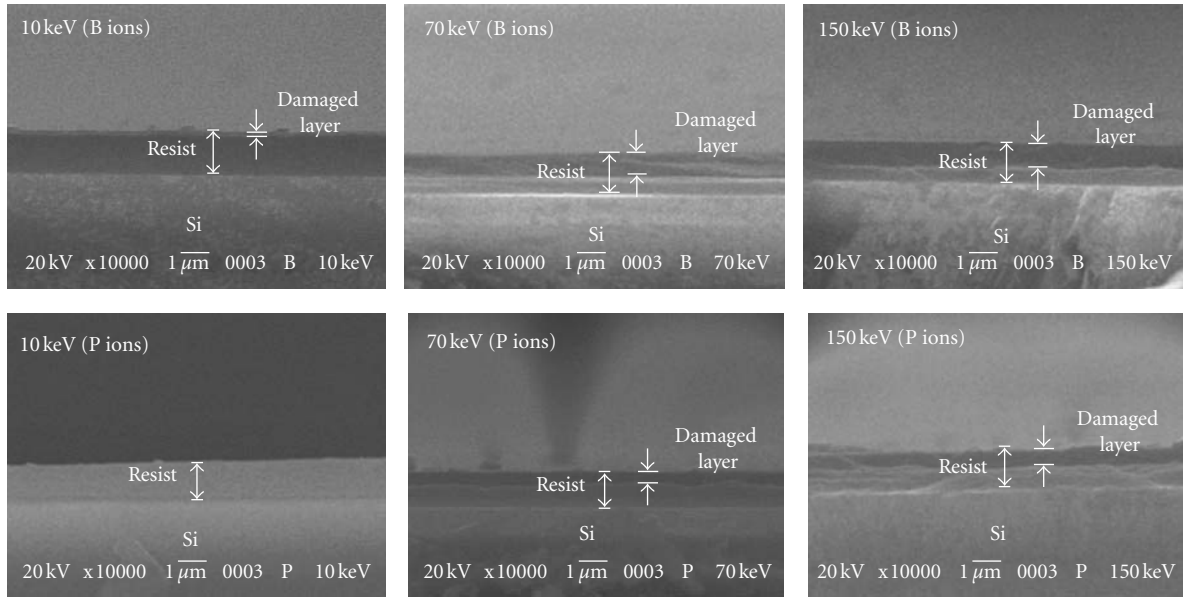

Figure 5: SEM images of B and P ion-implanted resist with various acceleration energies.

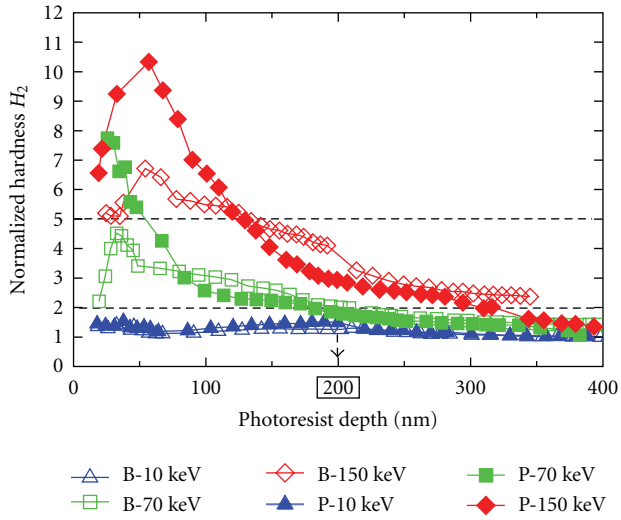

Figure 6: Depth profiles of normalized plastic-deformation hardness H_2 of the B and P ion-implanted resists.

ion-implanted resist using chemicals. The percentage of ion-implanted resist damaged layer increased with increasing acceleration energy.

3.4. Plastic-Deformation Hardness of Ion-Implanted Resist. Figure 6 plots depth profiles of normalized plastic-deformation hardness of B and P ion-implanted resists versus photoresist depth. Normalized plastic-deformation hardness H_2 was obtained by dividing the plastic-deformation hardness of ion-implanted resists by that of non-ion-implanted resists. The plastic-deformation hardness and the thickness of ion-implanted resists increased with increasing acceleration energy. Therefore, removability of the ion-implanted resist using wet ozone decreased with increasing acceleration energy because the hardness of resist increases with increasing acceleration energy as determined by nanoindentation measurement. Based on the results of the removal of ion-implanted resists using wet ozone and nanoindentation,

Table 3: The damaged layer thickness measured by resist removal using wet ozone, SEM images, and resist removal using chemicals.

Sample	Resist removal (wet ozone) damaged layer	SEM observation damaged layer	Resist removal (chemicals) damaged layer
10 keV (B ions)	40 nm	110 nm	90 nm
70 keV (B ions)	200 nm	500 nm	407 nm
150 keV (B ions)	—	830 nm	660 nm
10 keV (P ions)	30 nm	—	40 nm
70 keV (P ions)	—	330 nm	140 nm
150 keV (P ions)	—	500 nm	400 nm

Table 4: Percentages of ion-implanted resist damaged layer by SEM and stripping of ion-implanted resist using chemicals.

Sample	Resist removal (wet ozone) damaged layer/total	SEM observation damaged layer/total	Resist removal (chemicals) damaged layer/total
10 keV (B ions)	0.04	0.09	0.08
70 keV (B ions)	0.25	0.60	0.50
150 keV (B ions)	—	0.72	0.60
10 keV (P ions)	0.03	—	0.03
70 keV (P ions)	—	0.34	0.25
150 keV (P ions)	—	0.46	0.36

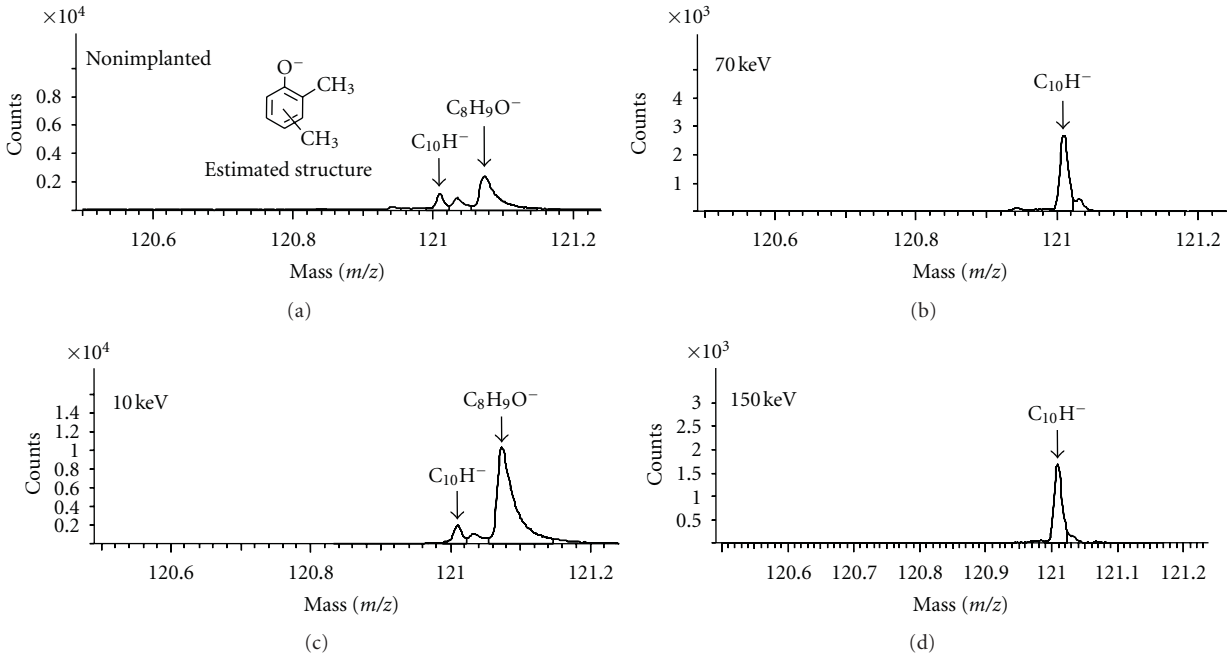

Figure 7: The second negative ion mass spectra of ion-implanted resists with various acceleration energies.

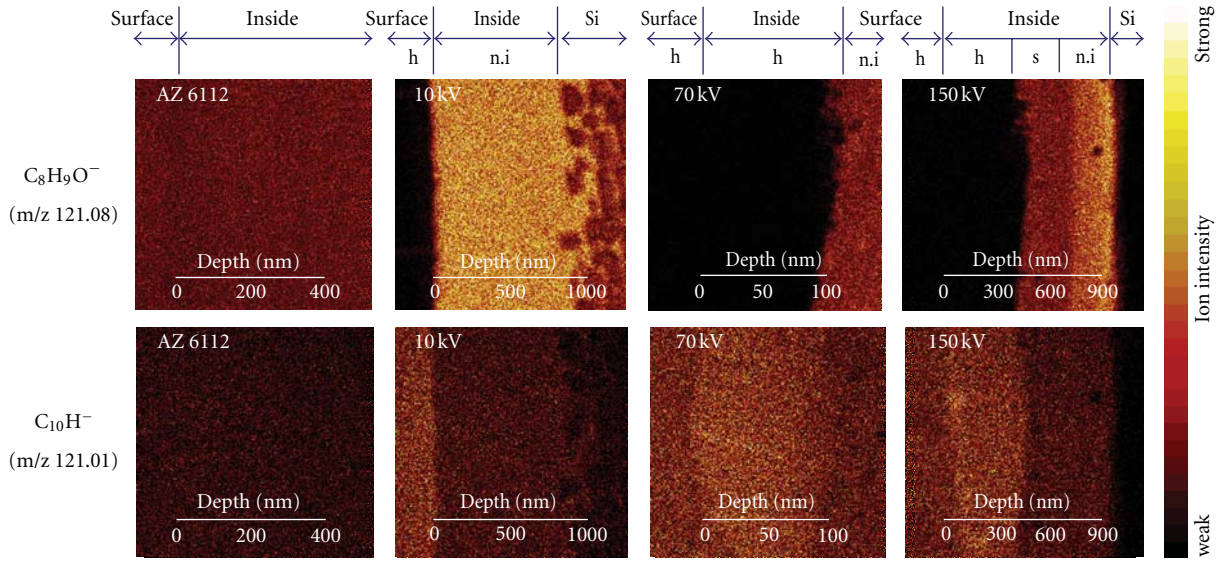

Figure 8: Secondary negative ion images of ion-implanted resists with various acceleration energies (h: hardened layer, n.i.: nonimplanted. s: stripped nonimplanted).

the resist with plastic-deformation hardness five times that of normal resist should not be removed. After the ion-implanted resist surfaces were removed, the resists were removed at the same rate as nonimplanted resist. The ion-implanted resists whose plastic-deformation hardness was less twice than that of normal resist should be removed similarly to nonimplanted resist.

3.5. TOF-SIMS Measurement of Ion-Implanted Resist. Figure 7 presents the secondary negative ion mass spectra of ion-implanted resists with various acceleration energies. "Counts" of the vertical axis of Figure 7 is a number of ions which entered the detector, and it becomes the number of counts for each area. The $C_8H_9O^-$ (m/z 121.08 Chemical structure is drawn in Figure 7) from cresol novolak resin was detected as a component of non-ion-implanted resists. In addition, $C_{10}H^-$ (m/z 121.01), which is a hydrocarbon with a saturated bond, was detected as a component of the damaged (hardened) layer of ion-implanted resist. $C_{10}H^-$ is described as follows. Hydrogen is escaped from the resist ($C_8H_9O^-$) by ion implant, and we think that it is

the compound such as graphitized and amorphous carbon. We do not understand whether the material is composed only of a saturated bond. The ion intensity of $C_{10}H^-$ increased with increasing acceleration energy. Therefore, it was assumed that removing ion-implanted resists would become difficult because cresol novolak resin was carbonized by ion implantation. The reason why the count of $C_{10}H^-$ of 150 keV is smaller than that of $C_{10}H^-$ of 70 keV is that the area where $C_{10}H^-$ in 150 keV is smaller than that of 70 keV. When Figure 8 is seen, it is understood that the area (h: harden layer) of $C_{10}H^-$ of 150 keV is narrower than that of 70 kev. Figure 8 presents the second negative ion images of ion-implanted resists with various acceleration energies. $C_{10}H^-$ was detected from the lower layer of resist with increasing acceleration energy.

In contrast, the ion intensity of $C_8H_9O^-$ was weak at the surface and strong at the lower layer. Therefore, resists are carbonized deeply with increasing acceleration energy. Also, the ion intensity of $C_8H_9O^-$ was greater than that of non-ion-implanted resist for all ion-implanted resists. It was assumed that the molecules of cresol novolak resin were easily ionized. For 10 keV, $C_8H_9O^-$ was detected at the lower layer than at the surface because the surface was stripped when it was cut at a slant. It was assumed that the hardened layer fell away.

Next, we measured the surface profile of the resist that was cut by SAICAS using a stylus-type surface-profile measurement instrument (DekTak 6 M; ULVAC). From the result of surface profile measurement, at the resist with ions implanted at 10 keV, the resist layer of 100 nm depth from the surface was stripped. At 70 keV, the resist of 400 nm depth was stripped and that at 150 keV was 600 nm. Therefore, the estimated thickness of the hardened layer of ion-implanted resist at 10 keV was above 100 nm, that at 70 keV was above 400 nm, and that at 150 keV was above 600 nm.

4. Conclusion

We investigated the removal of polymers with various chemical structures and the removal of ion-implanted resists using wet ozone. The removal rates of polymers that have C–C double bonds in the main chain (novolak resin and cis-1,4-polyisoprene) were the highest. The removal rates of polymers that have C–C double bonds in the side chain (PVP and PS) were lower than those of novolak resin and cis-1,4-polyisoprene. In novolak resin and cis-1,4-polyisoprene, the main chain may be decomposed by reaction with wet ozone. In PVP and PS, the benzene ring in the side chain changes into carboxylic acid by reaction with wet ozone. Thus, PVP and PS should be removed because their ability to dissolve in water increased. However, the polymers that have no C–C double bond (PMMA and PVC) were not removed.

Removal of B and P ion-implanted resists became difficult with increasing acceleration energy. Resist with B ions implanted at an acceleration energy of 150 keV could not be removed nor could resist with P ions implanted at acceleration energies of 70 keV and 150 keV. It was assumed that the reactivity of ozone and resists decreases with increasing acceleration energy. From the results of removal of ion-implanted resist using wet ozone and nanoindentation, a resist with plastic-deformation hardness five times that of normal resist could not be removed, and a resist with plastic-deformation hardness twice that of normal resist should be removable similarly to nonimplanted resist. Using TOF-SIMS, the $C_8H_9O^-$ (m/z 121.08) from cresol novolak resin was detected as a component of non-ion-implanted resists. $C_{10}H^-$ (m/z 121.01), which is a hydrocarbon with an unsaturated bond, was detected as a component of the damaged (hardened) layer of ion-implanted resist. The ion intensity of $C_{10}H^-$ increased with increasing acceleration energy. We clarified that the molecule of cresol novolak resin was destroyed and carbonized by ion implantation.

Acknowledgment

This study was supported by the Industrial Technology Research Grant Program (2004) from the New Energy and Industrial Technology Development Organization (NEDO) of Japan.

References

[1] M. Strobel, C. S. Lyons, and K. L. Mittal, *Plasma Surface Modification of Polymers Relevance to Adhesion*, VSP, Utrecht, The Netherlands, 1994.

[2] E. M. Liston, "Plasma modification of polymer surfaces," in *Polymer-Solid Interfaces*, J. J. Pireaux, P. Bertrand, and J. L. Bredas, Eds., pp. 429–442, Institute of Physics, Belgium, 1991.

[3] M. N. Kawaguchi, J. S. Papanu, B. Su, M. Castle, and A. Al-Bayati, "Surface characterization of ion-enhanced implanted photoresist removal," *Journal of Vacuum Science and Technology B*, vol. 24, no. 2, pp. 657–663, 2006.

[4] M. Yamamoto, T. Maruoka, A. Kono, H. Horibe, and H. Umemoto, "Substrate temperature dependence of the photoresist removal rate using atomic hydrogen generated by a hot-wire tungsten catalyst," *Japanese Journal of Applied Physics*, vol. 49, no. 1, Article ID 016701, 2010.

[5] H. Morinaga, M. Suyama, and T. Ohmi, "Mechanism of metallic particle growth and metal-induced pitting on Si wafer surface in wet chemical processing," *Journal of the Electrochemical Society*, vol. 141, no. 10, pp. 2834–2841, 1994.

[6] H. Morinaga, T. Futatsuki, T. Ohmi, E. Fuchita, M. Oda, and C. Hayashi, "Behavior of ultrafine metallic particles on silicon wafer surface," *Journal of the Electrochemical Society*, vol. 142, no. 3, pp. 966–970, 1995.

[7] A. Izumi and H. Matsumura, "Photoresist removal using atomic hydrogen generated by heated catalyzer," *Japanese Journal of Applied Physics Part 1*, vol. 41, no. 7, pp. 4639–4641, 2002.

[8] M. Yamamoto, H. Horibe, H. Umemoto et al., "Photoresist removal using atomic hydrogen generated by hot-wire catalyzer and effects on Si-wafer surface," *Japanese Journal of Applied Physics*, vol. 48, no. 2, Article ID 026503, 2009.

[9] H. Horibe, M. Yamamoto, E. Kusano, T. Ichikawa, and S. Tagawa, "Resist removal by using atomic hydrogen," *Journal of Photopolymer Science and Technology*, vol. 21, no. 2, pp. 293–298, 2008.

[10] T. Maruoka, Y. Goto, M. Yamamoto et al., "Relationship between the thermal hardenlng of ion-implanted resist and the

resist removal using atomic hydrogen," *Journal of Photopolymer Science and Technology*, vol. 22, no. 3, pp. 325–328, 2009.

[11] M. D. Gurol and R. Vatistas, "Oxidation of phenolic compounds by ozone and ozone + u.v. radiation: a comparative study," *Water Research*, vol. 21, no. 8, pp. 895–900, 1987.

[12] Y. Abe, A. Kaneko, T. Yagi et al., "Effects of UV-irradiation on removal process of photoresist by aqueous ozone," *Kagaku Kogaku Ronbunshu*, vol. 36, no. 1, pp. 41–50, 2010.

[13] H. Horibe, T. Kamimura, and K. Yoshida, "Removal of positive-tone diazonaphthoquinone/novolak resist using UV laser irradiation," *Journal of Photopolymer Science and Technology*, vol. 18, no. 2, pp. 181–185, 2005.

[14] H. Horibe, M. Fujita, I. Nishiyama, and A. Yoshikado, "Novolak resist removal by laser irradiation (532 nm) and adhesion between resist and substrate," *Japanese Journal of Applied Physics Part 1*, vol. 44, no. 12, pp. 8673–8675, 2005.

[15] T. Kamimura, S. Akamatsu, H. Horibe et al., "Enhancement of surface-damage resistance by removing subsurface damage in fused silica and its dependence on wavelength," *Japanese Journal of Applied Physics Part 2*, vol. 43, no. 9, pp. L1229–L1231, 2004.

[16] S. Noda, M. Miyamoto, H. Horibe, I. Oya, M. Kuzumoto, and T. Kataoka, "Development of a photoresist removal method using ozone gas with water vapor for LCD manufacturing," *Journal of the Electrochemical Society*, vol. 150, no. 9, pp. G537–G542, 2003.

[17] S. Noda, K. Kawase, H. Horibe, M. Kuzumoto, and T. Kataoka, "Development of a method for resist removal by ozone with acetic acid vapor," *Journal of the Electrochemical Society*, vol. 152, no. 1, pp. G73–G82, 2005.

[18] H. Horibe, M. Yamamoto, Y. Goto, T. Miura, and S. Tagawa, "Removal characteristics of resists having different chemical structures by using ozone and water," *Japanese Journal of Applied Physics*, vol. 48, no. 2, Article ID 026505, 2009.

[19] H. Horibe, M. Yamamoto, T. Ichikawa, T. Kamimura, and S. Tagawa, "Resist removal by using wet ozone," *Journal of Photopolymer Science and Technology*, vol. 20, no. 2, pp. 315–318, 2007.

[20] C. Geletneky and S. Berger, "The mechanism of ozonolysis revisited by 17O-NMR spectroscopy," *European Journal of Organic Chemistry*, no. 8, pp. 1625–1627, 1998.

[21] L. G. Wade Jr., *Organic-Chemistry*, Prentice Hall, Upper Saddle River, NJ, USA, 6th edition, 2006.

[22] M. Lichinchi, C. Lenardi, J. Haupt, and R. Vitali, "Simulation of Berkovich nanoindentation experiments on thin films using finite element method," *Thin Solid Films*, vol. 312, no. 1-2, pp. 240–248, 1998.

[23] X. Chen, Y. Xiang, and J. J. Vlassak, "Novel technique for measuring the mechanical properties of porous materials by nanoindentation," *Journal of Materials Research*, vol. 21, no. 3, pp. 715–724, 2006.

[24] B. D. Beake, G. A. Bell, W. Brostow, and W. Chonkaew, "Nanoindentation creep and glass transition temperatures in polymers," *Polymer International*, vol. 56, no. 6, pp. 773–778, 2007.

[25] S. Fujimura, J. I. Konno, K. I. Hikazutani, and H. Yano, "Ashing of ion-implanted resist layer," *Japanese Journal of Applied Physics Part 1*, vol. 28, no. 10, pp. 2130–2136, 1989.

[26] P. M. Visintin, M. B. Korzenski, and T. H. Baum, "Liquid clean formulations for stripping high-dose ion-implanted photoresist from microelectronic devices," *Journal of the Electrochemical Society*, vol. 153, no. 7, pp. G591–G597, 2006.

[27] K. K. Ong, M. H. Liang, L. H. Chan, and C. P. Soo, "Increase of etch resistance of deep ultraviolet photoresist by implantation," *Journal of Vacuum Science and Technology A*, vol. 17, no. 4, pp. 1479–1482, 1999.

[28] M. N. Kawaguchi, J. S. Papanu, B. Su, M. Castle, and A. Al-Bayati, "Surface characterization of ion-enhanced implanted photoresist removal," *Journal of Vacuum Science and Technology B*, vol. 24, no. 2, pp. 657–663, 2006.

Hindawi Publishing Corporation
International Journal of Polymer Science
Volume 2012, Article ID 574878, 14 pages
doi:10.1155/2012/574878

Review Article

Structure of Colloidal Flocs in relation to the Dynamic Properties of Unstable Suspension

Yasuhisa Adachi, Azusa Kobayashi, and Motoyoshi Kobayashi

Graduate School of Life and Environmental Science, University of Tsukuba, Tsukuba, Ibaraki 305-8572, Japan

Correspondence should be addressed to Yasuhisa Adachi, yas@sakura.cc.tsukuba.ac.jp

Received 15 August 2011; Accepted 29 September 2011

Academic Editor: Eri Yoshida

Dynamic behaviors of unstable colloidal dispersions are reviewed in terms of floc formation. Geometrical structure of flocs in terms of chemical conditions and formation mechanics is a key to predict macroscopic transportation properties. The rate of sedimentation and rheological properties can be described with the help of fractal dimension (D) that is the function of the number of contacts between clusters (N_c). It is also well known that the application of water soluble polymers and polyelectrolytes, which are usually used as a conditioner or flocculants in colloidal dispersions, critically affects the process of flocculation. The resulted floc structure is also influenced by the application of polymer. In order to reveal the roles of the polymers, the elementary rate process of polymer reaching to colloidal interface and subsequent reconformation process into more stable adsorption state are needed to be analyzed. The properties of permeable flocs and adsorbed polymer (polyelectrolyte) layers formed on the colloidal surfaces remain to be worked out in relation to inhomogeneous porous structure and electrokinetics in the future.

1. Introduction

Owing to the increasing social interest in environmental issues, interfacial phenomena and the behavior of colloidal particles have attracted attention [1]. Numerous colloidal particles exist in soil, water, and air environments. These particles have a large specific surface area where various chemicals can be adsorbed. Even substances that do not dissolve in water, such as dioxin, can be adsorbed and concentrated on the surface of colloidal particles with hydrophobic nature. If the colloidal particles are allowed to move with the water flow, they can be regarded as carriers for insoluble substances. Hence, it is important to analyze transport properties of colloidal particles to predict and control the movement and the fate of chemical substances in the environment. The dynamic behavior of colloidal particles depends critically on the way of flocculation. Therefore, the relationship between the microscopic flocculation process of colloidal particles and the macroscopic dynamics of the resultant flocculated system has been regarded as one of the most fundamental issues when considering the state and dynamics of chemical substances in aquatic environment. Figure 1 shows the relationship between various factors which control the flocculation process and macroscopic properties associated with flocculation. As shown in this figure, transport characteristics such as the rate of separation and rheological properties of the colloidal dispersion are largely affected by the structure of flocs. Consequently, many problems related to the transportation of colloidal particles are addressed by controlling the geometrical structure of flocs through kinetics of flocculation. As will be discussed later, an application of water soluble polymers and polyelectrolytes with an affinity to colloidal surfaces will critically influence flocculation processes. However, this process is not fully understood. In the present article, we introduce our effort using monodispersed spherical colloid as model system to establish the scheme of the study of the dynamics of unstable suspension placing an emphasis on the formation of colloidal flocs. Even though natural colloid does not obviously satisfy this condition, our strategy turned out to be useful to introduce the concept of fractal, to analyze the system on the basis of rate theory and evaluation of the role of polymer flocculants.

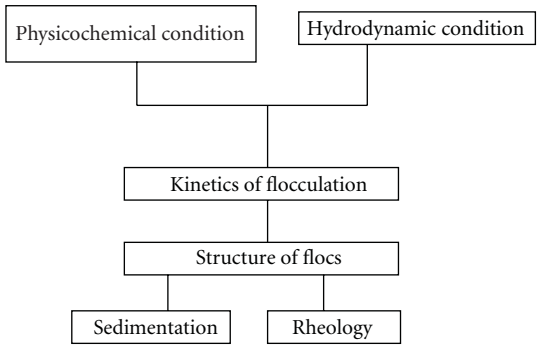

Figure 1: A correlation diagram of physical properties of a floc.

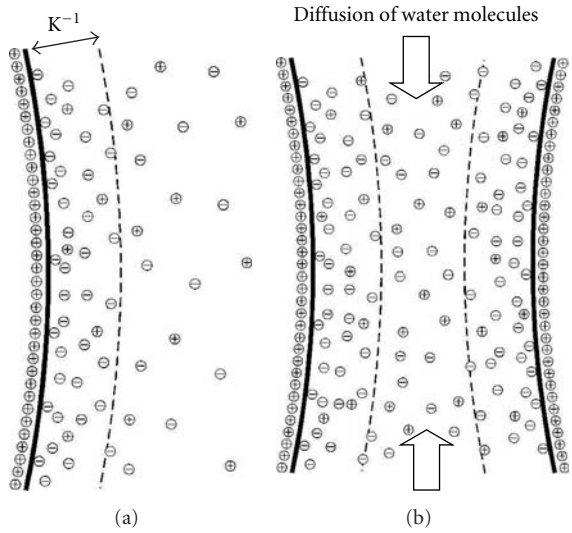

Figure 2: Schematic representations of a diffuse electrical double layer and the mechanism of generation of repulsive force by increasing the osmotic pressure. The chart was drawn on the basis of the ratio of the curvature radius of a colloidal particle to the Debye length κ^{-1} to be 30.

2. Natural Flocculation and Behavior of Colloidal Particles

Colloidal dispersions encountered in natural environments, such as suspension of clay minerals and organic substances in soil or turbid water, are usually thermodynamically unstable by themselves. If colloidal particles come close together, a universal van der Waals attractive force starts to interact between the particles. Because of this reason, when colloidal particles are brought close to each other by the effect of Brownian motion, fluid motion, and/or gravitational force, the colloidal particles start to flocculate and eventually form large flocs or aggregates.

The process of flocculation is usually analyzed by means of the rate theory. If all particle-particle collisions lead to flocculation, the flocculation rate is limited by particle-particle collisions; this type of flocculation is called rapid flocculation (or diffusion-limited aggregation). However, it is not always in reality, since a colloidal particle in water is

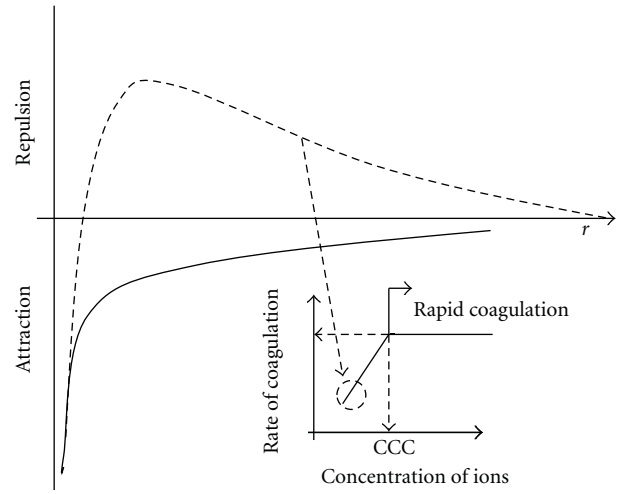

Figure 3: Potential between two particles and the coagulation velocity. When the salt concentration is low, the osmotic pressure results in the potential generation that causes positive repulsion (dotted line) with the expansion of a diffusion section of the electrical double layer. The coagulation velocity decreases because the particles overcome the potential.

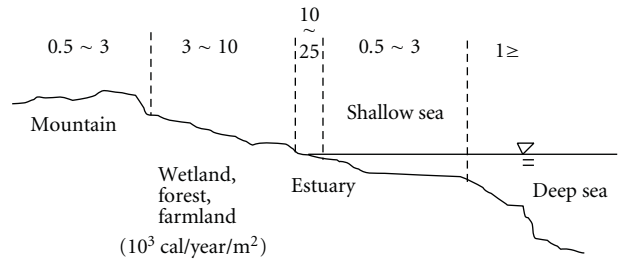

Figure 4: Biological primary production on the land and in the ocean.

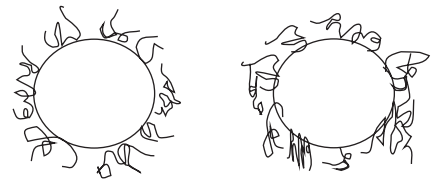

Figure 5: Coagulation inhibition by the steric hindrance of adsorptive polymers. When the polymer is adsorbed on colloidal particles, the protective effect hinders the particles from aggregation.

present with a considerable charge, thus attracting counter ions around the surface of the particles forming an ionic atmosphere. The development of the diffusive layer of ions will induce the increment in the osmotic pressure of the solvent in the gap region between the surfaces of two particles which are brought close together. Figure 2 shows a schematic representation of this situation. The development of the ionic diffusive layer prevents particles from adhesion. In other words, the flocculation of particles is inhibited by an energy barrier; hence, flocculation will take place at a significantly lower rate than that of rapid flocculation. This type of flocculation is called slow flocculation (or reaction-limited aggregation). Figure 3 shows schematically the relation between

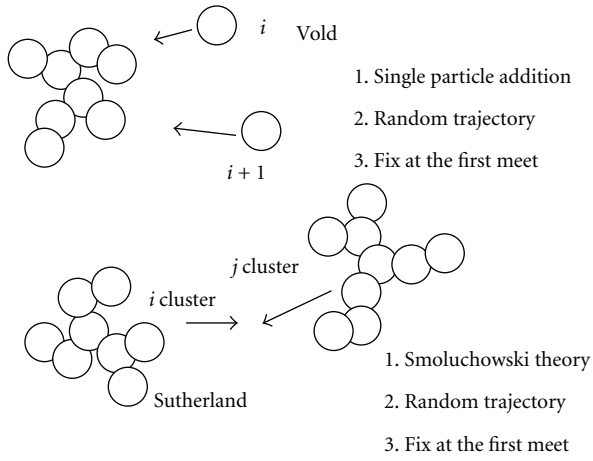

Figure 6: The single particle model (Vold) and the cluster-cluster addition model (Sutherlands).

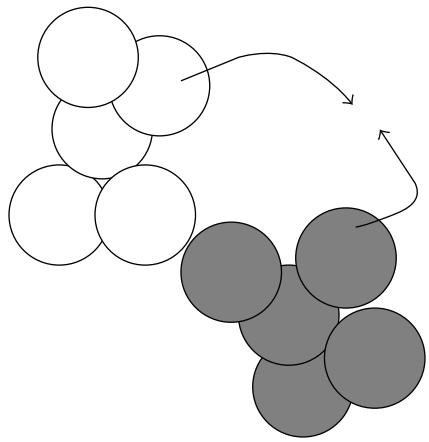

Figure 7: Rearrangement of collided clusters and increase in the number of their contacts.

the interacting potential and the rate of flocculation. In a low salt concentration, a positive potential that causes repulsion between particles is generated; hence, the rate of coagulation will become slow. The salt concentration corresponding to the point of inflection from slow to rapid flocculation is called the critical coagulation concentration (CCC).

In the case of slow coagulation, clear flocculation is not always induced. With a decrease of ionic strength, the tendency to remain cloudy will be increased. Even if the water in a freshwater area downstream near the river mouth is turbid, the transparency of water increases as it approaches to the marine environment. This is because the flocculation of colloidal particles or turbid components does not occur in water with a low salt concentration and the suspensions of small impalpable particles with a low sedimentation velocity can be maintained. On the other hand, the salt content of sea water is higher than CCC because of which the ionic diffusion layer gets compressed to induce rapid coagulation; thus, large flocs of the turbid components settle. Figure 4 depicts the process of biological primary production as summarized by Odum [2]; significantly high biological production is observed in a tidal flat in a coastal zone. The tidal ebb and flow causes the mixing of seawater and freshwater; the oxygen supplied by this mixture greatly contributes to the high biological production. In addition to this, aggregation of nutrient salts collected in flocs greatly contributes to a significant increase in the biological production capacity.

On the other hand, the seawater in contaminated areas such as Tokyo Bay does not always become transparent even when the salinity is high. This may be because organic matters adhere to the surfaces of the turbid colloidal particles. For instance, when organic macromolecules such as surface-active agents and proteins are adsorbed on the surfaces of colloidal particles, the thermal motions of their molecular chains, which have a fixed end and are projected like sea grass, prevent coagulation of the colloidal particles (Figure 5). This coagulation inhibition caused by the steric hindrance of the absorbed macromolecules is called the steric stabilization by absorbed polymer chains. Hunter et al. reported that water-soluble natural organic matters such as humic substances were adsorbed on colloidal particles such as clay minerals and metal hydroxides, thereby hindering the coagulation of the colloidal particles in the estuary [3, 4].

In the coagulation and settlement processes involved in the water treatment, the physicochemical conditions in the region containing colloidal particles are artificially modified to induce flocculation of the particles. Generally, in wastewater, the particle surfaces are contaminated. Hence, a flocculant is added in order to modify the particle surfaces and to increase/promote coagulation. A water-soluble polymer (or polyelectrolyte) is widely used as a flocculating agent to form large flocs of the colloidal particles. As will be discussed later, the details of the mechanism behind the formation of floc structures including the effect of the properties of a polymer flocculant [5] have not been fully understood.

3. Fractal Structure of the Floc

A floc of colloidal particles has a very high void ratio and an irregular shape. As a floc grows, its density decreases exponentially as a function of the floc diameter. The exponential reduction of the density reflects the fractal structure of the floc. The geometrical property of such flocs can be analyzed by methods such as the computer simulation by Monte Carlo method. In particular, since 1980s, a vast amount of data on the geometrical properties of flocs has been obtained with the development of the concept of fractals. However, the original model, other than the current fractal model, of the floc simulation was reported already in the late 1950s. Vold [6, 7] proposed a model involving a single particle addition in which individual spherical particles on a randomly selected straight line collide sequentially with the mother floc positioned at the origin, and a flocgrows when the particles are fixed at the point of the first contact with the mother floc. Flocs made of up to 60 particles were numerically reproduced. The flocs had random and irregular shapes. However, the exponential reduction of their densities with the growth of the floc could not be reproduced in their study.

(a) (b)

Figure 8: Floc model developed using ping-pong balls (number of particles: 256). (a) One cluster-to-cluster contact model. (b) Two cluster-to-cluster contacts model [13].

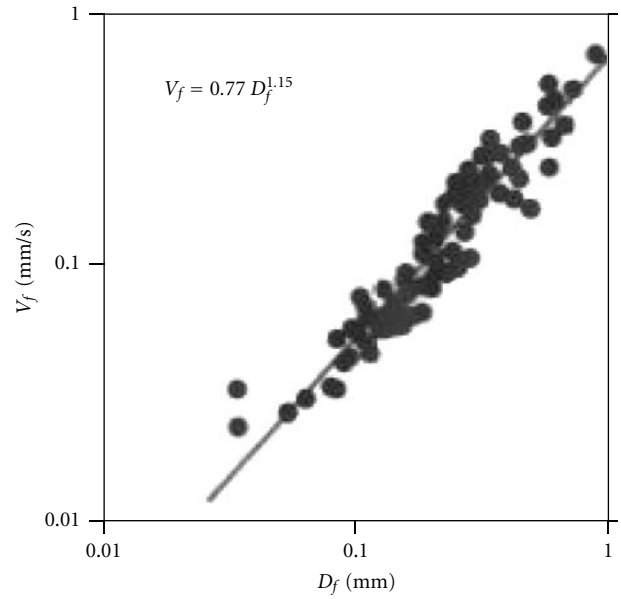

Figure 9: Relationship between the diameter and the settling velocity of kaolinite flocs [15].

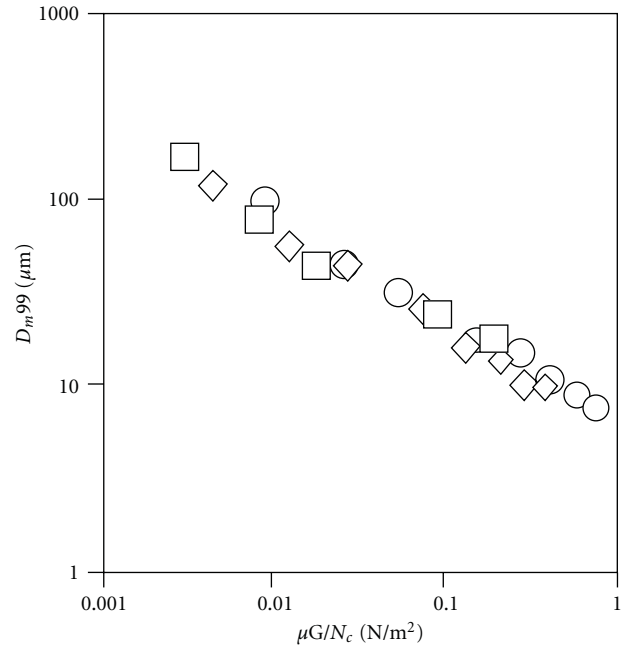

Figure 10: Relationship between the maximum diameter (D_m99) of the floc of polystyrene latex particles existing in the agitating tank and the strength of agitation. G is the practical shearing velocity and μ is the viscosity coefficient. ◇; N_c= 1; ◯: N_c = 2; □: N_c= 3 [17].

Sutherland and Goodarz-Nia [8, 9] improved Vold's model and proposed a model of cluster-cluster aggregation by assuming that two clusters of colloidal particles collide repeatedly in sequence resulting in the growth of the floc; they proposed this model on the basis of computer simulations performed by applying the rate theory of coagulation developed by Smoluchowski [10], and they succeeded in reproducing the exponential reduction of the density with the floc growth (Figure 6). On the basis of the results obtained, the number of the colloidal particles in a floc is expressed in terms of a floc diameter function, as follows:

$$i = \left(\frac{D_f}{d_0}\right)^D, \tag{1}$$

where d_0 is the diameter of primary particle and D is the fractal dimension. From the simulation performed on the basis of Sutherland's model, D is determined to be approximately 1.83; however, experimental results [11] are greater than this value and distributed. Considering that the difference between these values is a result of the way of formation of clusters, the authors proposed a two-point contact model. In this model, the clusters can roll and move to the next point of contact after a collision (Figure 7) [12, 13]. Figure 8 shows the result of the simulation in which ping-pong balls were considered. From the figure, it is apparent

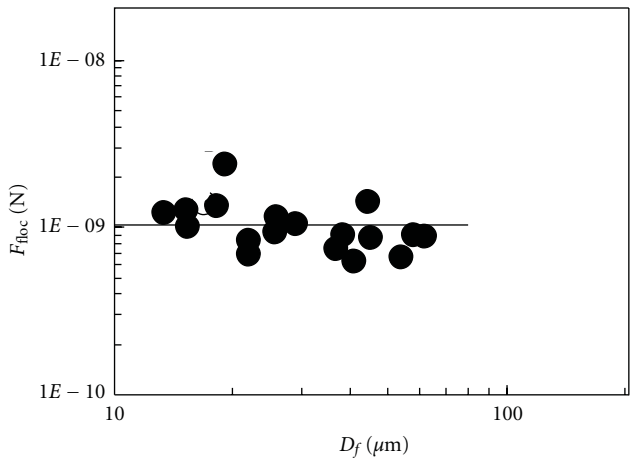

Figure 11: Cluster-to-cluster adhesive force calculated by a fracture experiment for contractile flow through the orifice. The experiment was conducted with a floc of polystyrene latex particles of the diameter of 2.8 μm.

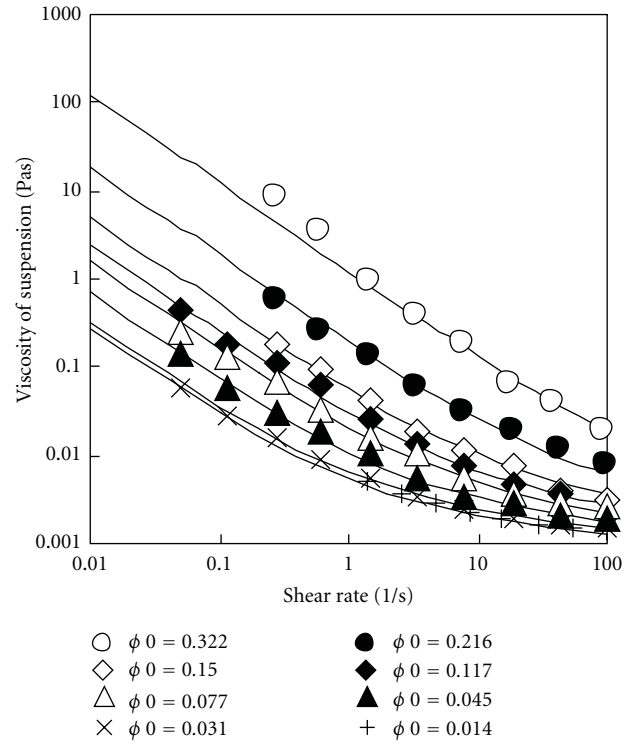

Figure 12: Analysis of the shear thinning viscosity of flocculated suspension of polystyrene latex with our model [19].

that by using the two-point contact model, a floc made of dense packing of particles can be obtained. Meakin and Jullien [14] performed the same simulation and confirmed that the fractal dimension increased to 2.13, 2.18, and 2.19 as the number of contacts between clusters (N_c) was increased to 2, 3, and 4, respectively.

4. Fractal Structure and Physical Properties of Flocs

The settling velocity of a single floc, V_f, is an indicator used to design a settling tank in the process of water and waste water treatment or to evaluate the transport diffusion of coagulated contaminants in the aquatic environments. V_f can be obtained by analyzing the force balance involving terms for gravity, buoyancy, and the fluid resistance acting on a floc with fractal structure as follows [15]:

$$V_f = \frac{g}{18\alpha\mu}(\rho_s - \rho_w) \cdot {d_0}^{3-D} \cdot {D_f}^{D-1}, \tag{2}$$

where ρ_s and ρ_w are the densities of the colloidal particles and water (known), μ is the viscosity coefficient, and g is the acceleration due to gravity, respectively. α is a coefficient reflecting the floc shape; for a spherical floc, the value of this coefficient is 1. Figure 9 shows an example of experimental measurement of the settling velocity of flocs as a function of the floc diameter. On the basis of (2), the fractal dimension of the structure is determined from the slope of the plots presented in this figure.

As can be easily understood, the determination of the floc diameter at a given flow field is the most important issue to evaluate the rate of sedimentation. This is a so-called problem of floc strength and has been worked out for many years [16]. Kobayashi [17] proposed a simple model on the fracture strength of a floc that exists in a turbulent flow. That is, the floc will break up when the shear force F_{hyd} of the fluid acting on the floc in the flow field exceeds the force retaining the floc F_{floc}:

$$F_{\text{hyd}} \geq F_{\text{floc}}. \tag{3}$$

The force retaining the floc is assumed to be the product of the adhesive force per contact between clusters (f) and the number of cluster-to-cluster contacts (N_c):

$$F_{\text{floc}} = f \cdot N_c. \tag{4}$$

On the other hand, the shear force of the fluid acting on the floc is expressed by substituting the term for shear stress per unit area into the expression for the surface area of the floc:

$$F_{\text{hyd}} \propto \mu G D_f^2, \tag{5}$$

where μ is the viscosity coefficient and G is the substantive velocity gradient. By assuming (3) to be the condition for the fracture, D_f is derived as follows:

$$D_f \propto \left(\frac{N_c}{G}\right)^{0.5}. \tag{6}$$

Figure 10 shows the size of the floc in a turbulent flow as a function of the fluid mixing intensity. The experimental result was plotted on a master curve by applying different N_c values to flocs with different fractal dimensions. This result validates the concepts expressed in (4) and (5).

Equation (4) was validated by a floc fracture test by considering a contract flow through an orifice. The adhesive

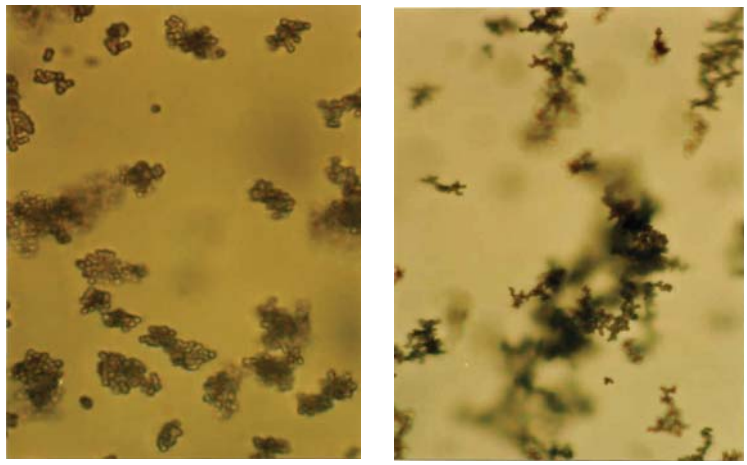

Slow coagulation in turbulent flow (a)

Rapid Brownian coagulation (KCI 1.19 M) (b)

Figure 13: Flocs of polystyrene latex particles of the primary diameter 1.356 μm formed in a turbulent flow (a) and flocs of the same particles formed by the rapid Brownian coagulation (b).

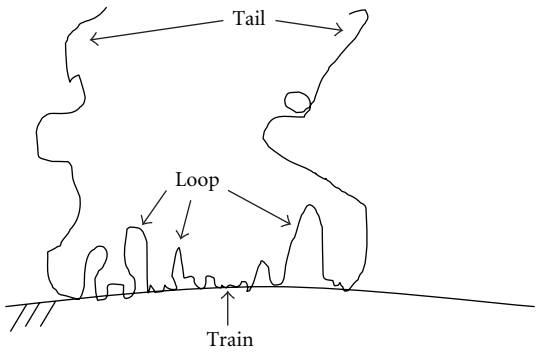

Figure 14: A typical conformation of a polymer chain adsorbed on the surface.

strength per contact within the floc was estimated to be of the same order as that of the adhesive force, including AFM measurements between surfaces (Figure 11) [18]. It is also interesting to note that (4) and (6) can be easily incorporated into a rheology model owing to simple forms of the terms used in these equations and can be used to describe non-Newtonian flows such as softening of materials (Figure 12) [19, 20].

5. Rearrangement of Floc Structures

As mentioned in the previous chapters, the number of contacts between clusters (N_c) and the corresponding fractal dimension (D) characterizing floc structures are of essential importance in settling/sedimentation and transport phenomena. However, physical mechanisms by which these factors are determined have not been fully understood as well as their contributions to floc formation. Meakin et al. [14, 21] ascribed the rearrangement of clusters to the condition of reaction-limited (or slow) coagulation, That is, there exists interparticle repulsion within a cluster, and demonstrated that the resulting flocs in this condition are more compact than those formed by diffusion-limited (or rapid) coagulation. On the other hand, we observed a cluster-to-cluster rearrangement when the initial particle concentration is high [22, 23] or the fluid flow is involved, even under the region of rapid coagulation (Figure 13) [24]. That is, interparticle repulsion is screened by the presence of concentrated salt ions. As indicated in Figure 13, the presence of the shear flow would induce rearrangement of the flocs leading to the formation of dense flocs.

6. Formation of Flocs Enhanced by Polymers

For polymer-induced flocculation, the presence of polymers additionally influences rearrangement and corresponding floc properties. In fact, water soluble polymers are often utilized as flocculants in water and waste water treatments to enhance the rate of flocculation and produce large, dense, and strong flocs to facilitate solid-liquid separation. When the flocs are large in size, having a nearly spherical, dense, and packed structure, they are referred to as pellet flocs. Napper [25] conducted experiments varying physicochemical conditions during flocculation operation and reported that pellet flocs are formed in the concentrated colloidal suspension only when a certain level of polymer is mixed under a proper stirring intensity. The fractal dimension of pellet flocs approaches to 3.0 since branching structures within a cluster are diminished. Formation of these pellet flocs provides obvious evidence for rearrangement of interacting clusters. It is noteworthy that they are formed only in the presence of shear flow. This observation leads us to a possible explanation that the contact points of the clusters are flexible due to the adsorbed polymers in between so that the clusters can rearrange themselves quite easily driven by the shear force.

Let us now summarize the process of floc flocculation enhanced by adsorbing polymers. Two flocculation mechanisms are well known: bridging and charge neutralization.

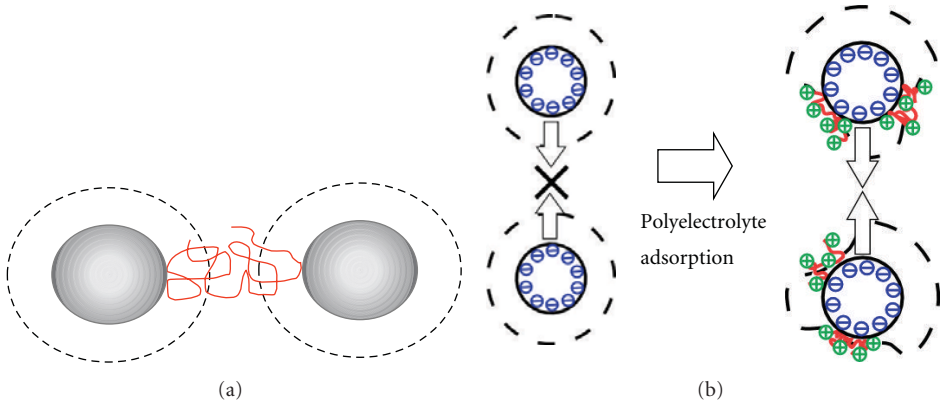

Figure 15: Flocculation mechanisms: (a) bridging and (b) charge neutralization. The dashed line represents the electric double layer.

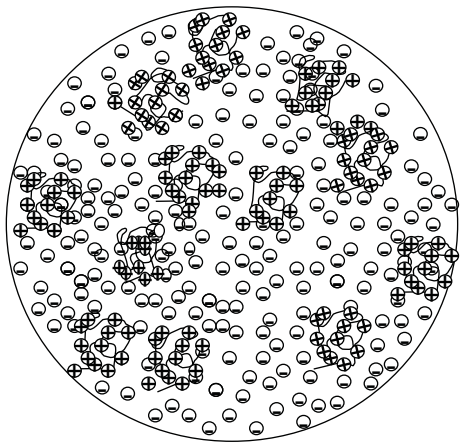

Figure 16: A mosaic-like distribution of highly charged polyelectrolytes on a particle of the oppositely charge.

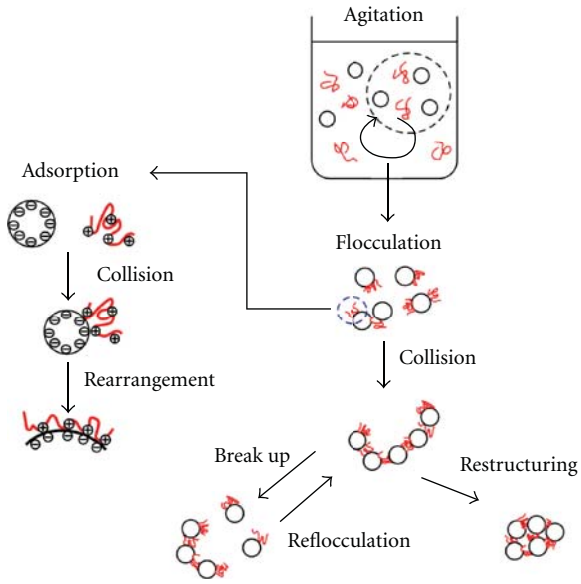

Figure 17: A schematic diagram of flocculation with adsorbing polymers [40].

Whether which mechanism is dominant is markedly dependent on the conformation of adsorbing polymers at colloidal surfaces. Once a polymer chain is adsorbed onto the surface of a particle, the attached chain undergoes a conformational change (referred to as reconformation) after a characteristic time toward a more stable configuration with loops, tails, and trains (Figure 14) [26]. If the adsorbing polymer has a high molecular weight, or the polymer chain is long, it is likely to result in the formation of protruding loops and tails extending into the solution side. These protruding segments on a particle can reach to other particles and adsorb thereon, thus bridging the particles together as a floc as illustrated in Figure 15(a). Flocculation on this basis is referred to as bridging flocculation, which is firstly proposed by Smellie Jr. and La Mer in 1958 [27]. For bridging there must remain an unoccupied portion on the surface where polymer chains adsorbed on another particle can attach to, otherwise the particles will be stabilized and flocculation will not take place. A very first work on the efficiency of bridging flocculation with an account of the surface coverage was proposed by Fleer and Lyklema [28]. According to their concept, the probability of bridge formation is proportional to the fractional surface coverage θ and the uncovered fraction $(1-\theta)$. Although this model accounts for the experimental observation that the formation of bridges is more facilitated when the surface coverage is low, a quantitative estimation based on this idea is hardly achieved since numerous kinetic factors regarding adsorption are involved as well as complex structures of adsorbed polymers which make the measurement of surface coverage complex. The extending polymer chains must have a greater than twice the thickness of the electric double layer κ^{-1} around a particle to form a bridge. That is, bridging flocculation can take place if the extent of the adsorbed polymer layer δ is greater than $2/\kappa$, while no bridging flocculation develops as $\delta < 2/\kappa$. This is confirmed experimentally, for instance, by Gregory [29].

Another mechanism of flocculation is called charge neutralization. Adsorption of a charged polymer onto the surface of an oppositely charged particle results in the reduction in the net charge of the particle. The neutralization of the surface charge lowers electrostatic repulsion acting between the particles, thus induces flocculation. Figure 15(b)

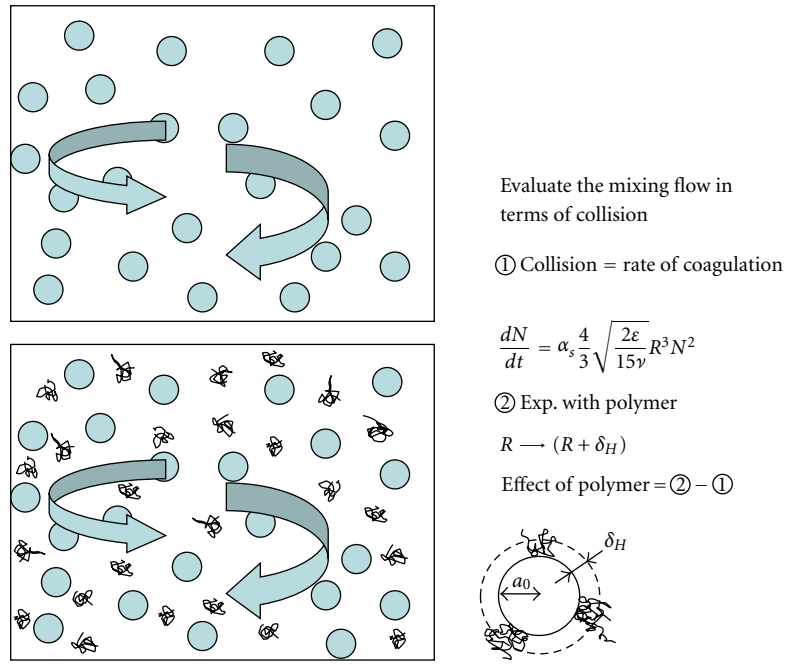

Figure 18: Normalization of mixing condition applied to analyze the influence of polymer addition.

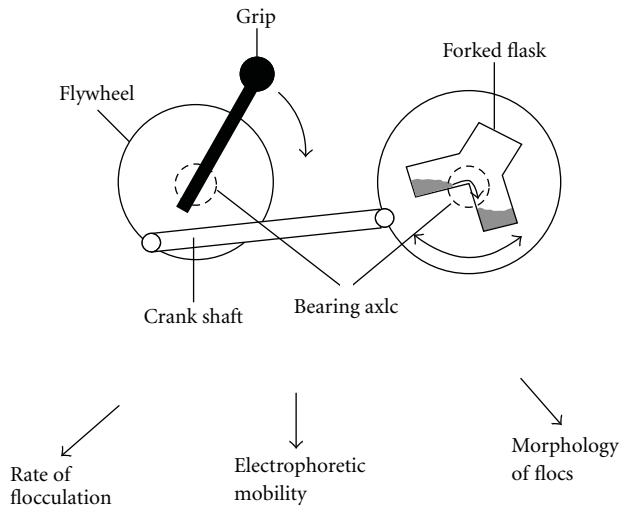

Figure 19: The end-over-end rotation apparatus to generate standardized mixing with a small volume of samples. After the mixing of a predetermined period, samples are taken up to be monitored by the rate of flocculation, the electrophoretic mobility and the morphology of flocs.

shows a schematic representation of this mechanism. One can imagine that the charged surface may not be completely covered with adsorbed polyelectrolytes even if the net electric potential of the particle is neutralized. In this case, mosaic-like distributed polyelectrolytes can interact with unoccupied surfaces of other particles to form a floc (Figure 16). The attraction in this manner is called electrostatic patch effects, which is proposed by Higashitani et al. [30] through a flocculation experiment of polystyrene particles with strongly charged cationic polyelectrolytes. Electrostatic interaction acting between a particle and polyelectrolyte is a function of the ionic strength of the solution as well as the charge density of polyelectrolyte; accordingly, the process of charge neutralization is affected by both parameters.

Each of the flocculation mechanisms described above is governed by the process of polymer adsorption and collision of colloidal particles, which markedly influence the conformation of the polymers at the surfaces. A schematic diagram of flocculation induced by polymer addition is shown in Figure 17. When polymers are added to the colloidal dispersion, the system is brought to the state far from the equilibrium. As seen in the diagram, the flocculation procedure consists of following several elementary processes under the mixing conditions, which usually is the turbulent flow:

(i) mixing of the polymeric flocculants into a homogeneous solution,

(ii) collision between colloidal particles,

(iii) transportation of a polymer chain toward the surface of a particle,

(iv) reconformation of an adsorbed polymer chain on the surface of a particle,

(v) formation of bonds (or bridges) between colloidal particles,

(vi) rearrangement and breakage of floc structures.

All these elementary processes occur simultaneously. That is, a cluster fixation would take place at the same time with or at the early stages of polymer adsorption and collision of the particles. Variations in floc structures produced in

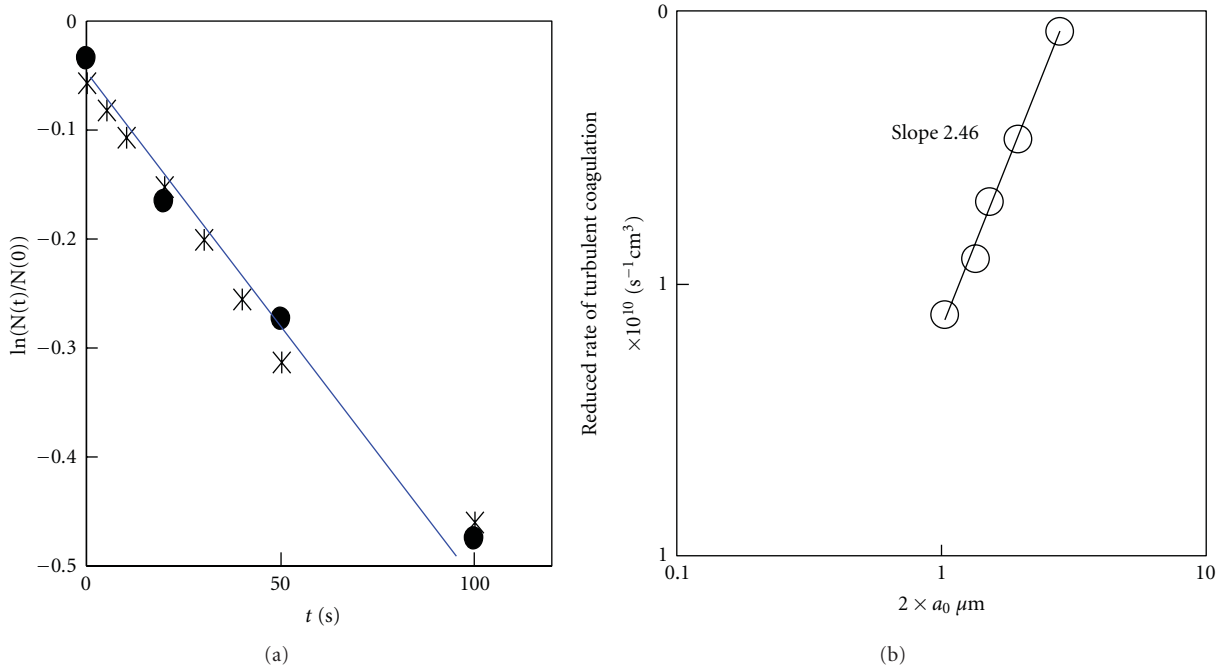

Figure 20: The result of the progress of salt-induced rapid coagulation in the standardized mixing. (a) Temporal evolution of the number concentration of flocs. (b) Reduced rate of coagulation as a function of the particle diameter.

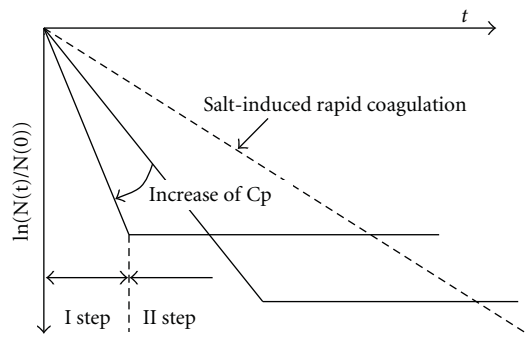

Figure 21: Concept of the progress of flocculation with addition of the excess amount of adsorbing polymers [47].

different physicochemical conditions support this idea [23–25]. Therefore, the analysis of kinetic aspects listed previously is an essential requirement in order to elucidate the process of rearrangement of flocs structures.

7. Monitoring Rearrangement of Floc Structures

Although it is now obvious that the process of particle collision as well as polymer adsorption at early stages of flocculation has significant impacts on the floc formation, including cluster fixation and corresponding rearrangement of floc structures, few studies are available on the mechanism of action. In order to investigate dynamic aspects of colliding particles under the turbulent flow, the authors developed a reproducible method of colloidal mixing and applied this technique to assess nonequilibrium behavior of polymer adsorption (Figure 18). Assuming that all collisions between particles lead to coagulation, one can evaluate the turbulent flow of mixing by monitoring the rate of coagulation. First, let us consider a monodispersion of colloidal particles undergoing rapid coagulation with a sufficient content of salt. The rate of coagulation under the mixing flow was worked out by Adachi et al. [31]. Also, Saffman and Turner [32] confirmed the correlation of collision efficiently owning to hydrodynamic interaction derived by van de Ven and Mason [33] evoking the concept of the local isotropy of turbulence proposed by Komogrov. The progress of coagulation is expressed with a temporal variation of the total particle number concentration $N(t)$ as

$$\frac{dN(t)}{dt} = -\frac{1}{2}\alpha_T \sqrt{\frac{8\pi\varepsilon}{15\nu}}(2a_0)^3 N(t)^2, \tag{7}$$

where ε, ν, and a_0 are the rate of energy dissipation per unit mass of the fluid, kinematic viscosity, and the radius of a colloidal particle, respectively. α_T is the collision efficiency reflecting the hydrodynamic interaction. For rapid coagulation, an approximate expression for α_T is derived by substituting the effective shear rate of turbulent flow in the numerical calculation result of Adachi et al. [34] taking into account van der Waals attractive forces in the trajectory analysis of two colloidal particles in the laminar shear field. That is,

$$\alpha_T = \left(\frac{A}{36\pi\mu a^3{}_0\sqrt{4\varepsilon/15\pi\nu}}\right)^{0.18}, \tag{8}$$

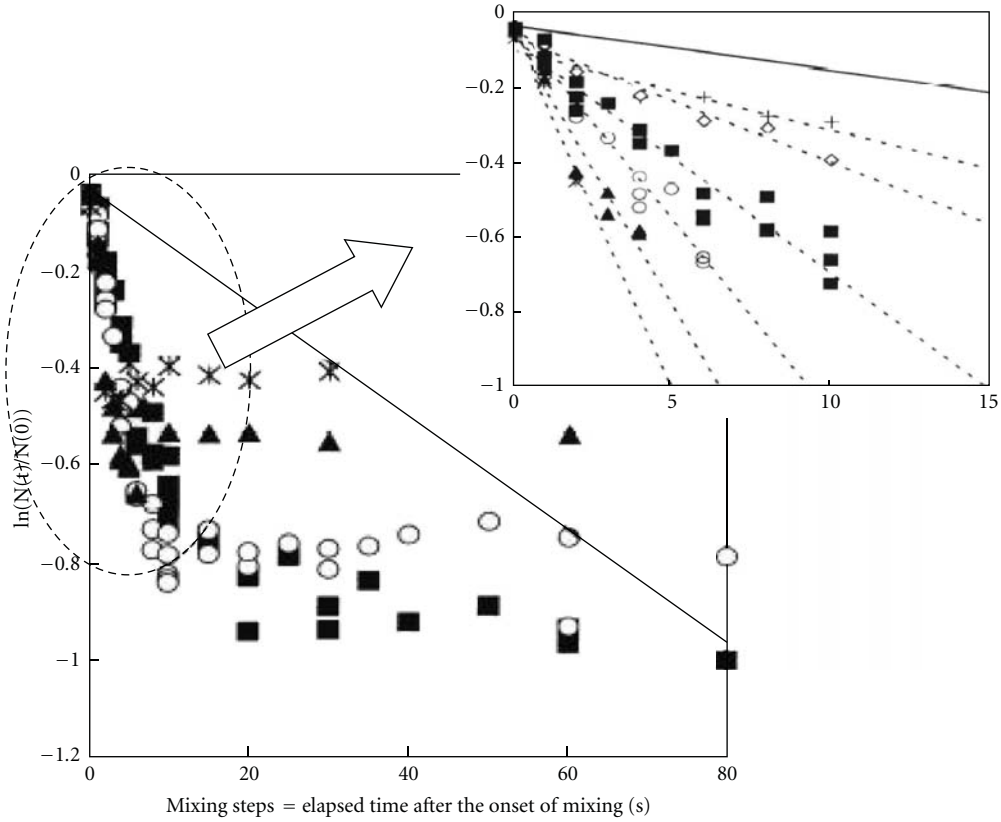

FIGURE 22: $\ln(N(t)/N(0))$ versus time for PEO-induced flocculation [47].

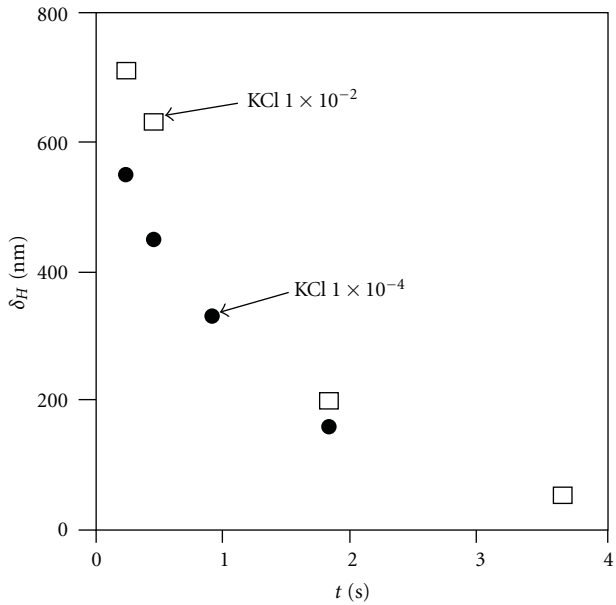

FIGURE 23: The thickness of a polymer layer δ_H as a function of the interval of polymer supply [47].

where A is the Hamaker constant and μ is the viscosity. If the discussion is restricted to the early stage of coagulation, where the volume fraction of clusters can be assumed as

$$\phi = N(t) \times \frac{4\pi}{3} \times a_0^3, \tag{9}$$

then (7) yields the following approximate solution:

$$\ln \frac{N(t)}{N(0)} = -\alpha_T \sqrt{\left(\frac{24\varepsilon}{5\pi\nu}\right)} \phi t. \tag{10}$$

Evaluation of mixing flow is now possible by simply measuring the number concentration of coagulating colloidal particles as a function of elapsed time using the monodispersed colloidal particles under the condition of rapid coagulation. In our experiment, an end-over-end mixing device was developed to realize normalization of mixing flow (Figure 19). Coagulation was performed with this apparatus and the rate of coagulation, the electrophoretic mobility, and the morphology of the resultant complex were monitored at each step of mixing. A typical result of the evolution of coagulation is given in Figure 20.

Furthermore, the authors used the aforementioned technique to investigate the effect of polymers on the flocculation of the same system. The temporal evolution of flocculation is shown in Figure 21. Flocculation is enhanced immediately after the addition of polymers (stage I) until the surface of the particles reaches saturation (stage II). Since the flocculation rate is greatly dependent on the size of colloidal particles as seen in (7), the effective thickness of the adsorbed polymeric layer δ_H can be obtained from the ratio of the flocculation rate enhanced by polymers to that of without polymer addition, using

$$\eta = \frac{(a_0 + \delta_H)^3}{\alpha_T a_0^3}. \tag{11}$$

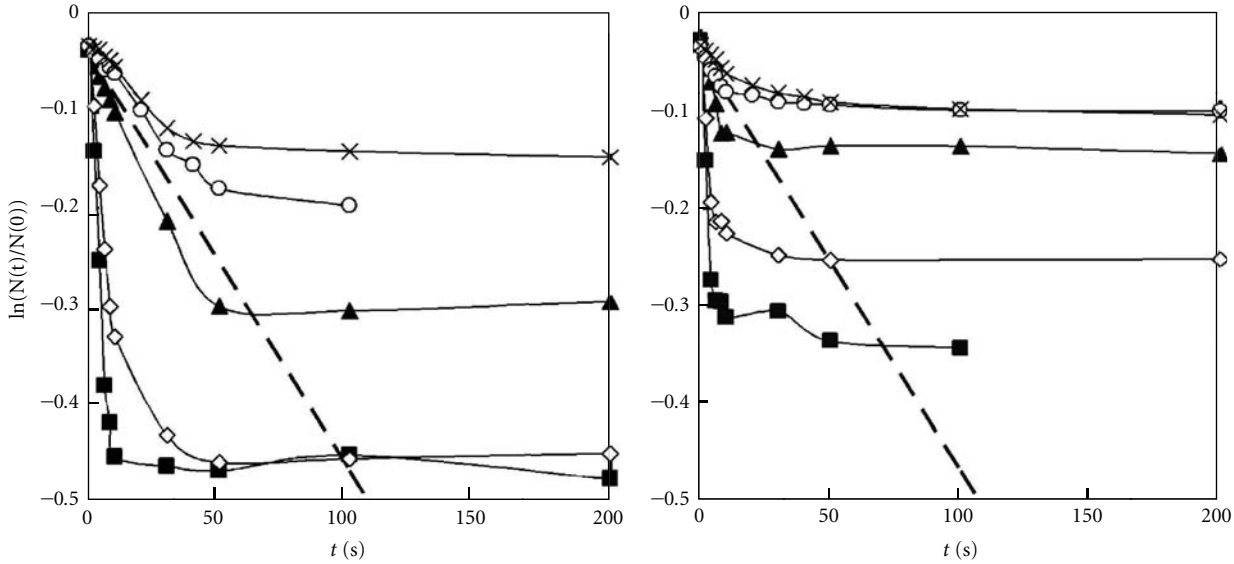

FIGURE 24: $\ln(N(t)/N(0))$ versus time for flocculation with polyelectrolytes of the concentration of 0.5 mg/L. (a) KCl $= 1.0 \times 10^{-2}$ M. (b) KCl $= 1.0 \times 10^{-4}$ M. The molecular weights of the polyelectrolytes are (■) 4.9 million, (◇) 3.5 million, (▲) 1.2 million, (◯) 0.49 million, and (×) 0.16 million.

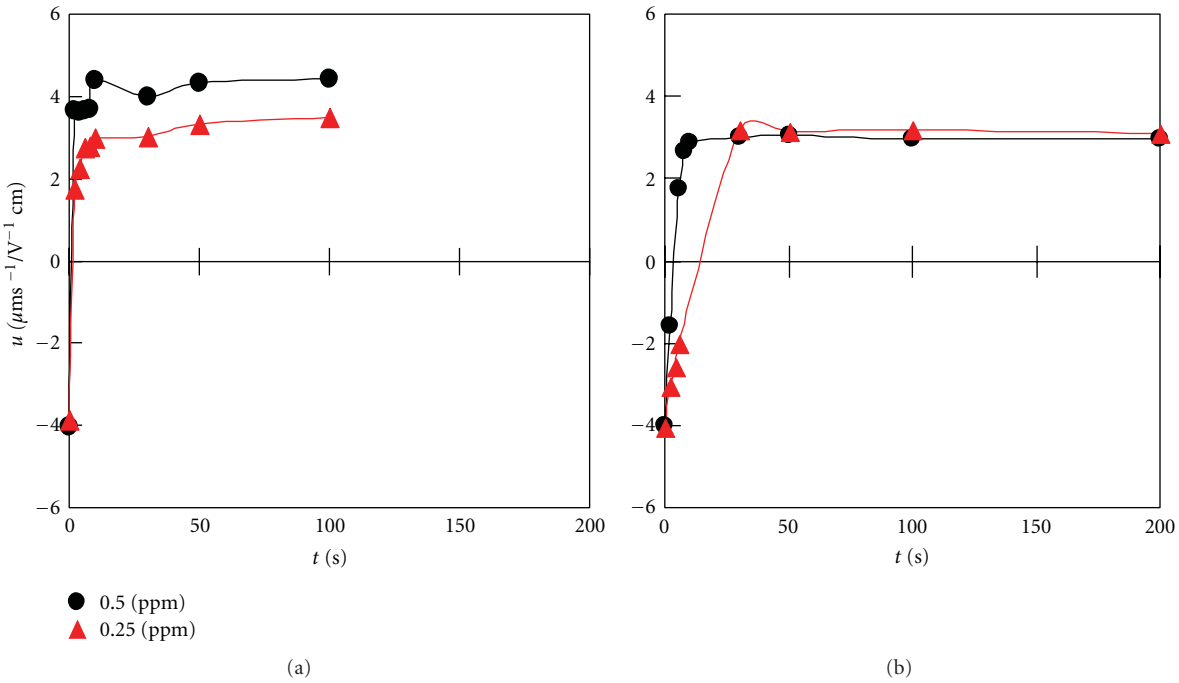

FIGURE 25: Electrophoretic mobility of the polyelectrolyte-PSL particle complexes versus the agitation time. (a) KCl $= 1.0 \times 10^{-4}$ M. (b) KCl $= 1.0 \times 10^{-2}$ M. The molecular weight of the polyelectrolyte was 4.9 million.

When the polymer concentration is high, it is likely that the particles carry freshly adsorbed polymers, and thus the effective collision radius is detected higher. Meanwhile, δ_H will be detected small if the polymer reconforms to a flattened structure on the surface when the polymer concentration is low. The time required for the saturation decreases with the polymer concentration, as expected. The flux of polymers toward a reference particle can be quantified by assuming a simple addition of the diffusion flux by Brownian motion and the collision induced by the turbulent flow, as

$$J_p = 4\pi D_{OP} R_{OP} N_p + \sqrt{\frac{8\pi\varepsilon}{15\nu}} \left(a_0 + a_p\right)^3 N_p, \qquad (12)$$

where D_{OP} and R_{OP} are the relative diffusion constant and collision radius of a polymer chain and a particle,

respectively, and a_p and N_p are the radius and the number concentration of polymers, respectively. The authors conducted a flocculation experiment of polystyrene latex (PSL) particles induced by the excess addition of polyethylene oxide (PEO) of a nominal molecular weight of 5.0×10^6 g/mol (Figure 22) [35]. Enhancement of the flocculation rate provides evidence for bridging flocculation. The initial rate of flocculation is greater for higher PEO concentration cases, indicating that δ_H for the collision radius grows with the PEO concentration. On the basis of (12) and defining the projected area of a single PEO chain as a square of its diameter, the relationship between δ_H and the interval of the polymer supply is clarified as shown in Figure 23. One can see that the reconformation of a polymer chain is disturbed when the surface is crowded with previously adsorbed polymers, that is, when the flux of polymers toward a particle is high. Note that the reconformation occurs within the order of a few seconds.

Most polymeric flocculants in practical applications are polyelectrolytes. They carry charged groups on their segments and thus have a strong adsorption affinity to the surface of oppositely charged particles. The temporal progress of flocculation of PSL particles induced by strong polyelectrolytes is shown in Figure 24 as a function of the molecular weight and ionic strengths [36]. The rate of flocculation is enhanced compared to that of salt-induced coagulation when the polymeric molecular weight is high because of formation of bridges; meanwhile the flocculation is not facilitated greatly when the shorter polyelectrolyte chains are used. Taking into account the neutralized net charge of the PSL-polyelectrolyte complex, one can reasonably estimate that charge neutralization was dominant in the latter case [37, 38]. Interestingly, the electrophoretic mobility of PSL particle-polyelectrolyte complexes converges on the same plateau value regardless of the polymer concentration if the chain length is the same, except for the cases of high molecular weight chains under low ionic strength (Figure 25) [39]. Furthermore, the observation of the morphology of the complexes produced under the low ionic strength revealed that the rearrangement of particles is significantly hindered and the flocs are resulted in an open structure as shown in Figure 26. The explanation for the aforementioned results is given as follows. Under lower ionic strengths, polymer chains are rigidly adsorbed on the oppositely charged particles while they repel each other with strong electrostatic repulsion among charged segments, making both polymers and particles difficult to move as illustrated in Figure 27 [39–41]. In contrast, under the high ionic strength, that is, when polymer-particle electrostatic attraction and polymer-polymer repulsion are screened, adsorbed polyelectrolytes smoothly undergo reconformation and subsequently produced flocs easily rearrange their structures to have increased contact points. Interestingly, dependency of ease of rearrangement and structures of flocs on the ionic strength is reversed with and without polymer flocculants. The same trend is observed in a comparative study on floc structures of humic acids produced by various dual-coagulants of different electric properties [42]. Experimental results discussed previously imply the necessity of introducing a new concept on the way to fix contact points of clusters instead of a traditional idea of simple energy barrier.

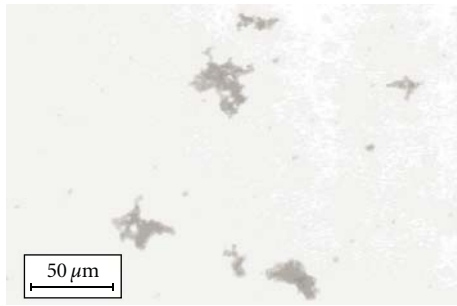

KCl: 1×10^{-4} (mol/l)

Polyelectrolyte Mw: 4.9×10^6

Concentration: 0.6 (mg/l)

(a)

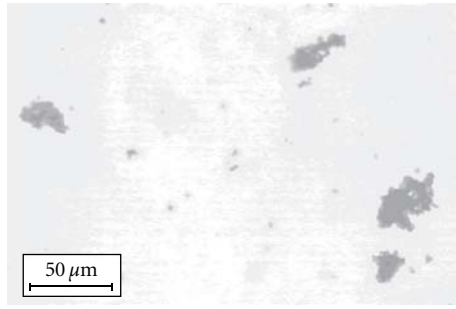

KCl: 1×10^{-2} (mol/l)

(b)

Figure 26: Microscopic photographs of polystyrene latex flocs formed by polyelectrolyte flocculants of a large molecular weight. When the ionic strength is low (a), low-density bulky flocs are formed. In contrast, high-density flocs are formed when the ionic strength is high (b) so that adsorbed polyelectrolytes undergo reconformation smoothly [39].

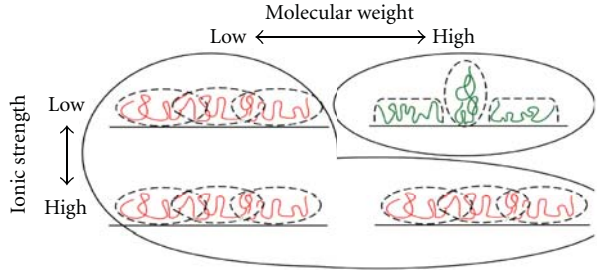

Figure 27: Polyelectrolytes adsorbed on the surface of a colloidal particle. The final pattern is affected by the adsorptive process when the ionic strength is low and the molecular weight is high.

8. Future Perspectives

We have discussed the importance of floc rearrangement in the earlier part of this review. Thus far, our discussion had been based on the fact that floc structures are determined by

the process of coagulation/flocculation. Interestingly, some reports suggest that a further growth of flocs leads to the rise in the rate of coagulation [43, 44]. That is, the floc structure itself has some influence on the progress of coagulation. Their interdependency remains to be elucidated. Also, in the system where flocculation is induced only by salt, the time scale involved in the rearrangement is estimated to be very short, possibly less than 1 second. Even for the polymer-induced flocculation, it is accepted that the rearrangement of the flocs takes place within a few seconds after adsorption, as demonstrated in the experiment using PEO as a flocculant [35]. However, a recent study by the authors [45] revealed that the order of a few hours is required for a polymeric layer adsorbed on a single colloidal particle to reach the state of equilibrium. Analysis on floc structures as well as factors acting on their determination in a system of well-proceeding levels of coagulation would be important to evaluate long-term behaviors of colloidal dispersions, such as the stability of the system and the breakage and/or re-grow of the flocs. Electrophoresis, despite the ease of the measurement, remains unrevealed for the problem dealing with a particle carrying an ion-permeable polymeric layer around it. Theoretical work on the electrophoresis of so-called soft particles has been developed [46], though quantitative discussions are still under development including the charge distribution and internal polymer structures inside the polymeric layer and their correspondence to the experimental results. Furthermore, interior floc structures and the presence of polymeric interparticle matrix markedly influence the fluid flow within the flocs. This is regarded as a great importance for the electrophoretic transport, settling behavior of flocs, and biochemical interactions such as the exchange of substrates among microbial cells within a colony, and we expect further investigations.

Acknowledgments

The authors express their thanks to Dr. Kenji Aoki, Dr. Yasuyuki Kusaka, and Dr. Tomonori Fukasawa for their frank discussions. This work is partly funded by Grants-in-Aid for scientific research (222408025) from JSPS.

References

[1] Y. Adachi and S. Iwata, Eds., "Tsuchi no koroido genshou," *Gakkai-Shuppan Sentar*, pp. 1–451, 2003 (Japanese).
[2] E. P. Odum, *Basic Ecology*, CBS College Publishing, 1988.
[3] K. A. Hunter and P. S. Liss, "The surface charge of suspended particles in estuarine and coastal waters," *Nature*, vol. 282, no. 5741, pp. 823–825, 1979.
[4] L. M. Mosley, K. A. Hunter, and W. A. Ducker, "Forces between colloid particles in natural waters," *Environmental Science and Technology*, vol. 37, no. 15, pp. 3303–3308, 2003.
[5] K. Aoki and Y. Adachi, "Flocculation mechanisms of colloidal particles with polyelectrolytes bridging vs. Charge neutralization," *Transactions of The Japanese Society of Irrigation, Drainage and Rural Engineering*, vol. 245, pp. 65–71, 2006.
[6] M. J. Vold, "A numerical approach to the problem of sediment volume," *Journal of Colloid Science*, vol. 14, no. 2, pp. 168–174, 1959.
[7] M. J. Vold, "Computer simulation of floc formation in a colloidal suspension," *Journal of Colloid Science*, vol. 18, no. 7, pp. 684–695, 1963.
[8] D. N. Sutherland, "A theoretical model of floc structure," *Journal of Colloid And Interface Science*, vol. 25, no. 3, pp. 373–380, 1967.
[9] D. N. Sutherland and I. Goodarz-Nia, "Floc simulation: the effect of collision sequence," *Chemical Engineering Science*, vol. 26, no. 12, pp. 2071–2085, 1971.
[10] M. V. Smoluchowski, "Versuch einer mathematichen theorie der koagulations kinetik kollider losungen," *Zeitschrift fur Physikalische Chemie*, vol. 92, pp. 129–168, 1917.
[11] N. Tambo and Y. Watanabe, "Physical characteristics of flocs—I. The floc density function and aluminium floc," *Water Research*, vol. 13, no. 5, pp. 409–419, 1979.
[12] Y. Adachi and S. Ooi, "Structure of a floc," in *Proceedings of the World Congress III of Chemical Engineering*, vol. 3, pp. 156–159, 1986.
[13] Y. Adachi and S. Ooi, "Geometrical structure of a floc," *Journal of Colloid And Interface Science*, vol. 135, no. 2, pp. 374–384, 1990.
[14] P. Meakin and R. Jullien, "The effects of restructuring on the geometry of clusters formed by diffusion-limited, ballistic, and reaction-limited cluster-cluster aggregation," *The Journal of Chemical Physics*, vol. 89, no. 1, pp. 246–250, 1988.
[15] Y. Adachi and Y. Tanaka, "Settling velocity of an aluminium-kaolinite floc," *Water Research*, vol. 31, no. 3, pp. 449–454, 1997.
[16] R. C. Sonntag and W. B. Russel, "Structure and breakup of flocs subjected to fluid stresses. I. Shear experiments," *Journal of Colloid And Interface Science*, vol. 113, no. 2, pp. 399–413, 1986.
[17] M. Kobayashi, "Breakup of fractal floes in a turbulent flow," *Langmuir*, vol. 15, no. 13, pp. 4351–4356, 1999.
[18] Y. Adachi, M. Kobayashi, and Y. Fukuhara, "Break-up strength of floes analyzed using orifice converging flow," *Nihon Reoroji Gakkaishi*, vol. 35, no. 2, pp. 69–72, 2007 (Japanese).
[19] M. Kobayashi, Y. Adachi, and S. Ooi, "On the steady shear viscosity of coagulated suspensions," *Nihon Reoroji Gakkaishi*, vol. 28, no. 3, pp. 143–144, 2000.
[20] M. Kobayashi, S. Ooi, and Y. Adachi, "On the yield stress of sheared coagulated suspensions," *Annual Journal of Hydraulic Engineering*, vol. 46, pp. 637–640, 2002.
[21] M. Y. Lin, H. M. Lindsay, D. A. Weitz, R. C. Ball, R. Klein, and P. Meakin, "Universality in colloid aggregation," *Nature*, vol. 339, no. 6223, pp. 360–362, 1989.
[22] T. Fukasawa and Y. Adachi, "Direct observation on the Brownian coagulation of PSL particles through optical microscope in the regime near critical coagulation concentration (CCC)," *Journal of Colloid and Interface Science*, vol. 344, no. 2, pp. 343–347, 2010.
[23] Y. Kusaka, T. Fukasawa, and Y. Adachi, "Cluster-cluster aggregation simulation in a concentrated suspension," *Journal of Colloid and Interface Science*, vol. 363, no. 1, pp. 34–41, 2011.
[24] Y. Adachi, M. Kobayashi, and T. Yanagibashi, "Densification of small flocs formed in the mixing flow under the condition of rapid coagulation," *Transactions of the Japanese Society of Irrigation, Drainage and Reclamation Engineering*, vol. 233, pp. 49–56, 2004.
[25] K. Higashitani and T. Kubota, "Pelleting flocculation of colloidal latex particles," *Powder Technology*, vol. 51, no. 1, pp. 61–69, 1987.
[26] D. H. Napper, *Polymeric Stabilization of Colloidal Dispersions*, Academic Press, 1983.

[27] R. A. Ruehrwein and D. W. Ward, "Mechanism and clay aggregation by polyelectrolytes," *Soil Science*, vol. 73, pp. 485–492, 1952.

[28] R. H. Smellie Jr. and V. K. La Mer, "Flocculation, subsidence and filtration of phosphate slimes. VI. A quantitative theory of filtration of flocculated suspensions," *Journal of Colloid Science*, vol. 13, no. 6, pp. 589–599, 1958.

[29] G. J. Fleer and J. Lyklema, "Polymer adsorption and its effect on the stability of hydrophobic colloids. II. The flocculation process as studied with the silver iodide-polyvinyl alcohol system," *Journal of Colloid And Interface Science*, vol. 46, no. 1, pp. 1–12, 1974.

[30] J. Gregory, "Rates of flocculation of latex particles by cationic polymers," *Journal of Colloid And Interface Science*, vol. 42, no. 2, pp. 448–456, 1973.

[31] K. Higashitani, T. Shibata, and H. Kage, "Formation of pellet flocs from kaoline suspension and their properties," *Journal of Chemical Engineering of Japan*, vol. 20, no. 2, pp. 152–157, 1987.

[32] Y. Adachi, M. A. Stuart, and R. Fokkink, "Kinetics of turbulent coagulation studied by means of end-over-end rotation," *Journal of Colloid and Interface Science*, vol. 165, no. 2, pp. 310–317, 1994.

[33] P. G. Saffman and J. S. Turner, "On the collision of drops in turbulent clouds," *The Journal of Fluid Mechanics*, vol. 1, pp. 16–30, 1956.

[34] T. G. M. van de Ven and S. G. Mason, "The microrheology of colloidal dispersions VII. Orthokinetic doublet formation of spheres," *Colloid and Polymer Science*, vol. 255, no. 5, pp. 468–479, 1977.

[35] Y. Adachi, M. A. Stuart, and R. Fokkink, "Dynamic aspects of bridging flocculation studied using standardized mixing," *Journal of Colloid And Interface Science*, vol. 167, no. 2, pp. 346–351, 1994.

[36] Y. Adachi, "Dynamic aspects of coagulation and flocculation," *Advances in Colloid and Interface Science*, vol. 56, pp. 1–31, 1995.

[37] Y. Adachi and T. Matsumoto, "Dynamics of initial stage flocculation of polystyrene latex spheres with polyelectrolytes," *Colloids and Surfaces A*, vol. 113, no. 3, pp. 229–236, 1996.

[38] T. Matsumoto and Y. Adachi, "Effect of ionic strength on the initial dynamics of flocculation of polystyrene latex with polyelectrolyte," *Journal of Colloid and Interface Science*, vol. 204, no. 2, pp. 328–335, 1998.

[39] K. Aoki, *Koubunshi denkaishitsu niyoru koroid ryushi no gyoshukatei ni kansuru kenkyu*, Ph.D. thesis, University of Tsukuba, 2007.

[40] K. Aoki and Y. Adachi, "Kinetics of polyelectrolyte adsorption onto polystyrene latex particle studied using electrophoresis: effects of molecular weight and ionic strength," *Journal of Colloid and Interface Science*, vol. 300, no. 1, pp. 69–77, 2006.

[41] Y. Adachi and K. Aoki, "Restructuring of small flocs of polystyrene latex with polyelectrolyte," *Colloids and Surfaces A*, vol. 342, no. 1–3, pp. 24–29, 2009.

[42] J. Wei, B. Gao, Q. Yue, Y. Wang, W. Li, and X. Zhu, "Comparison of coagulation behavior and floc structure characteristic of different polyferric-cationic polymer dual-coagulants in humic acid solution," *Water Research*, vol. 43, no. 3, pp. 724–732, 2009.

[43] T. Fukasawa and Y. Adachi, "Effect of floc structure on the rate of Brownian coagulation," *Journal of Colloid and Interface Science*, vol. 304, no. 1, pp. 115–118, 2006.

[44] D. Sato, M. Kobayashi, and Y. Adachi, "Effect of floc structure on the rate of shear coagulation," *Journal of Colloid and Interface Science*, vol. 272, no. 2, pp. 345–351, 2004.

[45] Y. Adachi, Y. Kusaka, and A. Kobayashi, "Transient behavior of adsorbing/adsorbed polyelectrolytes on the surface of colloidal particles studied by means of trajectory analysis of Brownian motion," *Colloids and Surfaces A*, vol. 376, pp. 9–13, 2011.

[46] H. Ohshima, *Biophysical Chemistry of Biointerfaces*, John Wiley & Sons, 2010.

[47] Y. Adachi and T. Wada, "Initial stage dynamics of bridging flocculation of polystyrene latex spheres with polyethylene oxide," *Journal of Colloid and Interface Science*, vol. 229, no. 1, pp. 148–154, 2000.

Hindawi Publishing Corporation
International Journal of Polymer Science
Volume 2012, Article ID 816163, 8 pages
doi:10.1155/2012/816163

Review Article

Synthesis of Hyperbranched Polymer Using Slow Monomer Addition Method

Toshifumi Satoh

Division of Biotechnology and Macromolecular Chemistry, Faculty of Engineering, Hokkaido University, Sapporo 060-8628, Japan

Correspondence should be addressed to Toshifumi Satoh, satoh@poly-bm.eng.hokudai.ac.jp

Received 17 August 2011; Accepted 13 October 2011

Academic Editor: Eri Yoshida

This paper details the synthesis of a well-defined hyperbranched polymer using a slow monomer addition method. The polymerization under slow monomer addition conditions results in a very low monomer concentration actually present in the reaction mixture, and the exclusive reaction of the monomer with the growing polyfunctional macromolecules occurs, resulting in a high molecular weight and a high degree of branching value. Thus, the slow monomer addition is a versatile and preferential method for the controlled synthesis of a well-defined hyperbranched polymer with both a high molecular weight and a high degree of branching value.

1. Introduction

The novel architectures of highly branched polymers, such as a dendrimer and hyperbranched polymer, have attracted much attention from the viewpoint of nanotechnology, because these polymers exhibit different characteristic features, such as a lower viscosity, higher solubility, and higher amount of terminal groups, compared with those of the corresponding linear polymers [1–15]. The dendrimers have a number of advantages, such as a monodispersity and a highly ordered structure. However, the synthesis of dendrimers has required multistep procedures of protection, deprotection, and purification. In contrast to dendrimers, the hyperbranched polymers have an irregular structure. However, the hyperbranched polymers possess properties similar to the dendrimer and can be easily synthesized via the one-pot polymerization of the A_2 and B_m monomers, AB_m-type monomer, and AB* monomer (inimer), in which the A functional group of a monomer can react with the B group of another monomer [1, 9, 14, 15]. Therefore, the hyperbranched polymers have more extensive prospects for application and have attracted increasing interest in polymer science.

Since Kim and Webster first synthesized the hyperbranched polyphenylene by AB_2-type monomers [16], numerous hyperbranched polymers have been prepared by step-growth polycondensation, self-condensing vinyl polymerization, ring-opening multibranching polymerization, self-condensing ring-opening polymerization, proton transfer polymerization, and so forth [1, 9, 14, 15]. According to the experimental results and theoretical calculations, the hyperbranched polymers prepared by a one-pot reaction have a very wide polydispersity index (PDI) and the ordinary degree of branching (DB) values that limit the specification of hyperbranched polymers for advanced application, that is, the maximum DB value, is only about 0.5 for the AB_2-type monomer or AB* monomer and the PDI of the hyperbranched polymers is extremely broad for a high conversion [17, 18]. In contrast, the slow monomer addition method is a highly effective way to produce the very ordered hyperbranched polymer with a controlled molecular weight, high DB, and narrow PDI [19–25]. The slow monomer addition method results in a very low monomer concentration actually present in the reaction mixture. Thus, the exclusive reaction of the monomer with the growing polyfunctional macromolecules occurs, resulting in a high molecular weight and a high DB. In the field of advanced polymer particles, it is very important to finely tune the structure of the hyperbranched polymer.

In this paper, the comprehensive study of the synthesis of hyperbranched polymers using the slow monomer addition method is described.

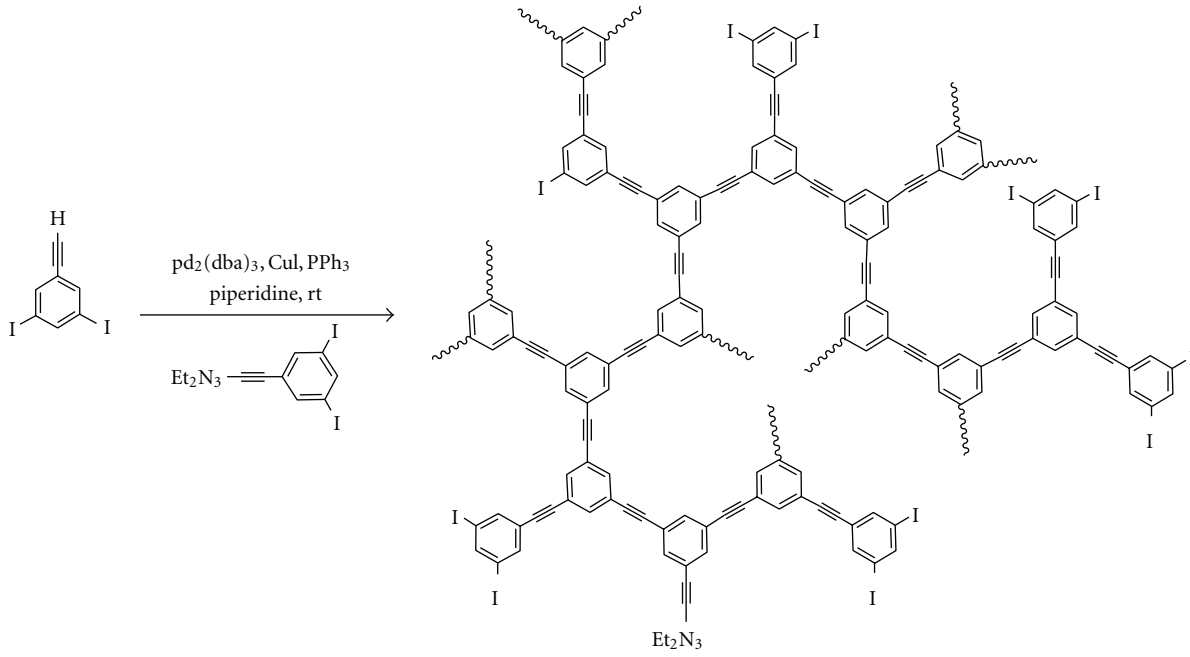

Scheme 1: Synthesis of hyperbranched polyphenylacetylene.

2. Step-Growth Polycondensation by Slow Monomer Addition

2.1. Synthesis of Hyperbranched Polyphenylacetylene. Bharathi and Moore first reported the synthesis of hyperbranched polyphenylacetylene by the slow monomer addition (SMA) of 3,5-diiodophenylacetylene as an AB_2-type monomer, as shown in Scheme 1 [26, 27]. When the slow addition of the monomer into piperidine was carried out in the presence of 1-(3,5-diiodophenyl)-3,3-diethyltriazene as a B_2 core molecule and Pd_2(dibenzylideneacetone)$_3$ as a catalyst, a soluble hyperbranched polymer with the weight-average molecular weight (M_w) = 8220 g·moL^{-1} and PDI = 1.28 (monomer : core ratio = 17.5) was formed after the capping reaction. In contrast, the M_w of the hyperbranched polymer prepared by the one-pot approach in piperidine was around 35300 g·moL^{-1} with a polydispersity near 2.4 after the capping reaction. The slow monomer addition to the catalyst solution without the core resulted in a hyperbranched polymer with a bimodal SEC profile consisting of a narrow high-molecular-weight peak and a broad tail on the low-molecular-weight side of M_w = 490000 g·moL^{-1} and PDI = 33.3.

They also achieved the control of molecular weight (M_w = 8000–90000 g·moL^{-1}) by varying the monomer : core ratio. The experimental results are in good qualitative agreement with computer simulations reported by Frey et al. and the theoretical work reported by Müller et al. [19–21].

2.2. Synthesis of Hyperbranched Poly(siloxysilane). Fréchet and coworkers reported the progressive SMA method to control the molecular weight and polydispersity in hyperbranched poly(siloxysilane) prepared from methylvinylbis(dimethylsiloxysilane), as shown in Scheme 2 [28]. The SMA method effectively increases the molecular weight of the final hyperbranched polymers and improves the preparation yield by reducing the occurrence of intramolecular cyclization. In addition, both the molecular weight and polydispersity could be controlled by changing the rate of addition or the amount of the monomer feed, that is, the slower the monomer addition or the higher the amount of added monomer, the higher the molecular weight (M_w = 8700–61000 g·moL^{-1} after precipitation) and polydispersity (2.3 to 9.2) of the resulting hyperbranched polymer. They also reported that the use of a monodisperse polyfunctional core showed a similar trend and led to a product with a higher molecular weight (a maximum M_w = 84000 g·moL^{-1} in 81% yield after precipitation).

2.3. Synthesis of Hyperbranched Aromatic Homo- and Copolyesters. Möck and coworkers reported the random bulk polycondensation with the SMA method leading to hyperbranched aromatic homo- and copolyesters based on 3,5-bis(trimethylsiloxy)benzoyl chloride (AB_2-type monomer) and 3-(trimethylsiloxy)benzoyl chloride (AB-type monomer), as shown in Scheme 3 [29].

For the bulk homopolycondensation of the AB_2-type monomer using 1,3,5-trihydroxybenzene as the B_3 core molecules under the SMA conditions, the M_n (75000 g·moL^{-1}) of the obtained polymer was higher than that (M_n = 2900 g·moL^{-1}) without the SMA conditions. In addition, the DB values were significantly enhanced above the theoretical value of 0.5 [17, 18] for the one-pot polycondensation to 0.61–0.66, in agreement with the theoretical predictions (DB = 0.66) [19, 20]. A remarkably

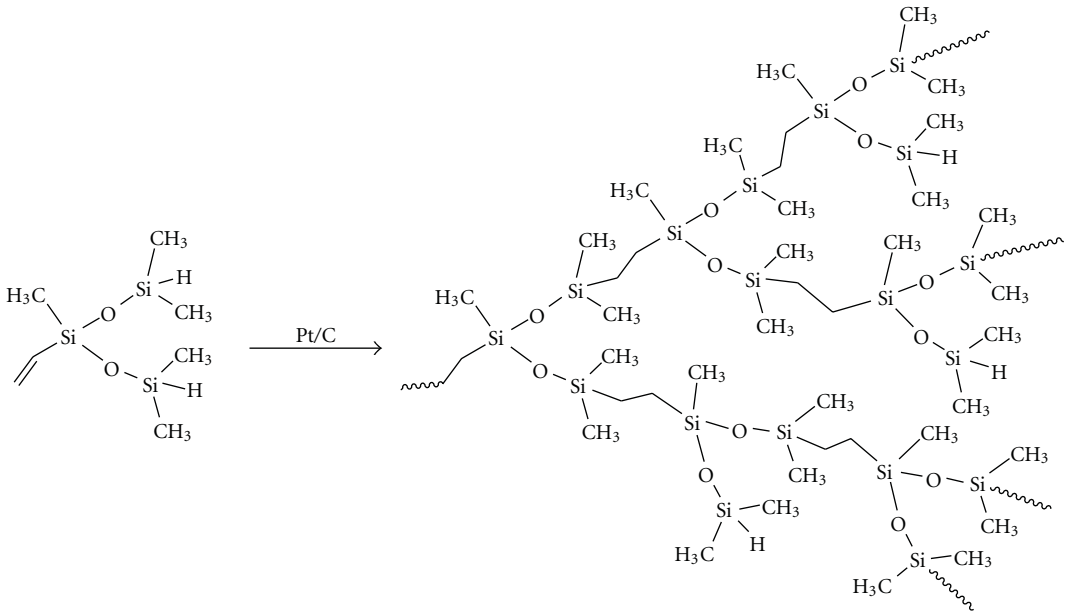

Scheme 2: Synthesis of hyperbranched poly(siloxysilane).

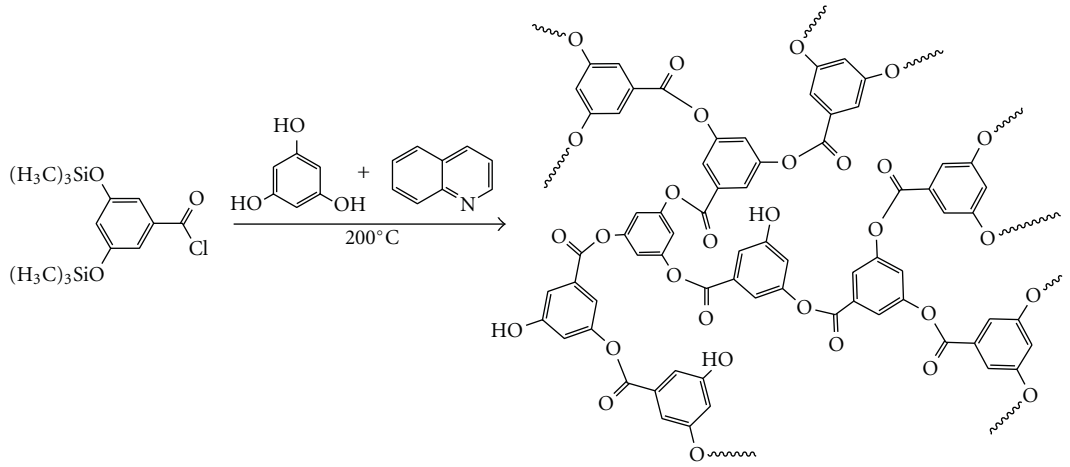

Scheme 3: Synthesis of hyperbranched aromatic polyester.

low Mark-Houwink-Sakurada (MHS) exponent, α, of only 0.18 in DMF (including guanidine hydrochloride) was also obtained for the hyperbranched homopolymer prepared under the SMA conditions.

For the random copolymerization using SMA conditions, the copolymer with a higher molecular weight and lower polydispersity was obtained (M_n = 83000–278000 g·moL^{-1}, PDI = 1.09–1.49), compared to the random copolymerization without SMA method (M_n = 2900–8400 g·moL^{-1}, PDI = 1.37–2.15). For the copolycondensation, the variation in the molar feed ratio of the AB-type monomer to AB_2-type monomer allows varying the branching density over a broad range; that is, the DB values increased with the decreasing monomer feed ratio in good agreement with the DB value expected from theory [19, 20]. The MHS exponents, α, also clearly decreased with the increasing DB and were in the range of 0.23 to 0.55.

3. Ring-Opening Multibranching Polymerization by Slow Monomer Addition

3.1. Synthesis of Hyperbranched Poly(3-ethyl-3-hydroxymethyloxetane). Magnusson and coworkers prepared hyperbranched polyethers by the cationic ring-opening multibranching polymerization of 3-ethyl-3-hydroxymethyloxetane using benzyltetramethylenesulfonium hexafluoroantimonate (BTS-SbF_6) as a catalyst, as shown in Scheme 4 [30]. When 3-ethyl-3-hydroxymethyloxetane was polymerized under SMA conditions (1.6 mmoL·min^{-1}) using a trifunctional core molecule, trimethylolpropane (TMP), the polymers with DB values ranging from 0.15 to 0.28, that were a lower value compared to the one-pot synthesis without the core (DB = 0.40-0.41), were obtained. When the monomer was very slowly added to the core (0.08 mmoL·min^{-1}), the polymer with a high DB (0.40) was obtained. The

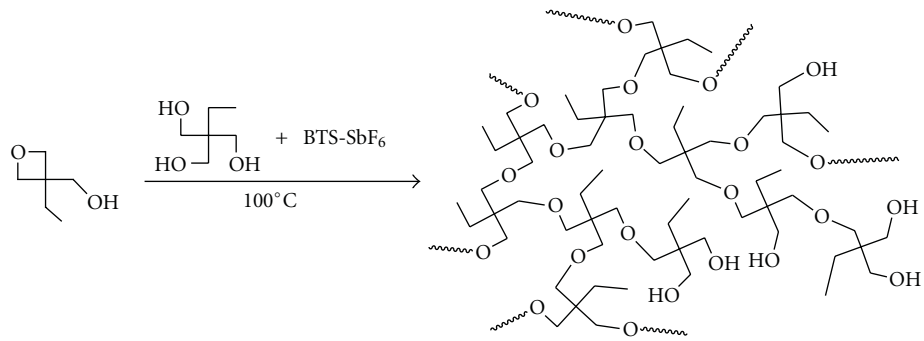

Scheme 4: Synthesis of hyperbranched poly(3-ethyl-3-hydroxymethyloxetane).

polydispersities were also slightly lower than those of the polymer from the one-pot synthesis.

They also reported the synthesis of the dumbbell-shaped triblock copolymer consisting of a linear polyethylene glycol and hyperbranched poly(3-ethyl-3-hydroxymethyloxetane) through the cationic ring-opening polymerization using the SMA method [31]. The obtained materials were of relatively low polydispersities ranging from 1.2 to 1.4.

Smith and Mathias first reported the anionic ring-opening multibranching polymerization of 3-ethyl-3-hydroxymethyloxetane using NaH as a strong base catalyst and TMP as a trifunctional initiator core [32]. The polymerization was carried out under SMA conditions at high temperatures (>100°C) because of the high activation energy of the ring opening. The obtained polymers were of low molecular weight, and the acetone-soluble part has a higher DB value (0.48) than the acetone-insoluble one (0.20).

3.2. Synthesis of Hyperbranched Poly(2-hydroxymethyloxetane). Satoh and coworkers recently reported the cationic ring-opening multibranching polymerization of 2-hydroxymethyloxetane as a novel latent AB_2-type monomer using the SMA method, as shown in Scheme 5 [33]. The polymer yield ranged from ca. 62–88%, which increased with the increasing monomer addition time using the SMA method. The M_w and the polydispersity of the polymer were in the range of 12,000–43,500 g·moL^{-1} and 1.60–4.53, respectively, which also increased with the increasing monomer addition time. In contrast, the polymerization without the SMA method produced a polymer with a lower M_w and yield, but narrower PDI. The MHS exponents, α, in 0.2 M $NaNO_3$ aq. were determined to be 0.02–0.25, which decreased with the increasing monomer addition time. The DB value of the polymer, which was calculated by Frey's equation [18], ranged from ca. 0.50 to 0.58, increased with the increasing monomer addition time.

Satoh and coworkers also applied the SMA method for the cationic polymerization of tetrahydrofurfuryl alcohol [33]. The M_w values also increased with the increasing addition time, as well as the cationic ring-opening multibranching polymerization of 2-hydroxymethyloxetane, for example, M_w was 18,200 g·moL^{-1} for the polymerization with the addition time of 20 h, and 32,200 g·moL^{-1} for 50 h, whereas only the oligomer was obtained without the SMA.

3.3. Synthesis of Hyperbranched Polyglycerol. In 1999, Sunder and coworkers reported the anionic ring-opening multibranching polymerization of glycidol, a latent cyclic AB_2-type monomer, under SMA conditions with TMP as a trifunctional coreinitiator, leading to polyglycerols with narrow PDIs (1.13–1.47), as shown in Scheme 6 [34]. The polymerization proceeded in a controlled manner, and the hyperbranched aliphatic polyether, possessing an M_n in the range of 1250 to 6500 g·moL^{-1}, can be prepared under the SMA conditions. The determined DB values were found to be enhanced (0.53–0.59) in comparison with the value of 0.5 expected for the one-pot polymerization. The MALDI-TOF mass spectra of the obtained polymers revealed complete attachment of the hyperbranched structures to the TMP initiator and the absence of macrocyclics due to the SMA. The chiral hyperbranched polyglycerols have also been prepared in a similar manner using the enantiomerically pure glycidol [35].

Satoh and coworkers also reported the cationic ring-opening multibranching polymerization of glycidol using the SMA method [33]. The polymer yield increased using the SMA method, for example, an 81.1% yield for the polymerization without the SMA and a 91.1% yield for the polymerization with the addition time of 2.08 h. The M_w values (9500–10100 g·moL^{-1}) of the polymer obtained with $BF_3{\cdot}OEt_2$ showed a small change for the addition time, though the M_w values increased with the increasing amount of the cationic agent. The polydispersities of the resulting polymers were broad in the range of 2.06–2.11. The MHS exponents, α, were determined to be 0.03–0.26 in 0.2 M $NaNO_3$ aq., which decreased with the increasing monomer addition time. The DB values also increased with the increasing monomer addition time, but the change was moderate, for example, the DB was 0.47 without the SMA method and 0.50 for the 6.66 h addition time.

A further important improvement in the ring-opening multibranching polymerization of glycidol was reported in 2006 by Kainthan and coworkers [36]. They synthesized very high molecular weight (up to M_n = 670000 g·moL^{-1}) and narrow polydispersed (1.1–1.4) hyperbranched polyglycerols by the anionic ring-opening multibranching polymerization of glycidol in dioxane as an emulsifying agent using the SMA method. The isolated polymer yields were between 80 and 90%, and the MHS exponents, α, were in the range

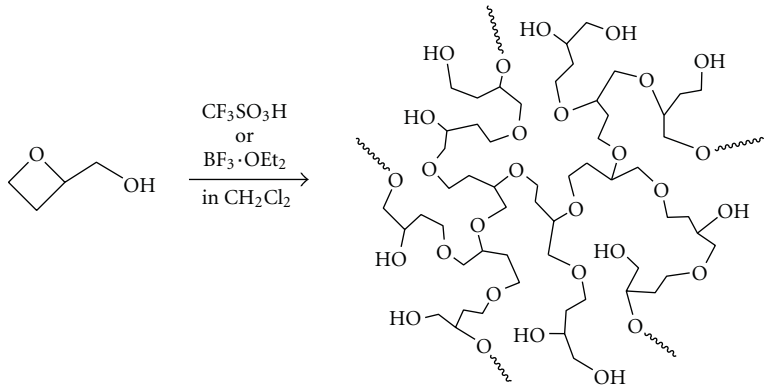

Scheme 5: Synthesis of hyperbranched poly(2-hydroxymethyloxetane).

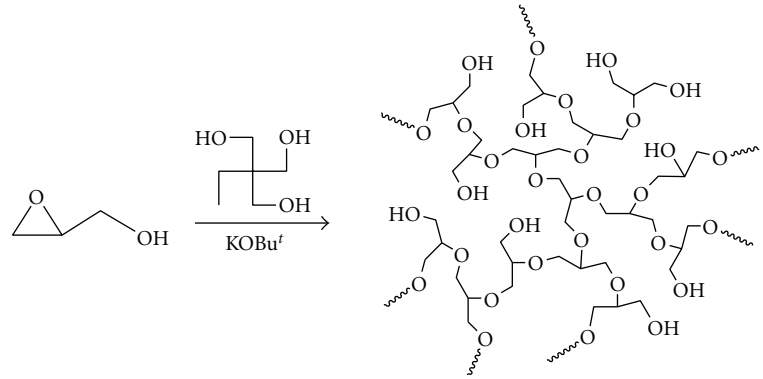

Scheme 6: Synthesis of hyperbranched polyglycerol from glycidol.

of 0.31–0.34. In contrast, broader polydispersities with low-molecular-weight fractions were obtained when the more polar diglyme was used as the emulsifying agent.

In past year, a facile two-step approach via low-molecular-weight polyglycerol macroinitiators (M_n = 500 and 1000 g·moL^{-1}) using the SMA method was developed by Wilms and coworkers for preparing a hyperbranched polyglycerol with a controlled molecular weight [37]. The polyfunctionality of the macroinitiator affords a higher concentration of alkoxide sites even at an elevated degree of polymerization and thus permits the preparation of hyperbranched polyglycerols up to M_n = 24000 g·moL^{-1} under controlled SMA conditions. The polydispersities of the obtained samples were in the range of 1.3 to 1.8, and the DB values were obtained in the range of 0.60 to 0.63.

Rokichi and coworkers recently reported the synthesis of hyperbranched polyglycerol by the anionic ring-opening multibranching polymerization of the environmentally benign monomer, glycerol carbonate, as shown in Scheme 7 [38]. The polymerization using the SMA method and partially deprotonated TMP as an initiator led to the formation of the hyperbranched polyglycerol upon CO_2 liberation. The obtained polymers were of low molecular weight, and the polydispersities ranged between 1.2 and 1.3. The polymerization with the alkoxide proceeded through two reaction pathways in which attack at the carbonyl or alkyl carbon atoms of the cyclic carbonate group takes place. Although the chemical structure of the polymer was very similar to that from glycidol, the polymer contained the terminal 1,3-dihydroxy unit, which was the result of an intramolecular rearrangement. In addition, the MALDI-TOF mass analysis confirmed the relatively small amount of macrocyclic units in the polymer.

The high concentration of hydroxy groups on the hyperbranched polyglycerol, which can be easily transformed into other functional groups, enables the use of new materials for nanotechnology and biomedical applications such as drug carriers, molecular labels or probe moieties, and hydrogels.

3.4. Synthesis of Hyperbranched Glycopolymer. Tamaki and coworkers reported the cationic ring-opening multibranching polymerization of 5,6-anhydro-1,2-*O*-isopropylidene-*α*-D-glucofuranose as a latent cyclic AB_2-type monomer using $BF_3 \cdot OEt_2$ as an initiator in order to synthesize a novel hyperbranched glycopolymer, as shown in Scheme 8 [39]. The cationic polymerization without the SMA method produced the glycopolymer with M_w = 15000 g·moL^{-1} and PDI = 1.45. On the other hand, the cationic polymerization with the SMA method is a facile method leading to hyperbranched glycopolymers with high molecular weights and highly branched structures; that is, the M_w values (37000–122400 g·moL^{-1}) increased with the increasing monomer

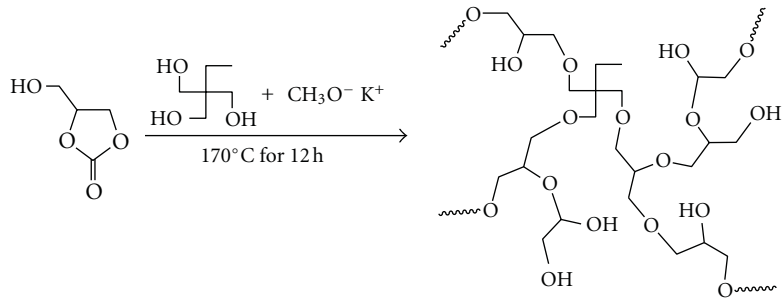

Scheme 7: Synthesis of hyperbranched polyglycerol from glycerol carbonate.

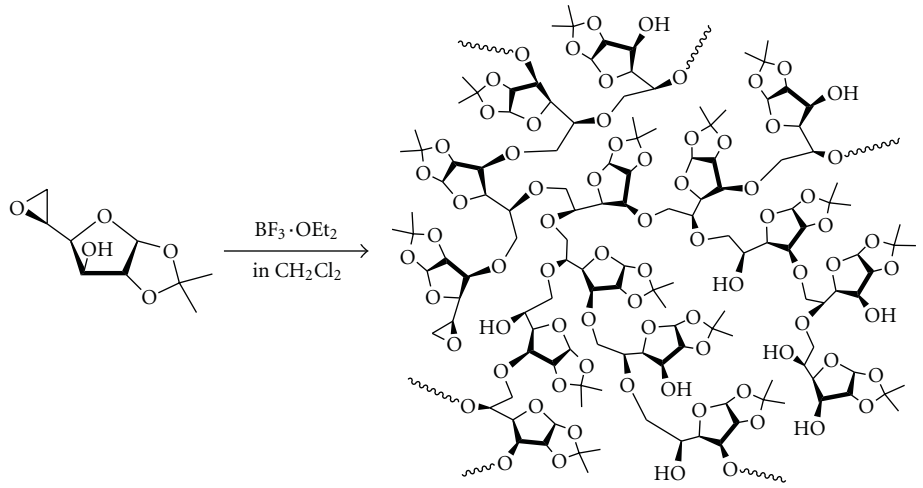

Scheme 8: Synthesis of hyperbranched glycopolymer.

addition time and the MHS exponents, α, were calculated to be 0.08-0.09 in 0.2 M $NaNO_3$ aq., suggesting that the resulting polymers have a highly branched spherical structure. The polydispersities were found to be in the relatively narrow range of 1.19–1.70.

The resulting polymer is a novel hyperbranched glycopolymer arranged with numerous sugar units on the peripheries of the polymer. Thus, a water-soluble hyperbranched 5,6-glucan synthesized by the hydrolysis of the hyperbranched glycopolymer has a high reducing ability derived from the glycol-cluster effect of the reducing D-glucose units; that is, the "reducing sugar ball" effectively acts as a sugar-based reductant. Such a hyperbranched glycopolymer with numerous reducing sugar units can be expected to be useful in a wide variety of fields such as biochemical and medicinal applications, for examples, a biocompatible reductant, antioxidant, and a part of the carrier for a drug delivery system, and so forth.

4. Conclusion

This paper describes that the slow monomer addition is a versatile and preferential method for the controlled synthesis of a well-defined hyperbranched polymer with both a high molecular weight and a high degree of branching value. The slow monomer addition method also reduced the undesired intramolecular cyclization reactions during the polymerization. Because the hyperbranched polymers have many characteristic features and their numerous terminal units can be easily converted into various functional groups leading to novel advanced polymer particles, the well-defined hyperbranched polymers prepared using the slow monomer addition method can be expected to be useful in a wide variety of industrial and research fields, for example, molecular capsules as a carrier for a drug delivery system [40–44], a nanoreactor [45], a mixture separator [46], a viscosity modifier, a cross-linker for preparing functional gels, and so forth.

Acknowledgments

The author acknowledges the contributions of T. Kakuchi, R. Sakai, M. Tamaki, Y. Kitajyo, K. Mori, S. Nakabayashi, T. Taguchi, H. Misaka, and N. T. Hoai.

References

[1] J. M. J. Frechet, "Functional polymers and dendrimers: reactivity, molecular architecture, and interfacial energy," *Science*, vol. 263, no. 5154, pp. 1710–1715, 1994.

[2] C. J. Hawker and W. Devonport, "Design, synthesis, and properties of dendritic macromolecules," *ACS Symposium Series*, vol. 624, pp. 186–196, 1996.

[3] F. Zeng and S. C. Zimmerman, "Dendrimers in supramolecular chemistry: from molecular recognition to self-assembly," *Chemical Reviews*, vol. 97, no. 5, pp. 1681–1712, 1997.

[4] K. Uhrich, "Hyperbranched polymers for drug delivery," *Trends in Polymer Science*, vol. 5, pp. 388–393, 1997.

[5] O. A. Matthews, A. N. Shipway, and J. F. Stoddart, "Dendrimers—branching out from curiosities into new technologies," *Progress in Polymer Science*, vol. 23, no. 1, pp. 1–56, 1998.

[6] A. Huit, M. Johansson, and E. Malmström, "Hyperbranched polymers," *Advances in Polymer Science*, vol. 143, pp. 1–34, 1999.

[7] F. Vogtle, S. Gestermann, R. Hesse, H. Schwierz, and B. Windisch, "Functional dendrimers," *Progress in Polymer Science*, vol. 25, no. 7, pp. 987–1041, 2000.

[8] N. Hadjichristidis, M. Pitsikalis, S. Pispas, and H. Iatrou, "Polymers with complex architecture by living anionic polymerization," *Chemical Reviews*, vol. 101, no. 12, pp. 3747–3792, 2001.

[9] M. Jikei and M. A. Kakimoto, "Hyperbranched polymers: a promising new class of materials," *Progress in Polymer Science*, vol. 26, no. 8, pp. 1233–1285, 2001.

[10] H. Frey and R. Haag, "Dendritic polyglycerol: a new versatile biocompatible material," *Reviews in Molecular Biotechnology*, vol. 90, no. 3-4, pp. 257–267, 2002.

[11] C. Gao and D. Yan, "Hyperbranched polymers: from synthesis to applications," *Progress in Polymer Science*, vol. 29, no. 3, pp. 183–275, 2004.

[12] B. D. Mather, K. Viswanathan, K. M. Miller, and T. E. Long, "Michael addition reactions in macromolecular design for emerging technologies," *Progress in Polymer Science*, vol. 31, no. 5, pp. 487–531, 2006.

[13] T. Satoh and T. Kakuchi, "Synthesis of hyperbranched carbohydrate polymers by ring-opening multibranching polymerization of anhydro sugar," *Macromolecular Bioscience*, vol. 7, no. 8, pp. 999–1009, 2007.

[14] S. Peleshanko and V. V. Tsukruk, "The architectures and surface behavior of highly branched molecules," *Progress in Polymer Science*, vol. 33, no. 5, pp. 523–580, 2008.

[15] B. I. Voit and A. Lederer, "Hyperbranched and highly branched polymer architectures-synthetic strategies and major characterization aspects," *Chemical Reviews*, vol. 109, no. 11, pp. 5924–5973, 2009.

[16] Y. H. Kim and O. W. Webster, "Water-soluble hyperbranched polyphenylene: a unimolecular micelle?" *Journal of the American Chemical Society*, vol. 112, no. 11, pp. 4592–4593, 1990.

[17] C. J. Hawker, R. Lee, and J. M. J. Fréchet, "One-step synthesis of hyperbranched dendritic polyesters," *Journal of the American Chemical Society*, vol. 113, no. 12, pp. 4583–4588, 1991.

[18] D. Halter, A. Burgath, and H. Frey, "Degree of branching in hyperbranched polymers," *Acta Polymerica*, vol. 48, no. 1-2, pp. 30–35, 1997.

[19] D. Halter and H. Frey, "Degree of branching in hyperbranched polymers," *Acta Polymerica*, vol. 48, no. 8, pp. 298–309, 1997.

[20] R. Hanselmann, D. Hölter, and H. Frey, "Hyperbranched polymers prepared via the core-dilution/slow addition technique: computer simulation of molecular weight distribution and degree of branching," *Macromolecules*, vol. 31, no. 12, pp. 3790–3801, 1998.

[21] W. Radke, G. Litvinenko, and A. H. E. Müller, "Effect of core-forming molecules on molecular weight distribution and degree of branching in the synthesis of hyperbranched polymers," *Macromolecules*, vol. 31, no. 2, pp. 239–248, 1998.

[22] G. I. Litvinenko and A. H. E. Müller, "Molecular weight averages and degree of branching in self-condensing vinyl copolymerization in the presence of multifunctional initiators," *Macromolecules*, vol. 35, no. 12, pp. 4577–4583, 2002.

[23] K. C. Cheng, T. H. Chuang, J. S. Chang, W. Guo, and W. F. Su, "Effect of feed rate on structure of hyperbranched polymers formed by self-condensing vinyl polymerization in semibatch reactor," *Macromolecules*, vol. 38, no. 20, pp. 8252–8257, 2005.

[24] Z. P. Zhou, Z. W. Jia, and D. Y. Yan, "Effect of slow monomer addition on molecular parameters of hyperbranched polymers synthesized in the presence of multifunctional core molecules," *Science China Chemistry*, vol. 53, no. 4, pp. 891–897, 2010.

[25] L. Wang, X. He, and Y. Chen, "Diffusion-limited hyperbranched polymers with substitution effect," *The Journal of Chemical Physics*, vol. 134, no. 10, pp. 104901–104909, 2011.

[26] P. Bharathi and J. S. Moore, "Controlled synthesis of hyperbranched polymers by slow monomer addition to a core," *Macromolecules*, vol. 33, no. 9, pp. 3212–3218, 2000.

[27] P. Bharathi and J. S. Moore, "Solid-supported hyperbranched polymerization: evidence for self-limited growth," *Journal of the American Chemical Society*, vol. 119, no. 14, pp. 3391–3392, 1997.

[28] C. Gong, J. Miravet, and J. M. J. Fréchet, "Intramolecular cyclization in the polymerization of ABx monomers: approaches to the control of molecular weight and polydispersity in hyperbranched poly(siloxysilane)," *Journal of Polymer Science, Part A*, vol. 37, no. 16, pp. 3193–3201, 1999.

[29] A. Möck, A. Burgath, R. Hanselmann, and H. Frey, "Synthesis of hyperbranched aromatic homo- and copolyesters via the slow monomer addition method," *Macromolecules*, vol. 34, no. 22, pp. 7692–7698, 2001.

[30] H. Magnusson, E. Malmström, and A. Hult, "Influence of reaction conditions on degree of branching in hyperbranched aliphatic polyethers from 3-ethyl-3-(hydroxymethyl)oxetane," *Macromolecules*, vol. 34, no. 17, pp. 5786–5791, 2001.

[31] M. Rahm, R. Westlund, C. Eldsäter, and E. Malmström, "Triblock copolymers of polyethylene glycol and hyperbranched poly-3-ethyl-3-(hydroxymethyl)oxetane through cationic ring opening polymerization," *Journal of Polymer Science, Part A*, vol. 47, no. 22, pp. 6191–6200, 2009.

[32] T. J. Smith and L. J. Mathias, "Hyperbranched poly(3-ethyl-3-hydroxymethyloxetane) via anionic polymerization," *Polymer*, vol. 43, no. 26, pp. 7275–7278, 2002.

[33] T. Satoh, M. Tamaki, T. Taguchi et al., "Synthesis of novel hyperbranched polymer through cationic ring-opening multibranching polymerization of 2-hydroxymethyloxetane," *Journal of Polymer Science, Part A*, vol. 49, no. 11, pp. 2353–2365, 2011.

[34] A. Sunder, R. Hanselmann, H. Frey, and R. Mülhaupt, "Controlled synthesis of hyperbranched polyglycerols by ring-opening multibranching polymerization," *Macromolecules*, vol. 32, no. 13, pp. 4240–4246, 1999.

[35] A. Sunder, R. Mülhaupt, R. Haag, and H. Frey, "Chiral hyperbranched dendron analogues," *Macromolecules*, vol. 33, no. 2, pp. 253–254, 2000.

[36] R. K. Kainthan, E. B. Muliawan, S. G. Hatzikiriakos, and D. E. Brooks, "Synthesis, characterization, and viscoelastic properties of high molecular weight hyperbranched polyglycerols," *Macromolecules*, vol. 39, no. 22, pp. 7708–7717, 2006.

[37] D. Wilms, F. Wurm, J. Nieberle, P. Böhm, U. Kemmer-Jonas, and H. Frey, "Hyperbranched polyglycerols with elevated molecular weights: a facile two-step synthesis protocol based on polyglycerol Macroinitiators," *Macromolecules*, vol. 42, no. 9, pp. 3230–3236, 2009.

[38] G. Rokicki, P. Rakoczy, P. Parzuchowski, and M. Sobiecki, "Hyperbranched aliphatic polyethers obtained from environmentally benign monomer: glycerol carbonate," *Green Chemistry*, vol. 7, no. 7, pp. 529–539, 2005.

[39] M. Tamaki, T. Taguchi, S. Nakabayashi et al., "Hyperbranched 5,6-glucan as reducing sugar ball," *Polymer Chemistry*, vol. 1, no. 1, pp. 82–92, 2010.

[40] R. K. Kainthan, C. Mugabe, H. M. Burt, and D. E. Brooks, "Unimolecular micelles based on hydrophobically derivatized hyperbranched polyglycerols: ligand binding properties," *Biomacromolecules*, vol. 9, no. 3, pp. 886–895, 2008.

[41] T. Satoh, M. Tamaki, Y. Kitajyo et al., "Synthesis of unimolecular reversed micelle consisting of a poly(L-lactide) shell and hyperbranched D-mannan core," *Journal of Polymer Science, Part A*, vol. 44, no. 1, pp. 406–413, 2006.

[42] Y. Kitajyo, T. Imai, Y. Sakai et al., "Encapsulation-release property of amphiphilic hyperbranched d-glucan as a unimolecular reverse micelle," *Polymer*, vol. 48, no. 5, pp. 1237–1244, 2007.

[43] Y. Kitajyo, Y. Nawa, M. Tamaki et al., "A unimolecular nanocapsule: encapsulation property of amphiphilic polymer based on hyperbranched polythreitol," *Polymer*, vol. 48, no. 16, pp. 4683–4690, 2007.

[44] T. Satoh, "Unimolecular micelles based on hyperbranched polycarbohydrate cores," *Soft Matter*, vol. 5, no. 10, pp. 1972–1982, 2009.

[45] K. R. Kumar and D. E. Brooks, "Comparison of hyperbranched and linear polyglycidol unimolecular reverse micelles as nanoreactors and nanocapsules," *Macromolecular Rapid Communications*, vol. 26, no. 3, pp. 155–159, 2005.

[46] T. Satoh, Y. Kitajyo, R. Sakai et al., "Size-selective encapsulation property of unimolecular reverse micelle consisting of hyperbranched D-glucan core and L-leucine ethyl ether shell," *Macromolecular Symposia*, vol. 279, no. 1, pp. 145–150, 2009.

Hindawi Publishing Corporation
International Journal of Polymer Science
Volume 2012, Article ID 609767, 10 pages
doi:10.1155/2012/609767

Review Article

Self-Assembly of Cholesterol-Containing Water-Soluble Polymers

Shin-ichi Yusa

Department of Materials Science and Chemistry, University of Hyogo, 2167 Shosha, Himeji, Hyogo 671-2280, Japan

Correspondence should be addressed to Shin-ichi Yusa, yusa@eng.u-hyogo.ac.jp

Received 15 August 2011; Accepted 29 September 2011

Academic Editor: Eri Yoshida

Self-assembly of amphiphilic polymers containing cholesteryl groups has proved to be attractive in the field of nanotechnology research. Some cholesterol derivatives are known to form ordered structures which indicate thermotropic and lyotropic liquid-crystalline, monolayers, multilayers, micelles, and liposomes. This paper involves the synthesis and characterization of various kinds of amphiphilic polymers bearing cholesteryl moieties.

1. Introduction

Self-assembling water-soluble polymers are of current scientific and technological interest because of their relekvance to biological macromolecular systems and also to various industrial applications [1–3]. Macromolecular self-assemblies can be driven by noncovalent interactions including Coulombic, hydrogen bonding, van der Waals, exchange repulsive, and hydrophobic interactions. Among others, hydrophobic interaction is a major driving force for the self-organization of amphiphilic polymers in water.

Various types of self-assembling amphiphilic polymers have so far been synthesized by various methods. A practical approach to the synthesis of such polymers is to covalently introduce hydrophobes into water-soluble polymers. A large number of hydrophobes can be incorporated into a water-soluble polymer chain by copolymerization of hydrophilic and hydrophobic monomers with a block, alternating, or random sequence distribution. The incorporation of hydrophobic groups into a hydrophilic polymer can alter its solution properties in an aqueous solution. Water forms an organized, ice-like structure around hydrophobic molecules, which is entropically unfavorable [4, 5]. Therefore, water forces hydrophobic molecules together so that the amount of water structuring is minimized. If the hydrophobic groups are covalently attached to a hydrophilic polymer, associations of hydrophobes either within or between polymer chains occur in water.

The micelle formation of amphiphilic block copolymers in aqueous solutions has been the focus of great interest in a number of excellent reviews [6–8]. It is well established that block copolymers dissolved in a selective solvent—a solvent good for one block and poor for the other—undergo self-organization, leading to the formation of various morphologies, for example, spheres, rods, or lamellae. Water is a selective solvent for amphiphilic block copolymers, allowing for the formation of spherical micelles. Typically, they are formed with hydrophobic cores and hydrophilic outer layers (i.e., shells).

On the other hand, a great deal of effort has also been devoted to the investigations of random copolymers because of their relative ease of synthesis and wide range of monomer selections, compared to block copolymers. A wide variety of self-association phenomena may be anticipated for amphiphilic random copolymers. The self-association is dependent on the type of hydrophobic groups, their content in the copolymer, their sequence distribution, and the type of hydrophilic monomer units.

An important starting point for understanding the self-assembling behavior of hydrophobically modified water-soluble polymers is to know whether polymer-bound hydrophobes associate within the same polymer chain or among different polymer chains in water. The association of polymer-bound hydrophobes in water can occur either within a single polymer chain or between different polymer chains; an intrapolymer association will result in a chain loop while interpolymer association will cross-link (Figure 1).

Figure 2 illustrates an extreme case where all polymer-bound hydrophobes undergo interpolymer association.

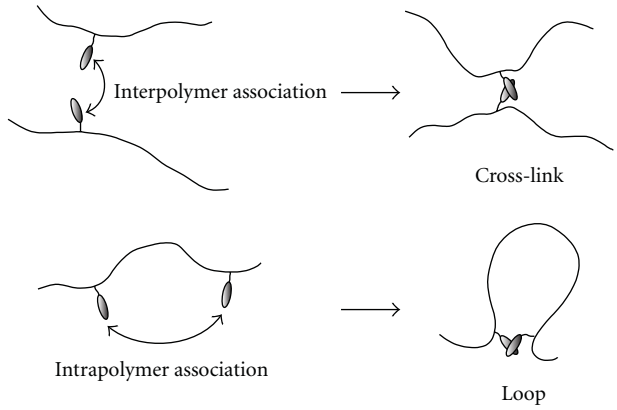

Figure 1: Inter- versus intrapolymer hydrophobe association.

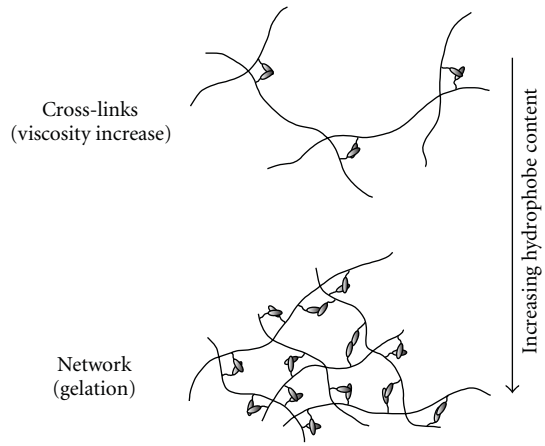

Figure 2: Interpolymer hydrophobe association.

When hydrophobe content is low, the interpolymer hydrophobic association may lead to a situation where several polymer chains are cross-linked, causing a large increase in solution viscosity. As the hydrophobe content is increased, infinite networks may be formed, leading to gelation or bulk phase separation.

Figure 3 depicts another extreme case where all polymer-bound hydrophobes undergo complete intrapolymer associations. In this extreme case, hydrophobic associations lead to the formation of single molecular self-assemblies or unimolecular micelles. When the content of hydrophobes in a polymer is sufficiently low, a "flower-like" unimolecular micelle may be formed, which consists of a hydrophobic core surrounded by hydrophilic loops shaped into "petals." This type of micelle has been theoretically predicted by Halperin [9] and Semenov et al. [10] for the self-organization of sequential multiblock copolymers in selective solvents. The flower-like micelles can be viewed as a second-order structure formed by a linear polymer chain. As the content of hydrophobes in a copolymer is increased, the size of the hydrophobic core increases and, in turn, the size of the hydrophilic petals decreases. Accordingly, the second-order structure may become unstable because part of the surface of the hydrophobic core is exposed to water. This leads to a further collapse of the second-order structure into a third-order structure due to secondary association of hydrophobic cores. Such third-order structures are composed of a number of flower-like micelles collapsed into a highly compact assembly.

Figure 4 shows a case where intrapolymer associations mainly occur, but a portion of hydrophobes undergo interpolymer association. In this situation, intermolecularly bridged flower-like micelles are likely to be formed. The extent of such micellar bridges may depend strongly on the content of hydrophobes in the polymer as well as the polymer concentration. As the content of hydrophobes in a polymer are increased, both the size of the micellar core and the number of micellar bridges would increase. A collapsed micelle network would eventually be formed, giving rise to gelation or bulk phase separation.

Morishima et al. [11–14] have extensively studied hydrophobic associations of amphiphilic random copolymers of sodium 2-(acrylamido)-2-methylpropanesulfonate (AMPS) or sodium acrylate and various hydrophobic comonomers. They have employed, as hydrophobic comonomers, methacrylamides, or methacrylates substituted with various types of hydrophobic groups via various spacer bonds. They have particularly focused on the macromolecular

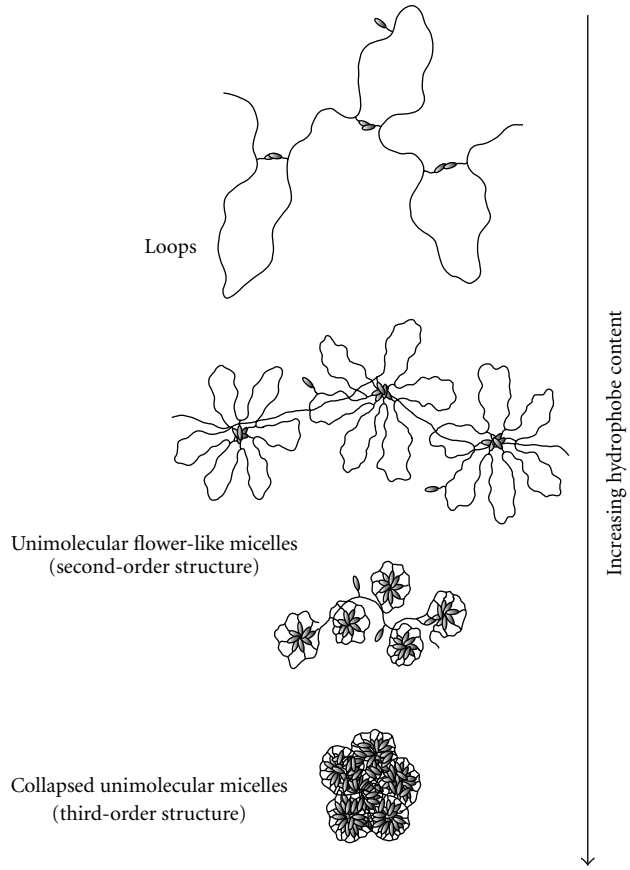

Figure 3: Intrapolymer hydrophobe association.

architecture which results in the two extreme cases, (i) completely intramolecular associations leading to single-macromolecular self-assemblies independent of polymer concentration and (ii) highly preferential interpolymer associations leading to multipolymeric "transient" networks. From the studies by Morishima et al. [15, 16] and others [17–19], it has been revealed that the sequence distribution of charged and hydrophobic units along the polymer chain is a very important structural factor to determine whether the hydrophobic self-association is an intra- or interpolymer event. Block sequences have a strong tendency for interpolymer association, whereas random and alternating sequences tend to associate in an intrapolymer mode. Chang and McCormick [20] have shown that even a subtle difference in the sequence distribution in random copolymers has a considerable effect on the association mode; if the sequence distribution is "block-like" in nature, there is a tendency for intermolecular association.

There is a class of amphiphilic polymers that have hydrophobic moieties at polymer chain ends. If the hydrophobes at chain ends interact strongly, micellar structures may be formed. Figure 5(a) shows schematically the formation of a core-corona type unicore micelle by water-soluble polymers possessing a hydrophobe at one chain end of each polymer. Such micelles may be formed spontaneously at equilibrium between micelles and single free polymer molecules (i.e., unimers) as described by a closed association model [21–23]. A characteristic feature of such equilibrium micelles is that they are nearly monodispersed in mass and size. At a thermodynamic equilibrium, aggregation numbers (numbers of polymer molecules that consist of a single micelle) are determined by the minimum free energy of the system, and therefore the distribution of aggregation numbers around the most stable state is quite narrow [24]. However, if polymers having hydrophobic moieties at both chain ends (doubly end-capped polymers) are present together with the singly end-capped polymers, bridged unicore micelles may be formed (Figure 5(b)). At a very low polymer concentration, a doubly end-capped polymer chain may exist as a looped or open chain-end conformation depending on whether or not the terminal hydrophobes associate in the same polymer chain. These two conformations may exist in equilibrium in aqueous solution and undergo multipolymer association as their own identities. This situation would give rise to the formation of looped coronas and intermicellar bridges. In the case where all polymers are doubly end-capped, polymer chains would form either looped coronas or intermicellar bridges, leading to infinite networks, as conceptually illustrated in Figure 5(c).

Winnik et al. [25, 26] synthesized amphiphilic derivatives of poly(*N*-isopropylacrylamide) (PNIPAM) consisting of a

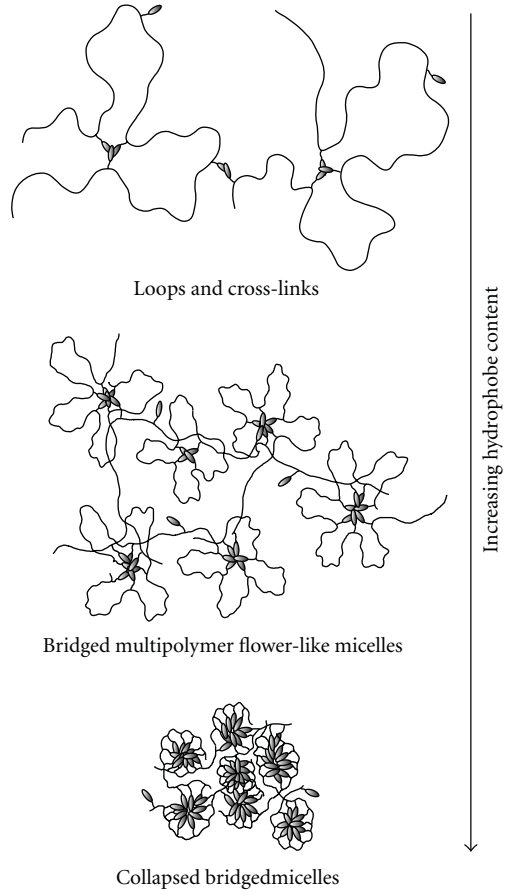

Figure 4: Inter- plus intrapolymer association.

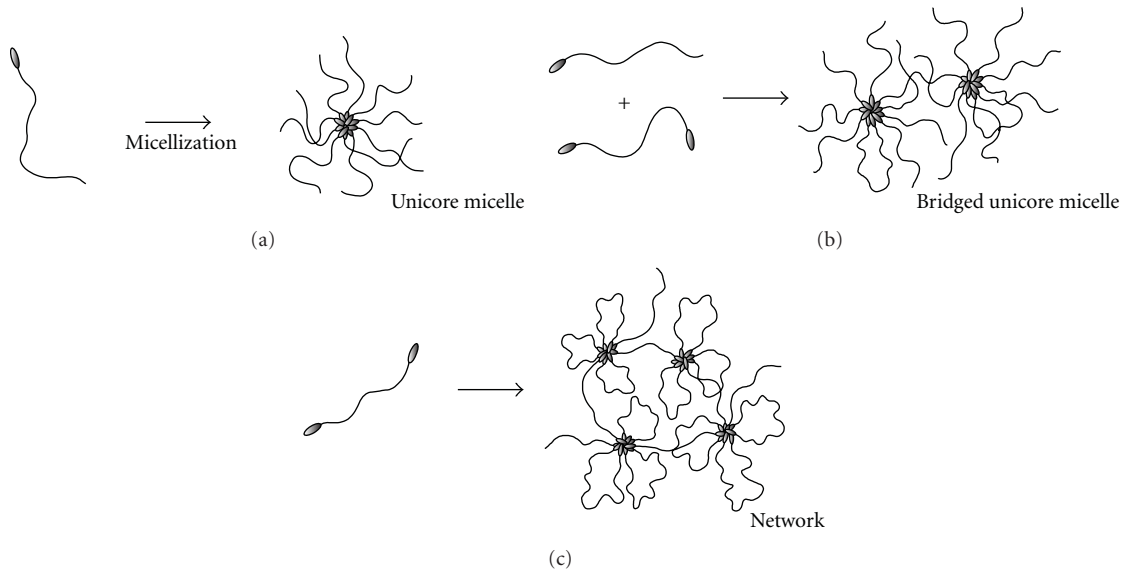

Figure 5: Association of hydrophobically end-modified polymers: (a) singly end-modified polymers; (b) a mixture of singly and doubly end-modified polymers; (c) doubly end-modified polymers.

PNIPAM chain substituted at one end with a dioctadecyl group by free radical polymerization of *N*-isopropylacrylamide using 4,4′-azobis(4-cyano-*N*,*N*-dioctadecyl) pentanamide as an initiator. In aqueous solution, the end-dioctadecylated PNIPAM forms a multimolecular core-corona type micelle under temperatures below the lower critical solution temperature (LCST). The micelle consists of a core of dioctadecyl chains and corona of solvated PNIPAM chains. Alami et al. [27] reported the aggregation behavior of hydrophobically doubly end-capped poly(ethylene oxide) in aqueous solutions. At very low concentrations, the polymers exist in the form of unimer, some of which are closed to loops, or in small oligomeric aggregates. In semidilute or concentrated regimes, micelle-like polymer aggregates are formed. At higher concentrations, the polymer chains form an infinite network.

2. Effects of Structural Variations of Amphiphilic Polymers on Association Behavior

Morishima et al. [28] have shown that (i) the type of hydrophobes, (ii) their content in a polymer, (iii) the sequence distribution of electrolyte and hydrophobic monomer units in a polymer chain, and (iv) the type of spacer bonding between hydrophobes and the polymer chain are particularly important structural parameters determining a preference for intra- or interpolymer hydrophobe association. Random copolymers of AMPS and methacrylamides carrying bulky hydrophobic groups with cyclic structures, such as cyclododecyl, 1-adamantyl, and 1-naphthyl groups, form unimolecular micelles (unimer micelles) in aqueous solutions of a wide range of concentrations if the hydrophobe contents are higher than a certain critical level ($\geq$ca. 20 mol %). This phenomenon is due to predominant intramolecular self-association of the hydrophobes with cyclic structure [29–31]. These unimer micelles are very different from the classical surfactant micelles in that (i) all charge and hydrophobes are covalently linked to the polymer backbone, (ii) the unimer micelles are "static" in nature as opposed to the "dynamic" nature of the surfactant micelles which exist in equilibrium between association and dissociation, (iii) the micellar structure is retained even at very low concentrations, and (iv) the unimer micelles remain as such even at very high concentrations.

Random copolymers of AMPS and methacrylamides *N*-substituted with a hydrophobic group such as dodecyl, cyclododecyl, or 1-adamantyl are soluble in water up to about 60 mol % of the hydrophobe content. In contrast, random copolymers of AMPS and dodecylmethacrylate are soluble in water only when the content of dodecylmethacrylate is $\leq$15 mol %. These results indicate that there is a great difference in solubility in water between the polymers with amide and ester spacer bonds connecting hydrophobes to the main chain. Both the amide-spacer and ester-spacer polymers show a tendency for interpolymer association when the hydrophobe contents are lower than about 10 mol %. This tendency is much more pronounced in the ester-spacer polymers than in the amide-spacer polymers. As the hydrophobe contents in the polymers are increased up to about 20 mol % or higher, the amide-spacer polymers show a strong preference for intrapolymer self-association even in a concentrated regime. On the other hand, the ester-spacer polymers give strongly turbid solutions when the hydrophobe content is increased to about 15 mol %.

Since the polymer chain exerts steric constraints to polymer-bound hydrophobes, the degree of the motional and geometrical freedom of polymer-bound hydrophobes has an important effect on their self-association. Therefore, the spacing between hydrophobes and the polymer backbone is a key element to control the hydrophobic association.

3. Cholesterol-Bearing Pullulan

Cholesterol (Chol) plays an important role in controlling membrane fluidity in biological systems, arising from its strong tendency for hydrophobic interactions and rigidity of the steroid ring [32]. The hydrophobicity of Chol is stronger than that of other hydrophobic groups such as dodecyl, cyclododecyl, 1-adamantyl, and 1-naphthyl groups. Some Chol derivatives are known to form ordered structures which indicate thermotropic and lyotropic liquid-crystalline (LC), monolayers, multilayers, micelles, and liposomes [33]. Especially, it is well known that comb-like polymers with Chol groups attached to the main chain via a flexible spacer show a thermotropic LC phase [34–36].

Akiyoshi et al. [37–41] have reported that Chol-bearing polysaccharides (Figure 6), especially Chol-bearing pullulan (CHP), formed colloidally stable particles in dilute aqueous solutions when the aqueous solutions were sonicated. A pullulan (weight-average molecular weight (M_w) = 5.5×10^4, molecular weight distribution (M_w/M_n) = 1.6) derivative carrying two Chol groups per 100 glucose units was prepared, which was characterized by size exclusion column chromatography (SEC), dynamic light scattering (DLS), static light scattering (SLS), transmission electron microscopy (TEM), ^{1}H NMR, and fluorescence spectroscopy. SEC results indicated that CHP intermolecularly aggregates and provides relatively monodispersive particles upon ultrasonication. Spherical particles with relatively uniform size (the diameter = 25 $\pm$ 5 nm) can be observed in the negatively stained TEM of CHP. The hydrodynamic radius (R_h) of the CHP self-aggregate estimated from DLS is approximately 13 nm, and the aggregation number determined by SLS was approximately 13; M_w of the self-aggregate was 7.6×10^6, the radius of gyration (R_g) was 16.8 nm, and the second virial coefficient (A_2) was 2.6×10^{-4} mol/$\cdot$mL/g^2. The mean aggregation number of the Chol moieties (N_{Chol}) can be estimated by fluorescence quenching experiments to be 4.2 $\pm$ 0.5. The CHP self-aggregate carries about 59 Chol moieties, which corresponds to 14 times the mean aggregation number of the Chol moieties. This suggests that approximately 14 independent domains are distributed in one nanoparticle. The critical aggregation concentration of CHP was 0.01 g/L, estimated from fluorescence

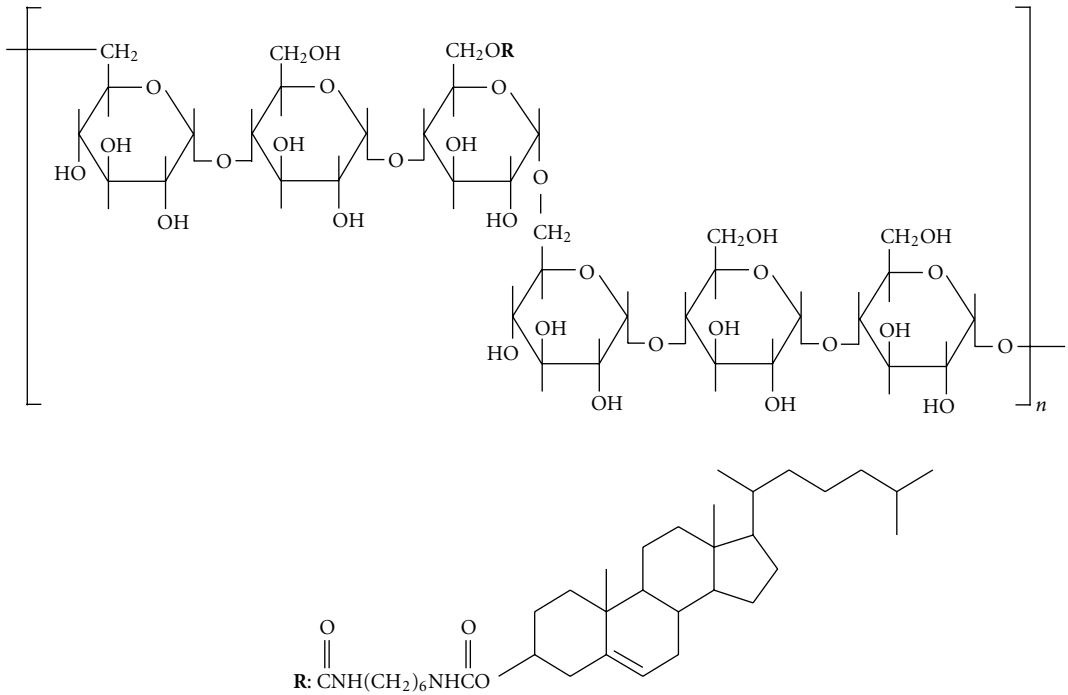

Figure 6: Chemical structure of cholesterol-bearing pullulan (CHP).

measurements using *N*-phenyl-1-naphtylamine (PNA) as a fluorescence probe. CHP shows no surface activity at all up to the concentration of 0.145 g/L. Existence of microdomains consisting of both the rigid core of hydrophobic Chol and the relatively hydrophilic polysaccharide shell was suggested by the line broadening of ^{1}H NMR proton signals of Chol moieties in CHP, and the incorporation of several hydrophobic fluorescence probes in the CHP aggregates. The CHP aggregate by themselves in water and provide colloidally stable and monodispersed nanoparticles above the critical concentration. The CHP self-aggregate is crucial for making a stable complex with various hydrophobic and hydrophilic substances. The main driving force of the complexation is the hydrophobic interactions. The particle size varies with the substitution degree of Chol. However, the association number of polymer chains is about ten, independent of the Chol content.

These studies suggest that, because of a strong tendency for self-association of Chol as well as its structural rigidity, a polyelectrolyte may be modified into a strongly associative polymer by covalently incorporating a small amount of Chol moieties into the polymer chain.

4. Polyelectrolyte-Containing Pendant Cholesteryl Moieties

Chol moieties-containing polyanion (P(A/ChM-5), Figure 7) was synthesized via ordinary random radical copolymerization of sodium 2-(acrylamido)-2-methylpropanesulfonate (AMPS) and cholesteryl 6-methacryloyloxyhecanoate (ChM-5) [42, 43]. Copolymerization of varying molar ratios of AMPS and ChM-5 were performed in the presence of radical initiator in *N*,*N*-dimethylformamide (DMF) at 60°C, and the copolymers with ChM-5 contents ranging from 0.5 to 10 mol % were prepared. The copolymers with ChM-5 contents <5 mol % can be completely soluble in water. ^{1}H NMR spectra for P(A/ChM-5) were measured in deuterium oxide and deuterated dimethyl sulfoxide (DMSO-d_6) at room temperature. In deuterium oxide, resonance peaks due to Chol protons are not observed because of considerable line broadening. In DMSO-d_6, by contrast, no such line broadening was observed in the Chol resonance peaks. These results indicate that motions of Chol moieties in P(A/ChM-5) are highly restricted in deuterium oxide, arising from hydrophobic self-association of Chol groups. The M_w values P(A/ChM-5) with various ChM-5 contents are estimated by SEC. The interpolymer Chol association is absent in the water and acetonitrile (50/50) mixed solvent, and the molar masses of all the random copolymers are more or less the same. In contrast, the M_w values for P(A/ChM-5) estimated by SLS in 0.1 M NaCl aqueous solution are much greater than those estimated by SEC using the water and acetonitrile mixed solvent. The apparent M_w values for the random copolymers with 1 and 5 mol % ChM-5 estimated by SLS are 4.93×10^5 and 1.90×10^6, respectively. The R_g values for the random copolymer with 1 and 5 mol % ChM-5 are 50.3 and 65.7 nm, respectively. The R_h distributions measured by DLS for the random copolymers with 1 and 5 mol % ChM-5 shows bimodal and unimodal distributions, respectively. The small and large R_h values for P(A/ChM-5) with 1 mol % ChM-5 are attributed to nonassociated polymers, that is, unimers and interpolymer

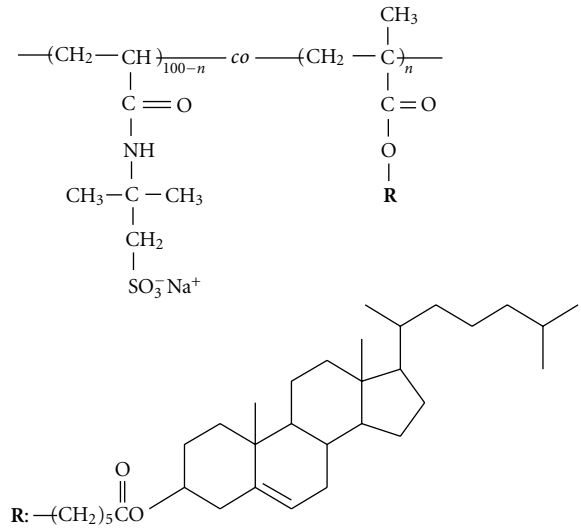

Figure 7: Chemical structure of cholesterol-bearing polyelectrolyte.

associations in water. P(A/ChM-5) with 5 mol % ChM-5 can be observed at only large R_h values, indicating that most polymer chains are intermolecularly associated in water. The aggregation number for P(A/ChM-5) with 5 mol % ChM-5 can be roughly calculated to be approximately 50 from the molecular weight determined by SLS and SEC.

All the results just presented led us to propose a conceptual model for interpolymer aggregated formed by P(A/ChM-5) with 5 mol % ChM-5 in water. The Chol pendants in the random copolymer associate both intra- and intermolecularly. Intrapolymer association leads to a flower-like micelle [9, 10] in which a hydrophobic microdomain—formed from Chol association—is surrounded by loops of polyanion segments. The concurrent interpolymer Chol association will link the flower-like micelle together, and thus intermolecularly-bridged flower-like micelles are formed. Generally, small amounts of large-size hydrophobic groups introduced into side chains in water-soluble polymers apt to associate intermolecularly.

The average number of Chol groups contained in one microdomain, that is, the average aggregation number of Chol groups (N_{chol}), is determined by a time resolved fluorescence quenching technique. For this experiment, P(A/ChM-5) with 5 mol % ChM-5, pyrene as a fluorescence probe, and 3,4-dimethylbenzophenoe (DMBP) as a fluorescence quencher were used. The number of polymer chains composed of one intermolecularly bridged flower-like micelle, that is, the apparent aggregation number (N_{agg}) of the polymer chains of P(A/ChM-5) with 5 mol % ChM-5, was roughly estimated based on molecular weight to be about 50. P(A/ChM-5) with 5 mol % ChM-5 possesses on average 3.5 Chol groups, as calculated from the molecular weight and the Chol content. Therefore, the number of Chol groups in the multipolymer associate is roughly estimated to be 175, consisting of 10 cross-linking sites with each site consisting 17–19 Chol moieties.

5. Cholesterol-End-Capped Polyelectrolyte

Chol-substituted azo initiator, 4,4-azobis(4-cyano-1-cholesteryl)pentanoate (AzCCP) was prepared [44]. Free radical polymerization of AMPS using AzCPP as an initiator was performed to obtain a Chol-end-capped polymer (Chol-PAMPS, Figure 8). The number-average degree of polymerization (DP) of Chol-PAMPS is estimated to be about 72 based on a ^{1}H NMR spectrum measured in DMSO-d_6 by assuming all the chain termination to occur via disproportionation. Using the DP estimated from ^{1}H NMR as a basis and assuming each polymer chain has one Chol group at the polymer chain end, the DP estimated from SEC was found to be very similar. It is anticipated that Chol-PAMPS would form a spherical core-shell type micelle with a Chol aggregate in the core and PAMPS chains in the shell. If that is the case, R_h of the micelle should be equal to or smaller than the length of the fully extended Chol-PAMPS chain. For Chol-PAMPS of DP = 72, this length is approximately 20 nm. However, R_h values observed by DLS in the various polymer concentrations are of the order of 50 nm, and this size is obviously too large for the core-shell micelle. It is concluded that the multipolymer aggregates of Chol-PAMPS are not spherical core-shell micelles. There is a possibility that some polymer chains possess Chol groups at both chain ends, which are produced by the recombination of growing chain radicals or by primary radical termination. Even if most of the polymers have one Chol group at one chain end and they form spherical micelles, a small number of polymer possessing Chol groups at both ends may bridge the micelles, leading to an increase in hydrodynamic size. Furthermore, it seems reasonable to consider that this bridging is more likely to occur at high polymer concentrations, thus leading to a large increase in R_h. Fluorescence emission and excitation spectra for pyrene probe solubilized in the aggregates of Chol-PAMPS suggested the presence of the critical micelle concentration (cmc) around 0.6 g/L in water.

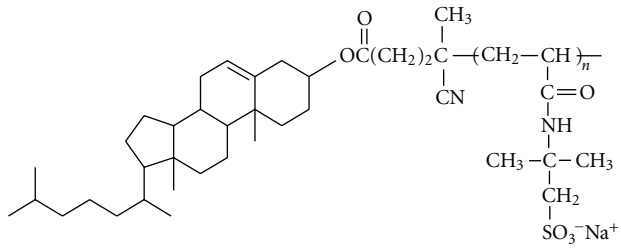

Figure 8: Chemical structure of cholesterol-end-capped polyelectrolyte.

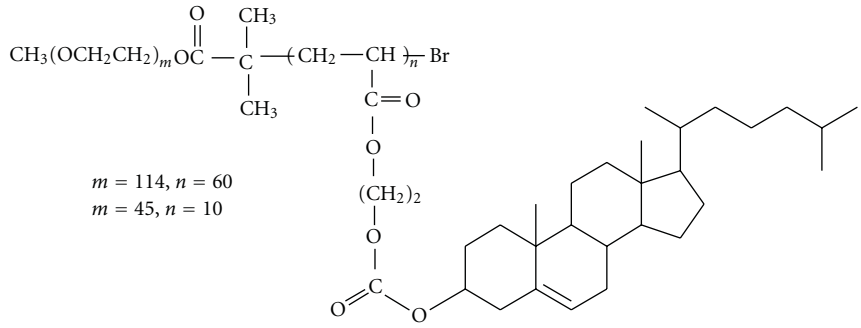

Figure 9: Chemical structure of amphiphilic block copolymers containing a Chol-based block.

6. Amphiphilic Block Copolymer Containing Cholesterol-Bearing Block

An amphiphilic block copolymer is a typical synthetic system that reveals a controlled balance of amphiphilicity and can assume various well-organized architectures, including spherical, rod, and lamellar structures [45, 46]. In the past decade, the studies on self-assembly of block copolymers in solution have been extensively pursued [47, 48]. Figure 9 shows the chemical structure of the amphiphilic LC diblock copolymers, PEG5000-*b*-PAChol(14/86) and PEG2000-*b*-PAChol(28/72), which are prepared by a typical atom transfer radical polymerization (14/86 and 28/72 are the hydrophilic/hydrophobic weight ratios) [49]. These diblock copolymers present LC mesophase measured by differential scanning calorimetry (DSC). X-ray scattering experiments on a bulk sample of PEG5000-*b*-PAChol(14/86) revealed a smectic A phase with lamellar period (d) of 4.29 nm. This period corresponds to a value being the wholly extended length of the Chol moieties. For PEG2000-*b*-PAChol(28/72) in the same position of reflection ($d = 4.3\,nm$), only diffuse layer reflection is observed, which corresponds to a fluctuation of smectic structure in the LC block. The mesophase in the LC part is a chiral nematic from the polarizing microscope observation. Self-assembly of the amphiphilic block copolymers in water was performed. Nanofibers with a lamellar fine structure were formed in water by the block copolymer PEG5000-*b*-PAChol(14/86). The lamellar structure in their hydrophobic core has the same origin as that of the smectic A phase observed in the bulk sample. Both of them result from the interdigital smectic A self-organization of the Chol-based mesogen. On the other hand, polymer vesicles instead of nanofibers are formed by PEG2000-*b*-PAChol(28/72), in bulk sample of which only a nematic phase with smectic fluctuation is observed.

7. Conclusion

Polymer-bound Chol moieties show a strong tendency for self-association in water. The strongly stacking nature and hydrophobically associating nature of Chol groups incorporated in polymers would allow one to design a variety of associative polymers that form a variety of nanoorganized structures. These Chol-bearing associative polymers may find usefulness in studies of interactions with lipid membranes as well as potentials for practical applications such as chemical delivery systems.

Acronyms

AMPS:	Sodium 2-(acrylamido)-2-methylpropanesulfonate
PNIPAM:	Poly(*N*-isopropylacrylamide)
LCST:	Lower critical solution temperature
Chol:	Cholesterol
LC:	Liquid crystalline
CHP:	Cholesterol-bearing pullulan
M_w:	Weight-average molecular weight
M_w/M_n:	Molecular weight distribution
SEC:	Size exclusion column chromatography
DLS:	Dynamic light scattering
SLS:	Static light scattering
TEM:	Transmission electron microscopy
^{1}H NMR:	Proton nuclear magnetic resonance

R_h:	Hydrodynamic radius
R_g:	Radius of gyration
A_2:	Second virial coefficient
N_{Chol}:	Aggregation number of cholesteryl moieties
PNA:	*N*-Phenyl-1-naphtylamine
P(A/ChM-5):	Poly(sodium 2-(acrylamido)-2-methylpropanesulfonate-co-cholesteryl 6-methacryloyloxyhecanoate)
ChM-5:	Cholesteryl 6-methacryloyloxyhecanoate
DMF:	*N,N*-Dimethylformamide
DMSO-d_6:	Deuterated dimethyl sulfoxide
DMBP:	3,4-Dimethylbenzophenoe
N_{agg} :	Aggregation number
AzCCP:	4,4-Azobis(4-cyano-1-cholesteryl)pentanoate
Chol-PAMPS:	Cholesterol-end-capped poly(sodium 2-(acrylamido)-2-methylpropanesulfonate)
DP:	Number-average degree of polymerization
cmc:	Critical micelle concentration
PEG5000-*b*-PAChol:	Poly(ethylene glycol)5000-block-poly(cholesteryl acryloyloxy ethyl carbonate)
PEG2000-*b*-PAChol:	Poly(ethylene glycol)2000-block-poly(cholesteryl acryloyloxy ethyl carbonate)
DSC:	Differential scanning calorimetry
d:	Lamellar period.

References

[1] C. L. McCormick, J. Bock, and D. N. Schulz, *Encyclopedia of Polymer Science and Engineering*, John Wiley and Sons, New York, NY, USA, 1989.

[2] P. Dubin, J. Bock, R. M. Davies, D. N. Schulz, and C. Thies, *Macromolecular Complexes in Chemistry and Biology*, Springer, Berlin, Germany, 1994.

[3] J. E. Glass, *Polymers in Aqueous Media: Performance through Association*, Advances in Chemistry Series 223, American Chemical Society, Washington, DC, USA, 1989.

[4] G. Némethy and H. A. Scheeaga, "Structure of water and hydrophobic bonding in proteins. I. A model for the thermodynamic properties of liquid water," *The Journal of Chemical Physics*, vol. 36, no. 12, pp. 3382–3400, 1962.

[5] G. Némethy and H. A. Scheraga, "Structure of water and hydrophobic bonding in proteins. II. Model for the thermodynamic properties of aqueous solutions of hydrocarbons," *The Journal of Chemical Physics*, vol. 36, no. 12, pp. 3401–3417, 1962.

[6] A. Halperin, M. Tirrell, and T. P. Lodge, "Tethered chains in polymer microstructures," *Advances in Polymer Science*, vol. 100, pp. 30–71, 1991.

[7] Y. Morishima, "Unimolecular micelles of hydrophobically modified polyelectrolytes," in *Solvents and Self-Organization of Polymers*, S. E. Webber, D. Tuzar, and P. Munk, Eds., pp. 331–358, Kluwer Academic Publishers, Dordrecht, The Netherlands, 1996.

[8] S. E. Webber, "Polymer micelles: an example of self-assembling polymers," *Journal of Physical Chemistry B*, vol. 102, no. 15, pp. 2618–2626, 1998.

[9] A. Halperin, "On the collapse of multiblock copolymers," *Macromolecules*, vol. 24, no. 6, pp. 1418–1419, 1991.

[10] A. N. Semenov, J. F. Joanny, and A. R. Khokhlov, "Associating polymers: equilibrium and linear viscoelasticity," *Macromolecules*, vol. 28, no. 4, pp. 1066–1075, 1995.

[11] M. W. Urban and T. Provder, *Multidimensional Spectroscopy of Polymers: Vibrational, NMR, and Fluorescence Techniques*, ACS Symposium Series 598, American Chemical Society, Washington, DC, USA, 1995.

[12] Y. Morishima, S. Nomura, T. Ikeda, M. Seki, and M. Kamachi, "Characterization of unimolecular micelles of random copolymers of sodium 2-(acrylamido)-2-methylpropanesulfonate and methacrylamides bearing bulky hydrophobic substituents," *Macromolecules*, vol. 28, no. 8, pp. 2874–2881, 1995.

[13] M. Seki, Y. Morishima, and M. Kamachi, "Characterization of the complexes of amphiphilic polyanions and double-chain cationic surfactants," *Macromolecules*, vol. 25, no. 24, pp. 6540–6546, 1992.

[14] Y. Morishima, M. Tsuji, M. Seki, and M. Kamachi, "Synthesis, NMR relaxation, and photoisomerization of amphiphilic polyelectrolytes covalently tethered with azobenzene moieties having bulky hydrophobic substituents," *Macromolecules*, vol. 26, no. 13, pp. 3299–3305, 1993.

[15] K. Kamioka, S. E. Webber, and Y. Morishima, "Solvent dependence of energy trapping in methacrylic acid-vinylphenanthrene block copolymers," *Macromolecules*, vol. 21, no. 4, pp. 972–978, 1988.

[16] Y. Morishima, H. S. Lim, S. I. Nozakura, and J. L. Sturtevant, "Effect of monomer sequence distribution in 2-vinylnaphthalene-maleic acid copolymers on energy migration excimer formation in aqueous solution," *Macromolecules*, vol. 22, no. 3, pp. 1148–1154, 1989.

[17] C. L. McCormick and Y. Chang, "Water-soluble copolymers. 58. Associative interactions and photophysical behavior of amphiphilic terpolymers prepared by modification of maleic anhydride/ethyl vinyl ether copolymers," *Macromolecules*, vol. 27, no. 8, pp. 2151–2158, 1994.

[18] K. Prochazka, D. Kiserow, C. Ramireddy, Z. Tuzar, P. Munk, and S. E. Webber, "Time-resolved fluorescence studies of the chain dynamics of naphthalene-labeled polystyrene-block-poly(methacrylic acid) micelles in aqueous media," *Macromolecules*, vol. 25, no. 1, pp. 454–460, 1992.

[19] C. L. McCormick and L. C. Salazar, "Water soluble copolymers: 46. Hydrophilic sulphobetaine copolymers of acrylamide and 3-(2-acrylamido-2-methylpropanedimethylammonio)-1-propanesulphonate," *Polymer*, vol. 33, no. 21, pp. 4617–4624, 1992.

[20] Y. Chang and C. L. McCormick, "Water-soluble copolymers. 49. Effect of the distribution of the hydrophobic cationic monomer dimethyldodecyl(2-acrylamidoethyl)ammonium bromide on the solution behavior of associating acrylamide copolymers," *Macromolecules*, vol. 26, no. 22, pp. 6121–6126, 1993.

[21] H. G. Elias, "Nonionic micelles," *Journal of Macromolecular Science: Part A*, vol. 7, no. 3, pp. 601–622, 1973.

[22] Z. Tuzar, P. Kratochvíl, K. Procházka, and P. Munk, "Block copolymer micelles in aqueous media," *Collection of Czechoslovak Chemical Communications*, vol. 58, no. 10, pp. 2362–2369, 1993.

[23] E. Matijevic, *Surface and Colloid Science Series*, vol. 51, Plenum, New York, NY, USA, 1993.

[24] M. Tian, A. Qin, C. Ramireddy et al., "Hybridization of block copolymer micelles," *Langmuir*, vol. 9, no. 7, pp. 1741–1748, 1993.

[25] F. M. Winnik, A. R. Davidson, G. K. Hamer, and H. Kitano, "Amphiphilic poly(N-isopropylacrylamides) prepared by using a lipophilic radical initiator: synthesis and solution properties in water," *Macromolecules*, vol. 25, no. 7, pp. 1876–1880, 1992.

[26] A. Yamazaki, J. M. Song, F. M. Winnik, and J. L. Brash, "Synthesis and solution properties of fluorescently labeled amphiphilic (N-alkylacrylamide) oligomers," *Macromolecules*, vol. 31, no. 1, pp. 109–115, 1998.

[27] E. Alami, M. Almgren, W. Brown, and J. François, "Aggregation of hydrophobically end-capped poly(ethylene oxide) in aqueous solutions. Fluorescence and light-scattering studies," *Macromolecules*, vol. 29, no. 6, pp. 2229–2243, 1996.

[28] Y. Morishima, Y. Tominaga, M. Kamachi, T. Okada, Y. Hirata, and N. Mataga, "Photoinduced charge separation by chromophores encapsulated in the hydrophobic compartment of amphiphllic polyelectrolytes with various aliphatic hydrocarbons," *Journal of Physical Chemistry*, vol. 95, no. 15, pp. 6027–6034, 1991.

[29] Y. Morishima, M. Tsuji, M. Kamachi, and K. Hatada, "Photochromic isomerization of azobenzene moieties compartmentalized in hydrophobic microdomains in a microphase structure of amphiphilic polyelectrolytes," *Macromolecules*, vol. 25, no. 17, pp. 4406–4410, 1992.

[30] Y. Morishima, Y. Tominaga, S. Nomura, M. Kamachi, and T. Okada, "Rapid migration and trapping of photoexcited electronic energy in amphiphilic polyelectrolytes containing naphthalene chromophores and pyrene traps," *Journal of Physical Chemistry*, vol. 96, no. 4, pp. 1990–1994, 1992.

[31] H. Aota, Y. Morishima, and M. Kamachi, "Compartmentalization of zinc (II) tetraphenylporphyrin in a hydrophobic microdomain of an amphiphilic polyelectrolyte: a physicochemical model of biological metalloporphyrin systems," *Photochemistry and Photobiology*, vol. 57, no. S1, pp. 989–995, 1993.

[32] R. A. Demel and B. De Kruyff, "The function of sterols in membranes," *Biochimica et Biophysica Acta*, vol. 457, no. 2, pp. 109–132, 1976.

[33] H. Ringsdorf, B. Schlarb, and J. Venzmer, "Molecular architecture and function of polymeric oriented systems: models for the study of organization, surface recognition, and dynamics of biomembrnaes," *Angewandte Chemie International*, vol. 27, no. 1, pp. 113–158, 1988.

[34] V. P. Shibaev, N. A. Platé, and Y. S. Freidzon, "Thermotropic liquid crystalline polymers. I. Cholesterol-containing polymers and copolymers," *Journal of Polymer Science*, vol. 17, no. 6, pp. 1655–1670, 1979.

[35] V. P. Shibaev, R. V. Tal'roze, F. I. Karakhanova, and N. A. Platé, "Thermotropic liquid crystalline polymers. II. Polymers with amino acid fragments in the side chains," *Journal of Polymer Science*, vol. 17, no. 6, pp. 1671–1684, 1979.

[36] T. Yamaguchi, T. Asada, H. Hayashi, and N. Nakamura, "Dependence of the packing structure of mesogenic groups on the flexible spacer length of liquid crystalline side-chain polymers," *Macromolecules*, vol. 22, no. 3, pp. 1141–1144, 1989.

[37] K. Akiyoshi, K. Nagai, T. Nishikawa, and J. Sunamoto, "Self-aggregates of hydrophobized polysaccharide as a host for macromolecular guests," *Chemistry Letters*, vol. 21, no. 9, pp. 1727–1730, 1992.

[38] K. Akiyoshi, S. Deguchi, N. Moriguchi, S. Yamaguchi, and J. Sunamoto, "Self-aggregates of hydrophobized polysaccharides in water. Formation and characteristics of nanoparticles," *Macromolecules*, vol. 26, no. 12, pp. 3062–3068, 1993.

[39] S. Deguchi, K. Akiyoshi, and J. Sunamoto, "Solution property of hydrophobized pullulan conjugated with poly(ethylene oxide)-poly(propylene oxide)-poly(ethylene oxide) block copolymer. Formation of nanoparticles and their thermosensitivity," *Macromolecular Rapid Communications*, vol. 15, no. 9, pp. 705–711, 1994.

[40] T. Nishikawa, K. Akiyoshi, and J. Sunamoto, "Supramolecular assembly between nanoparticles of hydrophobized polysaccharide and soluble protein complexation between the self-aggregate of cholesterol-bearing pullulan and α-chymotrypsin," *Macromolecules*, vol. 27, no. 26, pp. 7654–7659, 1994.

[41] K. Akiyoshi, S. Deguchi, H. Tajima, T. Nishikawa, and J. Sunamoto, "Self-assembly of hydrophobized polysaccharide. Structure of hydrogel nanoparticle and complexation with organic compounds," *Proceedings of the Japan Academy B*, vol. 71, no. 1, pp. 15–19, 1995.

[42] S. I. Yusa, M. Kamachi, and Y. Morishima, "Hydrophobic self-association of cholesterol moieties covalently linked to polyelectrolytes: effect of spacer bond," *Langmuir*, vol. 14, no. 21, pp. 6059–6067, 1998.

[43] S. I. Yusa, A. Hashidzume, and Y. Morishima, "Interpolymer association of cholesterol pendants linked to a polyelectrolyte as studied by quasielastic light scattering and fluorescence techniques," *Langmuir*, vol. 15, no. 26, pp. 8826–8831, 1999.

[44] S. I. Yusa, M. Kamachi, and Y. Morishima, "Self-association of cholesterol-end-capped poly(sodium 2-(acrylamido)-2-methylpropanesulfonate) in aqueous solution," *Macromolecules*, vol. 33, no. 4, pp. 1224–1231, 2000.

[45] B. Lindman and P. Alexandridis, *Amphiphilic Block Copolymer*, Elsevier, Amsterdam, The Netherlands, 2000.

[46] I. W. Hamley, *Block Copolymers in Solution*, John Wiley and Sons, New York, NY, USA, 2005.

[47] D. E. Discher and A. Eisenberg, "Polymer vesicles," *Science*, vol. 297, no. 5583, pp. 967–973, 2002.

[48] H. Kukula, H. Schlaad, M. Antonietti, and S. Förster, "The formation of polymer vesicles or "peptosomes" by polybutadiene-block-poly(L-glutamate)s in dilute aqueous solution," *Journal of the American Chemical Society*, vol. 124, no. 8, pp. 1658–1663, 2002.

[49] R. Piñol, L. Jia, F. Gubellini et al., "Self-assembly of PEG-b-liquid crystal polymer: the role of smectic order in the formation of nanofibers," *Macromolecules*, vol. 40, no. 16, pp. 5625–5627, 2007.